THE UNIVERSITY *of* EDINBURGH

Source apportionment of organic gas and particulate matter pollutants using concentration and flux measurements in Delhi

THE UNIVERSITY *of* EDINBURGH

James Cash

A thesis submitted in fulfilment of the requirements

for the degree of Doctor of Philosophy

The University of Edinburgh

2022

Declaration

I declare that this thesis was composed by myself, that the work contained herein is my own except where explicitly stated in the text.

Part of this work have been published in:

Cash, J. M., Langford, B., Di Marco, C., Mullinger, N. J., Allan, J., Reyes-Villegas, E., Joshi, R., Heal, M. R., Acton, W. J. F., Hewitt, C. N., Misztal, P. K., Drysdale, W., Mandal, T. K., Shivani, Gadi, R., Gurjar, B. R., and Nemitz, E.: Seasonal analysis of submicron aerosol in Old Delhi using high-resolution aerosol mass spectrometry: chemical characterisation, source apportionment and new marker identification, Atmos. Chem. Phys., 21, 10133–10158, https://doi.org/10.5194/acp-21-10133-2021, 2021.

James Cash

February 2022

Abstract

One of the world's worst cities for air pollution is Delhi, India. Past studies have shown air pollution in Delhi has a significant burden on the population's respiratory and cardiovascular health. It is therefore important to analyse the sources of these pollutants in order to improve air quality mitigation strategies. This thesis presents time-resolved source apportionments of the organic fraction of particulate matter (PM) and of the gaseous volatile organic compounds (VOCs) that were measured in Delhi. The results of this analysis are used to identify the sources of these air pollutants and determine their atmospheric implications.

Online aerosol mass spectrometry (AMS) measurements taken in Old Delhi during pre-monsoon, monsoon and post-monsoon seasons revealed concentrations of submicron particulate matter (PM_1) reaching ~750 μg m^{-3}. The largest contributing inorganic species to PM_1 in the post-monsoon is nitrate (8%) but this changes to sulphate during the monsoon (24%) and pre-monsoon (24%). PM_1 is dominated by the organics throughout the three measurement periods (54% - 68%). Source apportionment on the organics fraction using Positive Matrix Factorisation (PMF) revealed that PM_1 traffic emissions are the largest contributor of primary organic aerosol (POA) in the pre-monsoon (12%) and monsoon (16%) periods. Two traffic factors were resolved: a hydrocarbon-like organic aerosol (HOA) and another HOA factor rich in nitrogen (NHOA). The N within NHOA is previously undocumented within AMS measurements and is found to be linked to nitrile species. The two traffic factors are found to have separated due to fuel-type where NHOA is related to heavy goods vehicles (HGVs) and diesel emissions while HOA is related to petrol and compressed natural gas emissions. The highest PM_1 concentrations are observed in the post-monsoon period during which the highest form of POA is from a burning-related factor. These factors alone

contribute 35% to the total post-monsoon increase when concentrations increase by 188%. A high correlation between one burning factor, semi-volatility biomass burning organic aerosol (SVBBOA), and Earth observation fire counts in surrounding states demonstrates its link to crop residue burning. Another burning factor, solid-fuel OA (SFOA), is found to have a high composition of polyaromatic hydrocarbons (PAHs) and novel AMS-measured marker species for polychlorinated dibenzodioxins (PCDDs) and polychlorinated dibenzofurans (PCDFs). SFOA is therefore linked to local open-waste burning. There is also a 522% increase in chloride concentrations from pre-monsoon to post-monsoon. High correlations with SVBBOA and SFOA, suggest the post-monsoon increase in chloride is due to crop residue and open-waste burning. Future air quality mitigation strategies should concentrate on traffic emissions in order to cause a reduction PM_1 across the whole year. To reduce peak PM_1 concentrations during the post-monsoon, requires targeting of burning-related activities in future air quality policy.

The monitoring and measurements of volatile organic compounds (VOCs) in Delhi is often overlooked. While the effects of VOCs on people's heath is still being debated, the outcome of their interaction with the atmosphere can play a pivotal role in PM formation, OH reactivity and photochemical ozone creation potentials (POCP). For the first time, a novel approach to source apportionment was developed which allows for emission and deposition to be calculated for positive matrix factorisation (PMF) VOC source factors. Spatial flux patterns for PMF factors are presented, which give in-depth detail of the localised fluxes. A total of nine factors were resolved, of which traffic emissions are the largest (70% of total flux) and are the most significant source of OH reactivity flux and photochemical ozone creation potential (POCP). The two traffic factors separate based on the HGV restrictions causing the composition of one factor (TRAF1) to have a strong connection with diesel emissions and the other (TRAF2) with petrol and compressed natural gas. The second most significant source of emissions is an evaporative VOC (EVOC) source (10% of total flux) which has a high composition of marker species related to asphalt

emissions. These are found to be naphthalene and tetralin-based structures, along with 1,3-butadiene and styrene which are constituent species of the adhesives used in asphalt. The peak in emissions of EVOC occurs during midday and follows surface temperature and solar radiation. Due to their similar meteorological controls, most of the biogenic VOCs reside within the EVOC factor. It is estimated that biogenic emissions contribute 25% to total monoterpene concentrations and 18% to the localised monoterpene fluxes. However, the traffic factors have the highest composition of monoterpenes and, as a result, they dominate the monoterpene contributions to concentrations (60%) and localised fluxes (78%). Two burning-related factors were separated, one associated with solid-fuel combustion VOCs (SFVOC) and another associated with pyrotechnical activity VOCs (PVOC). The two factors are shown to share the largest percentage of the concentration-weighted OH reactivity. This is caused by a high content of furan-based species. The first observation of a strong urban deposition flux for PMF factors is also seen for SFVOC and an oxidised VOC (OVOC1) factor. Spatial deposition flux patterns suggest vegetation could act as a VOC sink in Delhi, however, the magnitude of which could show it to be small.

Over recent years, multiple PM mitigation strategies have been implemented in Delhi, but, how effective these changes have been to reduce PM is not clear. It is however possible to chart the changes in PM by analysing large archives of PM filter samples that have been collected over multiple years. An automated offline-AMS method was developed which has enabled high-throughput analysis, allowing PM concentrations to be charted over multiple years. This novel offline-AMS method uses an organic solvent mix of acetone and water which can extract high quantities of OA (95.4 ± 8.3 %). PM_{10} filter samples collected in Delhi for the years of 2011, 2015 and 2018, were analysed. PMF analysis was performed on the organic fraction and nine factors were resolved. These factors can be grouped into four source categories: cooking, traffic, coal-combustion and burning-related (solid fuel or open burning) OA. Burning-related OA is the highest contributor when total OA

concentrations are also at their highest, during the winter and post-monsoon. As a result, burning-related OA likely contributes significantly to acute PM-related health affects in Delhi. Annual averages show a decline in burning-related OA concentrations from 2015 to 2018 (47%). This could be linked to the 2015 ban on open-waste burning; however, compositional analysis of OA factors suggests municipal waste burning is still present in 2018. Further mitigation strategies are therefore required to reduce burning-related OA further. The shutdown of the two coal power stations in Delhi, along with initiatives to reduce the popularity of coal-use in businesses, residential homes, and industry, has led to a significant decrease (87%) in coal-combustion OA. Total OA concentrations were also predicted to be reduced by 17%, therefore, proving these measures brought effective reductions in PM_{10}. The Bharat stage emissions standards for vehicles likely supressed PM_{10} OA concentrations as the annual averages of traffic OA factors do not reflect the coinciding rapid increase in population and registered vehicles. However, restrictions on HGVs entering during the day shows possible links to increases in PM_{10} concentrations during the winter and post-monsoon months. This is likely due to the large influx of diesel-engine HGVs entering the city when the boundary layer is particularly low during the early mornings and evenings.

Lay Summary

Globally, air pollution is one of the leading causes of premature deaths, and one of the most polluted places in the world is Delhi, India. The air pollutant which has the greatest effect on human health is particulate matter (PM). These small particles, that are generally smaller than ten thousandths of a millimetre, are emitted directly into the atmosphere from point sources such as traffic or biomass burning. A substantial amount of PM is also formed in the atmosphere from reactions of volatile organic compounds (VOCs) that are also emitted into the air. These hydrocarbon compounds evaporate easily at room temperatures and cause the formation of near-surface ozone, which is toxic to most life. It is therefore crucial to understand their source origins in order to develop strategies to reduce their quantities.

Two measurement sites were used in this thesis and were selected based on their differences in emissions sources in the surrounding areas. One is situated in Old Delhi and represents an area containing a complex array of emission sources. The other site is situated towards the west of New Delhi and is closer to representing urban background concentrations. New ways of measuring PM and VOCs have been developed for this thesis. A novel method of measuring PM collected on filters in the past has enabled the possible sources of PM in Delhi to be charted over the seasons of 2011, 2015 and 2018. This information is supported by real-time measurements of PM throughout most of 2018, giving a briefer but highly time resolved view of PM and its sources. Measurements of VOCs were also taken during the post-monsoon of 2018. For the first time, this thesis presents the surface-exchange dynamics for a set of VOC sources contributing to these measurements. This means that instead of static concentrations, these measurements show the rate at which VOCs are emitted from, or deposited to, the surface due to a potential source or sink.

The main findings suggest traffic is a dominant source in Delhi for both PM and VOCs. Traffic VOC emissions are shown to be responsible for the greatest reduction in the atmosphere's ability to oxidise and remove air pollutants, and they have the greatest potential to form near-surface ozone. PM and VOC measurements also provide evidence to suggest restrictions that are designed to reduce emissions from heavy goods vehicles (HGV) are, instead, accentuating pollutant concentrations. This is due to the large influx of HGVs during times of the day when the meteorological conditions of the atmosphere are at their least favourable for pollution dispersion. This suggests that mitigation strategies surrounding HGV restrictions need to be rethought in order for them to have a positive impact on PM concentrations. However, annual changes in PM suggest that vehicle emissions standards are supressing what should be large yearly increases in PM. This shows that emission standards have been successful in reducing PM concentrations and, therefore, have reduced the adverse health impacts of air pollution on Delhi's population.

During the post-monsoon and winter seasons, PM originating from traffic is exceeded by the open burning of biomass, solid fuels and municipal waste. Burning-related PM is likely to be the greatest contributor to acute PM-related health affects in Delhi, as the highest concentrations of PM are also during the post-monsoon and winter seasons. Additionally, burning-related VOCs have the potential to be the second most significant source of ozone formation. Annual PM results suggest the complete ban on open waste burning in Delhi could have caused a small decrease in PM. However, the evidence from this work suggests that widespread open burning still occurs and contributes significantly to pollutant concentrations. Therefore, further consideration is required in order for the current open burning mitigation strategies to have a significant impact on Delhi's air quality.

Acknowledgements

I am deeply grateful to my supervisor at the University of Edinburgh, Prof. Mathew Heal. His inspirational lectures and fantastic teaching skills are why I decided to do a PhD in the atmospheric sciences. Without his patience and support, I would have struggled greatly.

I am very grateful to my supervisor, Dr. Eiko Nemitz, at the UK Centre for Ecology & Hydrology. His extensive knowledge and enthusiasm for the subject has inspired me and my work. I deeply appreciate his valuable time spent patiently describing concepts to me.

I would also like to pay special tribute to my supervisor, Dr. Ben Langford, at the UK Centre for Ecology & Hydrology, for being a good friend and mountain bike riding buddy. I have deeply enjoyed working with him and fully appreciate the huge amount of time he spent answering my many questions and inspiring me with his amazing ideas.

I am very grateful to Dr. Chiara Di Marco for her support and guidance with the HR-TOF-AMS measurements. Without her patient instruction I would have definitely broken more parts than I did.

I also want to thank Dr. Neil Mullinger for his field measurement support and for all the laughs along the way.

I thank the members of the MacAQUE (Modelling and measuring atmospheric chemistry and air quality at Edinburgh) group for their interesting discussions and helpful suggestions throughout my PhD.

I would like to thank Dr. Tuhin Mandal and his colleagues at the National Physics Laboratory in India. Without their support and guidance, this work simply would not have happened.

Finally, I am incredibly grateful to my friends; my mother, Sharon; my father, John; and my dog, Spuds, for keeping me sane over these last few years. I also owe my partner, Emily, a huge debt of gratitude for her support, patience, and encouragement.

Contents

List of Figures

List of Tables

List of Abbreviations

Abbreviations	*Meaning*
IGDTUW	**Indira Gandhi Delhi Technical University for Women, Old Delhi**
NPL-India	**National Physics Laboratory, New Delhi**
HR-TOF-AMS	**High-resolution time-of-flight aerosol mass spectrometer**
PTR-QiTOF-MS	**High-resolution proton transfer reaction mass spectrometer with a quadrupole ion guide**
EI	**Electron impact**
PM_1	**Sub-micron particulate matter**
$PM_{2.5}$	**Fine particulate matter**
PM_{10}	**The sum of fine and coarse PM**
OA	**Organic aerosol**
POA	**Primary organic aerosol**
SOA	**Secondary organic aerosol**
WSOA	**Water-soluble organic aerosol**
WIOA	**Water-insoluble organic aerosol**
OrgNO	**Organic nitrogen oxide species**
BC	**Black carbon**
OM	**Organic matter**
OC	**Organic carbon**
WSOC	**Water-soluble organic carbon**
TOC	**Total organic carbon**
EC	**Elemental carbon**
LWC	**Liquid water content**
PCDDs	**Polychlorinated dibenzodioxins**
PCDFs	**Polychlorinated dibenzofurans**
$\overline{OS}_C$	**Carbon oxidation state**
PMF	**Positive Matrix Factorisation**
ME-2	**Multilinear-Engine 2**
SNR	**Signal-to-noise ratio**
CCOA	**Coal-combustion organic aerosol**
COA	**Cooking organic aerosol**
NHOA	**Nitrogen-containing hydrocarbon-like organic aerosol**
SFOA	**Solid fuel organic aerosol**
HOA	**Hydrocarbon-like organic aerosol**
SVBBOA	**Semi-volatility biomass burning organic aerosol**
LVOOA	**Low-volatility oxygenated organic aerosol**
SVOOA	**Semi-volatility oxygenated organic aerosol**
PAH	**Polyaromatic hydrocarbons**
UnSubPAH	**Unsubstituted PAH**
MPAH	**Methyl-substituted PAH**
OPAH	**Oxidised PAH**
NOPAH	**Nitrogen-oxygen substituted PAH**
APAH	**Amino PAH**
VK	**Van Krevelen** **cont…**

Abbreviations	*Meaning*
VMR	**Volume mixing ratio**
PBL	**Planetary boundary layer**
SSRD	**Surface solar radiation downwards**
EC	**Eddy covariance**
TEA	**True-eddy accumulation**
POCP	**Photochemical ozone creation potential**
VOC	**Volatile organic compound**
VVOC	**Very volatile organic compound**
SVOC	**Semi-volatility organic compound**
LVOC	**Low-volatility organic compound**
ELVOC	**Extremely low volatility organic compound**
POCP	**Photochemical ozone creation potential**
MIR	**Maximum incremental reactivity**
SFVOC	**Solid fuel volatile organic compounds**
PVOC	**Pyrotechnical volatile organic compounds**
IND-VOC	**Industrial/solvent-use volatile organic compounds**
GEN-VOC	**Diesel-generator associated volatile organic compounds**
TRAF1	**Traffic-related volatile organic compounds**
TRAF2	**Traffic-related volatile organic compounds**
EVOC	**Evaporative volatile organic compounds**
OVOC1	**Oxidised volatile organic compounds**
OVOC2	**Oxidised volatile organic compounds**
BVOC	**Biogenic volatile organic compounds**
HGV	**Heavy goods vehicle**
CNG	**Compressed natural gas**

Chapter 1

Introduction

1.1. Particulate matter and volatile organic compounds

1.1.1. Definitions and classifications

Particulate matter (PM), often colloquially labelled ‘aerosol’, is a term which refers to a mixture of solid and liquid particles that are found in the atmosphere. PM is considered an atmospheric pollutant as it causes negative health effects when inhaled. Its component particles vary in size, and it is typically measured as the total particle mass (often in units of ug m^{-3}) below a threshold size which has led to defined size categories of PM. The size categories, going from smallest to largest, are as follows: ultrafine PM, defined as diameter < 100 nm; submicron PM, defined as diameter < 1 µm and often referred to as PM_1; fine PM, defined as diameter < 2.5 µm ($PM_{2.5}$); and coarse PM, defined as diameter < 10 µm (PM_{10}). PM_{10} is therefore the sum of fine and coarse PM.

The size categorisation of PM arises from its composition and its origins. Coarse PM is mostly formed through the physical abrasion of minerals or materials, such as sand or rock, whereas $PM_{2.5}$ is typically formed through chemical reactions, such as combustion. However, the size categories are also related to their effect on human health as different sizes of PM affect different parts of the respiratory system (Nurkiewicz et al., 2010). The lower respiratory tract, where gas exchange occurs, is affected by ultrafine PM and $PM_{2.5}$, whereas the upper respiratory tract is also affected by larger PM_{10}. Due to its greater penetration into the respiratory system, $PM_{2.5}$ is considered to have a greater effect on human health. This therefore creates the need to conduct measurements of PM at specific sizes.

Typically, the largest fraction of $PM_{2.5}$ by composition is the organic fraction which is composed primarily of C, H, O and N atoms. This thesis focuses on the organic fraction as it contains a complex mixture of compounds which, in effect, stores information about PM formation and its origins. $PM_{2.5}$ also includes the black carbon (BC) fraction which is composed of carbon atoms in different morphologies and is almost exclusively formed through combustion. The inorganic $PM_{2.5}$ fraction comprises the four main species of: Cl^-, NO_3^-, NH_4^+ and SO_4^{2-}. However, within the PM_{10} fraction there are also mineral salts (e.g. NaCl or K_2SO_4) and crustal metals species (e.g. Zn, Cr, Pb, Al, Ti, etc.).

PM is also defined into categories of primary emitted aerosol, where PM is emitted directly from its source, or secondary aerosol, where PM is formed through atmospheric reactions. Often the secondary inorganic aerosol (SIA) fraction is formed through reactions of acid gases, such as H_2SO_4 and HNO_3, which yields NH_4HSO_4, $(NH_4)_2SO_4$ and NH_4NO_3. On the other hand, the secondary organic aerosol (SOA) fraction is often formed through the atmospheric processing of volatile organic compounds (VOCs).

Non-methane VOCs, or what is referred to simply as VOCs throughout this thesis, are often defined as organic compounds with high vapour pressures such that they can evaporate under normal atmospheric conditions. A more refined definition is given by the US Environmental Protection Agency (EPA) who state that a VOC is an organic compound with a boiling point ≤ 250 ^oC at 101.3 kPa. However, the development of measurement technologies has meant a wider range of volatile compounds are measured. This has resulted in the need for more clarification when defining VOCs based on volatility. The World Health Organization (WHO) have therefore set out three categories of VOCs: very VOCs (VVOCs), defined as having a boiling point between 0 to 50-100 ^oC; VOCs, defined as having a boiling point between 50-100 to 240-260 ^oC; and semi VOCs (SVOCs), defined as having a boiling point between 240-260 to 380-400 ^oC (World Health Organization, 1989). This thesis focuses

on the VOC category (boiling point of 50-100 to 240-260 ^{o}C) which is the most understood and most relevant to ambient atmospheric measurements.

1.1.2. Interactions of PM and VOCs in the atmosphere

PM and VOCs within the atmosphere are interlinked. The schematic in Figure 1.1 shows their interactions and how they eventually lead to detrimental health effects. In general, VOCs and PM are emitted from point sources and undergo photochemical and OH radical reactions to form oxidation products. One result of VOC photochemistry is the formation of tropospheric ozone (O_3) which has adverse health effects on the cardiovascular system. PM is also known as one of the most harmful air pollutants due to its penetration of the respiratory system. In fact, the latest estimates from the World Health Organization suggest that PM contributes to ~7 million premature deaths each year (World Health Organization, 2021). This highlights the importance of understanding air pollutant concentrations and their origins.

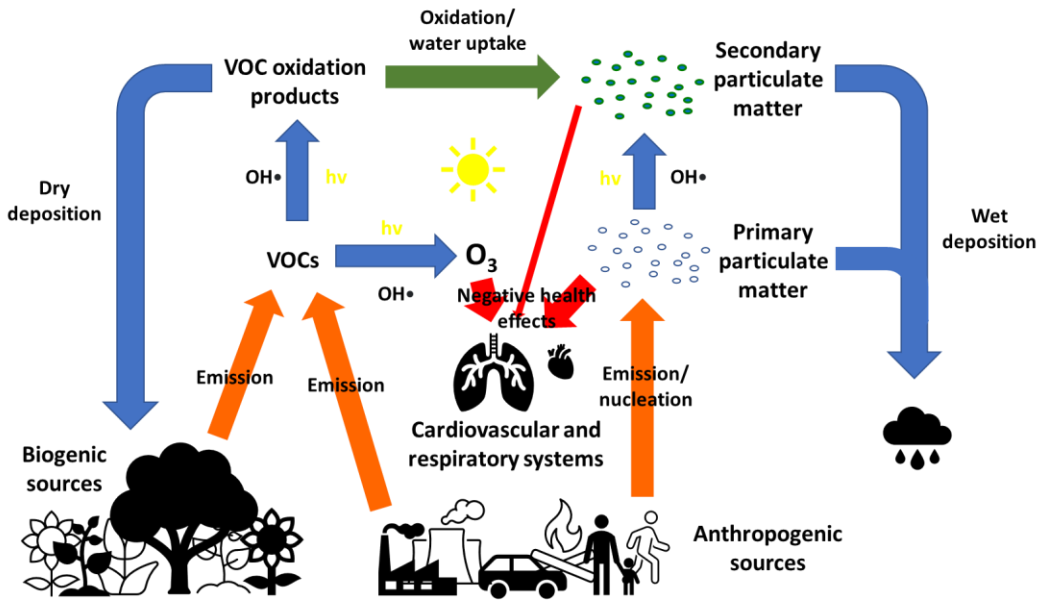

Figure 1.1. Schematic of the processes and interactions between organic particulate matter and volatile organic compounds in the atmosphere leading to negative health impacts.

The sources of PM and VOCs overlap when observing anthropogenic emissions. Both pollutants have been observed in the emissions from common sources such as traffic, biomass burning, industrial activities and cooking activities (Jimenez et al., 2009; Vlasenko et al., 2009; Wang et al., 2020). However, VOCs are also emitted in large quantities from less usual anthropogenic sources such as perfumes and personal-care products (Coggon et al., 2018; Steinemann, 2021).

Biogenic emissions are where PM and VOCs are no longer comparable. Globally, VOCs are emitted in their largest quantities through biogenic emissions which accounts for 90% of the total global VOC emission budget (Guenther et al., 1995). Although PM is emitted biogenically in the form of fungal spores and pollen, it is not one of the main sources of PM (Hyde and Mahalov, 2020). However, the photochemical oxidation products of biogenic VOCs go through a complex array of aerosol uptake reactions in the atmosphere, leading to the formation of SOA (Cash et al., 2016). Global modelling studies predict biogenic SOA to be responsible for between 74 – 95% of the total SOA production rate (Farina et al., 2010; Hodzic et al., 2016). From multiple mid-latitude PM_1 measurement campaigns across the northern hemisphere, SOA is consistently the largest form of OA measured, accounting for 64%, 83% and 95% of total OA in urban, urban downwind and rural/remote sites, respectively (Zhang et al., 2007). This shows the importance of measuring both VOCs and PM as their interactions in the atmosphere are strongly linked.

The importance of biogenic SOA changes however when observing PM in heavily polluted regions such as in Delhi, India. Here, anthropogenic emissions dominate both VOCs (Wang et al., 2020) and OA (Reyes-Villegas et al., 2021), and an aim of this thesis is to focus on the sources that are responsible.

1.1.3. Overview of sources of VOCs and OA in Delhi, India

Currently estimated at 31.2 million, the population of Delhi is increasing rapidly which is causing increases in industry, fossil fuel demands and land-use (Gulia et al., 2022; Sharma et al., 2021). The number of registered vehicles in Delhi increased from 6.35 million in 2011 to over 11 million in 2020 (Jain et al., 2020). The large numbers of vehicles in Delhi have led to recent measurement studies showing traffic emissions to be a dominant source of VOCs and PM concentrations (Cash et al., 2021; Reyes-Villegas et al., 2021; Stewart et al., 2021; Wang et al., 2020)

However, open burning of biomass, solid fuels and municipal waste is also common in Delhi. Waste management issues have led to residents clearing the streets by burning piles of municipal waste (Nagpure et al., 2015). Residents also use municipal waste, coal, wood and dried cow faeces, or 'dung cakes', for fuel to cook, or to stay warm during the colder months (Gulia et al., 2018). This produces high concentrations of OA and VOCs during the winter and post-monsoon.

Seasonal crop residue burning in the surrounding areas of Delhi causes the regional transport of OA during the summer and post-monsoon. The peak in crop residue burning is often seen during the post-monsoon (Kulkarni et al., 2020). This is timed with the festival of light, called "Diwali", which is a key contributor to pollutant concentrations as residents celebrate using pyrotechnics. All these burning-related sources together result in a peak in pollutant concentrations during the post-monsoon that has been responsible for Delhi being labelled as "the world's most polluted megacity" (Gani et al., 2019). Therefore, VOCs and OA emitted from burning emissions have become one of the biggest problems for air quality in Delhi.

1.2. Aerosol Mass Spectrometry

Two measurement methods involving aerosol mass spectrometry (AMS) are used within this thesis. One method involves the real-time measurement of PM_1 (online-AMS), while the other involves measuring the airstream of nebulised PM that has been extracted from PM filter samples (offline-AMS). An overview of each technique is described below. More specific details on operation and calibrations are described within the later chapters.

1.2.1. Online-AMS

Mass spectrometry (MS) is a technique in which the target chemical species is ionised using an ion source. The resultant ions are then separated based on their mass-to-charge ratio (*m/z*) before arriving at a detector. MS are versatile instruments that can be developed into small bench-sized units that quantitatively measure specific chemical species and give compositional information. Aerodyne Research Inc. developed the aerosol mass spectrometer (AMS) which is the most commonly used MS to measure atmospheric PM. In summary, an AMS instrument quantitatively measures size-resolved non-refractory PM_1 at a high-time resolution of seconds to minutes and costs ~ £400,000. A schematic of a high-resolution time-of-flight AMS (HR-TOF-AMS) is shown in Figure 1.2. This is the main instrument used in this thesis to measure PM and a detailed description is given below. However, it is worth noting that other types of AMS have been developed for different purposes. The first AMS had a quadrupole mass analyser (Q-AMS) which gave integer *m/z* resolution. The simplicity and reliability of this instrument has been carried over to the aerosol chemical speciation monitor (ACSM) which is now widely used in air monitoring networks. There is also a soot-particle AMS (SP-AMS) which is designed to quantify black carbon containing particles. Finally, more recent advances have led to a long-TOF-AMS which is fitted with a time-of-flight analyser capable of reaching a resolution power of ~8000 $m/\Delta m$.

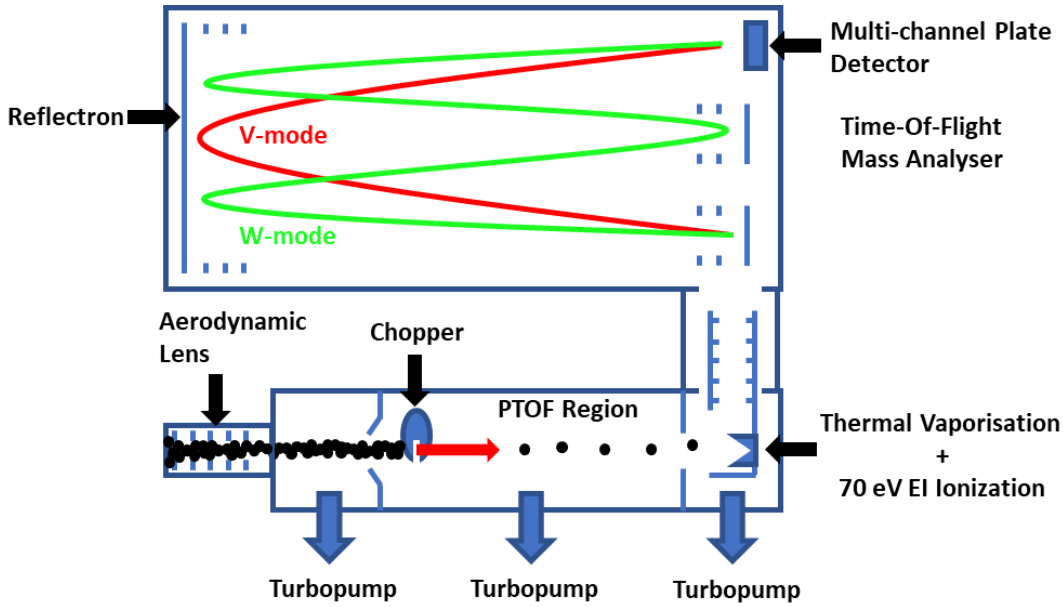

Figure 1.2. Schematic of a high-resolution time-of-flight aerosol mass spectrometer

As shown in Figure 1.2, the aerodynamic lens forms the inlet of the instrument which restricts the size of particles to only allow PM_1 to be measured. The lenses create a closely packed particle beam which is directed towards the high vacuum (10^{-13} Torr) particle-TOF (PTOF) chamber. Before entering the PTOF chamber, the particles have a size-dependent velocity which is controlled via an aperture, or critical orifice, which passively keeps the flow rate constant. The PTOF chamber gives PM sizing information using a servo-operated chopper to deliver discrete packets of particles along a flight path of known length. The mass spectrometer is then used as the detector but due to its complexity, which is described below, there is a delay of ~200 µs before detection. Counting statistics are therefore required in order to determine the time-of-flight through the PTOF chamber. This is achieved through acquiring a set number of mass spectra which are recorded for each chopper cycle. These mass spectra are then sorted as a function of extraction number from the time-

of-flight mass analyser. This creates a relationship between mass spectra and particle time-of-flight for each chopper cycle (DeCarlo et al., 2006).

The particles then impact a resistively heated vaporisation surface (600 ^{o}C) and are ionised through 70 eV electron impact (EI) ionisation. As a result, only non-refractory species are detected which, in AMS literature, means PM that is vaporised rapidly under vacuum at 600 ^{o}C. Measurements therefore do not include PM such as crustal material, black carbon and sea salt (DeCarlo et al., 2006).

The ions are then selected based on their *m/z* using, in this instance, a time-of-flight analyser. The HR-TOF-AMS has two modes: the V-mode and the W-mode (Figure 1.2). Their names describe the ion flight path in the Tofwerk AG analyser (H-TOF Platform, Thun, Switzerland) which is controlled by electric fields called reflectrons. These electric fields cause ions to be reflected via a set angle of reflection which is controlled by the diameter of the reflectron, the smallest of which is called a hardmirror. The V-mode ion trajectory follows a V from the entrance of the analyser, to a reflectron, and then to a multichannel plate (MCP) detector (flight path length = 1.3 m). Ion trajectory in W-mode follows a similar path via the reflectron; however, a hardmirror causes the ions to travel to the reflectron a second time before reaching the detector (flight path length = 2.9 m). The V-mode gives higher sensitivities (~2.9 ng/m^3 of nitrate over a 30 s averaging interval) and lower resolution (~2500 $m/\Delta m$) whereas the W-mode gives higher resolution (~5000 $m/\Delta m$) and lower sensitivities (~32 ng/m^3 of nitrate over a 30 s averaging interval) of *m/z* ions.

The resultant mass spectra are intercomparable between AMS instruments due to the separation of the flash vaporisation and 70 eV electron impact (EI) ionisation. This attenuates the possible plasma chemical transfer matrix effects and allows for the comparison with archival mass spectra such as the National Institute of Standards and Technology (NIST) library or the AMS spectral database (Canagaratna et al., 2007).

One study has assessed the differences between AMS and NIST spectra but they reported that similarities are only seen for species which are resistant to thermal decomposition (Alfarra, 2004). This is due to the additional thermal energy of flash vaporisation that is not present in standard 70 eV EI MS. This causes a greater amount of fragmentation and an ion distribution which is weighted more heavily towards lower *m*/*z* ions. An example of this is the increased signal of *m/z* 18 (H_2O^+), 28 (CO^+) and 44 (CO^{2+}) due to the thermal dehydration and decarboxylation of carboxylic acid species. This is shown in more detail in Figure 1.3 where fragmentation reactions of common PM species are presented along with an example AMS spectrum. The additional fragmentation of species means that AMS spectra are not useful to identify individual compounds unless the compound has characteristic peaks (or is resistant to thermal decomposition), such as inorganic compounds or polycyclic aromatic hydrocarbons (PAH). However, AMS spectra can be used to identify individual classes of compounds e.g. C_xH_y, $C_xH_yO_z$ or $C_xH_yO_zN_t$. This is particularly useful when observing the OA fragmentations and using multivariate analyses such as positive matrix factorisation (PMF). The latter is discussed in more detail later. Since AMS measurements have been ongoing for two decades (DeCarlo et al., 2006; Hunt and Petrucci, 2002), there are large number of past AMS studies to compare against in order to validate future measurements. This negates the inherent disadvantages of increased fragmentation when compared to other MS techniques.

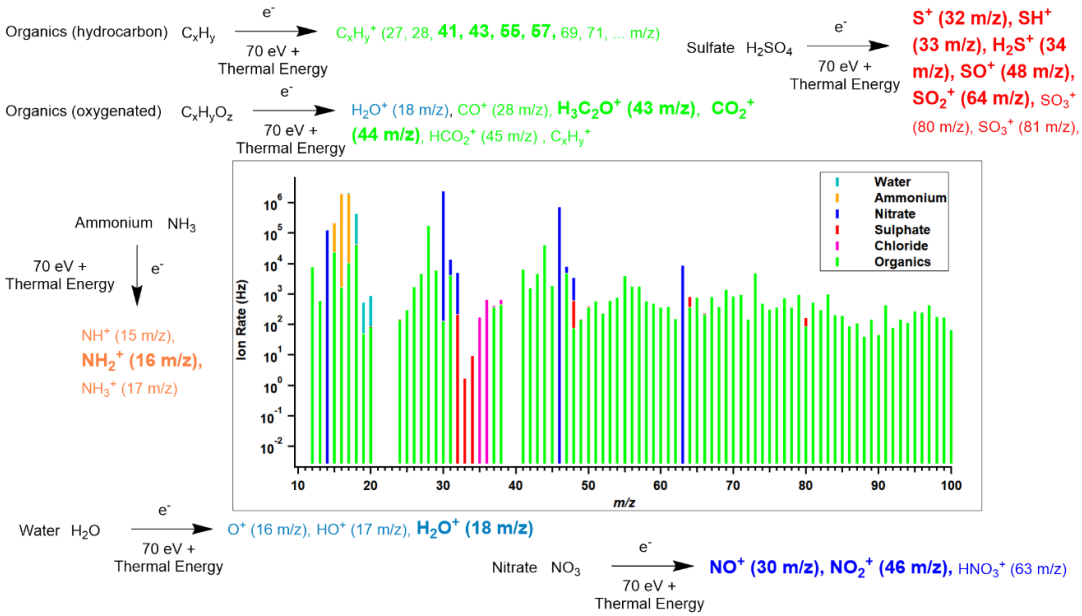

Figure 1.3. Example AMS mass spectrum of a nebulised ammonium nitrate standard. The fragmentation reactions of common species are shown, and the most abundant fragments are in bold. The species are colour coded to match the corresponding data presented in the spectrum.

1.2.2. Offline-AMS

The deployment of an AMS in the field is costly which limits its frequency of use and the number of measurement locations. The collection of PM filters however requires less specialist expertise to operate and is a fraction of the cost of installing an AMS. The offline measurement of filters using AMS therefore provides the possibility for improved spatial resolution at a lower cost. However, the main disadvantages of offline-AMS are the loss of temporal resolution and the possibility of introducing artefacts through filter handling.

The collection of PM filter samples has been ongoing for decades and research institutes often store filter archives for analysis at a later date. This creates the opportunity to measure PM from the past and the present using the same modern instrumental technique. When also combined with source apportionment techniques, the evolution of PM sources can be charted over

multiple years and the effects of air quality mitigation strategies can be evaluated.

The method of offline-AMS is summarised in schematic form in Figure 1.4. The first step involves the sampling of the PM filters. Pre-baked glass fibre filters are usually wrapped in pre-baked aluminium foil before and after sampling. The foil and filters are baked at ~800 ^{o}C for ~8 h to remove all organics.

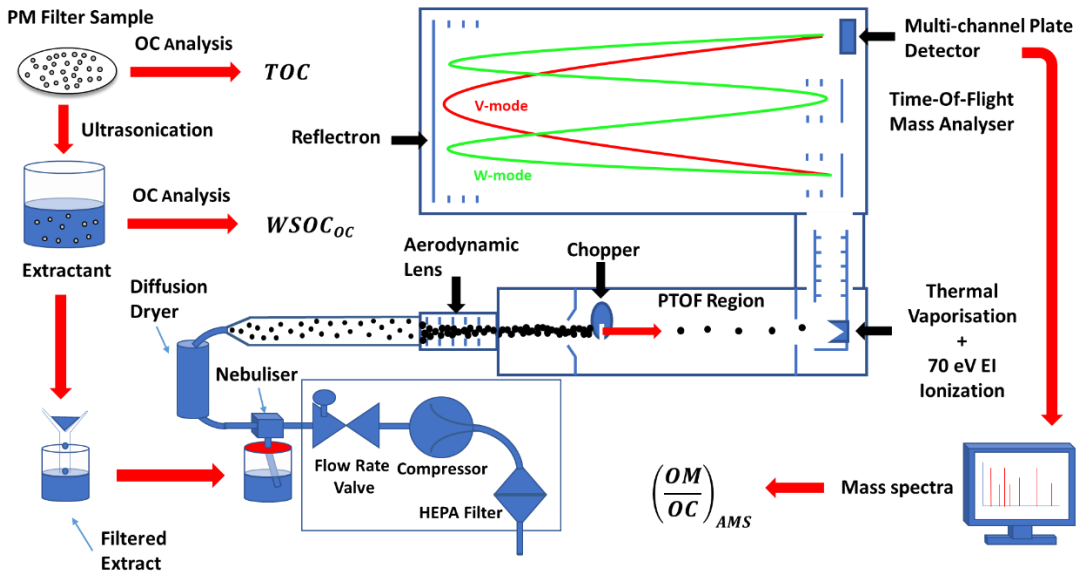

Figure 1.4. Schematic of the offline-AMS method showing the steps of filter extraction, organic carbon (OC) analysis, nebulisation, diffusion drying of the aerosol stream and HR-TOF-AMS analysis. The OC analysis is used to quantify PM concentrations, along with the AMS derived organic matter (OM) to OC ratio. The example illustrated here uses water extraction which gives measurements of water-soluble organic aerosol (WSOA).

The filter sampling parameters are often different between studies as there is a balance between high temporal resolution (i.e. filter collection times) and accumulating enough PM to be above the AMS limit of detection. Most studies use high-volume filter samplers which have a high flow rate (500 - 1100 L min^{-1}) allowing for lower sample collection times (usually ~24 h per sample). Once

sampled, the filters are stored at below freezing (~-18 ^{o}C) until needed for analysis.

Before being cut into smaller 'punches', the filters are often left to warm to room temperature in a controlled atmosphere (i.e. a sealed unit) to reduce contamination from volatile compounds condensing from the laboratory air. Once punched, the filter punches are ultrasonicated at 30 ^{o}C in a solvent. Most recent studies use ultrapure water as a solvent (Bozzetti et al., 2017a, 2017b; Daellenbach et al., 2016; Sun et al., 2011; Vlachou et al., 2019); however a small number of studies have explored using other solvents to extract a greater percentage of the total PM (Chen et al., 2016; Han et al., 2016; Mihara and Mochida, 2011).

The resultant extract is then filtered (0.45 µm pore) and aerosolised using a nebuliser. There are many types of nebulisers. The most common are pneumatic pressure nebulisers that use compressed HEPA filtered air to generate aerosol from the filter extract which is shown in Figure 1.4. The nebulised aerosol is then dried to remove as much solvent as possible from the particles. Most studies use silicon-filled diffusion dryers to remove water from the aerosol. The dried aerosol stream then enters the inlet of a HR-TOF-AMS, the principles of which are described in detail in the previous section. The resultant particle sizes generated from this procedure have been shown to be optimal for AMS measurements with a size-distribution mode of ~170 nm.

In offline-AMS, the extraction efficiency and the nebulisation efficiency need to be known in order to quantify absolute concentrations of PM. The extraction efficiency can be described as the proportion of PM dissolved into the solvent, while the nebulisation efficiency is the proportion of PM nebulised from the extract. The overall efficiency of the two has to be quantified using an external measurement. Using water extraction as an example method, this is often carried out using a dissolved organic carbon analyser to give an organic

carbon (OC) measurement (µg m^{-3}) for the filter extract, $WSOC_{OC}$. The quantification of water-soluble OA, $WSOA$, can then be calculated using the following equation:

$$WSOA = \left(\frac{WSOM}{WSOC}\right)_{AMS} . WSOC_{OC} \quad (1.1)$$

Here, $\left(\frac{WSOM}{WSOC}\right)_{AMS}$, is the organic matter (OM) to OC ratio measured by the AMS for the water extracted filter extract. The total OA on the filter can also be measured through OC analysis of the filter itself using a thermal optical transmission carbon analyser or a thermal optical reflectance carbon analyser. This gives a total OC measurement, TOC, which allows for the recovery, R, of OC to be calculated as follows:

$$R = WSOC/TOC \quad (1.2)$$

It is worth noting that for methods using other extractant solvents, such as methanol, the TOC measurement of the filter is crucial to calculate quantitative measurements of OA because OC analysis on the filter extract cannot be achieved when using organic solvents. For example, if using methanol as the extracting solvent, Equation (1.1) would be modified to give:

$$OA = \left(\frac{MSOM}{MSOC}\right)_{AMS} . TOC_{OC} \quad (1.3)$$

However, the TOC measurement includes all OC on the filter and not just methanol-soluble OC, $MSOC$. This means that when using Equation 1.3, the sum of OA will equate to atmospheric concentrations, although its composition is not a complete reflection of what exists in the atmosphere as insoluble compounds will not be included within the summed OA.

Further exploration and discussions of using organic solvents in the offline-AMS methodology developed in this thesis is provided in Chapter 4.

1.3. Proton transfer reaction mass spectrometry

The proton transfer reaction mass spectrometer (PTR-MS) is another MS instrument that has been used for more than two decades to measure atmospheric pollutants (Lindinger et al., 1998; Warneke et al., 1996). It was one of the first instruments to conduct online measurements of trace gases at ppbv levels. The first PTR-MS used quadrupole analysers capable of unit mass resolution with response times of 0.2 – 1 s. Now, PTR-MS technology has moved on to sensitivities < 1 pptv levels with response times of < 100 ms and resolutions of > 10000 $m/\Delta m$ (Fischer et al., 2021). These characteristics make a PTR-MS an ideal instrument for measuring micrometeorological fluxes of VOCs which requires fast response times in order to capture turbulent eddies.

As mentioned previously, MS depends on the ionisation of chemical compounds for their detection. There is a range of “soft” to “hard” forms of ionisation that produce weak to strong fragmentations of the analyte. Traditional MS, like the AMS, use electron impact (EI) and energy transfer is often set to 70 eV. This causes strong fragmentation patterns, making it hard to determine molecular structures. In contrast, PTR-MS uses hydronium ions (H_3O^+) as its ionisation source which is a particularly soft ionisation. The energy transfer can be adjusted using instrument parameters, but is generally of the order of ~ 10^{-1} eV (Lindinger et al., 1998; Warneke et al., 1996). The mass spectrum is therefore much simpler to interpret, and individual chemical compound can be identified.

The PTR-MS is comprised of four regions: the ion source (~5 cm in length), the drift tube (reaction chamber, ~30 cm in length), the ion transfer (~20 cm in length) and the TOF-MS region (chamber dimensions = 66.5 x 25.0 x 10.2 cm). These are shown in the schematic of an Ionicon PTR-TOF-MS (Ionicon Analytik G.m.b.H., Innsbruck, Austria) in Figure 1.5. The ion source is a high-voltage hollow cathode which is fed ultrapure water vapour to generate primary ions (H_3O^+). Both the water vapour flow rate and the electric discharge used

to form the primary ions, are controlled by the user. The aim is to increase sensitivity by producing the highest amount of primary ion counts possible, without saturating the signal. Increasing primary ions also generates NO^+ and O_2^+ which are species that cause charge transfer to some VOCs making fragmentation harder to interpret. The optimisation of primary ion counts is therefore a key consideration when operating a PTR-MS.

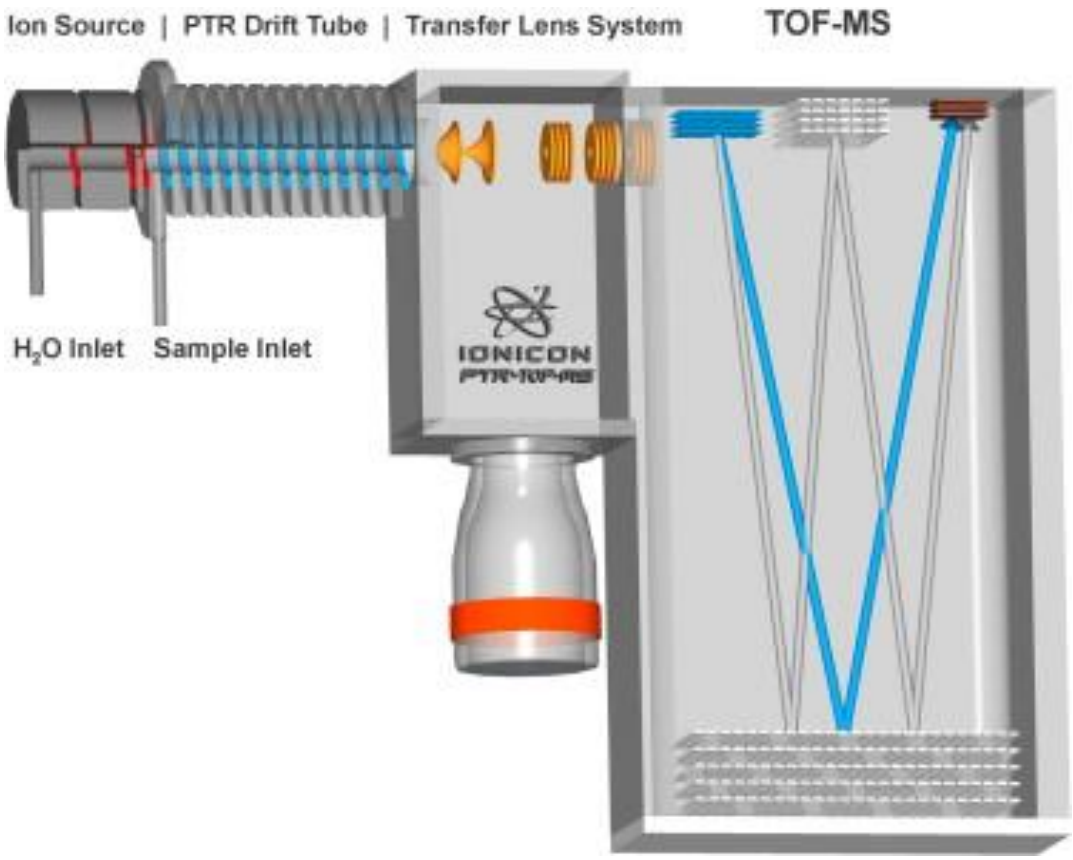

Figure 1.5. Schematic of a PTR-TOF-MS showing the ion source, drift tube, ion transfer and TOF-MS regions (Jordan et al., 2009).

The primary ions are then accelerated via a small aperture towards the low-pressure drift tube (~2 mbar) where they combine with sample air. Chemical species with proton affinities (PA) > 7.22 eV are protonated within the drift tube.

The range of species ionised is highly beneficial for atmospheric VOC measurements because the main components of air have lower PAs than water, as shown by the PA values in Table 1.1

.

Table 1.1. List of common atmospheric species and their proton affinities (Jolly, 1991; Lias et al., 1984; Wright, 2016).

Compound	PA (eV)
Argon	3.8
Oxygen	4.4
Nitrogen	5.1
Carbon Dioxide	5.7
Methane	5.7
Nitrous Oxide	5.9
Carbon Monoxide	6.2
Butane	7.1
Water	7.2
Hydrogen Sulphide	7.4
Hydrogen Cyanide	7.4
Formic Acid	7.8
Methanol	7.8
Acetonitrile	7.8
Benzene	7.9
Ethanol	8.2
Propanol	8.3
Water Cluster	8.4
Acetone	8.5
Ammonia	8.9

The drift tube is comprised of a series of stainless-steel rings separated by Teflon. A user-controlled voltage is applied across each ring to create an electric field, E (V cm^{-1}). The electric field is often normalised by the density of the sample gas, N (molecules cm^{-3}), and multiplied by 1 x 10^{-17} to give the commonly used instrument parameter E/N in Td. The value of E/N controls both the level of fragmentation and the dissociation of water cluster ions ($H_3O^+(H_2O)_n$). Water clusters make mass spectral interpretation harder as they

cause VOCs entering the drift tube to also cluster. A higher E/N leads to increased fragmentation and decreased water clusters, whereas the opposite applies for lower E/N. Therefore, there is a balance between the two and users often set the E/N to 120 - 140 Td.

The resultant protonated VOC ions are then accelerated through the lens transfer region. It is worth noting that the instrument used in this thesis is a slightly different model to what is shown in Figure 1.5, and uses a quadrupole to transfer ions between the drift tube and the TOF-MS (PTR-QiTOF-MS). The TOF-MS is the same Tofwerk AG analyser (H-TOF Platform, Thun, Switzerland) used in the HR-TOF-AMS and has been described in detail previously.

The proton transfer reaction between primary ions and a VOC analyte, R, can be described as follows:

$$R + H_3O^+ \rightleftharpoons RH^+ + H_2O. \quad (1.4)$$

For species of R that have a higher PA than water (7.22 eV), steady-state conditions are achieved, and the equilibrium strongly shifts to the right-hand side of the equation. The rate constant for this reaction, k_{19}, is therefore equivalent to the collision rate (~ 10^{-9} cm^3 $molecules^{-1}$ s^{-1}) and the change in concentrations of RH^+ are a linear reflection of the primary ion concentrations, $[H_3O^+]$. Therefore, the collision counts of R can be normalised by the primary ions to reflect the VOC analyte abundance:

$$[RH^+]_{norm} \approx \frac{1}{k_{19}t}\frac{R}{[H_3O^+]} \quad (1.5)$$

where, $[RH^+]_{norm}$, is the signal of R in normalised counts per second (ncps) and, t, is the dwell time in seconds. The volume mixing ratio of R, VMR_{RH^+}, can then be calculated using two different methods.

1.3.1. Sensitivity method

The sensitivity method essentially involves injecting VOC standards of known concentration, VMR_c (ppb), into the instrument and measuring the normalised signal of the calibrant, $[C]_{norm}$ (ncps). This gives a calibration factor called the normalized sensitivity, S_{norm} (ncps ppb^{-1}):

$$S_{norm} = \frac{[C]_{norm}}{VMR_c}. \quad (1.6)$$

This is then used to obtain VMR_{RH^+} in ppb by simply dividing its normalised signal (ncps), $[RH^+]_{norm}$, by S_{norm}:

$$VMR_{RH^+} = \frac{[RH^+]_{norm}}{S_{norm}}. \quad (1.7)$$

1.3.2. Kinetic method

The kinetic method relies on stable drift-tube conditions, known VOC k_{19} values and VOC fragmentation patterns. Again, this method uses a calibration standard containing a wide range of VOCs of known concentration. Briefly, the transmission efficiency, Tr_{RH^+}, of each calibration species is first determined through the relationship of its known VMR_{RH^+} and a number of instrument parameters, as described by the following equation:

$$VMR_{RH^+} = \frac{10^9 \cdot 22400 \cdot p_0^2 \cdot T_d^2 \cdot U_d \cdot \mu_o \cdot RH^+ \cdot Tr_{H_3O^+}}{p_d^2 \cdot T_0^2 \cdot k_{19} \cdot v_d \cdot N_A \cdot [H_3O^+] \cdot Tr_{RH^+}} \quad (1.8)$$

Here, p_d is the drift tube pressure, U_d is the drift tube voltage, T_d is the drift tube temperature, v_d is the drift tube length (~9.5 cm) and $Tr_{H_3O^+}$ is the transmission efficiency of primary ions. The ion mobility, μ_0, (~2.7 cm^2 V^{-1} s^{-1}) is calculated using equations described in de Gouw and Warneke (2007). Avogadro's constant, N_A, is also included, along with the pressure (p_0) and temperature (T_0) at standard conditions.

Using the Tr_{RH^+} values for each calibrant, a curve can be fitted through the data, such as in Figure 1.6. The fit can then be extrapolated to other masses to find Tr_{RH^+} for other VOCs not in the calibration standard. The resultant Tr_{RH^+} values can then be used in Equation 1.8 to find the VMR_{RH^+} for each *m/z* signal measured.

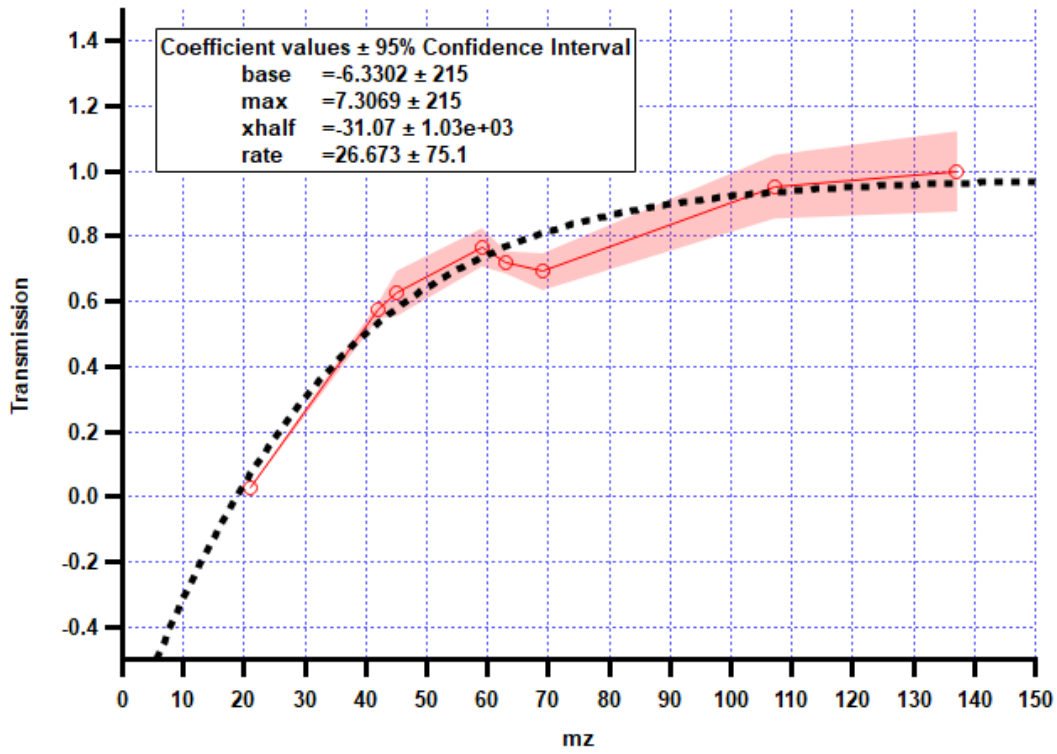

Figure 1.6. Example transmission efficiency curve fitted with a sigmoidal fit.

The kinetic method is used in this thesis because a broad spectrum of VOC compounds is used for source apportionment analysis. The sensitivity method is also limited by the number of VOC species in the calibration standard. It is worth noting that incorporating both the kinetic and sensitivity methods would impose artefacts on the source apportionment results. Therefore, the

concentrations were determined for all measured ions using the kinetic method.

1.4. Flux measurements

1.4.1. VOC emissions estimates

Modelling techniques have become increasingly popular in the atmospheric sciences. They are powerful tools which can help to understand the current state of the atmosphere. They also help to predict how the air quality changes due to increased anthropogenic activities, land-change, future climate change scenarios and changes caused by implementing air quality mitigation strategies. However, for models to produce accurate predictions, they rely on accurate input variables.

There are two types of approach to modelling: the top-down and the bottom-up approach. The top-down approach is based on generating national or global estimates from the disaggregation of variables measured or modelled at a regional or national level. The bottom-up approach is based on small scale estimates or point source observations, which are scaled-up to give regional, national or global estimates. Both approaches require emissions estimates (e.g. the amount of pollutant emitted due to traffic emissions) and activity factors (e.g. the total amount of cars in the city of interest).

Emissions inventories are often collected on a national scale for different source categories of the pollutant of interest (e.g. traffic emissions). These inventories can be determined from emission observations, but the majority are based on model estimates. Studies often point out that the largest source of uncertainty in an atmospheric model is the input emissions inventory (Guevara et al., 2017). Therefore, there is a need for accurate measurements of air pollutant emissions.

There is also a top-down and bottom-up approach to measuring VOC emissions. The bottom-up approach involves taking multiple point-location flux measurements across an area. The measurements are usually taken using chambers which can vary in size to cover a leaf, branch or plant. These measurements are then scaled-up to represent larger areas. This is a low-cost technique using robust equipment and samples can be collected for offline analysis using slow response and high-resolution instruments. This approach may be appealing for biogenic emissions, but it is not ideal for urban environments, such as Delhi, as anthropogenic VOC sources are not always static. Therefore, a different approach is required for measuring emissions in Delhi.

1.4.2. Micrometeorological VOC flux measurements

The top-down approach to measuring VOC emissions is through using fast-response sensors to measure micrometeorological fluxes taken at a height well-above the surface. This relies on the measurement of turbulent eddies which are generated by wind shear. Their size is based on their frequency, which ranges from 0.1 s to 1 h. For this reason, an instrument measurement response of ≥ 10 Hz is required if measuring fluxes directly.

An illustration of the turbulent transport of VOC compounds, χ, is shown in Figure 1.7. The random motion of turbulent eddies carry heat, mass and, ultimately, VOC compounds. When surface topography is uniform, the mean vertical wind velocity, w, equals zero. Therefore, the volume of air transported upwards equals that being displaced downwards. These conditions are achieved within the inertial sub layer, otherwise known as, the constant flux layer. In Figure 1.7, the emissions of χ from a point source on the surface will cause a concentration gradient to form. Only then can net transportation of χ occur through the instantaneous fluctuation of w about the mean. This can be described in simpler terms as follows: air from the upper layers with low concentrations of χ will travel randomly until it interacts with the air below that has high concentrations of χ. The concentration gradient moves χ into the

lower concentrated air. This air then moves via the random motions of turbulent eddies towards the upper layers and brings a higher concentration of χ with it. This causes a net movement of χ from the surface which would be observed as an emission. Conversely, the opposite occurs for deposition.

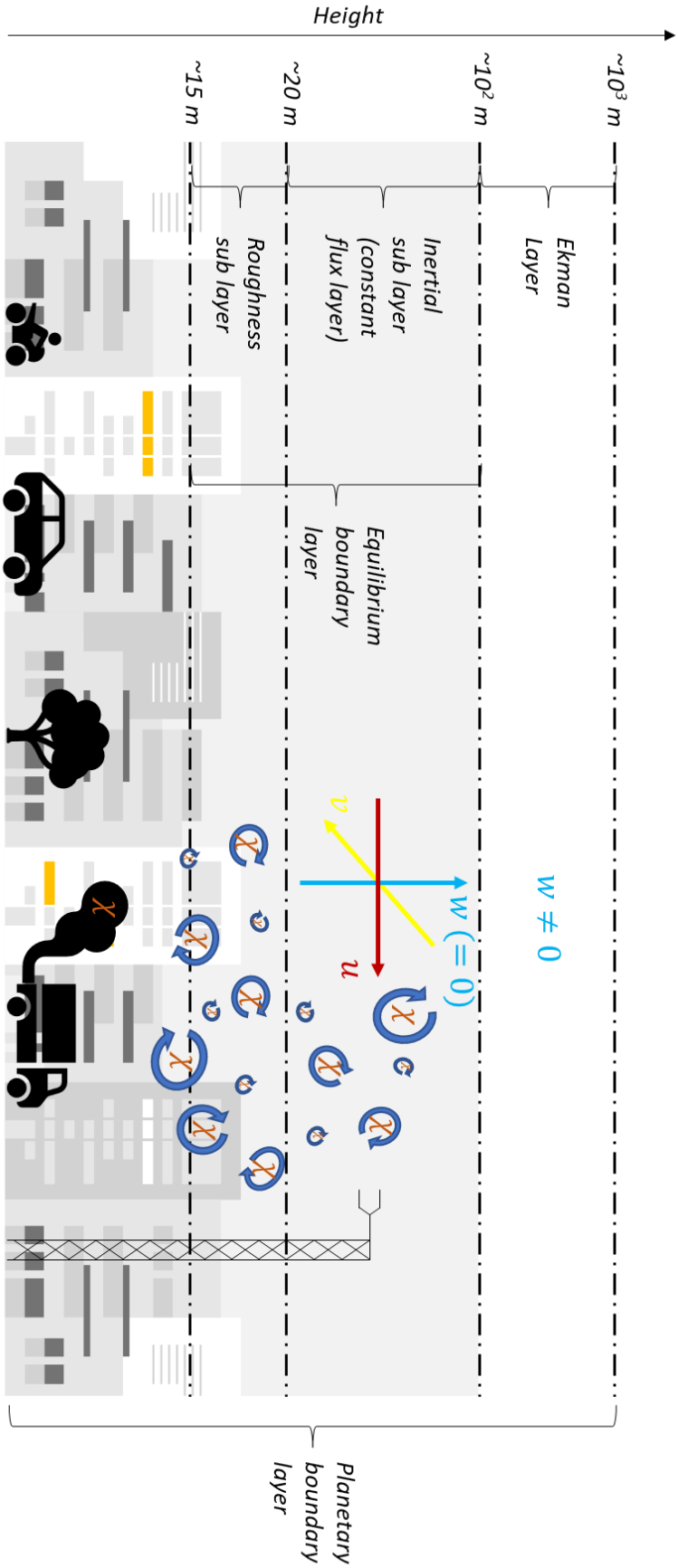

Figure 1.7. Illustration of the turbulent transport of VOC compounds, χ, within the planetary boundary layer.

Turbulent transport is one of the most occurrent form of transport within the planetary boundary layer (PBL) and occurs along the vertical plane. However, advection can also cause lateral or horizontal transport of VOC compounds. This occurs due to an obstruction in the topography preceding the measurement or it is driven by a pressure gradient. It is therefore vital for the upwind area, or what is known as the “fetch”, to be topographically uniform. The basis for choosing a measurement site that gives “ideal” flux measurement conditions is first to note the prevailing wind directions. The fetch along the prevailing wind is then checked for a level or uniform surface/canopy above which a measurement tower can be located. This effectively causes advection to be equal to zero. For urban environments, the topography is complex and often irregular due to buildings, roads and parks. Fluxes can however still be reliable if the measurement height is 3 times higher than the average building (Nemitz et al., 2002).

The measurement height is also related to the area measured. As a general rule, the higher the measurement height the greater the fetch. However, if it exceeds the equilibrium boundary layer (EBL) and lies within the Ekman layer, then advection may no longer be negligible (Figure 1.7). The maximum measurement height is consequently the height of the EBL which is characterised by the roughness height and the heat flux.

There is also one other complication to flux measurements other than advection: the sources and sinks of VOC compounds due to atmospheric chemical reactions. This could cause overestimation due to the formation of additional VOC compounds, or an underestimation due to their removal. Therefore, the assumption that VOCs are inert during turbulent transport could be a large source of uncertainty as some VOCs are highly reactive.

There are multiple methods to derive fluxes from measurements. The following two approaches are used within this thesis: the True Eddy Accumulation (TEA) approximation method, and Eddy Covariance. The TEA approach is used in

conjunction with source apportionment analysis to produce fluxes for source apportioned factors and is described in detail in Chapter 3. The Eddy Covariance method is described in the following section.

1.4.3. Eddy Covariance

The most direct approach to measuring vertical turbulent fluxes is Eddy Covariance (EC). This requires a fast-response instrument (≥ 10 Hz) and a measurement site with a topographically homogenous upwind fetch. The vertical flux, F, can be described in simple terms as follows:

$$F = \overline{\rho w \chi} \tag{1.9}$$

where $\bar{\rho}$ is the mean air density, $\bar{w}$ is the mean vertical wind velocity and $\bar{\chi}$ is the mean VOC concentration. Using Reynolds decomposition, the random motion of turbulence causes instantaneous fluctuations of all variables about their slow-moving mean (e.g. half-hourly averages). This can be written, for example, for vertical wind velocity as $w = \bar{w} + w'$. Once this is inserted into Equation 1.9 for each variable, it gives:

$$F = \overline{(\bar{\rho} + \rho')(\bar{w} + w')(\bar{\chi} + \chi')}. \tag{1.10}$$

The parentheses can then be opened to give:

$$F = \overline{(\bar{\rho}\bar{w}\bar{\chi} + \bar{\rho}\bar{w}\chi' + \bar{\rho}w'\bar{\chi} + \bar{\rho}w'\chi' + \rho'\bar{w}\bar{\chi} + \rho'\bar{w}\chi' + \rho'w'\bar{\chi} + \rho'w'\chi')} \tag{1.11}$$

and the terms $\bar{\rho}\bar{w}\chi'$, $\bar{\rho}w'\bar{\chi}$ and $\rho'\bar{w}\bar{\chi}$, represent the averaged deviations from the average, which equals zero. These are then removed to give:

$$F = \overline{(\bar{\rho}\bar{w}\bar{\chi} + \bar{\rho}w'\chi' + \rho'\bar{w}\chi' + \rho'w'\bar{\chi} + \rho'w'\chi')}. \tag{1.12}$$

This can be simplified further using the assumption that there are no fluctuations in air density. These fluctuations can occur if there are strong

winds over hills or mountains preceding or within the fetch, but for most measurement sites variation in air density is negligible. These terms can therefore be removed to give:

$$F = \overline{(\bar{\rho}\bar{w}\bar{\chi} + \bar{\rho}w'\chi')} \quad (1.13)$$

where, the final simplification assumes that effects due to advection/convection are negligible and the vertical wind velocity is equal to zero ($\bar{w} = 0$), which gives:

$$F = \bar{\rho}\overline{w'\chi'}. \quad (1.14)$$

This describes the flux being equal to the product of the mean air density and the mean covariance between instantaneous deviations in the vertical wind velocity and the VOC concentration. The flux can therefore be measured directly by measuring the VOC concentrations along with the vertical wind velocity.

1.5. Positive Matrix Factorisation

Positive matrix factorisation (PMF) is a bilinear unmixing receptor model that is a non-negative form of the more commonly-used principal component analysis (PCA) (Paatero and Tapper, 1994). The input of, in this case, mass spectral *m/z* intensities and corresponding ion concentration time series are put through a series of linear combination transformations to give an output of mass spectral profiles, named “factors”, and their time-dependent contributions. The model assumes the input dataset can conform to give factor profiles that are constant, meaning the ratios of *m/z* ion intensities stay the same, but their summed intensity changes with time (i.e. their factor time series).

The main difference between PCA and PMF is that PCA imposes orthogonality on factors (i.e. the scalar of two factor profiles would be zero). PMF therefore requires non-negative mass spectral and time series entries, hence its name. The model can also be described by the following equation:

$$x_{ij} = \sum_p (g_{ip} \times f_{pj}) + e_{ij} \quad (1.15)$$

where, i and j are the indices of the rows and columns of the matrix. The user-defined number of factors in the solution is p. The terms x_{ij}, g_{ip}, f_{pj}, and e_{ij} are, respectively, the matrix elements of the *m* x *n* measurement matrix (**X**), the *m* x *p* factor time series matrix (**G**), the *p* x *n* factor profiles matrix (**F**), and the *m* x *n* residual matrix (**E**).

The *m* rows of **X** in this thesis are either 5-min average AMS or 30-min average PTR-MS mass spectra. The *n* columns are the corresponding times series of each *m*/*z* ion. The rows of **F** are normalised to 1 and the mass concentration units are assigned to **G** (time series matrix). The user determines *p* with guidance from a fitting parameter, Q, which can be described by the equation:

$$Q = \sum_{i=1}^{m} \sum_{j=1}^{n} \left(\frac{e_{ij}}{\sigma_{ij}}\right)^2 . \quad (1.16)$$

This least-squares fit algorithm minimises Q through iteratively fitting values of **G** and **F** to the data. The standard operational controls of the PMF solver is called “robust mode”, and reweights outliers which cause $\left|\frac{e_{ij}}{\sigma_{ij}}\right| > 4$. The Q value is then recalculated using the reweighted outliers. In a second version of the PMF algorithm, PMF2 (Paatero, 1997), different pseudorandom starting values called “seeds” can be selected to find different solutions within the algorithm. This allows for the exploration of possible local minima in the Q output which may pull the algorithm towards an inaccurate solution.

The total Q value depends on the size of the data matrix and the number of factors which is not useful when defining the number of factors. It is therefore appropriate to normalise the Q value using an expected value Q_{exp} which incorporates the degrees of freedom of the model solution. The Q_{exp} value can be described as:

$$Q_{exp} \cong n\ x\ m\ -\ p(m+n) \tag{1.17}$$

and is used to evaluate the number of factor solutions as part of the expression Q/Q_{exp} (Canonaco et al., 2013). In a perfect scenario where all uncertainty is defined, the Q/Q_{exp} value would equal 1. However, the Q/Q_{exp} is skewed by artefacts such as an incorrectly chosen *p*, short-term localised factors which cannot be resolved by the algorithm, and unknown uncertainty in the measurement and the model uncertainty. The relative change in Q/Q_{exp} is therefore used instead of its absolute value. An example of this is when an increase in *p* causes a large step change in Q/Q_{exp} which indicates a significant improvement in the model's ability to explain the data. Further small relative changes in Q/Q_{exp} with a greater number of *p* would not suggest an improvement in the solution.

Despite non-negativity constraints within the model, there could be rotational ambiguity within the PMF solution, i.e. there may be linear transformations (rotations) of the dataset that result in solutions that have an identical fit to the data. This can be explored using a parameter called "Fpeak" which controls the approximate or "distorted" rotations.

Two types of rotation are allowed in the PMF model: pure and approximate. Pure rotations are what the algorithm uses to generate a solution and the Q value does not change after each rotation. A pure rotation can be described as follows:

$$\tilde{G} =\ GT\ and\ \tilde{F} = FT^{-1} \tag{1.18}$$

where, T, is a non-singular $p \times p$ matrix and, T^{-1}, is its inverse. The rotated matrices of G and F are $\tilde{G}$ and $\tilde{F}$, respectively. The product of either $\tilde{G}$ and $\tilde{F}$ or G and F are the same so therefore this does not change Q. The control of Fpeaks allows the user to explore the approximate rotations where T no longer complies with Equation 1.18. The most interesting approximate rotations are those that produce similar Q values and users are encouraged to explore the resultant solutions in more detail.

The controlled exploration of approximate rotations using Fpeaks involves either positive or negative "Fpeak" rotations. Positive Fpeaks result in one, or a series of, elementary rotations that increase the columns of **G** and decrease the rows of **F**. Conversely, negative Fpeaks decrease the columns of **G** and increase the rows of **F**. PMF users often do not reach the limits of the possible approximate rotations, but the signs of which are often the observation of large and sudden increases in Q/Q_{exp}. It is recommended by some studies to increase Q/Q_{exp} by 10% from its minimum at Fpeak = 0 (Ulbrich et al., 2009). However, varying Fpeaks does not cover all possible approximate rotations as it explores only one dimension out of multiple. This is where the multilinear-engine (ME-2) is advantageous over the PMF solver as it gives more control over Fpeak rotations.

1.5.1. Multilinear-engine 2

ME-2 was built around the PMF2 solver, a pre-existing solver that incorporated the Fpeak and seeds tools (Paatero, 2004). The aforementioned advantage of ME-2 is the increased control over Fpeak rotations. In ME-2, the user can add or subtract factors so that only parts of the data matrix are transformed and rotated.

Another key addition to ME-2 is the ability to supply *a priori* information into the model to constrain the solution. One such tool, named the "a-value approach", involves supplying the solver with factor mass profiles (**F** matrices) and/or factor or species time series (**G** matrices). The solution is then constrained to

the supplied profile or time series based on the variation parameter, a, as follows:

$$f_{j,solution} = f_j \pm a.f_j \text{ and } g_{j,solution} = g_j \pm a.g_j. \quad (1.19)$$

Here, f and g represent a row and a column of the matrices **F** and **G**, respectively. The a-value can therefore vary from 0 to 1; a-value = 0 results in an unconstrained solution, i.e. full variation from the supplied data allowed; and a-value = 1 results in 0% variation from the supplied data.

This therefore allows for further control of the PMF solution. However, the a-value approach can introduce bias towards certain solutions based on the user's input data. This is particularly the case when using measured data in new environments where the composition of air pollutants is unique. Therefore, if the solution were to be constrained, the ability of the solver to find new factors is reduced.

1.5.2. PMF factors present in literature

The source apportionment of organic air pollutants using PMF has been ongoing since 2004 (Lanz et al., 2007). This means there is a large archive of past studies to inform the identification of PMF factors. Identifying a source that is related to a factor often involves comparisons of PMF factors with external tracers and auxiliary measurements. For example, Zhang et al. (2005) found combustion tracers (elemental carbon, NO_x, CO) strongly correlated with a factor in their study. This traffic-related factor had high amounts of hydrocarbons (C_xH_y), hence its name "hydrocarbon-like" OA (HOA). It also had a distinctive mass profile with high *m/z* 55 and 57 peaks. This factor is now commonly separated in PMF analyses of AMS measurements.

Another method of identifying factors is through using laboratory-based measurements. For example, AMS measurements of wood-burning experiments showed high *m/z* 60 and 73 peaks in the OA mass spectrum

(Schneider et al., 2006; Weimer et al., 2008). It was theorised that these peaks were due to fragmentation of levoglucosan, a molecule commonly emitted from the combustion of cellulose-containing materials. These peaks are now commonly seen in AMS-measured biomass burning organic aerosol (BBOA) factor profiles.

There are a whole host of different PMF factors reported in both AMS and PTR-MS studies. An overview of some of the most commonly reported factors are shown in Figure 1.8. AMS PMF factors are often split into the two broad categories of SOA and POA. The SOA factors separate based on their volatility, giving factors such as semi-volatility oxygenated OA (SVOOA) and low-volatility oxygenated OA (LVOOA). The POA factors are found to be directly associated with specific primary emissions sources and have understandable names, such as cooking organic aerosol (COA). Figure 1.8 also shows some examples of less common PMF factors. The solid fuel OA factor (SFOA) is linked to a mixture of wood, charcoal and coal burning (Allan et al., 2010), meaning it could be considered a mixture of BBOA and coal-combustion OA (CCOA). The semi-volatility biomass burning OA (SVBBOA) and nitrogen-rich HOA (NHOA) factors in Figure 1.8a are unique to measurements made in Delhi (Cash et al., 2021). These two factors are described in detail in Chapter 2, but the diagram in Figure 1.8a is a visual representation of their origins. It is found that SVBBOA is secondary in its nature but contains tracers for biomass burning, hence, it is linked to both SVOOA and BBOA.

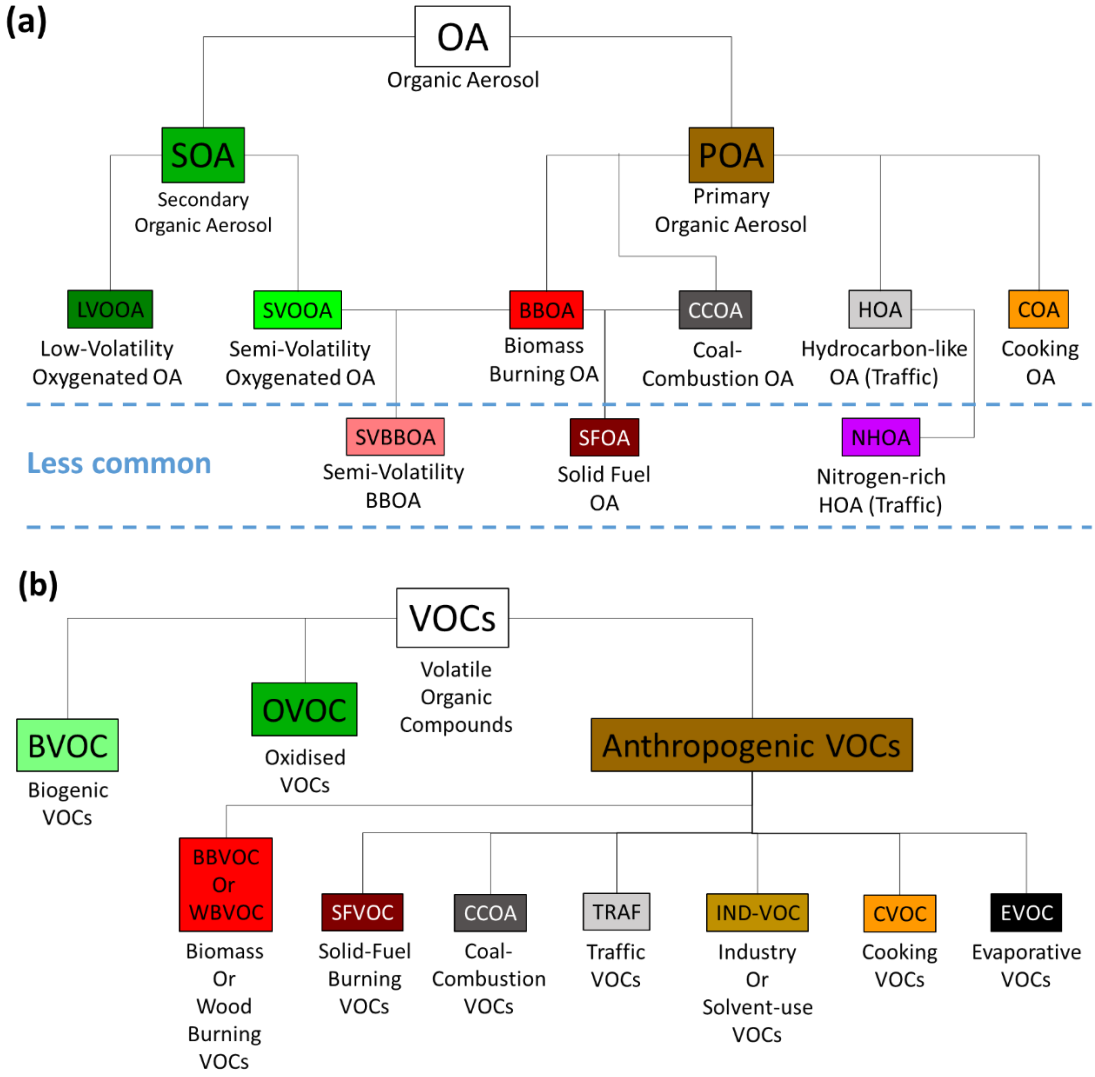

Figure 1.8. Summary of most commonly apportioned PMF factors for (a) organic aerosol and (b) volatile organic compounds. The blue dashed lines in (a) shows examples of less commonly apportioned PMF factors.

PTR-MS PMF factors split into similar categories where, much the same as the POA category, the anthropogenic VOC factors relate to specific VOC emission sources Figure 1.8(b). Often, the temporal emissions profile of two different VOC sources is highly correlated, which can mean PMF will not separate the measurements into two factors. This can be due to similar factors controlling their emissions, such as their response to temperature and light. It can also be due to the similarities of sources in time and space. For example,

what is named here as “IND-VOC”, can often relate to multiple industrial activities, such as solvent-use (Chen et al., 2014) or drug manufacturing (Jensen et al., 2021), due to their similarities in location and temporal emissions profiles. Therefore, PTR-MS PMF factors can often be related to a mixture of sources.

Oxidised VOC (OVOC) factors often separate based on their formation via atmospheric processing. For example, an OVOC factor in Wang et al., (2020) showed a strong link to photochemistry and, therefore, separated based on the temporal availability of light. Often, PTR-MS PMF analysis will also produce a factor related to biogenic VOCs (BVOCs). Their factor profiles usually have characteristic tracer peaks for biogenically emitted compounds such as, monoterpenes at *m/z* 137.

1.6. Aims and structure of this thesis

There are three main chapters in this thesis, and each presents a different measurement dataset taken in Delhi, India. Source apportionment using positive matrix factorisation (PMF) analysis has been performed to separate the organic PM and VOC measurements into PMF factors. The aims and contents of each chapter are as follows:

The aim of the work presented in Chapter 2 is the analysis of a high-resolution chemical dataset of PM_1 composition measured in Old Delhi. Using several auxiliary measurements, the aim is to produce well-defined source apportioned PMF factors against which future studies can compare. In-depth analysis of the polyaromatic hydrocarbon (PAH) component of each PMF factor is carried out to further the knowledge of their origins. Additional emphasis is also placed on the origin of the high PM_1 chloride concentrations observed in Delhi.

The aim of the work presented in Chapter 3 is to develop and apply a novel approach incorporating true eddy accumulation calculations which, for the first-time, make it possible to quantify bi-directional fluxes of VOC PMF factors. The spatial distribution of these PMF factor fluxes above Old Delhi is investigated. This, along with in-depth composition analyses, help to understand the sources associated with each PMF factor. Estimates are also made for each PMF factor of their quantitative impact on the atmospheric oxidising efficiency (OH reactivity) and of their potential to form ozone.

The aim of the work presented in Chapter 4 is to develop a novel offline-AMS methodology that enables the high-throughput analysis of PM filter samples. The changes in PM composition over multiple years can therefore be charted with a high temporal resolution. An emphasis is placed on developing the protocol to extract high amounts of primary organic aerosol (POA) from filter samples as Delhi is dominated by POA sources. The temporal resolution is aimed to be sufficient to incorporate seasonal changes in PM sources as some sources are known to emit on a seasonal basis. The seasonal analysis is then charted with the annual changes in PM, and the efficacy of past air quality mitigation strategies evaluated.

The final Chapter (5) focuses on the synthesis and comparisons of the outcomes generated from each chapter. Potential overlaps between datasets are assessed and a comprehensive picture is developed of the atmospheric composition and sources of VOCs and PM in Delhi.

References

Alfarra, M.: Insights into atmospheric organic aerosols using an aerosol mass spectrometer, PhD thesis, University of Manchester, UK., 2004.

Allan, J. D., Williams, P. I., Morgan, W. T., Martin, C. L., Flynn, M. J., Lee, J., Nemitz, E., Phillips, G. J., Gallagher, M. W. and Coe, H.: Contributions from transport, solid fuel burning and cooking to primary organic aerosols in two UK

cities, Atmos. Chem. Phys., 10(2), 647–668, doi:10.5194/acp-10-647-2010, 2010.

Bozzetti, C., Sosedova, Y., Xiao, M., Daellenbach, K. R., Ulevicius, V., Dudoitis, V., Mordas, G., Byčenkiene, S., Plauškaite, K., Vlachou, A., Golly, B., Chazeau, B., Besombes, J. L., Baltensperger, U., Jaffrezo, J. L., Slowik, J. G., El Haddad, I. and Prévôt, A. S. H.: Argon offline-AMS source apportionment of organic aerosol over yearly cycles for an urban, rural, and marine site in northern Europe, Atmos. Chem. Phys., 17(1), 117–141, doi:10.5194/acp-17-117-2017, 2017a.

Bozzetti, C., El Haddad, I., Salameh, D., Daellenbach, K. R., Fermo, P., Gonzalez, R., Minguillón, M. C., Iinuma, Y., Poulain, L., Elser, M., Müller, E., Slowik, J. G., Jaffrezo, J.-L., Baltensperger, U., Marchand, N. and Prévôt, A. S. H.: Organic aerosol source apportionment by offline-AMS over a full year in Marseille, Atmos. Chem. Phys., 17(13), 8247–8268, doi:10.5194/acp-17-8247-2017, 2017b.

Canagaratna, M. R., Jayne, J. T., Jimenez, J. L., Allan, J. D., Alfarra, M. R., Zhang, Q., Onasch, T. B., Drewnick, F., Coe, H., Middlebrook, A., Delia, A., Williams, L. R., Trimborn, A. M., Northway, M. J., DeCarlo, P. F., Kolb, C. E., Davidovits, P. and Worsnop, D. R.: Chemical and microphysical characterization of ambient aerosols with the aerodyne aerosol mass spectrometer, Mass Spectrom. Rev., 26(2), 185–222, doi:10.1002/mas.20115, 2007.

Canonaco, F., Crippa, M., Slowik, J. G., Baltensperger, U. and Prévôt, A. S. H.: SoFi, an IGOR-based interface for the efficient use of the generalized multilinear engine (ME-2) for the source apportionment: ME-2 application to aerosol mass spectrometer data, Atmos. Meas. Tech., 6(12), 3649–3661, doi:10.5194/amt-6-3649-2013, 2013.

Cash, J. M., Heal, M. R., Langford, B. and Drewer, J.: A review of stereochemical implications in the generation of secondary organic aerosol from isoprene oxidation, Environ. Sci. Process. Impacts, 18(11), 1369–1380, doi:10.1039/C6EM00354K, 2016.

Cash, J. M., Langford, B., Di Marco, C., Mullinger, N. J., Allan, J., Reyes-Villegas, E., Joshi, R., Heal, M. R., Acton, W. J. F., Hewitt, C. N., Misztal, P. K., Drysdale, W., Mandal, T. K., Gadi, R., Gurjar, B. R. and Nemitz, E.: Seasonal analysis of submicron aerosol in Old Delhi using high-resolution aerosol mass spectrometry: chemical characterisation, source apportionment and new marker identification, Atmos. Chem. Phys., 21(13), 10133–10158, doi:10.5194/acp-21-10133-2021, 2021.

Chen, Q., Ikemori, F., Higo, H., Asakawa, D. and Mochida, M.: Chemical Structural Characteristics of HULIS and Other Fractionated Organic Matter in Urban Aerosols: Results from Mass Spectral and FT-IR Analysis, Environ. Sci. Technol., 4(50), 1721–1730, doi:10.1021/acs.est.5b05277, 2016.

Chen, W. T., Shao, M., Lu, S. H., Wang, M., Zeng, L. M., Yuan, B. and Liu, Y.: Understanding primary and secondary sources of ambient carbonyl compounds in Beijing using the PMF model, Atmos. Chem. Phys., 14(6), 3047–3062, doi:10.5194/acp-14-3047-2014, 2014.

Coggon, M. M., McDonald, B. C., Vlasenko, A., Veres, P. R., Bernard, F., Koss, A. R., Yuan, B., Gilman, J. B., Peischl, J., Aikin, K. C., Durant, J., Warneke, C., Li, S. M. and De Gouw, J. A.: Diurnal Variability and Emission Pattern of Decamethylcyclopentasiloxane (D5) from the Application of Personal Care Products in Two North American Cities, Environ. Sci. Technol., 52(10), 5610–5618, doi:10.1021/acs.est.8b00506, 2018.

Daellenbach, K. R., Bozzetti, C., Křepelová, A., Canonaco, F., Wolf, R., Zotter, P., Fermo, P., Crippa, M., Slowik, J. G., Sosedova, Y., Zhang, Y., Huang, R., Poulain, L., Szidat, S., Baltensperger, U., El Haddad, I., H Prévôt, A. S., To, C.

and H Prévôt andreprevot, A. S.: Characterization and source apportionment of organic aerosol using offline aerosol mass spectrometry, Atmos. Meas. Tech, 9(1), 8599–8644, doi:10.5194/amt-9-23-2016, 2016.

DeCarlo, P. F., Kimmel, J. R., Trimborn, A., Northway, M. J., Jayne, J. T., Aiken, A. C., Gonin, M., Fuhrer, K., Horvath, T., Docherty, K. S., Worsnop, D. R. and Jimenez, J. L.: Field-Deployable, High-Resolution, Time-of-Flight Aerosol Mass Spectrometer, Anal. Chem., 78(24), 8281–8289, doi:10.1021/ac061249n, 2006.

Farina, S. C., Adams, P. J. and Pandis, S. N.: Modeling global secondary organic aerosol formation and processing with the volatility basis set: Implications for anthropogenic secondary organic aerosol, J. Geophys. Res. Atmos., 115(9), 1–17, doi:10.1029/2009JD013046, 2010.

Fischer, L., Breitenlechner, M., Canaval, E., Scholz, W., Striednig, M., Graus, M., Karl, T. G., Petäjä, T., Kulmala, M. and Hansel, A.: First eddy covariance flux measurements of semi-volatile organic compounds with the PTR3-TOF-MS, Atmos. Meas. Tech., 14(12), 8019–8039, doi:10.5194/amt-14-8019-2021, 2021.

Gani, S., Bhandari, S., Seraj, S., Wang, D. S., Patel, K., Soni, P., Arub, Z., Habib, G., Hildebrandt Ruiz, L. and Apte, J. S.: Submicron aerosol composition in the world's most polluted megacity: The Delhi Aerosol Supersite study, Atmos. Chem. Phys., 19(10), 6843–6859, doi:10.5194/acp-19-6843-2019, 2019.

de Gouw, J. and Warneke, C.: Measurements of volatile organic compounds in the earth's atmosphere using proton-transfer-reaction mass spectrometry, Mass Spectrom. Rev., 26(2), 223–257, doi:10.1002/mas.20119, 2007.

Guenther, A., Nicholas, C., Fall, R., Klinger, L., Mckay, W. A. and Scholes, B.: A global model of natural volatile organic compound emissions s Raja the

balance Triangle changes in the atmospheric accumulation rates of greenhouse Triangle Several inventories of natural and Exposure Assessment global scales have been two classes Fores, J. Geophys. Res., 100(94), 8873–8892, 1995.

Guevara, M., Lopez-Aparicio, S., Cuvelier, C., Tarrason, L., Clappier, A. and Thunis, P.: A benchmarking tool to screen and compare bottom-up and top-down atmospheric emission inventories, Air Qual. Atmos. Heal., 10(5), 627–642, doi:10.1007/s11869-016-0456-6, 2017.

Gulia, S., Mittal, A. and Khare, M.: Quantitative evaluation of source interventions for urban air quality improvement - A case study of Delhi city, Atmos. Pollut. Res., 9(3), 577–583, doi:10.1016/j.apr.2017.12.003, 2018.

Gulia, S., Shukla, N., Padhi, L., Bosu, P., Goyal, S. K. and Kumar, R.: Evolution of air pollution management policies and related research in India, Environ. Challenges, 6(December 2021), 100431, doi:10.1016/j.envc.2021.100431, 2022.

Han, Y., Kawamura, K., Chen, Q. and Mochida, M.: Formation of high-molecular-weight compounds via the heterogeneous reactions of gaseous C8-C10n-aldehydes in the presence of atmospheric aerosol components, Atmos. Environ., 126, 290–297, doi:10.1016/j.atmosenv.2015.11.050, 2016.

Hodzic, A., Kasibhatla, P. S., Jo, D. S., Cappa, C. D., Jimenez, J. L., Madronich, S. and Park, R. J.: Rethinking the global secondary organic aerosol (SOA) budget: Stronger production, faster removal, shorter lifetime, Atmos. Chem. Phys., 16(12), 7917–7941, doi:10.5194/acp-16-7917-2016, 2016.

Hyde, P. and Mahalov, A.: Contribution of bioaerosols to airborne particulate matter, J. Air Waste Manag. Assoc., 70(1), 71–77, doi:10.1080/10962247.2019.1629360, 2020.

Jain, S., Sharma, S. K., Vijayan, N. and Mandal, T. K.: Seasonal characteristics of aerosols (PM2.5 and PM10) and their source apportionment using PMF: A four year study over Delhi, India, Environ. Pollut., 262, 114337, doi:10.1016/j.envpol.2020.114337, 2020.

Jensen, A., Liu, Z., Tan, W., Dix, B., Chen, T., Koss, A., Zhu, L., Li, L. and Gouw, J.: Measurements of Volatile Organic Compounds During the COVID-19 Lockdown in Changzhou, China, Geophys. Res. Lett., 48(20), 1–11, doi:10.1029/2021GL095560, 2021.

Jimenez, J. L., Canagaratna, M. R., Donahue, N. M., Prevot, A. S. H., Zhang, Q., Kroll, J. H., DeCarlo, P. F., Allan, J. D., Coe, H., Ng, N. L., Aiken, A. C., Docherty, K. S., Ulbrich, I. M., Grieshop, A. P., Robinson, A. L., Duplissy, J., Smith, J. D., Wilson, K. R., Lanz, V. A., Hueglin, C., Sun, Y. L., Tian, J., Laaksonen, A., Raatikainen, T., Rautiainen, J., Vaattovaara, P., Ehn, M., Kulmala, M., Tomlinson, J. M., Collins, D. R., Cubison, M. J., null null, Dunlea, J., Huffman, J. A., Onasch, T. B., Alfarra, M. R., Williams, P. I., Bower, K., Kondo, Y., Schneider, J., Drewnick, F., Borrmann, S., Weimer, S., Demerjian, K., Salcedo, D., Cottrell, L., Griffin, R., Takami, A., Miyoshi, T., Hatakeyama, S., Shimono, A., Sun, J. Y., Zhang, Y. M., Dzepina, K., Kimmel, J. R., Sueper, D., Jayne, J. T., Herndon, S. C., Trimborn, A. M., Williams, L. R., Wood, E. C., Middlebrook, A. M., Kolb, C. E., Baltensperger, U. and Worsnop, D. R.: Evolution of Organic Aerosols in the Atmosphere, Science, 326(5959), 1525–1529, doi:10.1126/science.1180353, 2009.

Jolly, W. L.: Modern Inorganic Chemistry (2nd Edn.), New York: McGraw-Hill., 1991.

Jordan, A., Haidacher, S., Hanel, G., Hartungen, E., Märk, L., Seehauser, H., Schottkowsky, R., Sulzer, P. and Märk, T. D.: A high resolution and high sensitivity proton-transfer-reaction time-of-flight mass spectrometer (PTR-TOF-MS), Int. J. Mass Spectrom., 286(2–3), 122–128, doi:10.1016/j.ijms.2009.07.005, 2009.

Kulkarni, S. H., Ghude, S. D., Jena, C., Karumuri, R. K., Sinha, B., Sinha, V., Kumar, R., Soni, V. K. and Khare, M.: How Much Does Large-Scale Crop Residue Burning Affect the Air Quality in Delhi?, Environ. Sci. Technol., 54(8), 4790–4799, doi:10.1021/acs.est.0c00329, 2020.

Lanz, V. A., Alfarra, M. R., Baltensperger, U., Buchmann, B., Hueglin, C. and Prévôt, A. S. H.: Source apportionment of submicron organic aerosols at an urban site by factor analytical modelling of aerosol mass spectra, Atmos. Chem. Phys., 7(6), 1503–1522, doi:10.5194/acp-7-1503-2007, 2007.

Lias, S. G., Liebman, J. F. and Levin, R. D.: Evaluated Gas Phase Basicities and Proton Affinities of Molecules; Heats of Formation of Protonated Molecules, J. Phys. Chem. Ref. Data, 13(3), 695–808, doi:10.1063/1.555719, 1984.

Lindinger, W., Hansel, A. and Jordan, A.: Proton-transfer-reaction mass spectrometry (PTR-MS): On-line monitoring of volatile organic compounds at pptv levels, Chem. Soc. Rev., 27(5), 347–354, doi:10.1039/a827347z, 1998.

Mihara, T. and Mochida, M.: Characterization of solvent-extractable organics in urban aerosols based on mass spectrum analysis and hygroscopic growth measurement, Environ. Sci. Technol., 45(21), 9168–9174, doi:10.1021/es201271w, 2011.

Nagpure, A. S., Ramaswami, A. and Russell, A.: Characterizing the Spatial and Temporal Patterns of Open Burning of Municipal Solid Waste (MSW) in Indian Cities, Environ. Sci. Technol., 49(21), 12911–12912, doi:10.1021/acs.est.5b03243, 2015.

Nemitz, E., Hargreaves, K. J., McDonald, A. G., Dorsey, J. R. and Fowler, D.: Micrometeorological measurements of the urban heat budget and CO2 emissions on a city scale, Environ. Sci. Technol., 36(14), 3139–3146, doi:10.1021/es010277e, 2002.

Nurkiewicz, T. R., Frisbee, J. C. and Boegehold, M. A.: 6.08 - Assessment of Vascular Reactivity, in Comprehensive Toxicology (Second Edition), edited by C. A. McQueen, pp. 133–148, Elsevier, Oxford., 2010.

Paatero, P.: Least squares formulation of robust non-negative factor analysis, Chemom. Intell. Lab. Syst., 37(1), 23–35, doi:10.1016/S0169-7439(96)00044-5, 1997.

Paatero, P.: User's guide for positive matrix factorization programs PMF2 and PMF3, Univ. Helsinki, Helsinki, part1: tut, 2004.

Paatero, P. and Tapper, U.: Positive matrix factorization: A non-negative factor model with optimal utilization of error estimates of data values, Environmetrics, 5(2), 111–126, doi:10.1002/env.3170050203, 1994.

Reyes-Villegas, E., Panda, U., Darbyshire, E., Cash, J. M., Joshi, R., Langford, B., Di Marco, C. F., Mullinger, N. J., Alam, M. S., Crilley, L. R., Rooney, D. J., Acton, W. J. F., Drysdale, W., Nemitz, E., Flynn, M., Voliotis, A., McFiggans, G., Coe, H., Lee, J., Hewitt, C. N., Heal, M. R., Gunthe, S. S., Mandal, T. K., Gurjar, B. R., Shivani, Gadi, R., Singh, S., Soni, V. and Allan, J. D.: PM1 composition and source apportionment at two sites in Delhi, India, across multiple seasons, Atmos. Chem. Phys., 21(15), 11655–11667, doi:10.5194/acp-21-11655-2021, 2021.

Schneider, J., Weimer, S., Drewnick, F., Borrmann, S., Helas, G., Gwaze, P., Schmid, O., Andreae, M. O. and Kirchner, U.: Mass spectrometric analysis and aerodynamic properties of various types of combustion-related aerosol particles, Int. J. Mass Spectrom., 258(1–3), 37–49, doi:10.1016/j.ijms.2006.07.008, 2006.

Sharma, S. K., Banoo, R. and Mandal, T. K.: Seasonal characteristics and sources of carbonaceous components and elements of PM10 (2010–2019) in

Delhi, India, J. Atmos. Chem., 78(4), 251–270, doi:10.1007/s10874-021-09424-x, 2021.

Steinemann, A.: The fragranced products phenomenon: air quality and health, science and policy, Air Qual. Atmos. Heal., 14(2), 235–243, doi:10.1007/s11869-020-00928-1, 2021.

Stewart, G. J., Nelson, B. S., Drysdale, W. S., Acton, W. J. F., Vaughan, A. R., Hopkins, J. R., Dunmore, R. E., Hewitt, C. N., Nemitz, E., Mullinger, N., Langford, B., Shivani, Reyes-Villegas, E., Gadi, R., Rickard, A. R., Lee, J. D. and Hamilton, J. F.: Sources of non-methane hydrocarbons in surface air in Delhi, India, Faraday Discuss., 226, 409–431, doi:10.1039/d0fd00087f, 2021.

Sun, Y., Zhang, Q., Zheng, M., Ding, X., Edgerton, E. S. and Wang, X.: Characterization and Source Apportionment of Water-Soluble Organic Matter in Atmospheric Fine Particles (PM 2.5) with High-Resolution Aerosol Mass Spectrometry and GC–MS, Environ. Sci. Technol., 45(11), 4854–4861, doi:10.1021/es200162h, 2011.

Ulbrich, I. M., Canagaratna, M. R., Zhang, Q., Worsnop, D. R. and Jimenez, J. L.: Interpretation of organic components from Positive Matrix Factorization of aerosol mass spectrometric data, Atmos. Chem. Phys., 9(9), 2891–2918, doi:10.5194/acp-9-2891-2009, 2009.

Vlachou, A., Tobler, A., Lamkaddam, H., Canonaco, F., Daellenbach, K. R., Jaffrezo, J. L., Minguillón, M. C., Maasikmets, M., Teinemaa, E., Baltensperger, U., El Haddad, I. and Preávôt, A. S. H.: Development of a versatile source apportionment analysis based on positive matrix factorization: a case study of the seasonal variation of organic aerosol sources in Estonia, Atmos. Chem. Phys., 19(11), 7279–7295, doi:10.5194/acp-19-7279-2019, 2019.

Vlasenko, A., Slowik, J. G., Bottenheim, J. W., Brickell, P. C., Chang, R. Y. W., Macdonald, A. M., Shantz, N. C., Sjostedt, S. J., Wiebe, H. A., Leaitch, W. R. and Abbatt, J. P. D.: Measurements of VOCs by proton transfer reaction mass spectrometry at a rural Ontario site: Sources and correlation to aerosol composition, J. Geophys. Res., 114(D21), D21305, doi:10.1029/2009JD012025, 2009.

Wang, L., Slowik, J. G., Tripathi, N., Bhattu, D., Rai, P., Kumar, V., Vats, P., Satish, R., Baltensperger, U., Ganguly, D., Rastogi, N., Sahu, L. K., Tripathi, S. N. and Prévôt, A. S. H.: Source characterization of volatile organic compounds measured by proton-transfer-reaction time-of-flight mass spectrometers in Delhi, India, Atmos. Chem. Phys., 20(16), 9753–9770, doi:10.5194/acp-20-9753-2020, 2020.

Warneke, C., Kuczynski, J., Hansel, A., Jordan, A., Vogel, W. and Lindinger, W.: Proton transfer reaction mass spectrometry (PTR-MS): Propanol in human breath, Int. J. Mass Spectrom. Ion Process., 154(1–2), 61–70, doi:10.1016/0168-1176(96)04369-8, 1996.

Weimer, S., Alfarra, M. R., Schreiber, D., Mohr, M., Prévôt, A. S. H. and Baltensperger, U.: Organic aerosol mass spectral signatures from wood-burning emissions: Influence of burning conditions and type, J. Geophys. Res. Atmos., 113(10), D10304, doi:10.1029/2007JD009309, 2008.

World Health Organization: Indoor air quality: organic pollutants, Berlin, 23-27 August 1987. EURO Reports and Studies 111. Copenhagen., 1989.

World Health Organization: 7 million premature deaths annually linked to air pollution, [online] Available from: https://www.who.int/health-topics/air-pollution#tab=tab_1, 2021.

Wright, T.: Calibration Methodolgy for a Proton Transfer Reaction Mass, Thesis, Utrecht University., 2016.

Zhang, Q., Rami Alfarra, M., Worsnop, D. R., Allan, J. D., Coe, H., Canagaratna, M. R. and Jimenez, J. L.: Deconvolution and quantification of hydrocarbon-like and oxygenated organic aerosols based on aerosol mass spectrometry, Environ. Sci. Technol., 39(13), 4938–4952, doi:10.1021/es048568l, 2005.

Zhang, Q., Jimenez, J. L., Canagaratna, M. R., Allan, J. D., Coe, H., Ulbrich, I., Alfarra, M. R., Takami, A., Middlebrook, A. M., Sun, Y. L., Dzepina, K., Dunlea, E., Docherty, K., DeCarlo, P. F., Salcedo, D., Onasch, T., Jayne, J. T., Miyoshi, T., Shimono, A., Hatakeyama, S., Takegawa, N., Kondo, Y., Schneider, J., Drewnick, F., Borrmann, S., Weimer, S., Demerjian, K., Williams, P., Bower, K., Bahreini, R., Cottrell, L., Griffin, R. J., Rautiainen, J., Sun, J. Y., Zhang, Y. M. and Worsnop, D. R.: Ubiquity and dominance of oxygenated species in organic aerosols in anthropogenically-influenced Northern Hemisphere midlatitudes, Geophys. Res. Lett., 34(13), doi:10.1029/2007GL029979, 2007.

Chapter 2

Seasonal analysis of submicron aerosol in Old Delhi using high resolution aerosol mass spectrometry: Chemical characterisation, source apportionment and new marker identification

This chapter is based on a research paper published in Atmospheric Chemistry and Physics (*Cash, J. M., Langford, B., Di Marco, C., Mullinger, N. J., Allan, J., Reyes-Villegas, E., Joshi, R., Heal, M. R., Acton, W. J. F., Hewitt, C. N., Misztal, P. K., Drysdale, W., Mandal, T. K., Shivani, Gadi, R., Gurjar, B. R., and Nemitz, E.: Seasonal analysis of submicron aerosol in Old Delhi using high-resolution aerosol mass spectrometry: chemical characterisation, source apportionment and new marker identification, Atmos. Chem. Phys., 21, 10133–10158, https://doi.org/10.5194/acp-21-10133-2021, 2021*).

Author contributions: I took the PM_1 measurements using HR-TOF-AMS with help from Langford, B., Di Marco, C., Mullinger, N. J., and Nemitz, E. Reyes-Villegas, E. and Allan, J. measured co-located PM_1 using C-TOF-AMS along with black carbon measurements using an Aethalometer AE-31. Joshi, R. and Allan, J. measured black carbon using SP2. I took VOC measurements using PTR-QiTOF-MS along with Acton, W. J. F. and was supported by Langford, B., Hewitt, C. N., and Misztal, P. K. Drysdale, W. measured NO_x using an Aerolaser AL 5002 UVU and a dual-channel high-resolution chemiluminescence instrument. I interpreted the results with help from Langford, B., Heal, M. R., Di Marco, C., Allan, J., Reyes-Villegas, E., Nemitz, E. Mullinger, N. J., Mandal, T. K., Shivani, Gadi, R., Gurjar, B. R., and Nemitz, E., provided overall guidance with setup and logistics. I wrote the manuscript with subsequent contributions from all co-authors.

2.1. Abstract

We present the first real-time composition of submicron particulate matter (PM_1) in Old Delhi using high resolution aerosol mass spectrometry (HR-AMS). Old Delhi is one of the most polluted locations in the world, and PM_1 concentrations reached ~750 μg m^{-3} during the most polluted period, the post-monsoon, where PM_1 increased by 188% over the pre-monsoon period. Sulphate contributes the largest inorganic PM_1 mass fraction during the pre-monsoon (24%) and monsoon (24%) periods with nitrate contributing most during the post-monsoon (8%). The organics dominate the mass fraction (54-68%) throughout the three periods and using positive matrix factorisation (PMF) to perform source apportionment analysis of organic mass, two burning-related factors were found to contribute the most (35%) to the post-monsoon increase. The first PMF factor, semi-volatility biomass burning organic aerosol (SVBBOA), shows a high correlation with earth observation fire counts in surrounding states which links its origin to crop residue burning. The second is a solid-fuel OA (SFOA) factor with links to local open burning due to its high composition of polyaromatic hydrocarbons (PAH) and novel AMS measured marker species for polychlorinated dibenzodioxins (PCDDs) and polychlorinated dibenzofurans (PCDFs). Two traffic factors were resolved, one hydrocarbon-like OA (HOA) factor and another nitrogen-rich HOA (NHOA) factor. The N compounds within NHOA were mainly nitrile species which have not previously been identified within AMS measurements. Their PAH composition suggests that NHOA is linked to diesel, and HOA to compressed natural gas and gasoline. These factors combined make the largest relative contribution to primary PM_1 mass during the pre-monsoon and monsoon periods, while contributing the second highest in the post-monsoon. A cooking OA (COA) factor shows strong links to the secondary factor, semi-volatility oxygenated OA (SVOOA). Correlations with co-located volatile organic compound (VOC) measurements and AMS measured organic nitrogen oxides (OrgNO) suggest SVOOA is formed from aged COA. It is also found that a

significant increase in chloride concentrations (522%) from pre-monsoon to post-monsoon correlates well with SVBBOA and SFOA suggesting that crop residue burning and open waste burning are responsible. A reduction in traffic emissions would effectively reduce concentrations across most of the year. In order to reduce the post-monsoon peak, sources such as funeral pyres, solid waste burning and crop residue burning should be considered when developing new air quality policy.

2.2. Introduction

The number of premature deaths linked to fine particulate matter ($PM_{2.5}$) globally was estimated at 4.1 million in 2016 and 10.6% were in India alone (Gakidou et al., 2017). Some of the most polluted cities in the world are in India, with Delhi being in the top 10 cities listed by the World Health Organisation based on available annual $PM_{2.5}$ measurements in 2018 (World Health Organisation, 2018). This has a significant effect on the health of its population (26 million) and in 2016 it was estimated that fine particulate matter ($PM_{2.5}$) accounted for ~15,000 premature deaths per year (Maji et al., 2018). Therefore, it is important to investigate the sources of PM to improve air quality mitigation strategies.

The composition of sub-micron PM (PM_1) is a mixture of organic aerosol (OA), black carbon (BC) and inorganic aerosols including ammonium, sulphate, chloride and nitrate. The high-resolution aerosol mass spectrometer (HR-AMS) has helped to improve measurements of PM_1 as it gives detailed information on its chemical composition through elemental analysis and high-resolution compound identification. Combining these measurements with positive matrix factorisation (PMF), allows for the apportionment of aerosol mass into different sources (or factors). This provides detailed information needed to inform effective air quality interventions. To date, relatively few measurements of PM composition have been made by HR-AMS in India with

measurements made in Kanpur a notable exception (Chakraborty et al., 2015, 2016a, 2016b, 2018). These HR-AMS measurements however give multiple factor solutions, often of six or greater, which highlights the complexity of the source mix. Typical sources identified include components considered to be primary such as hydrocarbon-like organic aerosol (HOA) and biomass burning organic aerosol (BBOA) as well as components usually considered to be secondary such as low-volatility oxygenated organic aerosol (LVOOA), semi-volatility oxygenated organic aerosol (SVOOA), and oxidised-BBOA (O-BBOA). Throughout these studies there are multiple versions of the same source and requires additional auxiliary measurements to pin down their origin. This study aims to better assign factors to their original sources using additional measurements of volatile organic compounds (VOCs), black carbon (BC), carbon monoxide (CO), nitrogen oxides (NO_x) and Earth observations.

A growing number of studies in Delhi, and other locations in India, have reported large concentrations of chloride, especially during the morning hours at ~7-9 a.m. (Sudheer et al., 2014; Chakraborty et al., 2018; Gani et al., 2019; Acharja et al., 2020; Reyes-Villegas et al., 2020; Tobler et al., 2020; Lalchandani et al., 2021)**.** The source of this chloride is still widely debated and there are several possibilities including aluminium pickling, industrial activity, municipal waste burning and biomass burning. The aluminium pickling industry in the north-west of Delhi is thought to directly emit HCl and be the main contributor to chloride during the winter months when average concentrations increase from 1.5 µg m^{-3} in the summer to 23 µg m^{-3} in the winter (Gani et al., 2019). Studies in Mexico city suggest a substantial amount of chloride is from biomass and municipal waste burning and they also observe high concentrations from crop residue burning (Christian et al., 2010; Li et al., 2012). In Delhi, these sources may also be high contributors as it would explain why chloride concentrations show a larger elevation during the colder post-monsoon and winter months than other compounds.

During the post-monsoon, large-scale crop residue burning occurs along with large numbers of Delhi residents burning municipal waste to keep warm and clean streets. These open burning sources produce chloride in different organic and inorganic forms. Inorganic NH_4Cl is related to biomass burning through the release of particulate KCl that forms HCl and ultimately NH_4Cl once reacted with ammonia (Sullivan et al., 2007; Wang et al., 2017). Emissions of HCl are often associated with plastic burning but there are also organic species of chloride, such as polychlorinated dibenzo-furans (PCDF) and -dioxins (PCDD), that form readily from chloride-rich plastics such as polyvinyl chloride (PVC) and polychlorinated biphenyls (PCB) (Minh et al., 2003; Chakraborty et al., 2013; Stewart et al., 2020). Large-scale plastic burning practises in Delhi, such as electronic waste recycling centres situated in the north-west, could therefore be high contributors to chloride mass. The measurement of plastic burning markers is therefore important to understand the contribution of such practises to chloride concentrations.

This study focuses on the high-resolution aspect of the High-Resolution Time-of-Flight Aerosol Mass Spectrometer (HR-TOF-AMS) and investigates the detailed composition of aerosol. Using Positive Matrix Factorisation (PMF), the PM_1 source mass profiles in Delhi are compared to auxiliary measurements, including measurements of VOCs using a high-resolution proton-transfer-reaction time-of-flight mass spectrometer with a quadruple ion guide (PTR-QiTOF-MS), giving us a detailed picture of the origin of PMF factors. The polyaromatic hydrocarbon (PAH) composition of each factor is also investigated and helps to distinguish factors based on the combustion of different fuel types. A focus is also placed on investigating the origin of the high chloride concentrations observed in Delhi, where compositional aids help to establish a mixture of chloride sources and an indication to their contribution. There are two companion papers which use the HR-TOF-AMS measurement data from the Indira Gandhi Delhi Technical University for Women (IGDTUW). One study compares AMS datasets measured at different sites in Delhi and creates a city-wide perspective of PM_1 composition over an entire year (Reyes-

Villegas et al., 2020). The other study (which will be published separately) uses the unit-mass resolution measurements to calculate compositional aerosol fluxes for the first time and compares measurements in Delhi to measurements taken in two cities: London and Beijing. The three studies combine to produce a more comprehensive picture of PM_1 aerosol composition, concentrations and sources in Delhi.

2.3. Methods

2.3.1. Measurement location and instrumentation

Measurements were undertaken on the campus of the Indira Gandhi Delhi Technical University for Women (IGDTUW) which is located to the north of Old Delhi (28°39'51.8"N 77°13'55.2"E) (Figure 2.1). The measurements were made in three campaigns corresponding to three periods of the year in Delhi where the seasonal differences cause significant changes in meteorology. Here, we refer to the measurements taken during the summer months as the pre-monsoon period (26/05/2018 – 28/06/2018) when average temperatures were high (36 °C) and relative humidity (RH) was low (43%). During the monsoon campaign (03/08/2018 – 18/08/2018) the temperatures dropped slightly (31 °C) and RH was high (76%) coinciding with large rainfall events. The post-monsoon campaign (09/10/2018 – 23/11/2018) encompassed the periods of the 5-days of Diwali (05/11/18 – 10/11/18) and the seasonal stubble burning for rice crops in the neighbouring states of Punjab and Haryana situated to the NW. These two activities are combined with unfavourable meteorology where boundary layer height, temperatures (24 °C) and wind speeds are generally lower, causing a shallow inversion layer.

Figure 2.1 – Map showing the measurement site location (red circle) along with possible sources of PM (blue areas) and busy roads (yellow). A summary of the wind directional measurements for the three measurement campaigns are shown in the top right-hand corner.

A High-Resolution Time-of-Flight Aerosol Mass Spectrometer (HR-TOF-AMS, Aerodyne Research Inc.) was used in V-mode to measure 5-minute average mass spectra of non-refractory PM_1. The principle of operation of the instrument is described in detail elsewhere (DeCarlo et al., 2006; Canagaratna et al., 2007). Briefly, particles are sampled via a ~PM_1 aerodynamic lens and their size is measured using a time-of-flight chamber. Particles are then vaporised on a heated plate (600 °C), the non-refractory species ionised using a 70 eV electron impact source and the *m/z* values of the resultant ions determined with a time-of-flight analyser.

The HR-TOF-AMS was calibrated fortnightly over the three campaigns (11 calibrations in total) for its ionisation efficiency of nitrate (IE) and the relative ionisation efficiency (RIE) of other inorganic compounds using nebulised 300 nm ammonium nitrate, sulphate and chloride. A collection efficiency (CE) of

0.5 was confirmed through comparisons with gravimetric $PM_{2.5}$ filter measurements taken throughout the pre- and post-monsoon campaigns by Birmingham University. The AMS measurements were added to the BC measurements to give total PM_1 which was averaged to match the sample intervals of the filters (6 and 12 h). The comparison gave PM_1 vs. $PM_{2.5}$ gradients of 0.9 using a CE of 0.5 during most of the measurement campaigns. Considering the increased mass collected due to a higher size fraction for $PM_{2.5}$, the CE was set to 0.5 for these periods. However, for Diwali and a few days after (05 to 14/11/18) a higher CE of 0.8 was applied to obtain a similar PM_1 vs. $PM_{2.5}$ gradient of ~0.9. The reasons for this change are not the purpose of this study and further compositional analysis is required to understand the change. All CE, RIEs and IEs are summarised in Table S2.2 for the different measurement periods.

The HR-ToF-AMS data were analysed using the IGOR Pro (Wavemetrics, Inc., Portland, OR, USA) based software SQUIRREL (Sequential Igor data Retrieval) v.1.62B and PIKA (Peak Integration by Key Analysis) v.1.22B and a total of 2725 ions were fitted (including isotopes) in the range of *m/z* 12-328. This range extends to larger *m/z* than is typically used for ambient measurements and certainly for high resolution PMF calculations using AMS data (Aiken et al., 2009; Docherty et al., 2011; Sun et al., 2016; Zhang et al., 2018). This becomes possible due to the high concentration loading in Delhi (up to ~750 µg m^{-3}) providing considerable signal at high *m/z*. The fitting of heavier ions has also been shown to improve the strength of PMF solutions and their correlations with external tracers, as demonstrated in the Supplementary Information (SI) Section S2.1. However, fragment identification becomes increasingly ambiguous at higher *m/z.* The PIKA software allows the user to fit peaks based on a reduction in the residuals between the measured signal and the fit. There are measured signals for open (when the chopper is open), closed (when the chopper is closed) and diff (= open – closed), meaning there are also three sets of residuals. Neighbouring peaks may overlap and cause the diff residuals to improve whilst not improving the open and closed

residuals. This becomes more relevant when moving to higher *m/z* ions as peaks become broader. Therefore, only peaks which significantly improved the open and closed signal residuals were fitted. Peaks were also fitted based on signal intensity where peaks with an average signal of less than 10 Hz/ns were not included.

The extended *m/z* range included ions identified as polyaromatic hydrocarbons (PAH) which were fitted according to the protocol set out by Herring et al. (2015). Elemental analysis was also performed to derive oxygen-to-carbon (O:C), hydrogen-to-carbon (H:C), nitrogen-to-carbon (N:C) and organic mass to organic carbon (OM:OC) ratios using the Improved-Ambient (IA) method developed by Canagaratna et al. (2015) as implemented in PIKA.

The concentration of organic nitrogen oxide species (OrgNO) have been estimated using the NO_x ratio method described in detail by Farmer et al. (2010) and Kiendler-Scharr et al. (2016). The method involves calculating the fraction of OrgNO ($OrgNO_{frac}$) using the equation,

$$OrgNO_{frac} = \frac{(R_{obs}-R_{cal})(1+R_{ON})}{(R_{ON}-R_{cal})(1+R_{obs})}. \quad (2.1)$$

where R_{obs} is the measured NO_2^+/NO^+ ratio, R_{cal} is the NO_2^+/NO^+ ratio observed during NH_4NO_3 calibrations and R_{ON} is a fixed value (0.1) that has been determined as the lowest R_{obs} in multiple data sets (Kiendler-Scharr et al., 2016). The NO_2^+/NO^+ ratio described in Kiendler-Scharr et al. (2016) is used instead of NO^+/NO_2^+ to allow for signal reaching the limit of detection to approach zero rather than infinity because NO_2^+ is often the higher signal. The calculated $OrgNO_{frac}$ is then multiplied by the total nitrate concentration to give an estimate of the OrgNO mass ($OrgNO_{mass}$).

The ISORROPIA-II model was used to estimate the liquid water content (LWC) in aerosol using the input parameter of temperature and relative humidity along

with AMS measurements of ammonium, sulphate, chloride and nitrate (Fountoukis and Nenes, 2007).

The AMS measurements were compared to a number of co-located instruments including black carbon (BC) measurements which were taken using an Aethalometer AE-31. The BC measurements were corrected using the Weingartner method (Weingartner et al., 2003) and by using reference measurements from a Single Particle Soot Photometer (SP-2; Droplet Measurement Technology, Boulder, CO) which was co-located for ~7-days (Reyes-Villegas et al., 2020). Volatile organic compounds (VOC) were measured using a high-resolution proton-transfer-reaction time-of-flight mass spectrometer with a quadruple ion guide (PTR-QiTOF-MS, Ionicon Analytik GmbH, Innsbruck, Austria). A 5-minute average of the concentrations were used within this work and details of the setup are described in (Acton et al., 2020). CO and NO_x concentrations were measured using an Aerolaser AL 5002 UVU and a dual-channel high-resolution chemiluminescence instrument (Air Quality Designs Inc., Colorado), respectively. Meteorological measurements were taken using a HS-50 Gill research ultrasonic anemometer and a Vaisala weather transmitter (WXT530 Series) from the 11/10/2018 onwards. All measurements before this date were taken from the Indira Gandhi International Airport (available at: https://www.ncdc.noaa.gov/cdo-web/, last accessed: 20/04/2021).

2.3.2. Source apportionment

Positive Matrix Factorisation (PMF) is a bilinear receptor model which is used as a multivariate analysis tool to separate the total measured mass spectrum and its corresponding time series into individual sources or “factors” (Paatero and Tapper, 1994). The model can be summarised as:

$$\mathbf{X} = \mathbf{FG} + \mathbf{E}, \quad (2.2)$$

where $\mathbf{X}$ is the total measured matrix containing m rows of mass spectra for each time stamp and n columns of measured m/z ions. The factor mass spectral profiles are contained within the $m \times p$ matrix $\mathbf{F}$ and the time series contribution of each factor is expressed by the $p \times n$ matrix $\mathbf{G}$. The residuals of the model are represented by the $m \times n$ matrix $\mathbf{E}$ and the number of factors, p, are chosen by the model user but it requires no a priori information for matrices $\mathbf{F}$ and $\mathbf{G}$. The model iteratively fits $\mathbf{F}$ and $\mathbf{G}$ to the data in order to minimise the fitting parameter, Q, through a least-squares algorithm as:

$$Q = \sum_{i=1}^{m} \sum_{j=1}^{n} \left(\frac{e_{ij}}{\sigma_{ij}} \right)^2 . \quad (2.3)$$

Here the elements of the residual, e_{ij}, and uncertainty, σ_{ij}, matrices have rows, i, and columns, j, where in ideal circumstances Q = 1 and the model would create a minimised solution that would explain all the measured data and leave the uncertainty within the residual matrix.

The analysis was carried out using the PMF Evaluation Tool (PET, v3.00) using the PMF2 algorithm in robust-mode (Ulbrich et al., 2009). The error matrix was down-weighted based on the signal-to-noise ratio (SNR) where columns with an SNR <2 were down-weighted by a factor of two and SNR <0.2 by a factor of 10. Down-weighting of CO_2^+ and its associated (derived) ions CO^+, H^+, OH^-, H_2O, was also included to account for the influence of over-counting.

The primary PMF analysis was conducted on the organic matrix (2.39673 × 10^7 data points) and a 7-factor solution was chosen following the procedure and rationale set out in SI Sections S2.1 and S2.2. The procedure also includes multilinear regression analysis to help determine the chosen solution. The solution chosen is from PMF analysis carried out on all the measurement periods combined as multilinear regressions showed this to fit more closely with external tracers (see Section S2.1 for more details).

An alternative PMF solution was obtained, introducing inorganic species into the data matrix using the method set out by Sun et al. (2012). Briefly, selected ions for chloride (Cl^+ *m/z* 35, HCl^+ *m/z* 36), ammonium (NH^+ *m/z* 15, NH_2^+ *m/z* 16, NH_3^+ *m/z* 17), nitrate (NO^+ *m/z* 30, NO_2^+ *m/z* 46) and sulphate (SO^+ *m/z* 48, SO_2^+ *m/z* 64, SO_3^+ *m/z* 80, HSO_3^+ *m/z* 81, $H_2SO_4^+$ *m/z* 98) were chosen and it was confirmed that once combined to form one time series they correlated almost perfectly with the measured total mass of their represented inorganic species (r^2 ~1). All adjustments for relative ionisation and collection efficiencies were applied to the data before PMF analysis in order to determine accurate uncertainties and allow reasonable mixing of the organic and inorganic data. After PMF analysis, the selected ions were then divided by the total mass fraction of their represented inorganic species. This time a 9-factor solution was chosen (Section S2.3) and was developed partly to provide an analysis product that would be comparable with the earlier Aerosol Chemical Speciation Monitor (ACSM) PMF results for Delhi of Bhandari et al. (2019). Additionally, it provides information on the association between the organic factors and the ions that are normally associated with inorganic compounds.

Although there is some ambiguity in the choice of the ideal solutions, PMF was chosen over the more advanced Multi Linear engine (ME-2; Canonaco et al., 2013), which allows individual factors to be constrained with a priori information because, for India, reference spectra have not yet been established and especially not for high resolution spectra covering the wide range of *m/z* used in our analysis.

2.4. Results

2.4.1. Inorganic and organic PM concentrations

The concentrations of PM species during the pre-monsoon and monsoon periods are similar although slightly lower in the latter, presumably due to increased rainfall and associated washout (Figure 2.2). However, most PM component concentrations were considerably higher during the post-monsoon period and total-PM_1 mass increases by 188% over the pre-monsoon. Chloride and nitrate concentrations increase the most, by a factor of ~5-6, suggesting there is a significant additional source of chloride and nitrate during the post-monsoon period. This is also consistent with increased partitioning of (semi-)volatile aerosol compounds into the aerosol phase during the cooler post-monsoon period. Ammonium and organic aerosol underwent a ~2-3 fold increase, whereas sulphate is the only species whose absolute concentrations did not increase during the post-monsoon. This has also been noted in previous measurements taken in Delhi using an ACSM where sulphate was on average 10 μg m^{-3} across spring, summer and the monsoon period (Gani et al., 2019).

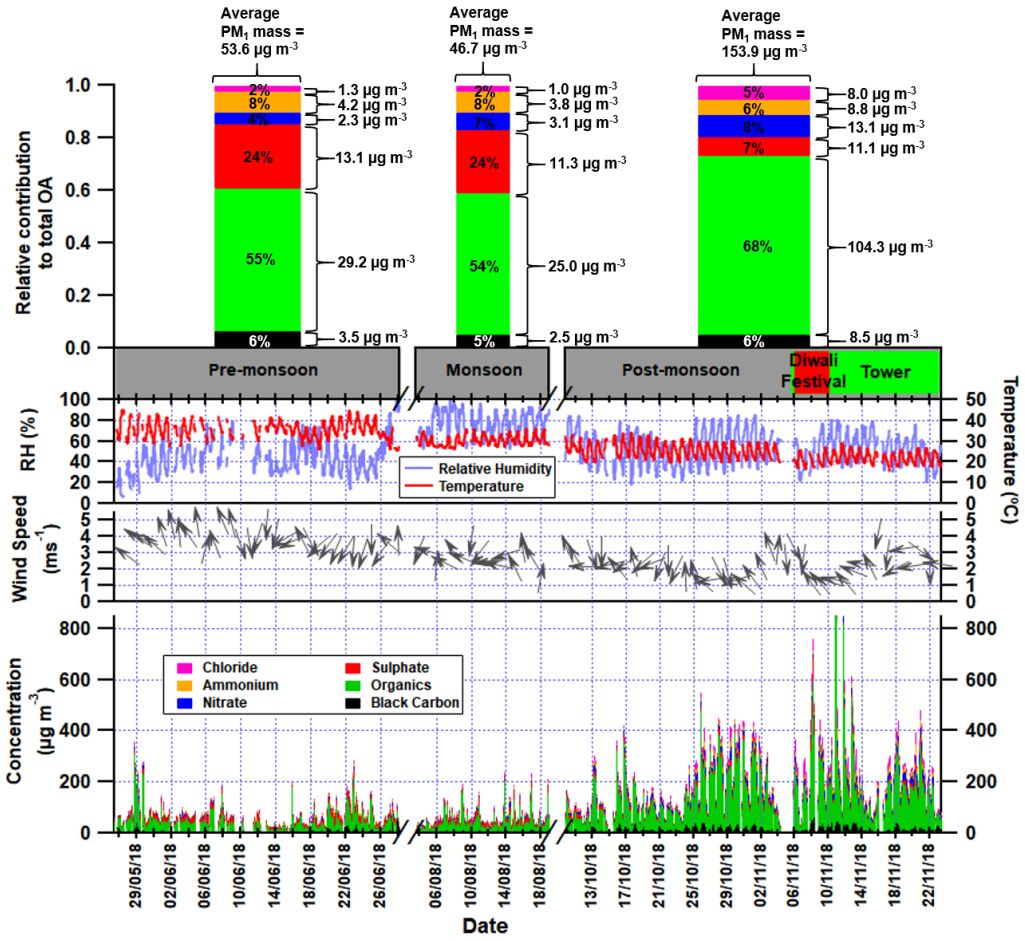

Figure 2.2. First Panel: Average relative contributions of chloride, ammonium, nitrate, sulphate, organic aerosol and black carbon to the total PM_1 mass loadings in the pre-monsoon, monsoon and post-monsoon periods. The average concentrations of each species are shown to the right of each bar (see Table S2.5 for values and statistics). Second panel: Gantt chart showing the measurement periods where the red region shows the Diwali festival and the green region shows when the inlet was moved to a 30 m tower. Third panel: time series of the relative humidity and the temperature for the three measurement periods. Fourth panel: time series of the wind speed with arrows showing wind direction. Fifth panel: time series of stacked concentrations of aerosol species showing total PM_1.

Preliminary analyses of the eddy-covariance flux measurements (Di Marco et al., 2019) made during the post-monsoon tower period suggest that whilst concentrations peaked at night, local emissions peaked during the late morning and afternoon, suggesting that boundary-layer dynamics exercised a dominant control over surface concentrations. Concentrations of all species, with the possible exception of sulphate, decreased significantly in the

afternoon during the post-monsoon (Figure 2.3). This was mainly due to the contraction of the boundary layer during the night and early hours of the morning being more pronounced which removes possible afternoon peaks from specific sources, e.g. lunch hour cooking activities (Nakoudi et al., 2019; Reyes-Villegas et al., 2020). The pre-monsoon and monsoon diurnal cycles show species concentrations, excluding nitrate and chloride, were less affected by the higher boundary layer in the afternoon. The monsoon is the least affected period as there were midday peaks for sulphate, ammonium and organic aerosol.

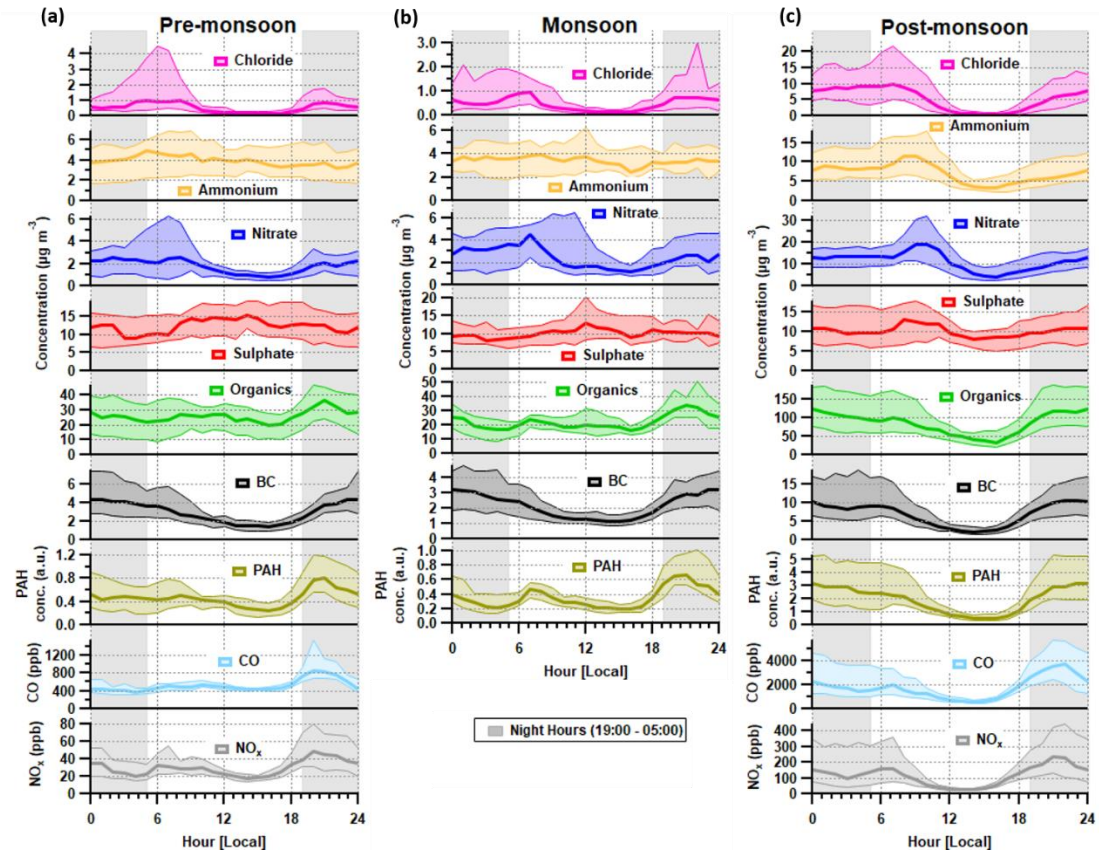

Figure 2.3. Median diurnal cycles for aerosol chemical species and for BC, CO and NO_x during the (a) pre-monsoon, (b) monsoon and (c) post-monsoon periods. The median concentration is represented by the thick line and the interquartile range is represented by the shading. Regions shaded in grey are night hours. Data for CO and NO_x are not available for the monsoon period.

Morning peaks were observed in the diurnal cycle for nitrate, ammonium and chloride (Figure 2.3). The nitrate peaks are earlier in the morning during the pre-monsoon compared to other periods which may relate to an earlier rise in temperature compared to monsoon and post-monsoon periods. The diurnal cycle for chloride shows a regular peak at ~ 6-8 a.m. and the details of possible sources will be discussed in Section 2.5.4.

The pollution roses (showing the concentration distribution by wind sector, Figure 2.4) for nitrate and ammonium show higher contributions to PM_1 mass with a south-westerly wind direction but there is no clear pattern. Figure S2.8 shows polar graphs (i.e. the wind-sector distribution of the raw 30-minute measurements) which in particular illustrate the wind direction corresponding to maximum concentrations. Nitrate and ammonium show scattered polar graphs which indicates no clear source directions were associated with extreme concentrations. The sulphate pollution rose shows a higher mass contribution with a south easterly wind, but its polar graph shows maximum concentrations originated from the north and north-east.

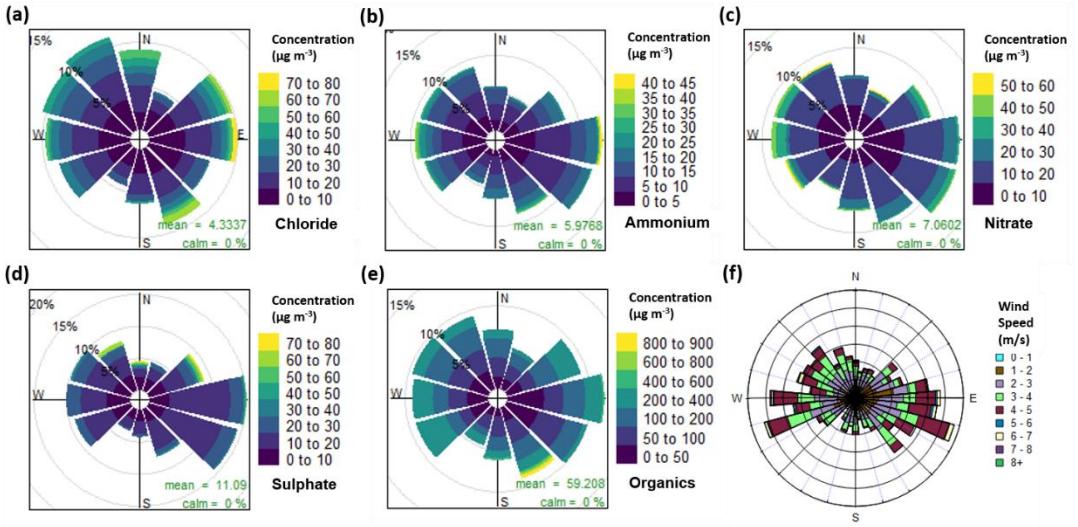

Figure 2.4. Pollution roses for (a) chloride, (b) ammonium, (c) nitrate, (d) sulphate and (e) organic aerosol, along with (f) a wind rose plot for all measurement periods combined. The pollution roses show 30º wind vectors and their size is proportional to the percentage contribution to the mean concentration. The vectors are divided into concentration bins based on the colour scale in the legend.

The pollution rose and polar graph for organic aerosol are highly spread. The pollution rose suggests there is a slight increase in the organic mass when originating from the east and south-east but this is closely followed by contributions from the west and north-west (Figure 2.4e). Its polar graph also shows some extreme values existing from the south-east (Figure S2.8). This spread can be explained by a low wind speed and a low boundary layer height causing a significant increase in concentrations. In Figure 2.2, PM_1 shows a large increase during periods of low wind speed and an exponential decay in PM_1 concentration with increasing wind speed. Meteorology therefore plays an important role during the high concentration periods.

The chloride pollution rose (Figure 2.4a) shows no clear pattern in its wind direction but there is a slightly higher contribution originating from the west, north-west and the east. The chloride polar graph in Figure S2.8 is also spread, showing large peaks which coincide with the southeast, east, north-east and north. The pollution roses for each diurnal hour in Figure S2.9 show the

directional trend of chloride in more detail. Here, the large peak in the morning (6-8 a.m.) corresponds to a mixed spread of wind directions with a slight preference for the west, south-west, south-east and north-west which suggests mixed sources of chloride.

2.4.2. Concentrations of polyaromatic hydrocarbons and OrgNO

The presence of OrgNO species is evident in Figure 2.5 and there is a gradual drop in concentration with time over the pre-monsoon, monsoon and earlier half of the post-monsoon period. This may suggest an increase in temperature and a decrease in relative humidity are key to OrgNO formation in Delhi. During Diwali (07/11/2018) there is also a sharp increase in OrgNO concentrations to > 20 µg m^{-3} and this is likely due to large amounts of pyrotechnical emissions. Similar peaks in AMS-measured OrgNO have been seen during a large pyrotechnical event in the UK called bonfire night (Reyes-Villegas et al., 2018b).

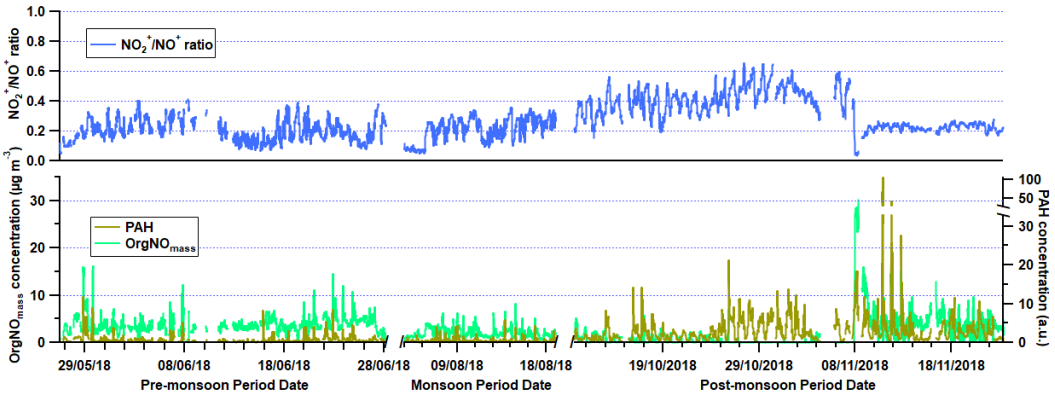

Figure 2.5. Upper panel: time series of NO_2^+/NO^+ ratio in the three measurement periods. Lower panel: time series of polyaromatic hydrocarbon (PAH) uncalibrated concentrations and organic nitrogen oxide species ($OrgNO_{mass}$) concentrations.

The time series of PAH concentrations in Figure 2.5 are uncalibrated concentrations and further lab work (such as the work carried out in Herring et al. (2015)) is required to establish absolute concentrations which goes beyond the scope of this study. The data does, however, show the relative change in PAHs is small between the pre-monsoon and monsoon periods suggesting consistent sources are responsible such as traffic, solid fuel burning or cooking activities. There is also a large increase in PAHs during the post-monsoon period when the burning of the rice crop residue begins (Kulkarni et al., 2020), but it is also likely a result of a lower boundary layer. Three large peaks are observed during the week of the Diwali holiday and each peak occurs during the late hours of the night (~10-12 p.m.), suggesting an infrequent local source. It is uncertain what this source is and through source apportionment analysis (see Section 2.4.3 below) the PAH contribution to these peaks is split between sources, suggesting they cannot be resolved through PMF without the unknown source occurring more often than these three occasions.

2.4.3. Source apportionment concentrations

The organic-only PMF solution is presented in Figure 2.6 and Figure 2.7 while the organic-inorganic solution is presented in the SI (Section S2.8). The organic-inorganic solution is not considered the most representative of sources, as it may be influenced by thermodynamic effects, i.e. factors may be resolved based on similarities in volatility rather than source. However, the organic-inorganic solution is referred to within this section as it provides insight into the combined behaviour of inorganic and organic species.

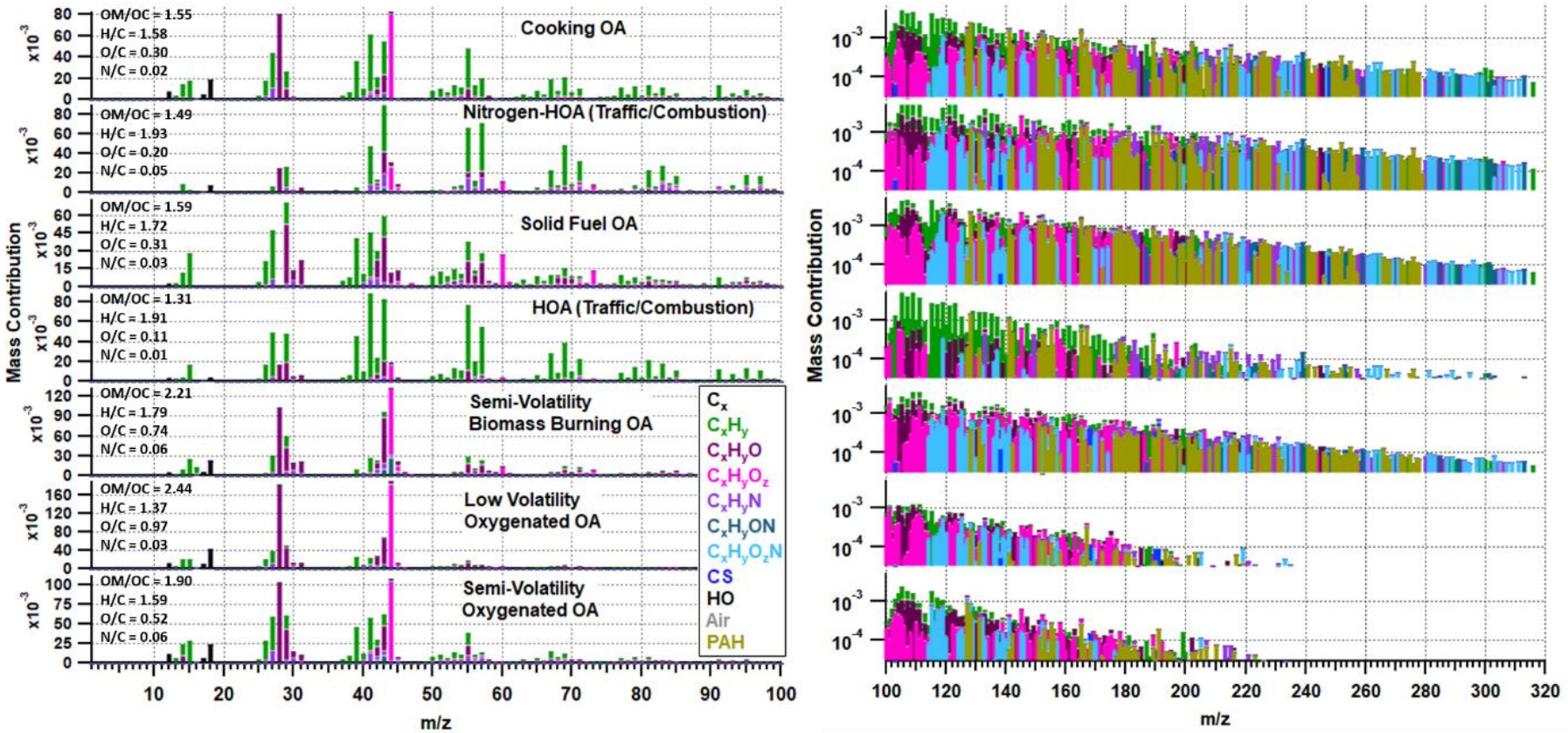

Figure 2.6. Organic-only PMF solution with elemental ratios shown for each factor in the left-hand corner of each spectrum. The mass spectra on the left show *m/z* 12-100 on a linear scale, while the spectra to the right show *m/z* 100-320 on a logarithmic scale. The peaks are coloured based on the chemical families shown in the legend.

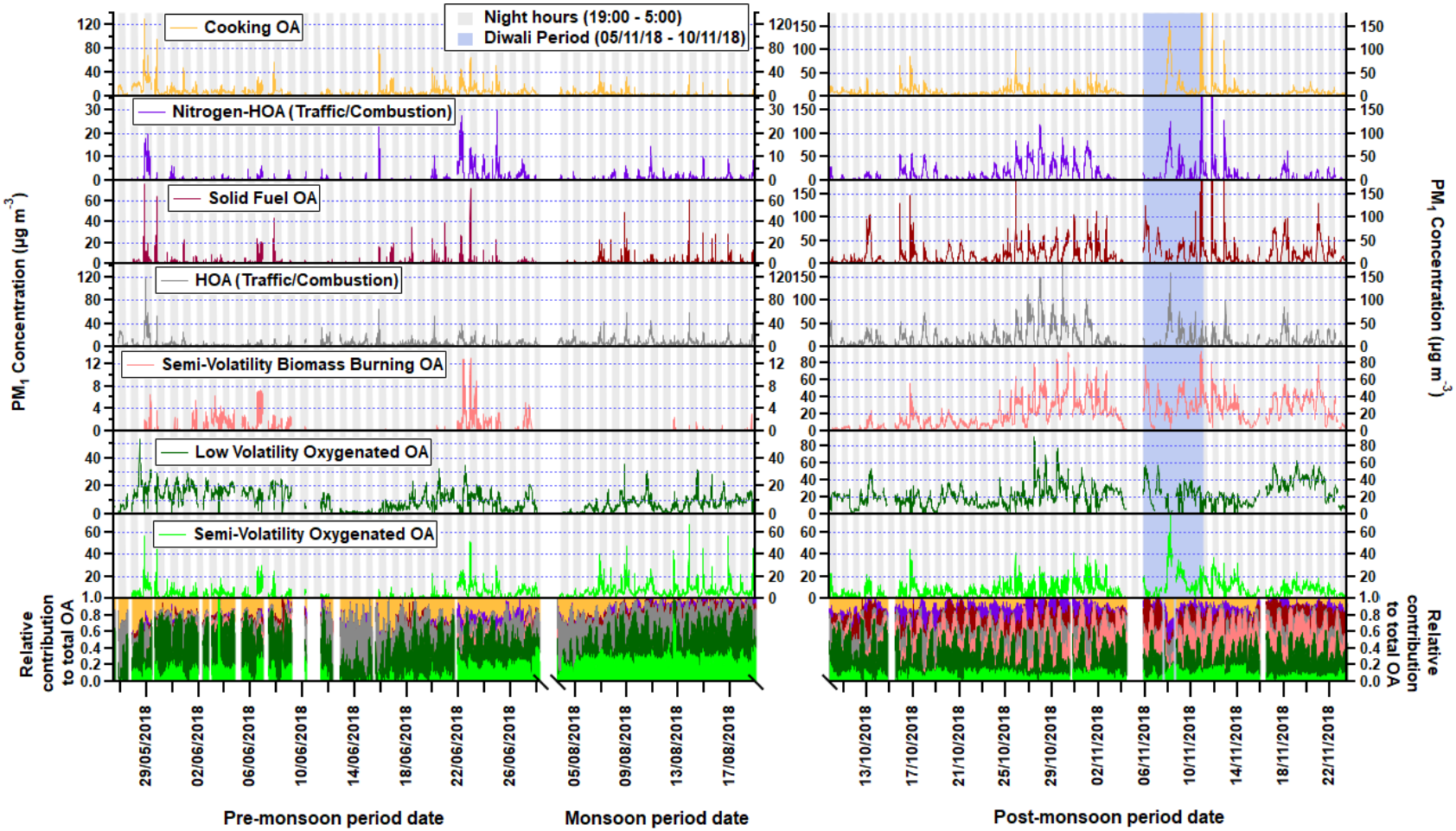

Figure 2.7. Time series for each factor where the x-axis is broken to show each measurement period. Regions shaded in grey are night hours and the Diwali period is shaded in light blue. The time series of the normalised concentrations are also shown in the bottom section of the graph

The 7-factor organic solution includes two hydrocarbon-like organic aerosol (HOA) factors relating to traffic, where one contains more nitrogen (NHOA) and is characterised by a larger contribution from higher *m/z* ions including PAHs (see below). Such N-rich HOA factors are rarely reported in the literature, but it was a persistent feature in our PMF sensitivity studies (see SI Section S2.2). There are also two burning related factors separated mainly by their oxygenation and source origin, which we interpret to reflect primary solid fuel organic aerosol (SFOA) and a semi-volatility biomass burning organic aerosol (SVBBOA), also on the basis of the correlation with regional fire counts (see Section 2.5.3 below). A cooking organic aerosol (COA) factor is also resolved along with two oxygenated organic aerosol factors (OOA) which are separated based on their volatility: low-volatility OOA (LVOOA) and semi-volatility OOA (SVOOA). Using multilinear regressions, the traffic and burning factors were determined to better correlate with external tracers when separated (see SI Section S2.2). This is further supported by a PMF study on PTR-MS measurements taken in Delhi which also resolved two traffic and two burning factors (Wang et al., 2020). A summary of the Pearson's *r* correlation coefficients for the combined and separated factors are shown in Table S2.4.

2.4.3.1. Hydrocarbon-like organic aerosol (HOA)

Both HOA and NHOA have characteristically large peaks at 55 and 57 *m/z* along with little evidence of oxidation (Figure 2.6). Their H:C values are the highest amongst the identified factors and they have the strongest correlations with measurements of BC, CO and NO_x (Figure 2.8). The diurnal cycle for both factors shows a clear peak in the evening when traffic is busy (Figure 2.9). The two factors are therefore assigned as traffic sources which is supported by strong correlations with co-located measurements of benzene, toluene and ethylbenzene, which are commonly used as tracers for traffic emissions (Slowik et al., 2010; Crippa et al., 2013).

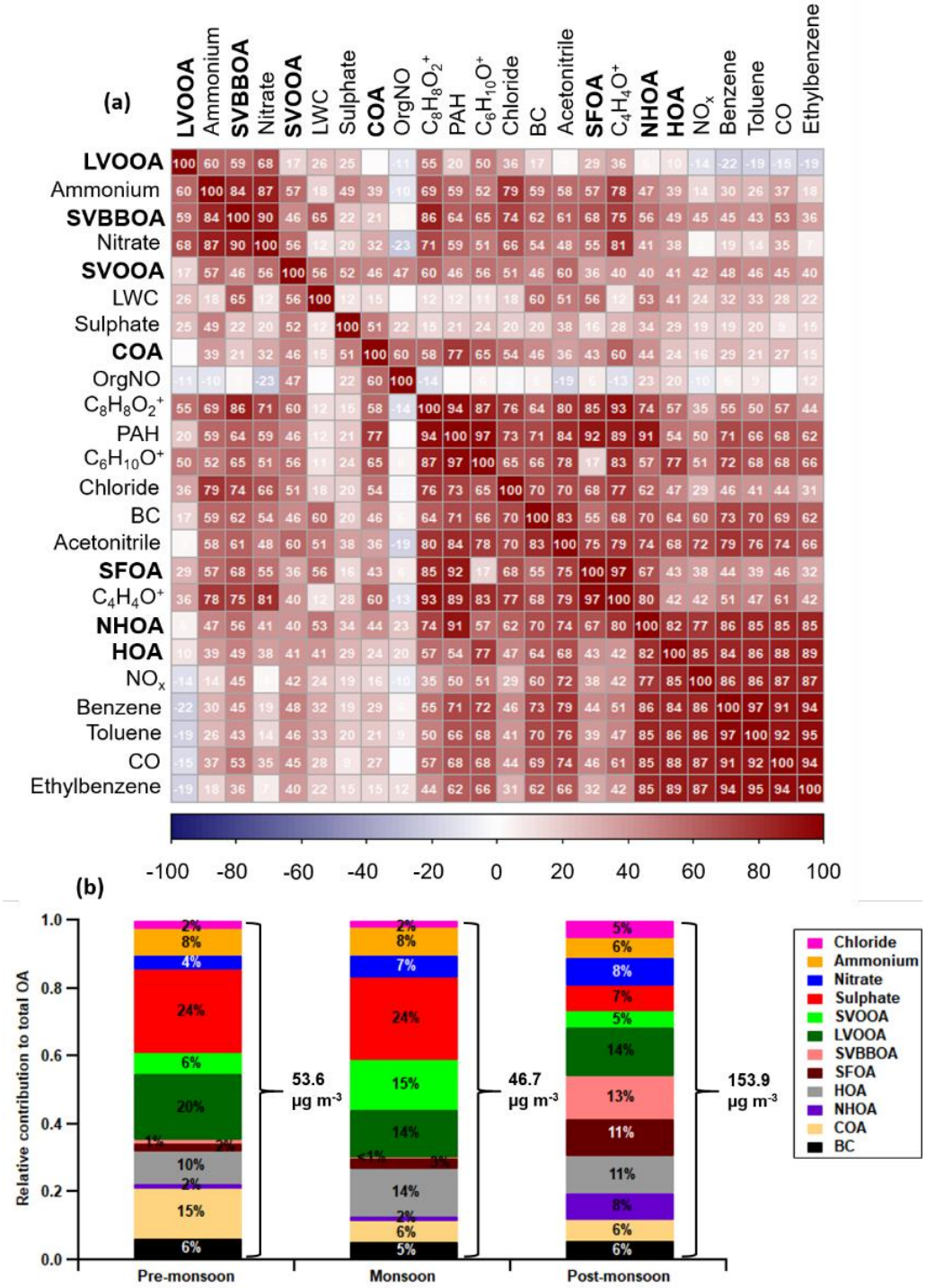

Figure 2.8. Correlation matrix (a) between the AMS OA factors (bold), internal tracers and external tracers for the combined dataset (all seasons). The correlation coefficients are ordered using hierarchical cluster analysis. The relative contribution of OA factors, BC and inorganic species to total PM_1 for each period (b) where the total average PM_1 is shown using right curly brackets (see Table S2.5 for values and statistics). The three ions $[C_6H_{10}O]^+$, $[C_8H_8O_2]^+$ and $[C_4H_4O]^+$ are, respectively: an organic acid fragment used for COA determination, a fragment of dibenzodioxin called benzodioxan and a fragment of dibenzofuran called furan.

From Figure 2.10, a large fraction of HOA mass follows a south westerly wind which points towards a nearby train station ~0.5 km from the measurement site. There is also a preference for westerly and north westerly winds which coincide with busy motorway intersections (~0.1 km and ~0.7 km). NHOA shows a similar preference for both the north-west and south-west however, there is a much larger spread of mass between wind directions. A larger spread for NHOA when compared to HOA could suggest that atmospheric processing is occurring as both have similar traffic origins. NHOA could, therefore, be a result of aged or oxidised traffic emissions allowing it to be transported further and causing a mixture of wind directional preferences.

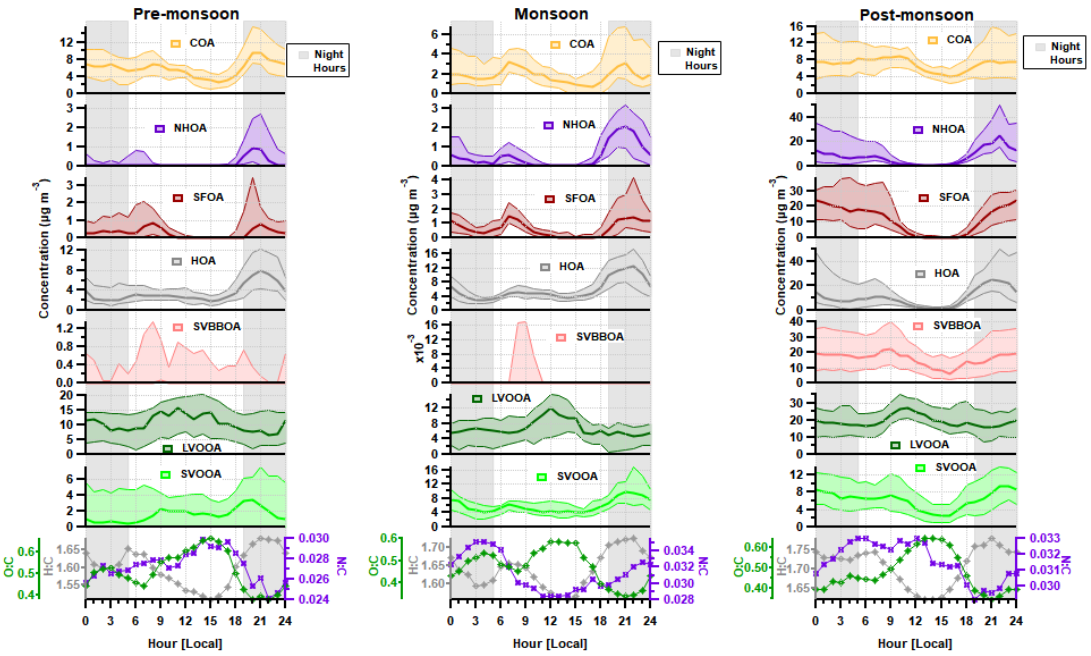

Figure 2.9. Median diurnal cycles of the factor solutions for the three measurement periods (interquartile range indicated by the shading) along with the elemental ratios. Regions shaded in grey are night hours.

One of the main compositional differences between NHOA and HOA is a higher nitrogen content in NHOA which is evident in the mass profiles (Figure

2.6). Peaks at *m/z* 41 ($[C_2H_3N]^+$), *m/z* 43 ($[C_2H_5N]^+$), *m/z* 55 ($[C_3H_5N]^+$), *m/z* 57 ($[C_3H_7N]^+$), *m/z* 83 ($[C_5H_9N]^+$), *m/z* 97 ($[C_6H_{11}N]^+$), are all prominent in NHOA but not in HOA. The PAH content of NHOA and HOA is also very different, with the fraction of PAHs within NHOA being high at 3.17 % compared with HOA at 1.00 %. The chemical functionality of the PAH fraction within each factor is shown in Figure 2.11. The NHOA factor contributes the highest relative amounts of amino PAHs (APAH) and nitrogen-oxygen substituted PAHs (NOPAH) which coincides with this factor containing more nitrogen. NHOA also has the second highest relative concentrations of oxidised PAH (OPAH), after SFOA. A large percentage of OPAH mass is due to the species dibenzodioxin, dibenzopyran and acenaphthoquinone (Figure S2.13). The presence of dibenzodioxin is also supported by a significant correlation with its mass spectral fragment, benzodioxan ($[C_8H_8O_2]^+$) (Pearson's r = 0.80) (Figure 2.8).

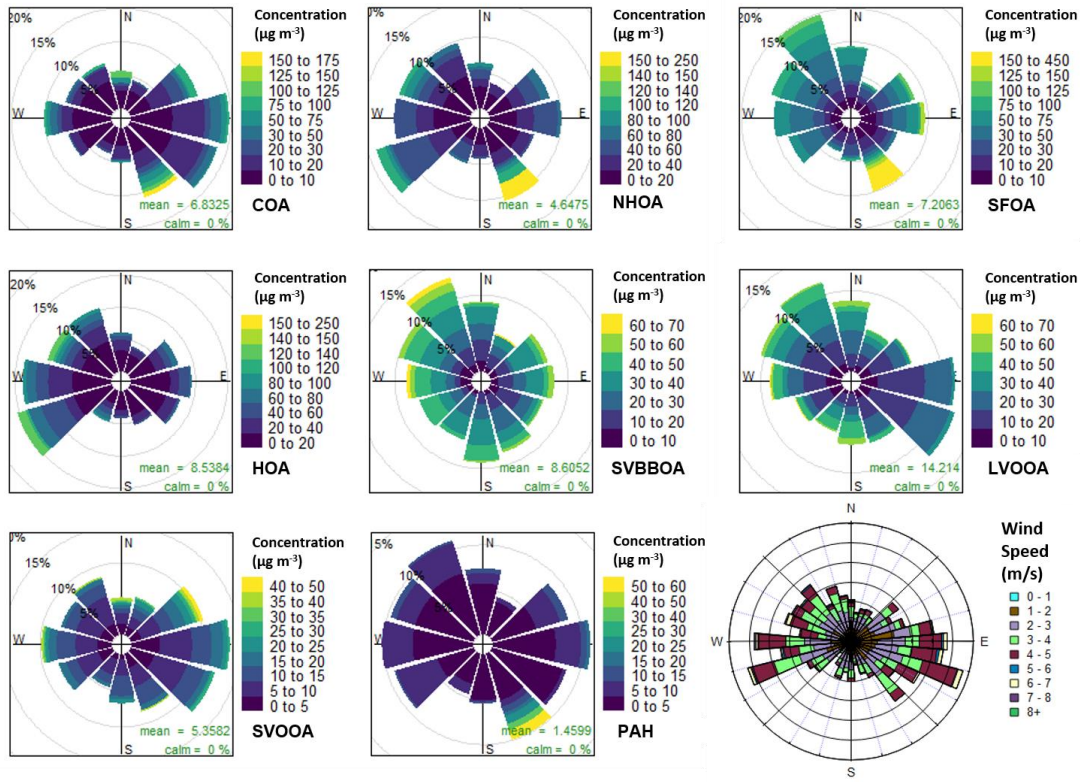

Figure 2.10. Pollution roses for each factor and uncalibrated PAH concentrations along with a wind rose. The pollution roses show 30º wind vectors and their size is proportional to the percentage contribution to the mean concentration. The vectors are divided into concentration bins based on the colour scale in the legend.

The total mass of traffic-related factors (HOA + NHOA) is the largest of the primary sources (compared with burning = SFOA + SVBBOA and cooking = COA) during the pre-monsoon and monsoon periods. It is also the joint second largest, similar to SOA (LVOOA + SVOOA), in the post-monsoon period where its average concentration reaches 29.13 µg m^{-3} (Figure 2.8).

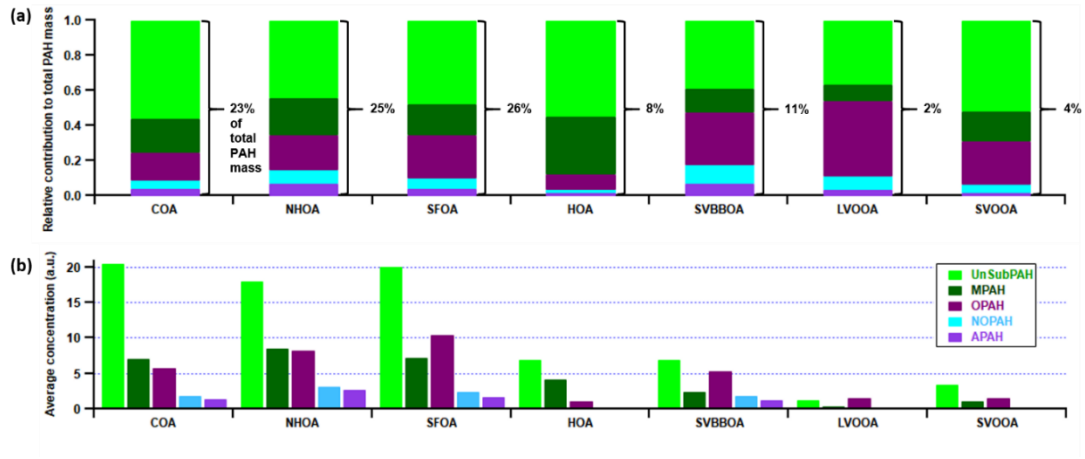

Figure 2.11. Relative contribution of PAH families to total PAH factor mass (a) and the PAH family average uncalibrated concentrations (b). The PAH families: UnSubPAH, MPAH, OPAH, NOPAH and APAH, are described within section S2.6 and in Herring et al. (2015).

2.4.3.2. Cooking organic aerosol (COA)

The COA mass profile in Figure 2.6 has a characteristically high *m/z* 55:57 nominal mass ratio (2.87) and high *m/z* 41 and 43 as seen in previous studies (Allan et al., 2010; Mohr et al., 2012; Sun et al., 2016). The COA time series also has a moderate correlation with the AMS measured $[C_6H_{10}O]^+$ peak (Pearson's $r = 0.65$) which is often used as an internal tracer for cooking related factors (Sun et al., 2016). The mass spectrum has an uncharacteristically large peak at *m/z* 44 (and the inferred *m/z* 28) and as a consequence a large O:C ratio (0.33) when compared to literature values presented in Table S2.6. There is also a deviation from literature when observing the Van Krevelen (VK) diagram in Figure S2.15 as the high O:C pulls it away from a gradient of -2 and towards a gradient of -1. This relates to a difference in composition from the normal aldehydes and ketones to carboxylic acids. The reasons for this are discussed in Section 2.5.2.

The diurnal cycle for COA has a clear morning peak across the three periods but it is hard to interpret the midday dynamics because of the pronounced boundary layer effect, whereas in other studies there is a clear lunchtime peak

(Figure 2.9). There is a slight rise in the median at 12 p.m. for the pre-monsoon and monsoon periods but the post-monsoon period shows a more defined lunchtime peak and supports this factor being related to cooking activities.

The wind rose for COA (Figure 2.10) is one of the few factors to have a clear pattern and shows that the majority of its mass is coming from the north-east, east and south-east. This is likely from food kiosks, shelters and vendors situated outside the grounds of IGDTUW. The polar graph shows a spread of large peaks matching a northerly wind (Figure S2.10) which coincides with the location of shared student kitchens at IGDTUW. The same observations were made by a study measuring n-alkanoic acids at IGDTUW (Gadi et al., 2019). The polar graph also shows maximum concentrations coincide with a south-easterly direction (Figure S2.10h). The timing of these peaks match with maxima seen in polar graphs for PAH, SFOA and NHOA (Figure S2.10), which suggests a common source.

The COA factor accounts for 23% of the total PAH mass and has a particularly high peak at *m/z* 91 which is seen in the majority of studies with COA measurements (Mohr et al., 2012; Dall'Osto et al., 2013). The PAH composition of COA is mainly unsubstituted PAHs (UnSubPAHs) and also contributes the largest amount of UnSubPAHs out of all factors (Figure 2.11). Its defining peaks described in Section S2.6 are similar to species seen in literature linked to cooking activities, although it is shown that they largely depend on the fuel used such as, dung cake, wood, etc. (Singh et al., 2010, 2016; Masih et al., 2012; Shivani et al., 2019).

The largest percentage mass contribution of COA to total OA was during the pre-monsoon period (15%) which equates to an average concentration of 7.84 μg m^{-3}. There was a relatively small (22%) increase to 9.60 μg m^{-3} in the post-monsoon, the lowest relative increase out of all factors and aerosol species (Figure 2.8). This suggests cooking activities were relatively consistent throughout the year. The monsoon period is, however, inconsistent with this

interpretation as there was a large 64% decrease in COA which is the largest percentage drop of all factors and aerosol species. This may be linked to meteorology or a decrease in outside cooking emissions as is discussed later.

2.4.3.3. Solid fuel organic aerosol and semi-volatility biomass burning organic aerosol (SFOA and SVBBOA)

The SFOA factor has a strong correlation with gas-phase acetonitrile (Pearson's *r* = 0.75) and has large peaks at *m/z* 60 and 73 which are the typical AMS biomass burning tracers (Weimer et al., 2008). SVBBOA shares the same peaks at *m/z* 60 and 73; however, it has a weaker correlation with acetonitrile (Pearson's *r* = 0.61). This may be due to the level of oxidation within SVBBOA as its mass spectrum has a large peak at *m/z* 44 (and consequently *m/z* 28), showing evidence that the aerosol is aged.

The O:C ratio for SVBBOA is relatively high (O:C = 0.74) and fits between the ratios for LVOOA and SVOOA (Figure 2.6) suggesting it is secondary in nature. This is consistent with the VK diagram in Figure S2.15 which shows SVBBOA lies between the oxidation states ($\overline{OS_C}$) of -1 and 0, typically where LVOOA and SVOOA literature values overlap. SVBBOA also appears to be closer to the alcohol functional group gradient (*m* = 0) which may explain the high correlation with LWC (Pearson's *r* = 0.65) due to alcohol functionalised compounds being more water-soluble. Additionally, SVBBOA has a particularly high N:C value (0.06) and has prominent $C_xH_yN_zO_t$ peaks which show similarities to primary amides through mass spectral comparisons described in Section S2.5. This shows SVBBOA has a complex composition of oxidised species.

The lower volatility of SVBBOA is also evident in its post-monsoon diurnal cycle as it is less affected in the afternoon by the temperature and boundary layer changes that appear to affect primary emitting factors significantly (Figure 2.9). SFOA however has more defined peaks in the morning and

evening, which is consistent with its aliphatic mass spectral composition, indicating it is fresh primary organic aerosol.

The pollution rose for SFOA shows the majority of its mass originates from the north-west but high concentrations also originate from the east and south-east (Figure 2.10). This can be seen more clearly in Figure S2.10 showing large peaks in SFOA originating from the south-east and east. These observations coincide with a large cremation site located east along the Yamuna River (~500 – 750 m) which likely contributes to SFOA mass (Figure S2.16). Conversely, SVBBOA mass shows a slight preference for a westerly and north westerly wind but overall, there is a larger spread. This further supports that SVBBOA is more secondary in origin.

SFOA and SVBBOA have the strongest correlations with chloride (Pearson's r = 0.68 and 0.74, respectively) which suggests they have an affinity with chloride sources (Figure 2.8). The application of the second PMF analysis where inorganic AMS measurements were combined with the organic matrix (SI Section S2.10) resulted in a biomass burning factor which included the majority of the ammonium chloride mass (Figure S2.17). Additionally, SVBBOA has the strongest correlations with ammonium and nitrate, out of all factors (Pearson's r = 0.84 and 0.90, respectively). These results suggest that the high levels of ammonium nitrate, and particularly ammonium chloride, in the post-monsoon are associated with SVBBOA.

SFOA and SVBBOA have substantially different correlations with PAHs (Pearson's r = 0.92 and 0.64, respectively). In fact, SFOA has the greatest contribution from PAHs (3.3 %) and contributes 26% to the total PAH mass (Figure 2.11). A large portion of its PAH mass is OPAH and the same is seen for SVBBOA. They both also have prominent UnSubPAHs, however, SFOA has a larger naphthalene (*m/z* 127 and 128) content (Figure S2.13). This is also seen in the PTR-QiTOF-MS correlation mass spectrum where SFOA has

a significantly stronger correlation with VOC furan and naphthalene when compared to SVBBOA (Figure S2.14).

One of the strongest correlations of AMS ions with SFOA (Figure S2.14) is the dibenzodioxin fragment, benzodioxan $[C_8H_8O_2]^+$, and this coincides with high correlations with furan ($[C_4H_4O]^+$) and chloride (Figure 2.8) which indicates SFOA may have a strong association with polychlorinated dibenzo-furans (PCDF) and -dioxins (PCDD).

The two factors SFOA and SVBBOA represent the overall burning-related aerosol. During the pre-monsoon and monsoon periods they are low in concentration and contribute ~3% to the total organic aerosol mass (Figure 2.8). During the post-monsoon, however, they combine to contribute 24% to the organic aerosol mass. The largest contributor of the two being SVBBOA at ~13% of total PM_1 mass, equivalent to ~19.6 µg m^{-3}. This increase means burning-related aerosol is the largest single contributor to the observed organic aerosol mass during the post-monsoon.

2.4.3.4. Semi-volatility oxygenated organic aerosol and low-volatility oxygenated organic aerosol (SVOOA and LVOOA)

LVOOA and SVOOA are separated based on their volatility and oxygenation and serve as proxies for aged and less aged secondary organic aerosol (SOA) (Jimenez et al., 2009). The large peak at *m/z* 44 in LVOOA (Figure 2.6) implies a high level of oxygenation which coincides with the highest O:C ratio (0.97) out of the resolved factors. It is also the only factor that consistently peaks in the afternoon, defying the pronounced boundary layer effect, demonstrating that it is low in volatility and forms through photochemistry (Figure 2.9). This is further supported by overall poor correlations with the PTR-QiTOF-MS mass spectrum, where its strongest correlations are mostly with $C_xH_yO_x$ family VOC species, such as methyl glyoxal and methacrolein (Figure S2.14). SVOOA has slightly stronger correlations with VOCs but the majority are still comparatively

poor (Pearson's $r < 0.6$). The strongest correlations are with ions from the $C_xH_yN_x$ and $C_xH_yN_xO_t$ families which coincides with SVOOA having the second strongest correlation with OrgNO however, it is very low (Pearson's $r = 0.47$).

There is also a substantial drop in LVOOA concentrations in the monsoon period, suggesting a decrease in light due to cloud cover could be responsible or increased washout from rainfall (Figure 2.8). In contrast, SVOOA increases significantly during this period which may be caused by the increase in relative humidity and LWC leading to increased aqueous-phase aerosol uptake. This is supported by SVOOA having the second strongest correlation with liquid water content (LWC), after SVBBOA for the combined dataset (all seasons) (Pearson's $r = 0.56$). Furthermore, it has the strongest correlation out of all factors with LWC during the monsoon (Pearson's *r* for: COA = 0.27, NHOA = 0.02, SFOA = 0.42, HOA = 0.04, SVBBOA = -0.07, LVOOA = 0.24 and SVOOA = 0.49).

Both SVOOA and LVOOA have the lowest PAH content and their PAH mass spectra are a mixture of peaks also seen in factors corresponding to primary aerosol composition. LVOOA is more oxygenated and has a large benzofuran peak (*m/z* 167), along with a naphthoquinone peak (*m/z* 158) which distinguishes it from the other factors. SVOOA conversely has a mixture of peaks seen in most primary factors but the difference is a particularly large amount of naphthalene (*m/z* 127 and 128).

The sum of LVOOA and SVOOA is considered the total PM_1-SOA and when compared to the total primary OA (POA = HOA + NHOA + SFOA + SVBBOA + BC), it is lower in concentration during all periods (Figure 2.8).

2.4.4. Elemental analysis

The measurements of elemental ratios are shown in Figure 2.12 where the VK diagram for each period can be used to determine the level of oxidation and chemical functionalisation within the aerosol composition. Here, there is a

similar aerosol composition between the pre-monsoon and monsoon periods which is a consistent theme throughout these analyses. There are however slight differences in gradient where the data for the pre-monsoon mainly falls across a gradient of -1. This equates to an increase in carboxylic acid or a simultaneous increase in carbonyl and alcohol functional groups. The formation of photooxidation products likely explains this because concentrations of LVOOA are particularly high (Section 2.4.3.4). The pre-monsoon has periods of low carbon oxidation states ($\overline{OS}_C$) which can be explained by simultaneous low concentrations in SOA and high primary OA concentrations. For example, the period ~12/06/18-16/06/18 relates to low concentrations in both SVOOA and LVOOA and high concentrations in HOA (Figure 2.7). There is also evidence of higher concentrations of aged aerosol during the pre-monsoon as higher carbon oxidation states ($\overline{OS}_C$) are observed. This shows higher levels of aging and oxygenation which is likely due to photochemistry (Heald et al., 2010). During the start of the monsoon, the data falls on a gradient of -1 but it gradually increases to a gradient which is similar to the post-monsoon. This shift is most likely due to the increase in SVOOA which suggests it is composed of alcohol and peroxide functionalities. The same can be said for the post-monsoon where the gradient increase will likely be due to the influence of SVBBOA and SVOOA.

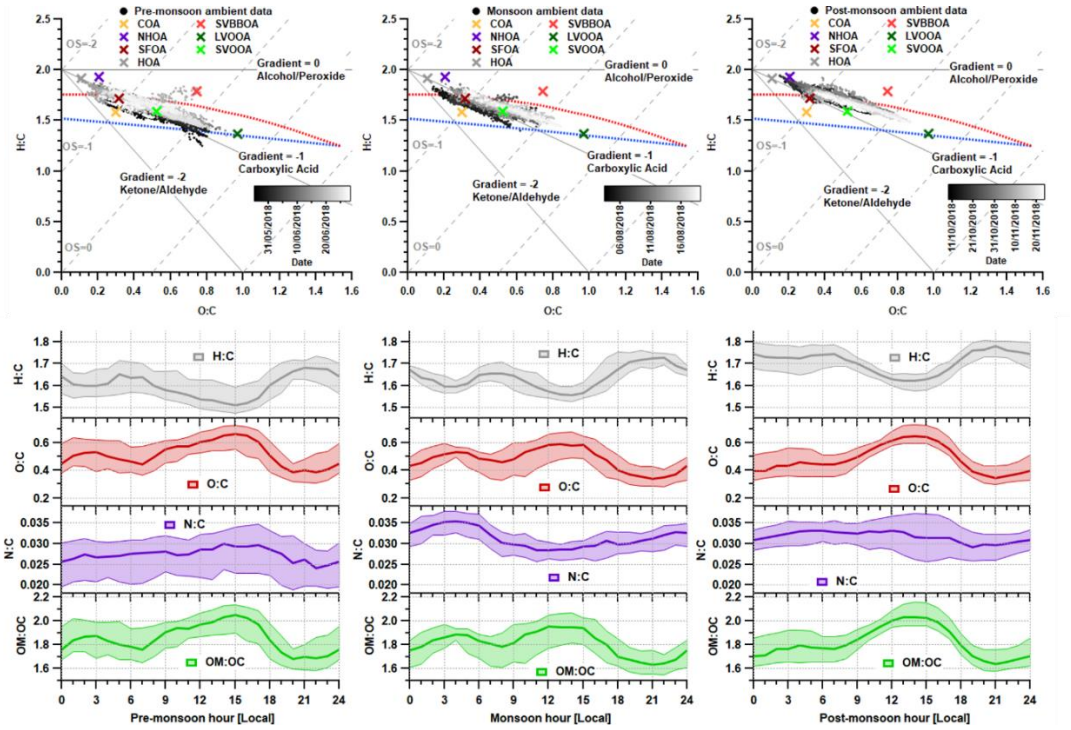

Figure 2.12. Van Krevelen (VK) diagrams and median diurnal cycles for elemental ratios during each measurement period. Each VK diagram contains the H:C vs O:C data for the PMF solutions and the raw AMS measurements which are coloured based on the time of the measurement. The carbon oxidation states ($\overline{OS}_C \approx 2O/C - H/C$) are shown using grey dashed lines and the functional group gradients are shown using solid grey lines. The blue and red dashed lines demarcate the region where published ambient OOA measurements are commonly found (Ng et al., 2011).

The diurnal profile for H:C almost perfectly mirrors that of O:C and follows the primary factors (HOA, NHOA and SFOA) for all three measurement periods (Figure 2.9 and Figure 2.12). The N:C however is highly variable across the three periods with significant changes in its diurnal pattern. During the pre-monsoon, nitrogen is mainly within the SOA fraction as the N:C ratio follows the O:C ratio in the diurnal cycle and peaks in the afternoon with LVOOA (Figure 2.12). This changes during the monsoon period as there is an early morning (00:00 – 06:00) peak in N:C. This simultaneous increase in N:C and O:C may suggest that dark oxidation via nitrate radicals is occurring. This is supported by the OrgNO diurnal cycle for the monsoon (Figure S2.20) which shows a small rise in the interquartile range during the morning hours (00:00-07:00) and could tentatively be linked to the same rise in N:C. There is also an

increase in LVOOA during these hours showing that it is composed of dark oxidation products. A small rise in N:C is also seen during the morning of the post-monsoon however, this is likely flattened due to the large increases in N-rich factor concentrations, such as NHOA and SVBBOA (Figure 2.9).

2.5. Discussion

2.5.1. Traffic sources: the existence of nitrile compounds and the separation of NHOA and HOA based on fuel type

The existence of nitrile compounds (R-C≡N) within NHOA is evident through mass spectral comparisons as explained in Section S2.5. VOC measurements also support this observation as the graph in Figure S2.14 shows correlations between PTR-QiTOF-MS measurements of $C_xH_yN_z$ species and PMF factors. Several of these species have previously been identified as nitrile compounds by Brilli et al. (2014). These species have a stronger correlation with NHOA over all factors which suggests possible partitioning of nitrile VOCs into the particle phase or vice versa. These compounds have not been identified in published AMS spectra; however, many have published amine peaks within factors. Most studies name these factors nitrogen organic aerosol (NOA) however, some relate to specific local organic aerosol (LOA) (Aiken et al., 2009; Docherty et al., 2011; Sun et al., 2011; Saarikoski et al., 2012; Hayes et al., 2013; Bottenus et al., 2018; Zhang et al., 2018). The main difference between Delhi measured NHOA and literature NOA (or LOA) is the absence of even *m/z* amine peaks in NHOA such as *m/z* 56 ($[C_3H_6N]^+$), *m/z* 58 ($[C_3H_8N]^+$), and *m/z* 84 ($[C_5H_{10}N]^+$). The Van Krevelen (VK) diagram in Figure S2.15 shows four examples of, what is collectively termed here as NOA, and shows a large variety of elemental compositions. Most studies relate the amine content to secondary sources or specific local sources. Ye et al. (2017) report a NHOA factor which they suggest is also composed of amines however they state this is inconsistent with their findings that NHOA was related to fossil fuel combustion. The NHOA factor they measured is the closest factor within the

VK diagram to NHOA measured in Delhi. They also measured similar odd nitrogen *m/z* peaks at 41 ($[C_2H_3N]^+$), 43 ($[C_2H_5N]^+$), 55 ($[C_3H_5N]^+$) and 57 ($[C_3H_7N]^+$) and it is therefore suggested that this factor may also contain nitrile compounds.

Nitrile compounds within PM are usually considered a sign of nitrogen-rich fuel combustion and these findings provide useful tracers for biomass burning such as acetonitrile (Simoneit et al., 2003; Weimer et al., 2008). However, there appear to be no publications reporting ambient atmospheric nitriles being linked to traffic sources. High molecular weight nitrile compounds with 7 to 22 carbon atoms (C_7-C_{22}) have been measured during high emission episodes of ammonia and 'fatty carboxylic' or alkanoic acids (Abas et al., 2004; Ozel et al., 2010; Simoneit et al., 2003). These observations are supported by laboratory studies which show atmospheric ammonia and alkanoic acids react to form alkyl cyanides via an amide intermediate (Simoneit et al., 2003; Zhao et al., 2009). The characteristically high ammonia concentrations in Delhi could therefore make this a viable reaction pathway (Saraswati et al., 2018; Nakoudi et al., 2019).

Studies that have measured C_9-C_{30} alkanoic acids suggest they originate from fossil fuel combustion, biomass burning, cooking and microbial activities (Abas et al., 2004; Kang et al., 2016; Gupta et al., 2018; Gadi et al., 2019). A substantial amount has been shown to be emitted from diesel engines where the majority originates from the engine lubricant (Lim et al., 2015). Emissions also increase with the use of biodiesel which is becoming a common fuel-type in Delhi (Cheung et al., 2010). Two previous studies measured PM_{10} composition at IGDTUW and found a large fraction of the organic aerosol is composed of n-alkanoic acids (Gupta et al., 2018; Gadi et al., 2019). They suggest that cooking and traffic emissions influence the n-alkanoic acid abundance and their concentrations are higher during the post-monsoon and winter months. This is a similar trend to NHOA and there are numerous studies which show traffic to be a large source of ammonia emissions in Delhi, different

cities in India, and in different cities worldwide (Sharma et al., 2014; Sun et al., 2017; Elser et al., 2018; Saraswati et al., 2018). It is therefore possible that the nitrile compounds within NHOA are formed through the reaction of alkanoic acids and ammonia.

The large differences in the PAH composition of NHOA and HOA described in Section 2.4.3.1 is a key characteristic which separates these two traffic factors. From the *m/z* 100-320 mass spectra in Figure 2.6, it is clear that masses are much higher in the later part of the NHOA spectrum than for HOA. These include (but are not restricted to) higher molecular weight UnSubPAHs and methyl-substituted PAHs (MPAHs) (Figure 2.11) and these are diagnostic markers for a diesel source (Singh et al., 2010). This suggests that HOA may originate from less dense traffic fuel types that have much lower aromatic content such as gasoline and compressed natural gas (CNG). What weakens this hypothesis is the absence of NHOA in the pre-monsoon and monsoon periods as diesel vehicles and trains are in operation throughout the year, although the additional contribution from diesel generators may vary throughout the year. This could, therefore, suggest NHOA is influenced by meteorology and forms during favourable conditions for aerosol partitioning in the post-monsoon. These conditions allow for the partitioning of more volatile fractions of NHOA, such as the nitriles. Diesel vehicles are not normally permitted on the roads directly adjacent to the measurement site. Thus, the low boundary layer post-monsoon may also result in more efficient advection and build-up of diesel emissions to the measurement site at low height, whilst emissions may be more efficiently dispersed during the other seasons.

Similar UnSubPAH and MPAH species in NHOA have been observed in laboratory studies measuring PAHs from diesel engines, but the ratios of these species largely depends on the mix of biodiesel and the running conditions of the engine (He et al., 2010; Tsai et al., 2011; Zheng et al., 2017). There is, however, a study which took place in Taj, India, which measured both indoor and outdoor PAH concentrations in homes along roadsides or in residential

areas. Through principal component analysis, the authors were able to separate factors based on different fuel types (Masih et al., 2012). At all measurement sites, factors were resolved relating to diesel and others relating to petrol and CNG. The latter is widely used in Delhi and is mandatory for public transport vehicles (taxis, moto-rickshaws). The diesel-related factors were high in acenaphthylene (*m/z* 151 and 152), acenaphthene (*m/z* 153 and 154), fluorene (*m/z* 165), anthracene and phenanthrene (*m/z* 178) and, carbazole (*m/z* 216 and 217), which is consistent with NHOA. The petrol and CNG-related factors were also consistent with HOA where methyl-naphthalene (*m/z* 141 and 142) and dimethyl-naphthalene (*m/z* 155 and 156) were particularly high and these are the distinguishing peaks in the PAH spectrum for HOA. The evidence gathered therefore suggests that NHOA and HOA are separated based on fuel-type, where NHOA is influenced by diesel emissions and HOA by gasoline and compressed natural gas. The separation of factors based on fuel-type is not often observed due to the almost identical diurnal patterns they often share. In Delhi however, this separation is most likely possible due to the restrictions of heavy goods vehicles during the day (07:00-23:00) which increases diesel emissions at night.

There is a strong correlation between NHOA and the dibenzodioxin fragment ion, benzodioxan ($[C_8H_8O_2]^+$) (Pearson's r = 0.80), and this is consistent with dibenzodioxin peaks seen in its PAH spectrum (Figure S2.13). There is also a mild correlation with chloride (Pearson's r = 0.62) which could be explained by the presence of polychlorinated dibenzodioxins (PCDD). It is well known that diesel combustion is a source of PCDDs and therefore could be a form of organic chloride associated with NHOA (Laroo et al., 2012; Wang et al., 2012). However, NHOA could also be similar in volatility to ammonium chloride which could also explain this.

Traffic-related organic aerosol (NHOA+HOA) amounts to the largest primary source of PM_1 across the pre-monsoon and monsoon periods (Figure 2.8). It is also the joint second highest source (with SOA) during the post-monsoon

period which suggest that a reduction in its emissions will result in a drop in PM_1 organic aerosol across the majority of the year. This conclusion is consistent with the analysis of unit mass resolution measurements from this and other AMS instruments operated in Delhi (Reyes-Villegas et al., 2020), which also found traffic to be the largest contributor to PM_1. Targeting emissions from traffic can therefore be viewed as the highest priority when developing air quality mitigation strategies for PM_1, especially considering that traffic sources also supply some of the precursor gases for the formation of the SOA components.

2.5.2. Sources of cooking activities and their link to OrgNO

The COA time series has a moderate correlation with the AMS measured $[C_6H_{10}O]^+$ peak (Pearson's r = 0.65) which is often used as an internal tracer for cooking related factors (Sun et al., 2016). This tracer has previously been used on AMS measurements taken in Western and East Asian countries. The reason for the reduced correlation in this study may be a difference in the style of cooking in Delhi and/or the contribution of other sources to this peak. Western and East Asian cooking is shown to produce short-chained organic acids through rapid and shallow frying (Reyes-Villegas et al., 2018a). In Delhi, however, food is generally cooked on a low heat and over a longer period of time. It is therefore hypothesised that longer-chained oxygenated fatty acids are associated with cooking activities in Delhi. This is supported by measurements taken at IGDTUW showing long-chained fatty acids being linked to cooking sources (Gupta et al., 2018; Gadi et al., 2019).

This difference in cooking style might also explain why the mass spectrum has an uncharacteristically large peak at *m/z* 44 $[CO_2]^+$ which is considered to be mainly due to carboxylic acid groups (Duplissy et al., 2011; Ng et al., 2011). Long-chains of C_xH_y atoms along with an increased number of –COOH groups fragment in the AMS resulting in mainly aliphatic ions and increased *m/z* 44. As a result, the COA factor has a particularly large O:C ratio (0.33) when compared to literature values (Table S2.6) which pulls it towards a carboxylic

acid composition gradient on the VK diagram in Figure S2.15. Additionally, some of the strongest correlations of VOCs with COA in the lower *m/z* part of the PTR-QiTOF-MS spectrum relate to the $C_xH_yN_z$ and $C_xH_yO_z$ families (Figure S2.14). These observations also support COA being composed of long-chained carboxylic acids and could also suggest that COA is influenced by the oxidation of organic acid VOCs.

The $C_xH_yN_zO_t$ family in both the AMS (*m/z* 210-300) and PTR-QiTOF-MS (*m/z* 120-210) correlation mass spectra are most closely correlated with COA (Figure S2.14). This coincides with the OrgNO having the strongest correlation with COA (Pearson's $r = 0.60$), out of all PMF factors (Figure 2.8). Furthermore, the COA spectrum for the inorg-org combined PMF solution shows a large NO^+ (*m/z* 30) peak with no associated ammonium peaks which implies the nitrate is organic (Figure S2.17). The evidence gathered, therefore suggests emissions associated with food preparation in Delhi is nitrogen rich and contributes the most to OrgNO concentrations. The presence of N-containing aromatic compounds (NACs) in $PM_{2.5}$ from wood and charcoal fuelled cooking stoves has also recently been measured experimentally (Xie et al., 2020). Again, the majority of the NACs identified in these measurements were of the $C_xH_yN_zO_t$ family. COA could also be influenced by the emissions of fuels used for food preparation as this would correlate highly in space and time. Äijälä et al. (2017) published a similar COA spectrum containing high *m/z* 44 (and *m/z* 28) peaks and found their measured COA is influenced by biomass burning. This could also be true for Delhi as residents, roadside stalls and restaurants (e.g. Dhabas) cook on open fire pits using fuels such as wood and dung cakes, and would explain a mixed factor profile of COA with BBOA influence.

The strong association of PAHs with cooking activities is well established and is an important component of cooking aerosol to consider due to its carcinogenicity (Svedahl, 2018; Lin et al., 2019). COA has a particularly high peak at *m/z* 91 (Figure 2.6) which is seen in the majority of studies with COA measurements but is not often highlighted (Mohr et al., 2012; Dall'Osto et al.,

2013). The fragment ion responsible is $[C_7H_7]^+$ and is observed when measuring PAHs (McLafferty and Turecek, 1993). It is also one of five AMS measured PAH fragment ions ($[C_6H_6]^+$, $[C_9H_9]^+$, $[C_{10}H_9]^+$ and $[C_{11}H_9]^+$) that give some of the highest correlations with COA in the AMS correlation mass spectra (Figure S2.14). This is consistent with the PAH composition of COA which is mainly UnSubPAHs (Figure 2.11) and shows that UnSubPAHs are a defining part of a COA signature. As the COA spectrum has strong similarities with SVOOA spectra (due to *m/z* 44), it's high PAH composition could help future studies. For AMS measurements in Delhi, *m/z* 91 could be a useful indicator of COA along with the *m/z* 55:57 ratio for studies that do not quantify *m/z* >120.

Unlike other source factors, COA does not significantly increase in concentration during the post-monsoon (Figure 2.8). Cooking activities are therefore relatively constant across the year in Old Delhi although there is a substantial drop in COA during the monsoon. This is likely because of the increased rainfall and RH (monsoon average ~76 %) causing increased rates of below cloud scavenging or washout. The propensity of this happening to COA over other organic aerosol could be down to composition as its high fatty acid content will increase its hygroscopicity, making it more likely to be scavenged. This could explain the reason for the low correlation with LWC (Pearson's r = 0.15) as an increase in water content and RH will most likely increase wet deposition. An alternate reason could simply be due to a decrease in outside cooking activity as more residents likely cook indoors to escape the rain.

2.5.3. Sources of burning

The results indicate the two burning-related PMF factors SFOA and SVBBOA are fresh and aged organic aerosol, respectively. The higher afternoon concentrations of SVBBOA and a high signal at *m/z* 44 are key indicators of its lower volatility and oxidation. This is also consistent with the analysis of AMS flux measurements taken during the post-monsoon (Di Marco et al., 2019). From the analysis, two burning factors were resolved where one had

higher emissions during the morning and evening suggesting it to be localised and a primary source. The other factor showed a lower and broader emission in the morning suggesting it is secondary. A similarly aged PMF factor to SVBBOA, named oxidised-BBOA, was also resolved from AMS measurements in Kanpur. They suggest this O-BBOA mainly formed through photochemical oxidation of primary emitted BBOA in the local area (Chakraborty et al., 2018). This may be the case in Delhi; however, there are peaks in the time series of SFOA which coincide with an absence of SVBBOA, particularly during peak photochemical conditions in the pre-monsoon (Figure 2.7). The origin of this source therefore may not be local to Delhi and instead the aerosol could have travelled from further afield.

The contribution of SVBBOA to the total PM_1 mass is insignificant during the pre-monsoon (~1%) and monsoon (~0%) periods. However, during the post-monsoon it is the second largest contributing factor (~13%) (Figure 2.8). This suggests a specific source that only occurs during the post-monsoon period. The most likely cause is large-scale crop residue burning after paddy fields are harvested in October and November which has been widely blamed for poor air quality in Delhi (Liu et al., 2018; Jethva et al., 2019; Beig et al., 2020; Mukherjee et al., 2020). In Figure 2.13, the SVBBOA time series is compared with fire counts data from the NASA Visible Infrared Imaging Radiometer Suite (VIIRS) sensor on the Suomi National Polar-orbiting Partnership (S-NPP) satellite (available at: https://earthdata.nasa.gov/earth-observation-data/near-real-time/firms, last accessed: 20/04/2021). The daily average fire counts are taken from a custom polygon of the Haryana region from which the city of Delhi itself has been removed. The strong correlation of SVBBOA with fire counts (Pearson's r = 0.73) suggests the source of this factor is mainly regional crop residue burning outside of Delhi. Whilst other factors, and particularly SFOA, also correlate significantly with the fire counts (as a result of all concentrations increasing post-monsoon), the PMF analysis identifies some SFOA but very little SVBBOA during the monsoon (Figure 2.7 and Figure 2.8). This suggests

that the distinction between SFOA and SVBBOA is fairly robust in quantifying the contribution of crop residue burning to Delhi's PM_1.

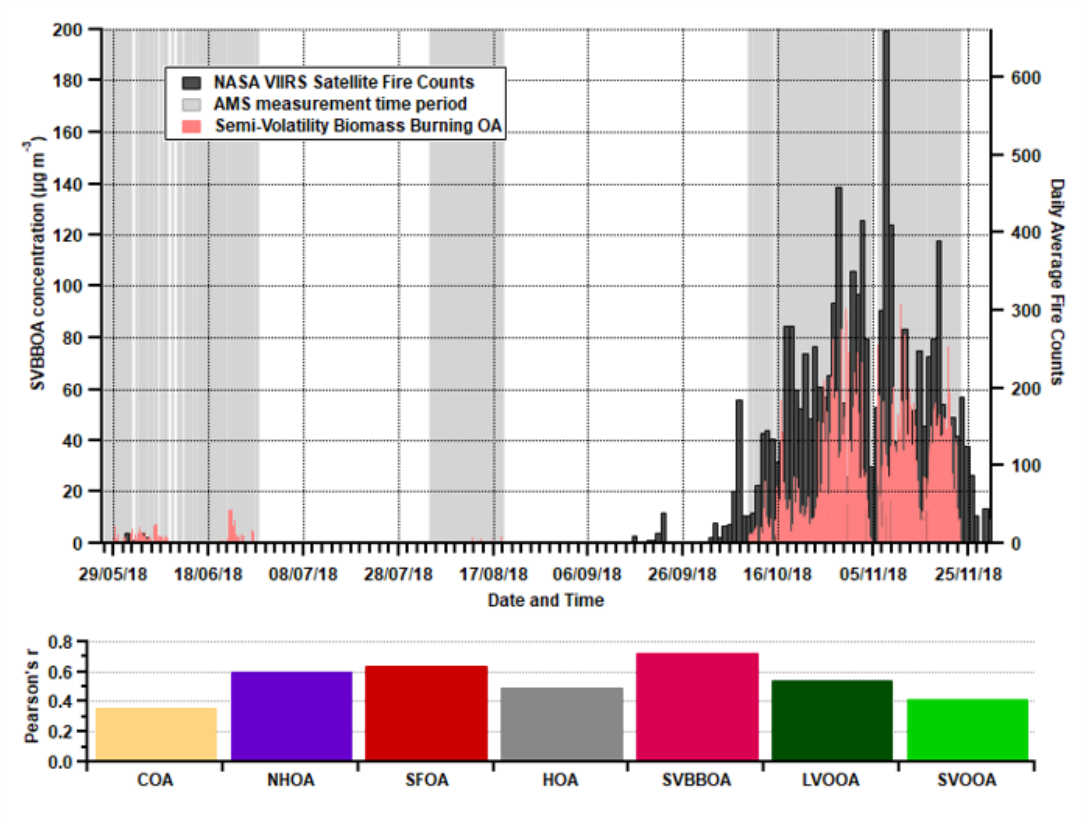

Figure 2.13. Upper panel: time series for SVBBOA along with the daily average fire counts from the NASA Visible Infrared Imaging Radiometer Suite (VIIRS) sensor on the Suomi National Polar-orbiting Partnership (S-NPP) satellite. Lower panel: Pearson's *r* correlations between daily average factor concentrations and the daily average fire counts. The VIIRS data covers all days displayed along the x-axis while the AMS measurements cover the grey shaded regions.

These findings show that crop burning is a major source of air pollution during the post-monsoon period when PM concentrations are at their highest. In 2018 a government initiative was introduced to improve air quality in Delhi by encouraging farmers outside the national capital region (NCR) to supply their agricultural waste for conversion to bioenergy (Bhuvaneshwari et al., 2019). Our measurements reveal that despite this intervention, the burning of crop

residues in the post-monsoon still accounted for ~19% of the total PM_1 increment over the pre-monsoon period. Our measurements suggest that in 2018 there was still scope for further reductions from the agricultural sector.

Studies have observed KNO_3 formation in aged smoke from biomass burning via the reaction of KCl with gaseous HNO_3 (Li et al., 2003; Wang et al., 2017). A subsequent substitution reaction with NH_3 forms NH_4NO_3 and this formation pathway could explain why SVBBOA has the strongest correlation with nitrate and ammonium (Figure 2.8). SFOA, however, is weakly correlated with nitrate which suggests it may not be linked to crop residue or wood burning. The defined morning and evening peaks in the SFOA diurnal cycle, and a less-oxidised composition shows SFOA is more likely to be linked to freshly emitted local area sources. It could, therefore, be due to municipal waste burning, which is a common practice in Delhi, particularly during the morning and evening (Nagpure et al., 2015). Municipal waste burning is also often found to produce higher PCDD and PCDF concentrations than biomass burning or traffic sources (Lavric et al., 2004; Chakraborty et al., 2013; Verma et al., 2016; Zhang et al., 2017; Stewart et al., 2020). The high dibenzodioxin and dibenzofuran peaks in the SFOA mass spectrum (Figure S2.13) coincide with strong correlations with our proposed novel-tracers for PCDDs and PCDFs, benzodioxan $[C_8H_8O_2]^+$ and furan $[C_4H_4O]^+$ (Figure 2.8). This shows SFOA has the strongest link to PCDDs and PCDFs which suggests a substantial fraction of its mass may be due to the burning of highly chlorinated municipal waste.

Although the results suggest strong links between SFOA and municipal waste burning, it is likely that this factor contains other solid fuel burning sources as well. The high correlation with acetonitrile (Figure 2.8) and mass spectral peaks at *m/z* 60 and 73 (Figure 2.6) show that SFOA includes a significant amount of organic aerosol from biomass burning. This will most likely include emissions from solid fuels such as dung cakes and wood which are used for cooking and warmth in Delhi (Sen et al., 2014; Pervez et al., 2019).

The measurement site is also positioned near large cremation grounds (~500-750 m) in the east along the Yamuna river where open funeral pyres and furnaces are used frequently. The largest of the two is directly east and coincides with frequent peaks in SFOA and PAH concentrations (Figure 2.10). Studies have shown that funeral pyres in India emit organic carbon and organic aerosol on a comparable level to transport emissions, where it was estimated to be equivalent to ~10-23% of organic aerosol mass emitted from regional fossil fuel and biofuel burning (Chakrabarty et al., 2013; Pervez et al., 2015). It is also shown that funeral pyres emit a significant amount of PAHs that are particularly high in benzene ring count (Dewangan et al., 2014) which is consistent with the high peaks later in the PAH mass spectrum for SFOA (Figure S2.13). SFOA is therefore also likely to include aerosol emitted from funeral pyres.

The large south-easterly peaks in the polar plots for SFOA, COA, NHOA and PAH, are concurrent which suggests a common source (Figure S2.10). These peaks occurred during the late hours of the night (~10-12 p.m.) and on three consecutive occasions which indicates the source is infrequent. They also occur during the Diwali festival and it is likely that they are due to pyrotechnical activity. A possible explanation is the PMF algorithm is unable to resolve these peaks into a single factor due to their infrequency. Further AMS studies on pyrotechnical activity may help to provide characteristic mass spectra which could be used, along with ME-2, to separate factors on occasions such as this.

Combining the two factors, SFOA and SVBBOA, shows that organic aerosol associated with burning-related sources contributes the highest PM_1 mass during the post-monsoon period (Figure 2.8). This is coincidentally the period when concentrations are the largest by a significant amount, in part, due to accentuated boundary layer dynamics. The post-monsoon is therefore a critical period which detrimentally decreases the health of Delhi's population. Combustion sources, including crop residue, municipal waste, funeral pyre

cremations and solid fuel burning, therefore need to be considered when creating new air quality mitigation strategies.

2.5.4. Sources of chloride

The concentrations of chloride in Delhi are particularly large relative to levels reported in other megacities, and a number of studies have linked it to biomass burning and industrial activities (Stone et al., 2010; Gani et al., 2019). There are possible industrial sources of chloride to the north-west of Delhi and these include steel pickling and electronic waste recycling sites that are suggested to emit gaseous HCl (Gani et al., 2019). The same early morning chloride peak reported by Gani et al. (2019) was measured at IGDTUW and occurs around 07:00-08:00 (Figure 2.3). This morning peak is however also seen using a HR-TOF-AMS in Kanpur, India, which suggests that this may not be linked to the same industrial sources (Chakraborty et al., 2018). Furthermore, there is no particular wind directional preference for the morning peak at IGDTUW (Figure S2.9) whereas Gani et al. (2019) show a preferred north westerly wind. Our findings instead suggest a nocturnal area source of HCl which preferentially partitions into the particle phase at night, accumulates in the shallow nocturnal boundary layer, and eventually evaporates in the morning. This is consistent with thermodynamic modelling results showing partitioning of HCl into aerosol water due to excess ammonia and a decrease in temperature and RH during the early morning (Gunthe et al., 2021). There is also no evidence to suggest the steel pickling and electronic waste recycling industries are more active during the post-monsoon and winter months when chloride concentrations are at their highest.

In both Delhi and Kanpur residents burn refuse either for warmth or to clear the streets and this is likely to be a significant source of chloride. Three Indian-based studies show that aerosol emitted from burning waste is composed of chlorine associated PAHs formed mainly from plastics such as polyvinylchloride (PVCs) and polychlorinated biphenyls (PCBs) (Chakraborty et al., 2013; Vreeland et al., 2016; Shivani et al., 2019). At IGDTUW, chloride

has a strong correlation with the PAH time series (Pearson's r = 0.72) which is significantly stronger than that of nitrate (Pearson's r = 0.58), sulphate (Pearson's r = 0.21) and ammonium (Pearson's r = 0.59). The diurnal cycle for PAHs also shares a similar temporal behaviour in the morning to chloride where the median peaks at ~07:00-08:00. This coincides with the regular occurrence of residents sweeping the previous days waste into piles and burning them. One study indicates that this behaviour results in larger amounts of municipal waste being burnt in the morning compared to the evening (Nagpure et al., 2015). Additionally, the temperature in Delhi does not drop until later in the evening making it less likely that residents burn refuse to stay warm in the earlier parts of the evening.

SFOA is strongly related to both PAHs and chloride and although SFOA concentrations in the pre-monsoon and monsoon are comparatively low (Figure 2.8), they are still comparable with chloride concentrations. The link with burning plastics through PCDDs and PCDFs further supports this, and the results gathered therefore suggest that municipal waste burning may be the largest source of PM_1 chloride during the pre-monsoon and monsoon periods.

Another possible source of chloride is from the annual crop burning that occurs during the post-monsoon period. It is well known that wood burning is a strong source of particulate KCl (Li et al., 2003; Lanz et al., 2008; Weimer et al., 2008) and while KCl itself is not quantifiable by the AMS, it goes on to form NH_4Cl via the intermediate reaction of HCl with NH_3 (Sullivan et al., 2007; Wang et al., 2017). SVBBOA has a strong correlation with chloride (Figure 2.8), and the additional results from the second (organic-inorganic) PMF analysis, which included the inorganic components, associate the majority of the post-monsoon ammonium chloride with SVBBOA (Figure S2.17). There are many studies which support this conclusion and show crop residue burning to be a significant source of chloride (Li et al., 2003; Sullivan et al., 2007; Lanz et al., 2008; Weimer et al., 2008; Christian et al., 2010; Wang et al., 2017). However, how much of this association is down to the PMF algorithm resolving

similarities in thermodynamics and thus reflect the volatile nature of both components is uncertain. Furthermore, SFOA has a strong correlation with chloride which suggests localised burning is an equally significant source. Crop burning therefore likely explains a significant fraction of the high levels of chloride in the post-monsoon while municipal waste burning is likely the dominant source during the pre-monsoon and monsoon periods.

2.5.5. Secondary organic aerosol

The two SOA factors LVOOA and SVOOA compare well with literature in the VK diagram (Figure S2.15) and they lie in areas which are consistent with their respective aged and less-aged SOA profiles. When compared to a few AMS studies measuring PM from around the world, only measurements in China gave an LVOOA factor with a larger O:C ratio (Table S2.6). This reflects how oxidised LVOOA is in Delhi and suggests a large amount of atmospheric processing. LVOOA is influenced mainly by photochemical oxidation as suggested by its afternoon peak (Figure 2.9) and its correlations with oxidised VOCs (Figure S2.14). SVOOA however may instead be more influenced by gas-aerosol partitioning and aqueous-phase aerosol uptake as it has a higher correlation with LWC (Pearson's r = 0.56, Figure 2.8).

The SVOOA mass spectrum is similar to the primary factor, COA, shown by a similarly high *m/z* 55:57 ratio (2.87) (Figure 2.6). They also share a similar affinity with OrgNO as both have the strongest correlations with OrgNO (Figure 2.8) and similar correlations with $C_xH_yO_zN_t$ VOC species (Figure S2.14). This is supported by the Inorg-Org PMF solution giving similar COA and SVOOA spectra, which includes both having a high NO^+ (30 *m/z*) peak (Figure S2.17). The largest difference between the two factors is the level of oxygenation where SVOOA has an O:C ratio of 0.52 and could suggest SVOOA may be formed via oxidised COA. The pollution rose plots support this as both COA and SVOOA show a similar wind directional preference (Figure 2.10). This may also explain the simultaneous drop in COA and increase in SVOOA during the

monsoon period as COA is oxidised through aqueous-phase chemistry to form SVOOA.

The diurnal cycles for N:C and O:C (Figure 2.9) appear to show a close relationship during the pre-monsoon indicating that nitrogen content is being driven by photochemistry. This suggests that the organic nitrogen species are mainly of the $C_xH_yN_zO_t$ family rather than the $C_xH_yN_z$ family during this period. A similar pattern is also seen in Kanpur where the N:C ratio closely follows the O:C ratio (Chakraborty et al., 2016a). There is however an increase in N-rich factors such as NHOA, SFOA and SVBBOA during the post-monsoon period which breaks the similarities in N:C and O:C diurnal cycles (Figure 2.9). NHOA and SVBBOA are shown to contain nitrogen in the form of nitrile and/or amine compounds which are of the $C_xH_yN_z$ family (see Sections 2.5.1 and 2.5.3). This shows the post-monsoon nitrogen species composition is a mixture of $C_xH_yN_zO_t$ and $C_xH_yN_z$ chemical families. During the monsoon however, the concentrations of N-rich factors (NHOA, SFOA and SVBBOA) are low which removes their influence on N:C during the night. This allows for the N:C ratio to be driven by dark oxidation via nitrate radicals which is seen in the early morning peak (Figure 2.12). The overall contribution of dark oxidation to SOA formation however is relatively small in Old Delhi. Evidence of which is shown by the coinciding rise in LVOOA concentrations which is small when compared to the following photochemically produced afternoon peak (Figure 2.9).

2.6. Conclusions

PM_1 measurements were taken using a HR-TOF-AMS in Old Delhi for the first time, covering three seasons (pre-monsoon, monsoon and post-monsoon). Results show large concentrations of aerosol species, particularly during the post-monsoon when ammonium and organic aerosol increase by a factor of ~2-3, and chloride and nitrate increase by a factor of ~5-6. These high post-monsoon concentrations have been linked to an increase in the boundary layer

height affect and an increase in burning emissions, mainly from crop residue and solid fuel.

A 7-factor solution was resolved from source apportionment analysis using PMF and this included two traffic-related factors (NHOA and HOA), two burning-related factors (SFOA and SVBBOA), a cooking factor (COA) and two SOA factors (LVOOA and SVOOA). NHOA is separated from HOA by the presence of what we believe to be nitrile species within its composition and their existence is previously unpublished in AMS literature. These nitrile compounds are hypothesised to form from the reaction of alkanoic acids and ammonia. Using a unique view of AMS factor PAH peaks, we establish that NHOA, unlike HOA, also includes higher mass PAHs. This suggests NHOA is heavily influenced by diesel engine emissions and coincides with the easing of heavy-goods vehicle restrictions during the night. HOA, however, was characterised by low molecular weight PAHs including key PAH species markers which suggest it, instead, originates from CNG and petrol engine emissions.

The existence of OrgNO species is evident with concentrations peaking at ~ 25 μg m^{-3} during the Diwali festival when large-scale pyrotechnical activity occurred. It was also found that COA is closely related to OrgNO through correlations with OrgNO and $C_xH_yN_zO_t$ PTR-QiTOF-MS ions. This may suggest that in Delhi OrgNO is formed mostly from cooking activities.

The same associations with OrgNO are also seen with the secondary SVOOA factor, which shares similarities in its mass spectrum to COA. This suggests it is formed from oxidised COA. The simultaneous loss of COA and increase in SVOOA during the monsoon period also indicate aqueous-phase oxidation occurs. LVOOA, however, is shown to form mainly through photochemistry but a small contribution is also made through dark oxidation via nitrate radicals.

The COA mass spectrum was found to have an unusually high degree of oxygenation. This may be explained by the difference in cooking style in Delhi

as food is cooked slowly and on a low heat which emits long-chained oxygenated fatty acids. PAHs are also shown to be an important component of COA composition, and it contributes a large proportion to the total PAH mass. A particularly high PAH fragment ion $[C_7H_7]^+$ peak (*m/z* 91), along with the literature established high *m/z* 55:57 marker, could be used as an additional indicator of COA in Delhi for future AMS studies, especially those measuring below *m/z* 120.

Chloride showed the largest relative increase out of the four inorganic species and organic aerosol, increasing 522% from an average of 1.29 µg m^{-3} in the pre-monsoon to 8.03 µg m^{-3} post-monsoon. Two burning-related factors, SFOA and SVBBOA, both show strong associations with chloride for different reasons. Using earth observations, SVBBOA is tightly linked to regional crop residue burning and is more secondary in character. A similar spectrum to SVBBOA was resolved using an alternative inorganic-organic PMF analysis but with large ammonium chloride peaks. This suggests that considerable amounts of ammonium chloride are linked with crop residue burning. We introduce novel AMS measured tracers which show the presence of polychlorinated dibenzo-furans (PCDF) and -dioxins (PCDD). This offers a new way to associate sources to plastic or Cl-rich fuel burning. Using these tracers, SFOA was found to have significant links to municipal waste burning. With SVBBOA concentrations being insignificant during the pre-monsoon and monsoon periods, municipal waste burning is therefore likely the most significant source of chloride during the pre-monsoon and monsoon periods. During the post-monsoon, however, it is concluded that both crop residue burning, and municipal waste burning are key contributors to the large increase in chloride.

SFOA was also linked to other sources of solid fuel burning such as wood and dung cakes which are commonly used in Delhi, particularly during the post-monsoon (and winter) when Delhi residents burn solid fuel to keep warm. Wind

directional data also suggests funeral pyres situated east of the measurement site likely contribute to SFOA as frequent excursions point in this direction.

Overall, the burning related sources (SFOA+SVBBOA) are the largest primary source of PM_1 during the post-monsoon. The high concentrations of SVBBOA suggest that there is further scope to mitigate PM_1 concentrations through strategies aimed at reducing crop residue burning. This, combined with reductions in other solid fuel burning sources, could significantly decrease the large peaks in PM_1 concentrations during the post-monsoon. However, overall, our measurements suggest that reducing traffic emissions will have the greatest reduction on PM_1 organic aerosol concentrations across the majority of the year, as total traffic aerosol (NHOA+HOA) is shown to be the highest primary contributor during the pre-monsoon and monsoon.

Acknowledgements

This work was supported by UK NERC project DelhiFlux under the Newton-Bhabha Fund Programme “Air Pollution and Human Health in a Developing Megacity (APHH-India)”, NERC reference numbers: NE/P016502/1 and NE/P016472/1. The NERC National Capability award SUNRISE (NE/R000131/1) supported the monsoon measurements and James M. Cash is supported by a NERC E^3 DTP studentship (NE/L002558/1). Tuhin K. Mandal is thankful to the Director of CSIR-National Physical Laboratory for allowing us to carry out this research. Authors gratefully acknowledge the financial support provided by the Earth System Science Organisation, Ministry of Earth Sciences, Government of India under the Indo-UK Joint collaboration grant no MoES/16/19/2017-APHH (DelhiFlux) to conduct the research. The paper does not discuss policy issues and the conclusions drawn in the paper are based on interpretation of results by the authors and in no way reflect the viewpoint of the funding agency or institutions authors are affiliated to.

Data availability

Time series data for AMS-measured organics, nitrate, ammonium, chloride and sulfate, along with PMF factors are available online (Cash, J.; Langford, B.; Di Marco, C.; Nemitz, E. (2021): APHH: High Resolution Time of Flight Mass Spectrometer measurements made at the Indira Gandhi Delhi Technical University for Women (IGDTUW) site during the DelhiFlux field campaigns. Centre for Environmental Data Analysis, Accessed: 20/04/2021. https://catalogue.ceda.ac.uk/uuid/5631c55a2caa4cd2bcdf1bf75365bcc8).

References

Abas, M. R. Bin, Rahman, N. A., Omar, N. Y. M. J., Maah, M. J., Samah, A. A., Oros, D. R., Otto, A. and Simoneit, B. R. T.: Organic composition of aerosol particulate matter during a haze episode in Kuala Lumpur, Malaysia, Atmos. Environ., 38(25), 4223–4241, doi:10.1016/j.atmosenv.2004.01.048, 2004.

Acharja, P., Ali, K., Trivedi, D. K., Safai, P. D., Ghude, S., Prabhakaran, T. and Rajeevan, M.: Characterization of atmospheric trace gases and water soluble inorganic chemical ions of PM1 and PM2.5 at Indira Gandhi International Airport, New Delhi during 2017–18 winter, Sci. Total Environ., 729, 138800, doi:10.1016/j.scitotenv.2020.138800, 2020.

Acton, W. J. F., Davison, B., Drysdale, W. S., Langford, B., Lee, J., Metzger, S., Mullinger, N., Nemitz, E., Vaughan, A. R. and Hewitt, C. N.: Surface-atmosphere fluxes of volatile organic compounds in Delhi, Atmos. Chem. Phys, 2020.

Äijälä, M., Heikkinen, L., Fröhlich, R., Canonaco, F., Prévôt, A. S. H., Junninen, H., Petäjä, T., Kulmala, M., Worsnop, D. and Ehn, M.: Resolving anthropogenic aerosol pollution types - Deconvolution and exploratory

classification of pollution events, Atmos. Chem. Phys., 17(4), 3165–3197, doi:10.5194/acp-17-3165-2017, 2017.

Aiken, A. C., Salcedo, D., Cubison, M. J., Huffman, J. A., DeCarlo, P. F., Ulbrich, I. M., Docherty, K. S., Sueper, D., Kimmel, J. R., Worsnop, D. R., Trimborn, A., Northway, M., Stone, E. A., Schauer, J. J., Volkamer, R. M., Fortner, E., de Foy, B., Wang, J., Laskin, A., Shutthanandan, V., Zheng, J., Zhang, R., Gaffney, J., Marley, N. A., Paredes-Miranda, G., Arnott, W. P., Molina, L. T., Sosa, G. and Jimenez, J. L.: Mexico City aerosol analysis during MILAGRO using high resolution aerosol mass spectrometry at the urban supersite (T0) - Part 1: Fine particle composition and organic source apportionment, Atmos. Chem. Phys., 9(17), 6633–6653, doi:10.5194/acp-9-6633-2009, 2009.

Allan, J. D., Williams, P. I., Morgan, W. T., Martin, C. L., Flynn, M. J., Lee, J., Nemitz, E., Phillips, G. J., Gallagher, M. W. and Coe, H.: Contributions from transport, solid fuel burning and cooking to primary organic aerosols in two UK cities, Atmos. Chem. Phys., 10(2), 647–668, doi:10.5194/acp-10-647-2010, 2010.

Beig, G., Sahu, S. K., Singh, V., Tikle, S., Sobhana, S. B., Gargeva, P., Ramakrishna, K., Rathod, A. and Murthy, B. S.: Objective evaluation of stubble emission of North India and quantifying its impact on air quality of Delhi, Sci. Total Environ., 709, 136126, doi:10.1016/j.scitotenv.2019.136126, 2020.

Bhandari, S., Gani, S., Patel, K., Wang, D. S., Soni, P., Arub, Z., Habib, G., Apte, J. S. and Hildebrandt Ruiz, L.: Sources and atmospheric dynamics of organic aerosol in New Delhi, India: Insights from receptor modeling, Atmos. Chem. Phys. Discuss., 2(2), 1–33, doi:10.5194/acp-2019-403, 2019.

Bhuvaneshwari, S., Hettiarachchi, H. and Meegoda, J. N.: Crop residue burning in India: Policy challenges and potential solutions, Int. J. Environ. Res. Public Health, 16(5), doi:10.3390/ijerph16050832, 2019.

Bottenus, C. L. H., Massoli, P., Sueper, D., Canagaratna, M. R., VanderSchelden, G., Jobson, B. T. and VanReken, T. M.: Identification of amines in wintertime ambient particulate material using high resolution aerosol mass spectrometry, Atmos. Environ., 180, 173–183, doi:10.1016/j.atmosenv.2018.01.044, 2018.

Brilli, F., Gioli, B., Ciccioli, P., Zona, D., Loreto, F., Janssens, I. A. and Ceulemans, R.: Proton Transfer Reaction Time-of-Flight Mass Spectrometric (PTR-TOF-MS) determination of volatile organic compounds (VOCs) emitted from a biomass fire developed under stable nocturnal conditions, Atmos. Environ., 97, 54–67, doi:10.1016/j.atmosenv.2014.08.007, 2014.

Canagaratna, M. R., Jayne, J. T., Jimenez, J. L., Allan, J. D., Alfarra, M. R., Zhang, Q., Onasch, T. B., Drewnick, F., Coe, H., Middlebrook, A., Delia, A., Williams, L. R., Trimborn, A. M., Northway, M. J., DeCarlo, P. F., Kolb, C. E., Davidovits, P. and Worsnop, D. R.: Chemical and microphysical characterization of ambient aerosols with the aerodyne aerosol mass spectrometer, Mass Spectrom. Rev., 26(2), 185–222, doi:10.1002/mas.20115, 2007.

Canagaratna, M. R., Jimenez, J. L., Kroll, J. H., Chen, Q., Kessler, S. H., Massoli, P., Hildebrandt Ruiz, L., Fortner, E., Williams, L. R., Wilson, K. R., Surratt, J. D., Donahue, N. M., Jayne, J. T. and Worsnop, D. R.: Elemental ratio measurements of organic compounds using aerosol mass spectrometry: Characterization, improved calibration, and implications, Atmos. Chem. Phys., 15(1), 253–272, doi:10.5194/acp-15-253-2015, 2015.

Canonaco, F., Crippa, M., Slowik, J. G., Baltensperger, U. and Prévôt, A. S. H.: SoFi, an IGOR-based interface for the efficient use of the generalized multilinear engine (ME-2) for the source apportionment: ME-2 application to aerosol mass spectrometer data, Atmos. Meas. Tech., 6(12), 3649–3661, doi:10.5194/amt-6-3649-2013, 2013.

Chakrabarty, R. K., Pervez, S., Chow, J. C., Watson, J. G., Dewangan, S., Robles, J. and Tian, G.: Funeral Pyres in South Asia: Brown Carbon Aerosol Emissions and Climate Impacts, Environ. Sci. Technol. Lett., 1(1), 44–48, doi:10.1021/ez4000669, 2013.

Chakraborty, A., Bhattu, D., Gupta, T., Tripathi, S. N. and Canagaratna, M. R.: Real-time measurements of ambient aerosols in a polluted Indian city: Sources, characteristics, and processing of organic aerosols during foggy and nonfoggy periods, J. Geophys. Res., 120(17), 9006–9019, doi:10.1002/2015JD023419, 2015.

Chakraborty, A., Gupta, T. and Tripathi, S. N.: Chemical composition and characteristics of ambient aerosols and rainwater residues during Indian summer monsoon: Insight from aerosol mass spectrometry, Atmos. Environ., 136, 144–155, doi:10.1016/j.atmosenv.2016.04.024, 2016a.

Chakraborty, A., Gupta, T. and Tripathi, S. N.: Combined effects of organic aerosol loading and fog processing on organic aerosols oxidation, composition, and evolution, Sci. Total Environ., 573, 690–698, doi:10.1016/j.scitotenv.2016.08.156, 2016b.

Chakraborty, A., Mandariya, A. K., Chakraborti, R., Gupta, T. and Tripathi, S. N.: Realtime chemical characterization of post monsoon organic aerosols in a polluted urban city: Sources, composition, and comparison with other seasons, Environ. Pollut., 232, 310–321, doi:10.1016/j.envpol.2017.09.079, 2018.

Chakraborty, P., Zhang, G., Eckhardt, S., Li, J., Breivik, K., Lam, P. K. S., Tanabe, S. and Jones, K. C.: Atmospheric polychlorinated biphenyls in Indian cities: Levels, emission sources and toxicity equivalents, Environ. Pollut., 182, 283–290, doi:10.1016/j.envpol.2013.07.032, 2013.

Cheung, K. L., Ntziachristos, L., Tzamkiozis, T., Schauer, J. J., Samaras, Z., Moore, K. F. and Sioutas, C.: Emissions of particulate trace elements, metals

and organic species from gasoline, diesel, and biodiesel passenger vehicles and their relation to oxidative potential, Aerosol Sci. Technol., 44(7), 500–513, doi:10.1080/02786821003758294, 2010.

Christian, T. J., Yokelson, R. J., Cárdenas, B., Molina, L. T., Engling, G. and Hsu, S. C.: Trace gas and particle emissions from domestic and industrial biofuel use and garbage burning in central Mexico, Atmos. Chem. Phys., 10(2), 565–584, doi:10.5194/acp-10-565-2010, 2010.

Crippa, M., Canonaco, F., Slowik, J. G., El Haddad, I., Decarlo, P. F., Mohr, C., Heringa, M. F., Chirico, R., Marchand, N., Temime-Roussel, B., Abidi, E., Poulain, L., Wiedensohler, A., Baltensperger, U. and Prévôt, A. S. H.: Primary and secondary organic aerosol origin by combined gas-particle phase source apportionment, Atmos. Chem. Phys., 13(16), 8411–8426, doi:10.5194/acp-13-8411-2013, 2013.

Dall'Osto, M., Ovadnevaite, J., Ceburnis, D., Martin, D., Healy, R. M., O'Connor, I. P., Kourtchev, I., Sodeau, J. R., Wenger, J. C. and O'Dowd, C.: Characterization of urban aerosol in Cork city (Ireland) using aerosol mass spectrometry, Atmos. Chem. Phys., 13(9), 4997–5015, doi:10.5194/acp-13-4997-2013, 2013.

DeCarlo, P. F., Kimmel, J. R., Trimborn, A., Northway, M. J., Jayne, J. T., Aiken, A. C., Gonin, M., Fuhrer, K., Horvath, T., Docherty, K. S., Worsnop, D. R. and Jimenez, J. L.: Field-Deployable, High-Resolution, Time-of-Flight Aerosol Mass Spectrometer, Anal. Chem., 78(24), 8281–8289, doi:10.1021/ac061249n, 2006.

Dewangan, S., Pervez, S., Chakrabarty, R. and Zielinska, B.: Uncharted sources of particle bound polycyclic aromatic hydrocarbons from South Asia: Religious/ritual burning practices, Atmos. Pollut. Res., 5(2), 283–291, doi:10.5094/apr.2014.034, 2014.

Docherty, K. S., Aiken, A. C., Huffman, J. A., Ulbrich, I. M., Decarlo, P. F., Sueper, D., Worsnop, D. R., Snyder, D. C., Peltier, R. E., Weber, R. J., Grover, B. D., Eatough, D. J., Williams, B. J., Goldstein, A. H., Ziemann, P. J. and Jimenez, J. L.: The 2005 Study of Organic Aerosols at Riverside (SOAR-1): Instrumental intercomparisons and fine particle composition, Atmos. Chem. Phys., 11(23), 12387–12420, doi:10.5194/acp-11-12387-2011, 2011.

Duplissy, J., De Carlo, P. F., Dommen, J., Alfarra, M. R., Metzger, A., Barmpadimos, I., Prevot, A. S. H., Weingartner, E., Tritscher, T., Gysel, M., Aiken, A. C., Jimenez, J. L., Canagaratna, M. R., Worsnop, D. R., Collins, D. R., Tomlinson, J. and Baltensperger, U.: Relating hygroscopicity and composition of organic aerosol particulate matter, Atmos. Chem. Phys., 11(3), 1155–1165, doi:10.5194/acp-11-1155-2011, 2011.

Elser, M., El-Haddad, I., Maasikmets, M., Bozzetti, C., Wolf, R., Ciarelli, G., Slowik, J. G., Richter, R., Teinemaa, E., Hüglin, C., Baltensperger, U. and Prévôt, A. S. H.: High contributions of vehicular emissions to ammonia in three European cities derived from mobile measurements, Atmos. Environ., 175, 210–220, doi:10.1016/j.atmosenv.2017.11.030, 2018.

Farmer, D. K., Matsunaga, A., Docherty, K. S., Surratt, J. D., Seinfeld, J. H., Ziemann, P. J. and Jimenez, J. L.: Response of an aerosol mass spectrometer to organonitrates and organosulfates and implications for atmospheric chemistry, Proc. Natl. Acad. Sci., 107(15), 6670–6675, doi:10.1073/pnas.0912340107, 2010.

Fountoukis, C. and Nenes, A.: ISORROPIA II: a computationally efficient thermodynamic equilibrium model for K+–Ca2+–Mg2+–NH4+–Na+–SO42−–NO3−–Cl−–H2O aerosols, Atmos. Chem. Phys., 7(17), 4639–4659, doi:10.5194/acp-7-4639-2007, 2007.

Gadi, R., Shivani, Sharma, S. K. and Mandal, T. K.: Source apportionment and health risk assessment of organic constituents in fine ambient aerosols

(PM2.5): A complete year study over National Capital Region of India, Chemosphere, 221, 583–596, doi:10.1016/j.chemosphere.2019.01.067, 2019.

Gakidou, E., Afshin, A., Abajobir, A. A., Abate, K. H., Abbafati, C., Abbas, K. M., Abd-Allah, F., Abdulle, A. M., Abera, S. F., Aboyans, V., Abu-Raddad, L. J., Abu-Rmeileh, N. M. E., Abyu, G. Y., Adedeji, I. A., Adetokunboh, O., Afarideh, M., Agrawal, A., Agrawal, S., Ahmad Kiadaliri, A., Ahmadieh, H., Ahmed, M. B., Aichour, A. N., Aichour, I., Aichour, M. T. E., Akinyemi, R. O., Akseer, N., Alahdab, F., Al-Aly, Z., Alam, K., Alam, N., Alam, T., Alasfoor, D., Alene, K. A., Ali, K., Alizadeh-Navaei, R., Alkerwi, A., Alla, F., Allebeck, P., Al-Raddadi, R., Alsharif, U., Altirkawi, K. A., Alvis-Guzman, N., Amare, A. T., Amini, E., Ammar, W., Amoako, Y. A., Ansari, H., Antó, J. M., Antonio, C. A. T., Anwari, P., Arian, N., Ärnlöv, J., Artaman, A., Aryal, K. K., Asayesh, H., Asgedom, S. W., Atey, T. M., Avila-Burgos, L., Avokpaho, E. F. G. A., Awasthi, A., Azzopardi, P., Bacha, U., Badawi, A., Balakrishnan, K., Ballew, S. H., Barac, A., Barber, R. M., Barker-Collo, S. L., Bärnighausen, T., Barquera, S., Barregard, L., Barrero, L. H., Batis, C., Battle, K. E., Baune, B. T., Beardsley, J., Bedi, N., Beghi, E., Bell, M. L., Bennett, D. A., Bennett, J. R., Bensenor, I. M., Berhane, A., Berhe, D. F., Bernabé, E., Betsu, B. D., Beuran, M., Beyene, A. S., Bhansali, A., Bhutta, Z. A., Bikbov, B., Birungi, C., Biryukov, S., Blosser, C. D., Boneya, D. J., Bou-Orm, I. R., Brauer, M., Breitborde, N. J. K., Brenner, H., et al.: Global, regional, and national comparative risk assessment of 84 behavioural, environmental and occupational, and metabolic risks or clusters of risks, 1990-2016: A systematic analysis for the Global Burden of Disease Study 2016, Lancet, 390(10100), 1345–1422, doi:10.1016/S0140-6736(17)32366-8, 2017.

Gani, S., Bhandari, S., Seraj, S., Wang, D. S., Patel, K., Soni, P., Arub, Z., Habib, G., Hildebrandt Ruiz, L. and Apte, J. S.: Submicron aerosol composition in the world's most polluted megacity: The Delhi Aerosol Supersite study, Atmos. Chem. Phys., 19(10), 6843–6859, doi:10.5194/acp-19-6843-2019, 2019.

Gunthe, S. S., Liu, P., Panda, U., Raj, S. S., Sharma, A., Darbyshire, E., Reyes-Villegas, E., Allan, J., Chen, Y., Wang, X., Song, S., Pöhlker, M. L., Shi, L., Wang, Y., Kommula, S. M., Liu, T., Ravikrishna, R., McFiggans, G., Mickley, L. J., Martin, S. T., Pöschl, U., Andreae, M. O. and Coe, H.: Enhanced aerosol particle growth sustained by high continental chlorine emission in India, Nat. Geosci., 14(2), 77–84, doi:10.1038/s41561-020-00677-x, 2021.

Gupta, S., Gadi, R., Sharma, S. K. and Mandal, T. K.: Characterization and source apportionment of organic compounds in PM10 using PCA and PMF at a traffic hotspot of Delhi, Sustain. Cities Soc., 39, 52–67, doi:https://doi.org/10.1016/j.scs.2018.01.051, 2018.

Hayes, P. L., Ortega, A. M., Cubison, M. J., Froyd, K. D., Zhao, Y., Cliff, S. S., Hu, W. W., Toohey, D. W., Flynn, J. H., Lefer, B. L., Grossberg, N., Alvarez, S., Rappenglück, B., Taylor, J. W., Allan, J. D., Holloway, J. S., Gilman, J. B., Kuster, W. C., De Gouw, J. A., Massoli, P., Zhang, X., Liu, J., Weber, R. J., Corrigan, A. L., Russell, L. M., Isaacman, G., Worton, D. R., Kreisberg, N. M., Goldstein, A. H., Thalman, R., Waxman, E. M., Volkamer, R., Lin, Y. H., Surratt, J. D., Kleindienst, T. E., Offenberg, J. H., Dusanter, S., Griffith, S., Stevens, P. S., Brioude, J., Angevine, W. M. and Jimenez, J. L.: Organic aerosol composition and sources in Pasadena, California, during the 2010 CalNex campaign, J. Geophys. Res. Atmos., 118(16), 9233–9257, doi:10.1002/jgrd.50530, 2013.

He, C., Ge, Y., Tan, J., You, K., Han, X. and Wang, J.: Characteristics of polycyclic aromatic hydrocarbons emissions of diesel engine fueled with biodiesel and diesel, Fuel, 89(8), 2040–2046, doi:10.1016/j.fuel.2010.03.014, 2010.

Heald, C. L., Kroll, J. H., Jimenez, J. L., Docherty, K. S., Decarlo, P. F., Aiken, A. C., Chen, Q., Martin, S. T., Farmer, D. K. and Artaxo, P.: A simplified description of the evolution of organic aerosol composition in the atmosphere, Geophys. Res. Lett., 37(8), doi:10.1029/2010GL042737, 2010.

Herring, C. L., Faiola, C. L., Massoli, P., Sueper, D., Erickson, M. H., McDonald, J. D., Simpson, C. D., Yost, M. G., Jobson, B. T. and Van Reken, T. M.: New Methodology for Quantifying Polycyclic Aromatic Hydrocarbons (PAHs) Using High-Resolution Aerosol Mass Spectrometry, Aerosol Sci. Technol., 49(11), 1131–1148, doi:10.1080/02786826.2015.1101050, 2015.

Jethva, H., Torres, O., Field, R. D., Lyapustin, A., Gautam, R. and Kayetha, V.: Connecting Crop Productivity, Residue Fires, and Air Quality over Northern India, Sci. Rep., 9(1), 1–11, doi:10.1038/s41598-019-52799-x, 2019.

Jimenez, J. L., Canagaratna, M. R., Donahue, N. M., Prevot, A. S. H., Zhang, Q., Kroll, J. H., DeCarlo, P. F., Allan, J. D., Coe, H., Ng, N. L., Aiken, A. C., Docherty, K. S., Ulbrich, I. M., Grieshop, A. P., Robinson, A. L., Duplissy, J., Smith, J. D., Wilson, K. R., Lanz, V. A., Hueglin, C., Sun, Y. L., Tian, J., Laaksonen, A., Raatikainen, T., Rautiainen, J., Vaattovaara, P., Ehn, M., Kulmala, M., Tomlinson, J. M., Collins, D. R., Cubison, M. J., Dunlea, E. J., Huffman, J. A., Onasch, T. B., Alfarra, M. R., Williams, P. I., Bower, K., Kondo, Y., Schneider, J., Drewnick, F., Borrmann, S., Weimer, S., Demerjian, K., Salcedo, D., Cottrell, L., Griffin, R., Takami, A., Miyoshi, T., Hatakeyama, S., Shimono, A., Sun, J. Y., Zhang, Y. M., Dzepina, K., Kimmel, J. R., Sueper, D., Jayne, J. T., Herndon, S. C., Trimborn, A. M., Williams, L. R., Wood, E. C., Middlebrook, A. M., Kolb, C. E., Baltensperger, U. and Worsnop, D. R.: Evolution of organic aerosols in the atmosphere, Science, 326(5959), 1525–1529, doi:10.1126/science.1180353, 2009.

Kang, M., Fu, P., Aggarwal, S. G., Kumar, S., Zhao, Y., Sun, Y. and Wang, Z.: Size distributions of n-alkanes, fatty acids and fatty alcohols in springtime aerosols from New Delhi, India, Environ. Pollut., 219, 957–966, doi:10.1016/j.envpol.2016.09.077, 2016.

Kiendler-Scharr, A., Mensah, A. A., Friese, E., Topping, D., Nemitz, E., Prevot, A. S. H., Äijälä, M., Allan, J., Canonaco, F., Canagaratna, M., Carbone, S., Crippa, M., Dall Osto, M., Day, D. A., De Carlo, P., Di Marco, C. F., Elbern, H.,

Eriksson, A., Freney, E., Hao, L., Herrmann, H., Hildebrandt, L., Hillamo, R., Jimenez, J. L., Laaksonen, A., McFiggans, G., Mohr, C., O'Dowd, C., Otjes, R., Ovadnevaite, J., Pandis, S. N., Poulain, L., Schlag, P., Sellegri, K., Swietlicki, E., Tiitta, P., Vermeulen, A., Wahner, A., Worsnop, D. and Wu, H. C.: Ubiquity of organic nitrates from nighttime chemistry in the European submicron aerosol, Geophys. Res. Lett., 43(14), 7735–7744, doi:10.1002/2016GL069239, 2016.

Kulkarni, S. H., Ghude, S. D., Jena, C., Karumuri, R. K., Sinha, B., Sinha, V., Kumar, R., Soni, V. K. and Khare, M.: How Much Does Large-Scale Crop Residue Burning Affect the Air Quality in Delhi?, Environ. Sci. Technol., 54(8), 4790–4799, doi:10.1021/acs.est.0c00329, 2020.

Lalchandani, V., Kumar, V., Tobler, A., M. Thamban, N., Mishra, S., Slowik, J. G., Bhattu, D., Rai, P., Satish, R., Ganguly, D., Tiwari, S., Rastogi, N., Tiwari, S., Močnik, G., Prévôt, A. S. H. and Tripathi, S. N.: Real-time characterization and source apportionment of fine particulate matter in the Delhi megacity area during late winter, Sci. Total Environ., 770, 145324, doi:10.1016/j.scitotenv.2021.145324, 2021.

Lanz, V. A., Alfarra, M. R., Baltensperger, U., Buchmann, B., Hueglin, C., Szidat, S., Wehrli, M. N., Wacker, L., Weimer, S., Caseiro, A., Puxbaum, H. and Prevot, A. S. H.: Source Attribution of Submicron Organic Aerosols during Wintertime Inversions by Advanced Factor Analysis of Aerosol Mass Spectra, Environ. Sci. Technol., 42(1), 214–220, doi:10.1021/es0707207, 2008.

Laroo, C. A., Schenk, C. R., Sanchez, L. J., McDonald, J. and Smith, P. L.: Emissions of PCDD/Fs, PCBs, and PAHs from legacy on-road heavy-duty diesel engines, Chemosphere, 89(11), 1287–1294, doi:10.1016/j.chemosphere.2012.05.022, 2012.

Lavric, E. D., Konnov, A. A. and De Ruyck, J.: Dioxin levels in wood combustion - A review, Biomass and Bioenergy, 26(2), 115–145, doi:10.1016/S0961-9534(03)00104-1, 2004.

Li, G., Lei, W., Bei, N. and Molina, L. T.: Contribution of garbage burning to chloride and PM 2.5 in Mexico City, Atmos. Chem. Phys., 12(18), 8751–8761, doi:10.5194/acp-12-8751-2012, 2012.

Li, J., Pósfai, M., Hobbs, P. V. and Buseck, P. R.: Individual aerosol particles from biomass burning in southern Africa: 2. Compositions and aging of inorganic particles, J. Geophys. Res. D Atmos., 108(13), 1–12, doi:10.1029/2002jd002310, 2003.

Lim, J., Lim, C., Kim, S. and Hong, J.: Characterizations of organic compounds in diesel exhaust particulates, J. Environ. Sci. (China), 34(2004), 171–183, doi:10.1016/j.jes.2015.03.013, 2015.

Lin, P. C., Peng, C. Y., Pan, C. H., Lin, P. I. D. and Wu, M. T.: Gender differences and lung cancer risk in occupational chefs: analyzing more than 350,000 chefs in Taiwan, 1984–2011, Int. Arch. Occup. Environ. Health, 92(1), 101–109, doi:10.1007/s00420-018-1358-8, 2019.

Liu, T., Marlier, M. E., DeFries, R. S., Westervelt, D. M., Xia, K. R., Fiore, A. M., Mickley, L. J., Cusworth, D. H. and Milly, G.: Seasonal impact of regional outdoor biomass burning on air pollution in three Indian cities: Delhi, Bengaluru, and Pune, Atmos. Environ., 172(October 2017), 83–92, doi:10.1016/j.atmosenv.2017.10.024, 2018.

Maji, K. J., Arora, M. and Dikshit, A. K.: Premature mortality attributable to PM2.5 exposure and future policy roadmap for ‘airpocalypse’ affected Asian megacities, Process Saf. Environ. Prot., 118, 371–383, doi:10.1016/j.psep.2018.07.009, 2018.

Di Marco, C. D., Langford, B., Cash, J. M., Mullinger, N., Helfter, C. and Nemitz, E.: Source apportionment analysis applied to aerosol eddy-covariance fluxes in Delhi, European Aerosol Conference. [online] Available from: https://www.costcolossal.eu/specialsessioneac2019/, 2019.

Masih, J., Singhvi, R., Kumar, K., Jain, V. K. and Taneja, A.: Seasonal variation and sources of polycyclic aromatic hydrocarbons (PAHs) in indoor and outdoor air in a semi arid tract of Northern India, Aerosol Air Qual. Res., 12(4), 515–525, doi:10.4209/aaqr.2011.11.0192, 2012.

McLafferty, W. F. and Turecek, F.: Interpretation of Mass Spectra., 1993.

Minh, N. H., Minh, T. B., Watanabe, M., Kunisue, T., Monirith, I., Tanabe, S., Sakai, S., Subramanian, A., Sasikumar, K., Viet, P. H., Tuyen, B. C., Tana, T. S. and Prudente, M. S.: Open dumping site in Asian developing countries: A potential source of polychlorinated dibenzo-p-dioxins and polychlorinated dibenzofurans, Environ. Sci. Technol., 37(8), 1493–1502, doi:10.1021/es026078s, 2003.

Mohr, C., DeCarlo, P. F., Heringa, M. F., Chirico, R., Slowik, J. G., Richter, R., Reche, C., Alastuey, A., Querol, X., Seco, R., Peñuelas, J., Jiménez, J. L., Crippa, M., Zimmermann, R., Baltensperger, U. and Prévôt, A. S. H.: Identification and quantification of organic aerosol from cooking and other sources in Barcelona using aerosol mass spectrometer data, Atmos. Chem. Phys., 12(4), 1649–1665, doi:10.5194/acp-12-1649-2012, 2012.

Mukherjee, T., Vinoj, V., Midya, S. K., Puppala, S. P. and Adhikary, B.: Numerical simulations of different sectoral contributions to post monsoon pollution over Delhi, Heliyon, 6(3), e03548, doi:10.1016/j.heliyon.2020.e03548, 2020.

Nagpure, A. S., Ramaswami, A. and Russell, A.: Characterizing the Spatial and Temporal Patterns of Open Burning of Municipal Solid Waste (MSW) in

Indian Cities, Environ. Sci. Technol., 49(21), 12911–12912, doi:10.1021/acs.est.5b03243, 2015.

Nakoudi, K., Giannakaki, E., Dandou, A., Tombrou, M. and Komppula, M.: Planetary boundary layer height by means of lidar and numerical simulations over New Delhi, India, Atmos. Meas. Tech., 12(5), 2595–2610, doi:10.5194/amt-12-2595-2019, 2019.

Ng, N. L., Canagaratna, M. R., Jimenez, J. L., Chhabra, P. S., Seinfeld, J. H. and Worsnop, D. R.: Changes in organic aerosol composition with aging inferred from aerosol mass spectra, Atmos. Chem. Phys., 11(13), 6465–6474, doi:10.5194/acp-11-6465-2011, 2011.

Ozel, M. Z., Ward, M. W., Hamilton, J. F., Lewis, A. C., Raventos-Duran, T. and Harrison, R. M.: Analysis of organic nitrogen compounds in Urban aerosol samples using GCxGC-TOF/MS, Aerosol Sci. Technol., 44(2), 109–116, doi:10.1080/02786820903410105, 2010.

Paatero, P. and Tapper, U.: Positive matrix factorization: A non-negative factor model with optimal utilization of error estimates of data values, Environmetrics, 5(2), 111–126, doi:10.1002/env.3170050203, 1994.

Pervez, S., Chakrabarty, R., Dewangan, S., Watson, J. G., Chow, J. C., Lal Matawle, J. and Pervez, Y.: Cultural and ritual burning emission factors and activity levels in india, Aerosol Air Qual. Res., 15(1), 72–80, doi:10.4209/aaqr.2014.01.0022, 2015.

Pervez, S., Verma, M., Tiwari, S., Chakrabarty, R. K., Watson, J. G., Chow, J. C., Panicker, A. S., Deb, M. K., Siddiqui, M. N. and Pervez, Y. F.: Household solid fuel burning emission characterization and activity levels in India, Sci. Total Environ., 654, 493–504, doi:10.1016/j.scitotenv.2018.11.019, 2019.

Reyes-Villegas, E., Bannan, T., Le Breton, M., Mehra, A., Priestley, M., Percival, C., Coe, H. and Allan, J. D.: Online Chemical Characterization of Food-Cooking Organic Aerosols: Implications for Source Apportionment, Environ. Sci. Technol., 52(9), 5308–5318, doi:10.1021/acs.est.7b06278, 2018a.

Reyes-Villegas, E., Priestley, M., Ting, Y. C., Haslett, S., Bannan, T., Le Breton, M., Williams, P. I., Bacak, A., Flynn, M. J., Coe, H., Percival, C. and Allan, J. D.: Simultaneous aerosol mass spectrometry and chemical ionisation mass spectrometry measurements during a biomass burning event in the UK: Insights into nitrate chemistry, Atmos. Chem. Phys., 18(6), 4093–4111, doi:10.5194/acp-18-4093-2018, 2018b.

Reyes-Villegas, E., Panda, U., Darbyshire, E., Cash, J. M., Joshi, R., Langford, B., Di Marco, C. F., Mullinger, N., Acton, W. J. F., Drysdale, W., Nemitz, E., Flynn, M., Voliotis, A., McFiggans, G., Coe, H., Lee, J., Hewitt, C. N., Heal, M. R., Gunthe, S. S., Shivani, Gadi, R., Singh, S., Soni, V. and Allan, J. D.: PM1 composition and source apportionment at two sites in Delhi, India across multiple seasons, Atmos. Chem. Phys. Discuss., 2020, 1–19, doi:10.5194/acp-2020-894, 2020.

Saarikoski, S., Carbone, S., Decesari, S., Giulianelli, L., Angelini, F., Canagaratna, M., Ng, N. L., Trimborn, A., Facchini, M. C., Fuzzi, S., Hillamo, R. and Worsnop, D.: Chemical characterization of springtime submicrometer aerosol in Po Valley, Italy, Atmos. Chem. Phys., 12(18), 8401–8421, doi:10.5194/acp-12-8401-2012, 2012.

Saraswati, Sharma, S. K. and Mandal, T. K.: Five-year measurements of ambient ammonia and its relationships with other trace gases at an urban site of Delhi, India, Meteorol. Atmos. Phys., 130(2), 241–257, doi:10.1007/s00703-017-0512-2, 2018.

Sen, A., Mandal, T. K., Sharma, S. K., Saxena, M., Gupta, N. C., Gautam, R., Gupta, A., Gill, T., Rani, S., Saud, T., Singh, D. P. and Gadi, R.: Chemical properties of emission from biomass fuels used in the rural sector of the western region of India, Atmos. Environ., 99, 411–424, doi:10.1016/j.atmosenv.2014.09.012, 2014.

Sharma, S. K., Kumar, M., Rohtash, Gupta, N. C., Saraswati, Saxena, M. and Mandal, T. K.: Characteristics of ambient ammonia over Delhi, India, Meteorol. Atmos. Phys., 124(1–2), 67–82, doi:10.1007/s00703-013-0299-8, 2014.

Shivani, Gadi, R., Sharma, S. K. and Mandal, T. K.: Seasonal variation, source apportionment and source attributed health risk of fine carbonaceous aerosols over National Capital Region, India, Chemosphere, 237, 124500, doi:10.1016/j.chemosphere.2019.124500, 2019.

Simoneit, B. R. T., Rushdi, A. I., Abas, M. R. B. and Didyk, B. M.: Alkyl amides and nitriles as novel tracers for biomass burning, Environ. Sci. Technol., 37(1), 16–21, doi:10.1021/es020811y, 2003.

Singh, A., Kamal, R., Mudiam, M. K. R., Gupta, M. K., Satyanarayana, G. N. V., Bihari, V., Shukla, N., Khan, A. H. and Kesavachandran, C. N.: Heat and PAHs emissions in indoor kitchen air and its impact on kidney dysfunctions among kitchen workers in Lucknow, North India, PLoS One, 11(2), 1–16, doi:10.1371/journal.pone.0148641, 2016.

Singh, D. P., Gadi, R. and Mandal, T. K.: Emissions of polycyclic aromatic hydrocarbons in the atmosphere: An indian perspective, Hum. Ecol. Risk Assess., 16(5), 1145–1168, doi:10.1080/10807039.2010.512258, 2010.

Slowik, J. G., Vlasenko, A., McGuire, M., Evans, G. J. and Abbatt, J. P. D.: Simultaneous factor analysis of organic particle and gas mass spectra: AMS and PTR-MS measurements at an urban site, Atmos. Chem. Phys., 10(4), 1969–1988, doi:10.5194/acp-10-1969-2010, 2010.

Stewart, G. J., Nelson, B. S., Acton, W. J. F., Vaughan, A. R., Farren, N. J., Hopkins, J. R., Ward, M. W., Swift, S. J., Arya, R., Mondal, A., Jangirh, R., Ahlawat, S., Yadav, L., Sharma, S. K., Yunus, S. S. M., Hewitt, C. N., Nemitz, E., Mullinger, N., Gadi, R., Sahu, L. K., Tripathi, N., Rickard, A. R., Lee, J. D., Mandal, T. K. and Hamilton, J. F.: Emissions of intermediate-volatility and semi-volatile organic compounds from domestic fuels used in Delhi, India, Atmos. Chem. Phys. Discuss., 2020, 1–45, doi:10.5194/acp-2020-860, 2020.

Stone, E., Schauer, J., Quraishi, T. A. and Mahmood, A.: Chemical characterization and source apportionment of fine and coarse particulate matter in Lahore, Pakistan, Atmos. Environ., 44(8), 1062–1070, doi:10.1016/j.atmosenv.2009.12.015, 2010.

Sudheer, A. K., Rengarajan, R., Deka, D., Bhushan, R., Singh, S. K. and Aslam, M. Y.: Diurnal and seasonal characteristics of aerosol ionic constituents over an urban location in Western India: Secondary aerosol formation and meteorological influence, Aerosol Air Qual. Res., 14(6), 1701–1713, doi:10.4209/aaqr.2013.09.0288, 2014.

Sullivan, R. C., Guazzotti, S. A., Sodeman, D. A., Tang, Y., Carmichael, G. R. and Prather, K. A.: Mineral dust is a sink for chlorine in the marine boundary layer, Atmos. Environ., 41(34), 7166–7179, doi:10.1016/j.atmosenv.2007.05.047, 2007.

Sun, K., Tao, L., Miller, D. J., Pan, D., Golston, L. M., Zondlo, M. A., Griffin, R. J., Wallace, H. W., Leong, Y. J., Yang, M. M., Zhang, Y., Mauzerall, D. L. and Zhu, T.: Vehicle Emissions as an Important Urban Ammonia Source in the United States and China, Environ. Sci. Technol., 51(4), 2472–2481, doi:10.1021/acs.est.6b02805, 2017.

Sun, Y., Du, W., Fu, P., Wang, Q., Li, J., Ge, X., Zhang, Q., Zhu, C., Ren, L., Xu, W., Zhao, J., Han, T., Worsnop, D. R. and Wang, Z.: Primary and secondary aerosols in Beijing in winter: Sources, variations and processes,

Atmos. Chem. Phys., 16(13), 8309–8329, doi:10.5194/acp-16-8309-2016, 2016.

Sun, Y. L., Zhang, Q., Schwab, J. J., Demerjian, K. L., Chen, W. N., Bae, M. S., Hung, H. M., Hogrefe, O., Frank, B., Rattigan, O. V. and Lin, Y. C.: Characterization of the sources and processes of organic and inorganic aerosols in New York city with a high-resolution time-of-flight aerosol mass apectrometer, Atmos. Chem. Phys., 11(4), 1581–1602, doi:10.5194/acp-11-1581-2011, 2011.

Sun, Y. L., Zhang, Q., Schwab, J. J., Yang, T., Ng, N. L. and Demerjian, K. L.: Factor analysis of combined organic and inorganic aerosol mass spectra from high resolution aerosol mass spectrometer measurements, Atmos. Chem. Phys., 12(18), 8537–8551, doi:10.5194/acp-12-8537-2012, 2012.

Svedahl, S. R.: Doctoral thesis: Cooks, work environment and health experimental studies of exposure to cooking fumes, and epidemiological investigations in a cohort, Norwegian University of Science and Technology., 2018.

Tobler, A., Bhattu, D., Canonaco, F., Lalchandani, V., Shukla, A., Thamban, N. M., Mishra, S., Srivastava, A. K., Bisht, D. S., Tiwari, S., Singh, S., Močnik, G., Baltensperger, U., Tripathi, S. N., Slowik, J. G. and Prévôt, A. S. H.: Chemical characterization of PM2.5 and source apportionment of organic aerosol in New Delhi, India, Sci. Total Environ., 745, 140924, doi:10.1016/j.scitotenv.2020.140924, 2020.

Tsai, J. H., Chen, S. J., Huang, K. L., Lee, W. J., Kuo, W. C. and Lin, W. Y.: Characteristics of particulate emissions from a diesel generator fueled with varying blends of biodiesel and fossil diesel, J. Environ. Sci. Heal. Part A, 46(2), 204–213, doi:10.1080/10934529.2011.532444, 2011.

Ulbrich, I. M., Canagaratna, M. R., Zhang, Q., Worsnop, D. R. and Jimenez, J. L.: Interpretation of organic components from Positive Matrix Factorization of aerosol mass spectrometric data, Atmos. Chem. Phys., 9(9), 2891–2918, doi:10.5194/acp-9-2891-2009, 2009.

Verma, R., Vinoda, K. S., Papireddy, M. and Gowda, A. N. S.: Toxic Pollutants from Plastic Waste- A Review, Procedia Environ. Sci., 35, 701–708, doi:10.1016/j.proenv.2016.07.069, 2016.

Vreeland, H., Schauer, J. J., Russell, A. G., Marshall, J. D., Fushimi, A., Jain, G., Sethuraman, K., Verma, V., Tripathi, S. N. and Bergin, M. H.: Chemical characterization and toxicity of particulate matter emissions from roadside trash combustion in urban India, Atmos. Environ., 147, 22–30, doi:10.1016/j.atmosenv.2016.09.041, 2016.

Wang, H., Wang, X., Yang, X., Li, W., Xue, L., Wang, T., Chen, J. and Wang, W.: Mixed chloride aerosols and their atmospheric implications: A review, Aerosol Air Qual. Res., 17(4), 878–887, doi:10.4209/aaqr.2016.09.0383, 2017.

Wang, L., Slowik, J. G., Tripathi, N., Bhattu, D., Rai, P., Kumar, V., Vats, P., Satish, R., Baltensperger, U., Ganguly, D., Rastogi, N., Sahu, L. K., Tripathi, S. N. and Prévôt, A. S. H.: Source characterization of volatile organic compounds measured by proton-transfer-reaction time-of-flight mass spectrometers in Delhi, India, Atmos. Chem. Phys., 20(16), 9753–9770, doi:10.5194/acp-20-9753-2020, 2020.

Wang, W. C., Lin, W. H., Kuo, C. P. and Wu, J. Y.: The relation between dioxin concentration from exhaust gas of diesel engine and chlorine content, J. Anal. Appl. Pyrolysis, 94, 10–16, doi:10.1016/j.jaap.2011.12.010, 2012.

Weimer, S., Alfarra, M. R., Schreiber, D., Mohr, M., Prévôt, A. S. H. and Baltensperger, U.: Organic aerosol mass spectral signatures from wood-

burning emissions: Influence of burning conditions and type, J. Geophys. Res. Atmos., 113(10), D10304, doi:10.1029/2007JD009309, 2008.

Weingartner, E., Saathoff, H., Schnaiter, M., Streit, N., Bitnar, B. and Baltensperger, U.: Absorption of light by soot particles: determination of the absorption coefficient by means of aethalometers, J. Aerosol Sci., 34(10), 1445–1463, doi:10.1016/S0021-8502(03)00359-8, 2003.

Xie, M., Zhao, Z., Holder, A. L., Hays, M. D., Chen, X. and Shen, G.: Chemical composition, structures, and light absorption of N-containing, Atmos. Chem. Phys. Discuss., 1–29, doi:10.5194/acp-2020-594, 2020.

Ye, Z., Liu, J., Gu, A., Feng, F., Liu, Y., Bi, C., Xu, J., Li, L., Chen, H., Chen, Y., Dai, L., Zhou, Q. and Ge, X.: Chemical characterization of fine particulate matter in Changzhou, China, and source apportionment with offline aerosol mass spectrometry, Atmos. Chem. Phys., 17(4), 2573–2592, doi:10.5194/acp-17-2573-2017, 2017.

Zhang, M., Buekens, A. and Li, X.: Open burning as a source of dioxins, Crit. Rev. Environ. Sci. Technol., 47(8), 543–620, doi:10.1080/10643389.2017.1320154, 2017.

Zhang, X., Xu, J., Kang, S., Liu, Y. and Zhang, Q.: Chemical characterization of long-range transport biomass burning emissions to the Himalayas: Insights from high-resolution aerosol mass spectrometry, Atmos. Chem. Phys., 18(7), 4617–4638, doi:10.5194/acp-18-4617-2018, 2018.

Zhao, J., Peng, P., Song, J., Ma, S., Sheng, G. and Fu, J.: Characterization of organic matter in total suspended particles by thermodesorption and pyrolysis-gas chromatography-mass spectrometry, J. Environ. Sci., 21(12), 1658–1666, doi:10.1016/S1001-0742(08)62470-5, 2009.

Zheng, X., Wu, Y., Zhang, S., Hu, J., Zhang, K. M., Li, Z., He, L. and Hao, J.: Characterizing particulate polycyclic aromatic hydrocarbon emissions from diesel vehicles using a portable emissions measurement system, Sci. Rep., 7(1), 1–12, doi:10.1038/s41598-017-09822-w, 2017.

Chapter 3

Source apportionment of micrometeorological VOC flux measurements above Old Delhi

This chapter is based on a research paper currently in preparation for submission for publication.

Author contributions: I took VOC measurements using PTR-QiTOF-MS along with Acton, W. J. F. and was supported by Langford, B., Hewitt, C. N., and Misztal, P. K. I interpreted the results with help from Langford, B., Heal, M. R., Di Marco, C., Nemitz, E. Overall guidance with setup and logistics were provided by Mullinger, N. J., Mandal, T. K., Shivani, Gadi, R., Gurjar, B. R., and Nemitz, E. I wrote the manuscript with subsequent contributions from all co-authors.

3.1. Abstract

Delhi is one of the most polluted cities in the world and its atmosphere contains a complex array of volatile organic compounds (VOCs) due to a large mixture of emission sources. To better understand these sources, we developed a novel approach where positive matrix factorization (PMF) is applied to the concentrations of VOCs measured in up and down drafts. The resulting factors were converted into fluxes by applying the true eddy accumulation approximation. In doing so, our approach is not constrained to periods of emission and can derive factor fluxes that show either emission or deposition, something not possible with conventional techniques. The spatial flux patterns for PMF factors are presented, giving spatial detail of the localised fluxes. A total of 9-factors were identified, of which traffic emissions were the largest (70% of total flux) and the most significant source of both the OH reactivity flux and photochemical ozone creation potential (POCP). One traffic factor

(TRAF1) was linked to diesel vehicle emissions while the other (TRAF2) was linked to petrol and compressed natural gas vehicle emissions. The second most significant source of VOCs were from evaporative emissions (EVOC) (10% of total flux) which had a significant contribution from species related to asphalt emissions. These included naphthalene and tetralin-based structures, along with 1,3-butadiene and styrene which are constituent species of the adhesives used in asphalt. The peak in emissions of EVOC occurred during midday and followed surface temperature and solar radiation. This behaviour reflects sources of evaporative and biogenic emissions and the majority of the biogenic VOCs detected were associated with this factor. Biogenic emissions contributed 25% to total monoterpene concentrations and 18% to the localised monoterpene fluxes. However, the traffic factors had the highest composition of monoterpenes and, as a result, they dominated the monoterpene contributions to concentrations (60%) and localised fluxes (78%). Two burning-related factors were identified, one associated with solid-fuel combustion VOCs (SFVOC) and another associated with pyrotechnical activity VOCs (PVOC). The two factors shared the largest percentage of the concentration weighted OH reactivity which was due to a high content of furan-based species. The first observation of an urban deposition flux is also seen for SFVOC and an oxidised VOC (OVOC1) factor, and their spatial deposition flux patterns suggest vegetation could be acting as a VOC sink in Delhi.

3.2. Introduction

Flux measurements of volatile organic compounds (VOCs) are paramount to understanding the sources from which they are emitted as well as their controls. Through reactions with NO_x and OH radicals, these trace-gas compounds are responsible for the formation of toxic tropospheric ozone and secondary organic aerosol (SOA). In recent years, studies have focused on naturally emitted biogenic VOCs (BVOC) as this is considered the largest global source of VOCs (Weng et al., 2020). However, there are also a

substantial number of VOCs which negatively affect human health, such as aromatic VOCs: toluene, benzene and phenols. The vast majority of these harmful VOC species are also emitted anthropogenically and are at their highest concentrations within the most densely populated areas. Therefore, knowledge of their origins and emission controls is important in order to understand how to reduce their effects on human health.

Delhi, India has recently been shown to be one of the most polluted cities in the world and is ranked within the top ten most polluted cities by the World Health Organization (World Health Organization, https://www.who.int/data/gho/data/themes/topics/topic-details/GHO/ambient-air-pollution, last access: 20 April 2021). A combination of waste management issues, an increasing population, surrounding agriculture and everchanging industry causes an aggregated air quality problem that affects millions of lives. The post-monsoon is the most polluted time of the year when seasonal crop-residue burning is timed with pyrotechnical activity associated with the festival of light, Diwali. This, combined with an exacerbation of pollutant concentrations due to a shallow boundary layer, creates a peak in air pollution that causes Delhi to be labelled as the “the world’s most polluted megacity” (Gani et al., 2019).

Recent work has shown that reductions in anthropogenic nitrogen oxide emissions in Delhi need to be accompanied by reductions in VOC emissions to avoid an increase in ozone production (Chen et al., 2021; Nelson et al, 2021). Traffic VOC emissions in particular, along with aromatic VOCs and monoterpenes, have a significant impact on ozone production (Nelson et al., 2021). The sources of aromatic VOCs has previously been well studied in Delhi (Stewart et al., 2021b; Wang et al., 2020b); however the sources of monoterpenes are uncertain. Wang et al. (2020b) observe monoterpene concentrations follow anthropogenic sources well and suggest a number of possible sources. Previous studies have shown monoterpenes originate from common anthropogenic sources such as traffic (Hellén et al., 2012) and

biomass burning (Hellén et al., 2006, 2012). Additionally, monoterpenes have recently been linked to a number of other less common anthropogenic sources such as cooking (Klein et al., 2016), domestic heating (Rouvière et al., 2006) and personal-care products (McDonald et al., 2018). One aim in this study is to further our understanding of monoterpene sources in Delhi in order for future studies to better quantify their impact on ozone.

The complex profile of VOC sources has been studied previously in Delhi using source apportionment techniques such as positive matrix factorisation (PMF). The two main sources contributing to VOC concentrations are traffic and burning of solid fuel and waste (Nelson et al., 2021; Stewart et al., 2021b; Wang et al., 2020b). A recent PMF-based study was conducted at two measurement sites in Delhi using proton-transfer-reaction time-of-flight mass spectrometers (PTR-ToF-MS) (Wang et al., 2020b), identifying two traffic-related, two solid fuel burning-related and two oxidised VOC factors. The traffic sources were separated based on the timing of restrictions for heavy good vehicles which has also been observed in PMF studies in Delhi that analysed the organic mass spectrum of sub-micron particulate matter (Cash et al., 2021). The two solid-fuel factors in Wang et al., (2020b) separated according to state of oxidation. One represents freshly emitted solid fuel burning, whilst the other is aged solid-fuel burning and includes marker species for atmospheric processing such as peroxyacetyl nitrate (PAN). Wang et al. (2020) describe that the solid fuel burning factors originate from domestic heating and cooking stoves. By contrast, another study using co-located dual-channel gas chromatography (DC-GC-FID) and two-dimensional gas chromatography (GCxGC-FID) described burning-related VOCs being related to municipal waste burning (Stewart et al., 2021b). It is therefore likely that burning-related VOCs are from a combination of these sources in Delhi.

Evaporative emissions are a source of VOCs that are highly uncertain. One study estimates that evaporative emissions from tarmac, also known as asphalt, exceed traffic-related sources of SOA precursors within megacities

(Khare et al., 2020). Controlled chamber experiments have identified key markers for surface evaporation from tarmac, such as anthracene, pyrene, fluoranthene, tetralin, tetralin derivatives, naphthalene and naphthalene derivatives. The experiments also found that tarmac emissions are driven by both temperature and light due to the combined evaporation of volatile species from increased heat and UV degradation. Only one study in Delhi has shown VOC concentrations to originate from evaporative surface sources such as from road surfaces and buildings (Srivastava et al., 2005b). Whilst other studies in India have shown the existence of large quantities of evaporative emissions, they focused on vehicle headspaces or hot soaking and the refuelling of vehicles (Sharma et al., 2015; Srivastava et al., 2005a; Srivastava and Majumdar, 2010).

It is likely that previous studies in Delhi have measured evaporative surface emissions, but their temporal concentration profile is too similar to separate them from other sources under similar control. Its evaporative behaviour is therefore often inseparable from its counterpart when using a multilinear model. However, the ability to measure fluxes of source factors may provide a tool to separate VOC mass based on its local emissions behaviour rather than its concentration. Until now, there has not been a method to fully utilise the power of PMF to apportion flux measurements.

Source apportionment has previously only been successfully implemented for flux measurements in two studies: one using non-negative matrix factorisation (NNMF) (Karl et al., 2018) and the other using the multilinear-engine 2 (ME-2) (Kota et al., 2014). This unique method to produce an emission flux for VOC source factors has the potential to create greater understanding of atmospheric processing and also provides emission factors for the use within atmospheric models. However, the normal positive constraint of PMF imposes limitations on the analysis. By removing negative net fluxes prior to the analysis and only allowing positive component fluxes, it cannot identify potential depositing VOCs and it does not allow for solutions in which a net positive flux

is the result of positive and negative component fluxes. Here, we propose a new method for the implementation of the PMF model which removes the issue of negative values and therefore allows for the calculation of emitting, depositing and bi-directionally exchanged VOC source factors. From these results, we are able to show the spatial distribution of fluxes within the flux footprint. We also estimate the OH reactivity flux and the flux-weighted POCP associated with each factor, thereby providing an estimate of the impact of the associated sources on atmospheric oxidising efficiency and ozone formation, rather than on individual compounds.

3.3. Methods

3.3.1. Measurement location and meteorological conditions

Measurements were taken during the post-monsoon (09/10/2018 – 23/11/2018) at the Indira Gandhi Delhi Technical University for Women (IGDTUW) in the north of Old Delhi (28°39'51.8"N 77°13'55.2"E) near Kashmiri Gate. IGDTUW is situated in an urban area and is surrounded by large road network systems, a nearby train station (~ 300-450 m southeast) and the Inter-State Bus Terminal (ISBT) (~ 350-500m northeast). There is a nearby automotive business district containing mostly businesses selling automotive parts (~50-100 m southeast) and a large cremation site on the shore of the Yamuna river (~500-750 m east). Some small-scale green areas also exist, including the IGDTUW playground (size ~0.01 km^2, ~50-100 m east), St James' Church (~100-150 m northwest) and a cluster of tree species directly underneath the measurement tower. There is a mixture of industry, businesses, residential living and rooftop slums within the area, creating a large mix of pollution sources.

The predominant wind direction was from the northwest with some contributions from the east. Temperatures (average ~21 ^oC, range ~15-30 ^oC) were lower than the annual average (~29 ^oC), while relative humidity (~52 %) is similar (annual average ~54%). Unfavourable meteorology, typical for the post-monsoon, meant there was often a low boundary layer during the evening

and late hours of the morning causing increased pollutant concentrations. Combined with generally low wind speeds (average ~2.17 m s^{-1}), this created a sharp increase in pollutant surface concentrations.

3.3.2. Instrumentation

VOC measurements were made at 10 Hz using a high-resolution PTR-QiTOF-MS (Ionicon Analytik G.m.b.H., Innsbruck, Austria) with a drift pressure (p_d) of 3.2 mbar, drift tube voltage (U_d) of 750 V, drift tube temperature (T_d) of 60 ºC, corresponding to an *E*/*N* of 118.8 Td. The inlet was positioned on a ~30 m tower which sampled air below (~0.5-1 m) a horizontally mounted (~3 m) sonic anemometer (Gill R3, Gill Instruments, Lymington, UK). A PFA inlet line (0.5 inch) ran into an air-conditioned lab where the PTR-QiTOF-MS subsampled from. The inlet line flow rate (~20 L min^{-1}) was measured using a TSI Mass Flowmeter 4043 (TSI, Shoreview, USA) and a Teflon filter was used to remove particulate matter from the airstream and was replaced every ~4-5 days. The flow rate into the instrument was 100 cm^3 min^{-1} and the mass spectrum was recorded over the range 0 - 511 *m/z*.

The volume mixing ratio (VMR) for species RH^+ in ppb was calculated using a transmission efficiency (Tr) of detected ions through the PTR-QiTOF-MS as described in the following equation:

$$VMR_{RH^+} = \frac{10^9 \cdot 22400 \cdot p_0^2 \cdot T_d^2 \cdot U_d \cdot \mu_o \cdot RH^+ \cdot Tr_{H_3O^+}}{p_d^2 \cdot T_0^2 \cdot k_1 \cdot v_d \cdot N_A \cdot H_3O^+ \cdot Tr_{RH^+}} \quad (3.1)$$

Here, μ_0 is the ion mobility which is calculated (~2.7 cm^2 V^{-1} s^{-1}) using equations described in de Gouw and Warneke (2007), k_1 is the collision reaction rate constant (~2 x 10^{-9} cm^3 s^{-1}), v_d is the drift tube length (9.5 cm) and N_A is Avogadro's constant. The product ion signal (RH^+) and the primary ion signal (H_3O^+) are used, along with the pressure (p_0) and temperature (T_0) at standard conditions.

The transmission efficiency was calibrated weekly using a mixture of VOC compounds (Apel-Reimer Inc. uncertainty ±5%) of known concentration (methanol, acetonitrile, acetaldehyde, acetone, dimethyl sulphide, isoprene, methacrolein, methyl vinyl ketone, methyl ethyl ketone, 2-butanol, benzene, toluene, 2-hexanone, m-xylene, heptanal, 3-octanone, 3-octanol, a-pinene and B-caryophyllene). The standards were diluted using a zero-air generator and a total of nine calibrations were conducted.

The measurement uncertainty (ΔVMR) was calculated using the equation:

$$\Delta VMR = \sqrt{\frac{\mathrm{VMR}_{RH^+}}{\tau} + \frac{\mathrm{VMR}_{RH^+,zero}}{\tau_{zero}}} \quad (3.2)$$

where τ and τ_{zero} are the dwell times for the ambient measurement and measurement background, and $\mathrm{VMR}_{RH^+,zero}$ is the background mixing ratio for species RH^+. It is assumed that the majority of the uncertainty can be quantified using statistical error as the PTR-QiTOF-MS is highly sensitive (de Gouw et al., 2003).

3.3.3. True eddy accumulation measurements

The fast response time of the PTR-MS allows its application in standard eddy-covariance (EC) flux measurements, where the flux is calculated (typically over 30-min periods) as the covariance between concentration (c_{voc}) and vertical wind velocity (w):

$$F_{VOC} = \overline{w' c_{voc}'} \quad (3.3)$$

where w' is the instantaneous fluctuation about the mean wind velocity (i.e. $w' = w - \bar{w}$) and overbars denote the mean. These need to be measured at a high temporal resolution (typically 10 to 20 Hz). This approach is not ideal for the application of PMF: as mentioned above, fluxes do not lend themselves to this analysis because they can be positive and negative, but PMF can also

not be applied to 10 Hz data points because they are noisy and because of computational constraints. Here, the approach in Langford et al. (in prep) is used to calculate average concentrations prior to the flux calculation using the fast data to numerically simulate true eddy accumulation (TEA).

The TEA method was devised for instruments unable to measure at a frequency sufficient for eddy covariance (Desjardins, 1977). Instead, the vertical wind velocity (w') is measured at the required frequency (> 5 Hz) and this is used to trigger separate sampling of the air during upward ($w'\uparrow$) or downward ($w'\downarrow$) eddies. The samples are collected in two separate reservoirs, each containing upward or downward draughts, and accumulated until a sufficient averaging period is reached. Measurements of these reservoirs thus yield a time series of positive upward ($c_{VOC}\uparrow$) and downward ($c_{VOC}\downarrow$) concentrations. As long as the samples of air are collected at a flowrate that is proportional to |*w*'|, TEA is numerically identical to EC. In practice, it is not easy to adjust the flowrate every 100 ms and TEA has rarely been implemented. Later, the Relaxed Eddy Accumulation (REA) approach was developed in which air could be sampled at a constant flow rate, but this relies on empirical parameterisations and can no longer be considered a direct flux measurement. Whilst TEA sampling is difficult, the approach can easily be implemented numerically to already acquired EC data, where averages of $c_{VOC}\uparrow$ and $c_{VOC}\downarrow$ can be calculated that are weighted by the magnitude of |*w*'|. Here, we apply the PMF model to a time series of the up and down draft concentrations, which are always positive. The flux (F_{VOC}) for each factor can then be calculated using the true eddy accumulation equation:

$$F_{VOC} = \left(\frac{(\sum|w'\uparrow|c_{VOC}\uparrow)}{\sum|w'\uparrow|} - \frac{(\sum|w\prime\downarrow|c_{VOC}\downarrow)}{\sum|w'\downarrow|}\right)\left(\frac{|w'|}{2}\right) \quad (3.4)$$

The error matrix is composed of errors calculated using Eq. (3.2) which are then weighted using the same scaling factors as used on the up and down draught concentrations. The weighting calculation is summarised in Eqs. (3.5) and (3.6),

$$\uparrow \Delta F = \sqrt{\frac{(\sum |w\prime\uparrow|\Delta VMR\uparrow)^2}{\sqrt{(N\uparrow)}\ \sum |w'|}} \quad (3.5)$$

$$\downarrow \Delta F = \sqrt{\frac{(\sum |w\prime\downarrow|\Delta VMR\downarrow)^2}{\sqrt{(N\downarrow)}\ \sum |w'|}} \quad (3.6)$$

where $N \uparrow$ and $N \downarrow$ are the number of measurements used for the averaging period for the up and down draughts, respectively.

For quality control purposes, EC was also calculated for individual VOC species and, when averaged to 30-min intervals, gave r^2 = 1 for acetonitrile, acetone, toluene, benzene, isoprene and acetic acid, when compared to TEA calculated fluxes. For further assurance, all time-series data points used for all ions measured (total of 1286) were compared by dividing each EC ion flux time series by the corresponding ion flux time series calculated by TEA. The average value generated was 0.9999 ± 0.0089 (± standard deviation) with 95th lower and upper confidence intervals of 0.999973 and 1.00001, respectively.

As the inlet and the sonic anemometer are not located immediately adjacent to the PTR-QiTOF-MS, there is a time-lag between the VOC concentration and the vertical wind speed measurements. The time lag was calculated using the maximum of the co-variance between these two measurements (Taipale et al., 2010). However, compound-specific traits such as polarity and chemical functionality cause differential absorption of compounds in the sample line and hence to variable lag times. This introduces large uncertainty into the maximum of the covariance function, particularly for higher masses which were highly polar and/or oxygenated. The time-lag was therefore determined for species with high signal-to-ratio (SNR) and strong covariance peaks (isoprene and toluene) and fixed for all other masses (Langford et al., 2015).

To increase the limit of detection (LoD) of fluxes, linear detrending rather than block averaging was applied to the VOC concentrations and vertical wind velocity (Langford et al., 2015). In this approach a linear fit is applied to each

30-min period which is used to remove the trend from the time series before it is averaged for the final flux calculation.

Finally, 2-dimensional co-ordinate rotations were applied to generate an average vertical wind velocity of zero which accounts for tilting of the sonic anemometer sensor (Nemitz et al., 2009).

3.3.4. Source apportionment

The positive matrix factorisation (PMF) bilinear receptor model is a multivariate analysis tool that is frequently used to resolve individual sources or "factors" from environmental measurements such as atmospheric mass spectral time series (Paatero and Tapper, 1994). In brief, the PMF model can be summarised as:

$$\mathbf{X} = \mathbf{FG} + \mathbf{E} \quad (3.7)$$

where $\mathbf{X}$ is the measured data matrix of mass spectral rows, m, for each *m/z* time series column, n, and $\mathbf{E}$ is the $m \times n$ residual matrix. The number of factors, p, is chosen by the user which determines the number of mass spectral profiles in the $m \times p$ matrix, $\mathbf{F}$, and the number of factor time series in the $p \times n$ matrix, $\mathbf{G}$. The solution is chosen based on the minimisation of Q which is calculated as:

$$Q = \sum_{i=1}^{m} \sum_{j=1}^{n} \left(\frac{e_{ij}}{\sigma_{ij}}\right)^2. \quad (3.8)$$

Here, e_{ij} and σ_{ij} are the residuals and uncertainties, respectively, for rows, i and columns, j. A value of Q = 1 and zero model error would therefore leave all measurement uncertainty in the residuals and a solution that perfectly explains all the measured data. The PMF2 algorithm was used in robust-mode using the PMF Evaluation Tool (PET, v3.00) (Ulbrich et al., 2009). For SNR values < 2, the error matrix was down-weighted by a factor of 2 and for SNR <

0.2 the error matrix was down-weighted by a factor of 10. All ions relating to the reagent ions and to non-VOCs were removed including: $^{18}H_3O^+$, N_2H^+, ON^+, O_2^+, CO^+, $H_5O_2^+$, CO_2^+.

The linear relationship between a total of 7 solutions and auxiliary measurements of NO_x, BC and CO were explored using multilinear regression analysis. A 9-factor solution was chosen which showed the strongest correlation with external tracers following the procedure set out in the Section 3.4.2.

3.3.5. Spatial flux patterns

A 30 m × 30 m gridded spatial flux pattern was estimated using the model described in Kormann and Meixner (2001) whereby the contributions of each grid to the total flux are estimated using the friction velocity, u_*, the Obukhov length, L, and the effective aerodynamic measurement height, z_m. The spatial flux can be expressed as:

$$F(0,0,z_m) = \int_{-\infty}^{\infty}\int_{0}^{\infty} F(x,y,0)\phi(x,y,z_m)\mathrm{d}x\mathrm{d}y \quad (3.9)$$

Here, the *x*-axis is aligned with the average horizontal wind direction and the flux footprint, $\phi(x,y,z_m)$, describes the flux contribution of species, s**,** from a point source, $F_s(x,y,0)$, to the total measured flux, $F_s(x,y,z_m)$. Using a defined 30 m × 30 m grid, the equation can be simplified to give:

$$F_s(0,0,z_m) = \Sigma_{g=1}^{N} F_s\phi_g. \quad (3.10)$$

where the species flux, F_s, is multiplied by the flux footprint calculated for each 30 m grid square, g. The total number of grid squares is N (= 100) and the KM Excel tool described by Neftel et al. (2008) was used to calculate ϕ_g. It should be noted that this method does not attempt to derive a weighted average flux for each grid square or apply a fitting regime to better distribute the total measured flux between grid squares. Each grid square, $F_s\phi_g$, represents the

maximum contribution to the flux of a species from the defined area in the footprint (x, y). Therefore, the magnitude of each grid square is not quantitative, and the results are to be interpreted with caution. Here, they are used as an indication of spatial flux patterns and further analysis to derive quantitative information would go beyond the scope of this study.

The intensities of each grid were superimposed onto an image of the flux footprint and the natural neighbour interpolation of each grid square was calculated using Voronoi tessellation. This describes the Delaunay triangulation of x, y when F_s = 0 and the interpolation of F_s values for a new specified domain of x, y from the Voronoi dual.

The 300 m radius was found as the optimum distance from the measurement site after $\phi(x, y, z_m)$ was calculated using a radius of 200, 250, 300, 350 and 400. Results showed that past 300 m, the contributions to the total flux were minimal.

3.3.6. Factor OH reactivity and photochemical ozone creation potential estimates

The OH reactivity for each factor was calculated using a method similar to that described in Millet et al. (2018) whereby OH reaction rate constants, k_s, for each VOC species, s, are used to determine the OH reactivity, $R_{OH,s}$ (in units of s^{-1}). The concentration of each VOC species, c_s, calculated for each PMF factor, f, can then be used to find the first-order loss rate for ambient OH due to each factor:

$$R_{OH,f} = \sum_{s=0}^{N} k_s c_s \quad (3.11)$$

A similar equation can be used to describe the OH reactivity flux (in units of cm s^{-2}) for each factor, $F_{OH,f}$, where the concentration of each species is replaced with the flux, F_s:

$$F_{OH,f} = \sum_{s=0}^{N} k_s F_s \quad (3.12)$$

The Estimate Program Interface (EPI Suite™) developed by the United States (US) Environmental Protection Agency (EPA) (EPI Suite™ for Microsoft® Windows, v3.20. US EPA, Washington, DC, USA) was used to estimate k_s values for known VOC species. A best-guess approach was used the assign measured ions that have multiple possibilities using additional information such as vapour pressure and boiling point temperature. For unassigned species which have an unambiguous molecular formula, the k_s values were estimated using the approach described in Donahue et al. (2013):

$$k_s = \sim 1.2x10^{-12}(N_C + 9N_O - 10(O{:}C)^2) \quad (3.13)$$

Here, N_C and N_O respectively represent the numbers of carbon and oxygen atoms in species s, and $O{:}C$ is the oxygen to carbon ratio.

The photochemical ozone creation potential (POCP) of a VOC quantifies its propensity to form ozone from photochemical reactions in the troposphere. It is calculated through model simulations of the reactions of the individual VOC species under a specified, or a range of, atmospheric conditions. The magnitude of a POCP depends on atmospheric conditions such as NO_x concentrations and VOC:NOx ratio, in addition to the intrinsic reactive properties of the VOC compound itself. In this study, a POCP was estimated for each factor using a Maximum Incremental Reactivity (MIR) scale. The IR is calculated as the change in ozone divided by the amount of a VOC species that is added to the system. The 'maximum' IR relates to high-NO_x conditions which is highly applicable to conditions in Delhi during 2018 (Chen et al., 2021). The MIR scale used was calculated using the SAPRC-07 chemical mechanism developed by Carter (2010) and updated by Venecek et al. (2018). Using the same principles as for the OH reactivity, the weighted-POCP was estimated for concentrations and fluxes using the following equations:

$$POCP_{c,f} = \sum_{s=0}^{N} MIR_s c_s \quad (3.14)$$

and

$$POCP_{F,f} = \sum_{s=0}^{N} MIR_s F_s \quad (3.15)$$

where the sum of the species-specific MIRs, MIR_s, for each factor is multiplied by the species factor concentration and flux to give the total factor POCP-weighted concentration, $POCP_{c,f}$, and flux, $POCP_{F,f}$.

3.3.7. Auxiliary measurements

Concentrations of PM_1 for comparison were measured using a co-located high-resolution time-of-flight aerosol-mass-spectrometer (HR-TOF-AMS, Aerodyne Research Inc.). The 5-min average concentrations were measured in V-mode and source apportionment of the organic fraction was performed using positive matrix factorisation (PMF). The full details of instrument operation, calibrations and source apportionment are in Cash et al. (2021). Concentrations of PM_1 Zn and Pb were also used in this study for the identification of a VOC PMF factor. Although the slow vaporisation of Zn and Pb within the HR-TOF-AMS means that calibration is required to give quantitative concentrations, the relative pattern of their time series still provides helpful insight. Contamination of the signal in the form of neighbouring peaks was observed on the most abundant isotopes of these elements. The signals at ^{66}Zn and ^{204}Pb showed low correlations (Pearson's $r < 0.25$) with the time series of neighbouring peaks, showing minimal contamination. The time series for Zn and Pb were therefore derived from the signals for ^{66}Zn and ^{204}Pb multiplied by their respective natural abundances.

Other data used here include NO_x and CO concentrations measured by a dual-channel high-resolution chemiluminescence instrument (Air Quality Designs Inc., Colorado) and a Aerolaser AL 5002 UVU, respectively. Black carbon (BC) concentrations were derived from Aethalometer AE-31 absorptions corrected

using the Weingartner method (Weingartner et al., 2003). Meteorological measurements were made with a Vaisala weather transmitter (WXT530 Series) and ultrasonic anemometer (HS-50 Gill research). The boundary layer height and surface solar radiation downwards (SSRD) were obtained from the ERA5 land model (download at: https://cds.climate.copernicus.eu/cdsapp#!/home).

3.4. Results

3.4.1. Overview of source apportionment factor profiles, concentrations and fluxes

The 9-factor PMF solution was initially derived for TEA-weighted up- and down-draught concentrations before the flux was calculated (see section 3.4.2). This solution includes two factors that relate to burning, named solid-fuel combustion VOC (SFVOC) and pyrotechnical-activity VOC (PVOC), and two factors that relate to traffic emissions (named TRAF1 and TRAF2). A factor that is associated with diesel-generators is named 'GEN-VOC' and another factor, whose composition is dominated by ethyl acetate, appears to be linked to industrial solvent use and is named 'IND-VOC'. A factor seemingly related to evaporative emissions is named evaporative VOC (EVOC). This was found to comprise sources of surface evaporation, such as asphalt emissions, and also includes biogenic emissions. The last two factors are composed of oxidised VOCs (OVOC1 and OVOC2). The mass spectral profiles for each of these factors are shown in Figure 3.1a and their average flux and concentration are shown in Figure 3.2. This section first gives an overview of the factor concentrations and fluxes, before describing the method for choosing the final solution. This is followed by the identification of each factor along with detailed information on their composition.

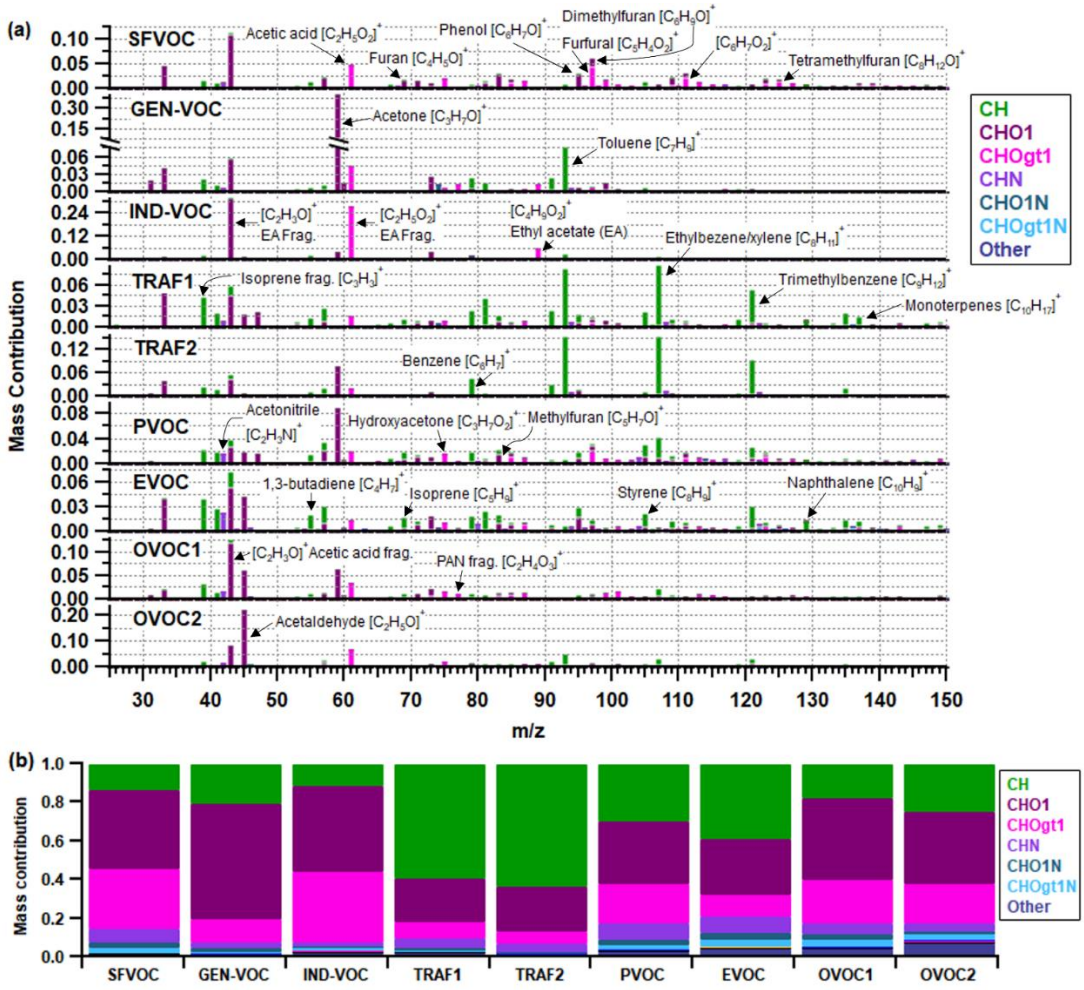

Figure 3.1. (a) 9-Factor PMF solution mass spectra showing peaks that are coloured according to their chemical family, as indicated in the legend. The masses of each high-resolution ion are averaged to the closest nominal *m/z* and then presented as a unit mass resolution spectrum. (b) The mass contribution of each family to the total mass of each factor.

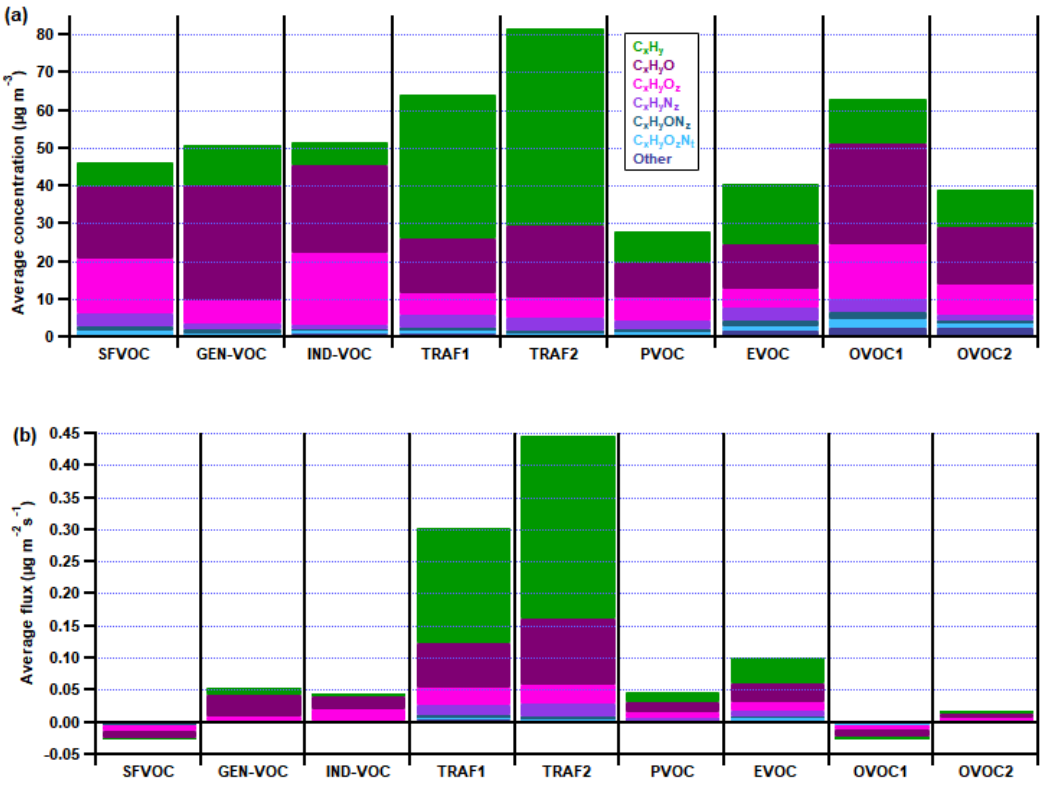

Figure 3.2. Average concentrations (a) and average fluxes (b) for the 9-factor solution. Each factor is separated into chemical families and coloured according to the legend.

The 9 factors can be assigned to one of 6 source-related categories. Traffic-related factors contribute the largest average concentrations (TRAF1 + TRAF2 = 293 µg m^{-3}) and oxidised factors contribute the second largest average concentrations (OVOC1 + OVOC2 = 205 µg m^{-3}). The next highest contribution is from burning-related factors (SFVOC + PVOC = 149 µg m^{-3}), followed by industrial emissions (IND-VOC = 51.7 µg m^{-3}) and diesel generators (GEN-VOC = 51.2 µg m^{-3}). The source category contributing least on average is evaporative emissions (EVOC = 40.9 µg m^{-3}). The majority of the traffic factor mass derives from hydrocarbon species (C_xH_y). All other factors are dominated by oxygen-containing species (Figure 3.1b).

The two factors with the highest composition of C_xH_yO (CHO1) and $C_xH_yO_z$ (CHOgt1) groups, IND-VOC (82%) and GEN-VOC (72%), contain individual oxygen-containing species that make up the majority of their mass. This includes acetone (*m/z* 59) in GEN-VOC and the acetic acid fragment ions, $[C_2H_3O]^+$ (*m/z* 43) and $[C_2H_5O_2]^+$ (*m/z* 61), in IND-VOC. However, most other oxygen-containing species are spread across all factors. In fact, the two chemical families of C_xH_yO and $C_xH_yO_z$ account for 54% of the total VOC concentrations whereas C_xH_y accounts for 34%, which highlights the importance of studying complex oxygen containing VOC species.

Overall, there are net emissions of VOC at the IGDTUW site, which is largely due to traffic emissions (Figure 3.2b) (70% of total average flux). The two traffic factors largely comprise hydrocarbon species including benzene, toluene, xylene and trimethylbenzene. Despite having the lowest concentrations, the EVOC factor has the third largest flux (10% of total average flux). EVOC is composed of 41% C_xH_yO and $C_xH_yO_z$ compounds and 39% C_xH_y compounds. This is mainly due to methanol (*m/z* 33), the fragment ion, $[C_2H_3O]^+$ (*m/z* 43), and acetaldehyde (*m/z* 45). EVOC also has the highest contribution of N-containing species (i.e. $C_xH_yN_z$, $C_xH_yN_zO$ and $C_xH_yN_zO_t$ combined) at 15% of its mass, which is mostly due to acetonitrile (*m/z* 42) and a series of $C_xH_yN_zO$ and $C_xH_yN_zO_t$ species.

The only two factors to show a net deposition flux are SFVOC and OVOC1. SFVOC has the second lowest composition of C_xH_y compounds (14%) and is mostly composed of oxygenated compounds (C_xH_yO and $C_xH_yO_z$, 72%). Both OVOC factors have a large contribution from C_xH_yO and $C_xH_yO_z$ species (66% for OVOC1 and 60 % for OVOC2) and OVOC1 has the largest contribution from $C_xH_yO_zN_t$ species (4%). More detailed discussion of specific compounds is presented in the following section.

3.4.2. Selection of PMF solution

This section describes the steps of choosing a PMF solution for the concentration data, and is similar to the method used in Cash et al. (2021). The number of factors chosen for comparison were between 8-9. Solutions with greater than 9 factors, resulted in one factor splitting into two with little or no reduction in the residuals, a small incremental drop in Q/Q_{exp} and no further explanation of possible sources from the dataset. Exploration of the rotational ambiguity of the solution was performed by an assessment of the FPEAKS (-3 to 3) for each solution. This showed little variation and the FPEAK was set to zero for each solution (Figure 3.3a). All 8-factor solutions showed little to no variation with initialisation SEED (Figure 3.3b). In contrast, the 9-factor solutions did show some variation with initialisation SEED (Figure 3.3c). When the SEED is equal to zero, the 9^{th} factor (PVOC) separates using a combination of leftover residual mass, along with mass from OVOC2, EVOC and SFVOC (Figure 3.3e). The difference in the residuals between the 8- and 9-factor solutions is also small which shows elements of splitting. This scenario has been previously observed in a study analysing organic mass spectra from an AMS, where evidence of splitting was found in a 5-factor solution. Further multilinear regression analysis found the 5-factor solution to be equal in its fit with external tracers when compared to its non-splitting 4-factor solution (Young et al., 2015). We therefore go on to compare the 8- and 9-factor solutions using a similar method, described later in this text. However, the 9-factor solutions at different SEEDS required exploration first in order to select the best solution to compare with the 8-factor solution.

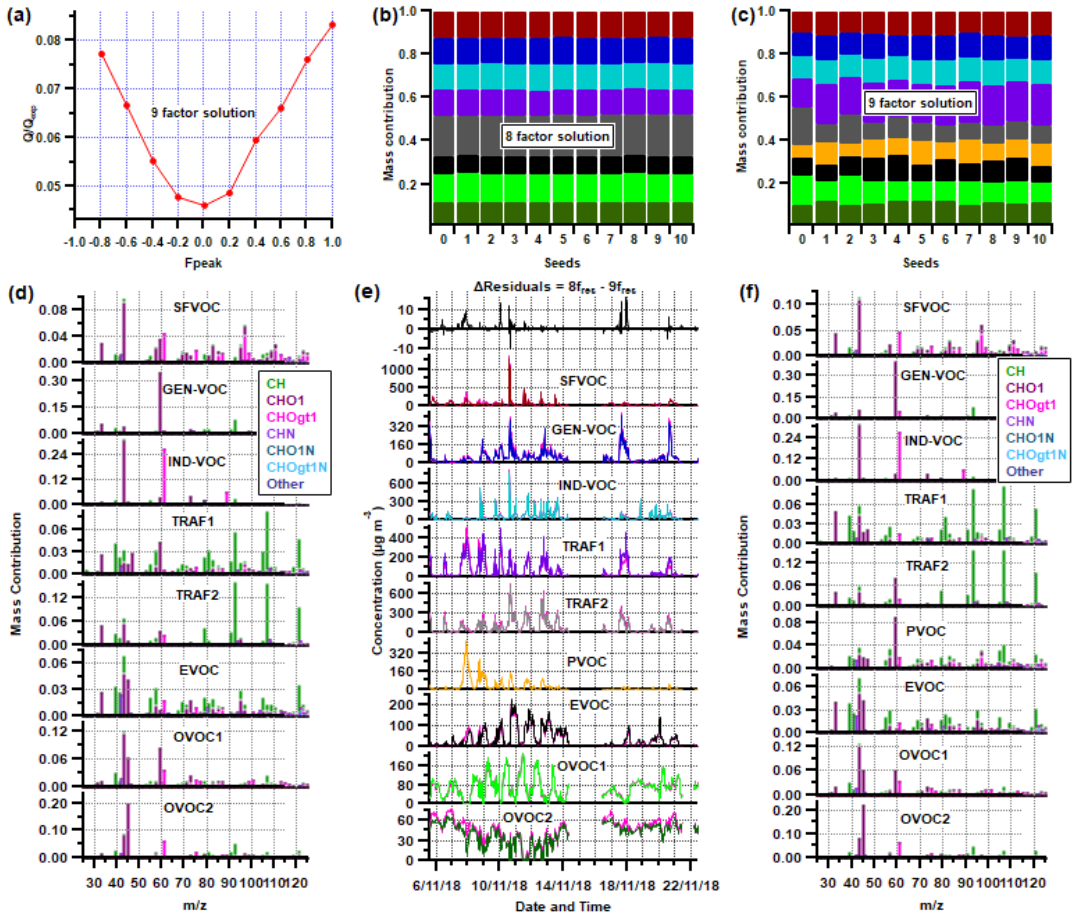

Figure 3.3. A comparison of 8 and 9 factor solutions. The Q/Q_{exp} values for the 9-factor solution using different FPEAKS are shown in (a), along with the differences in mass for the 8-factor (b) and 9-factor (c) solution using different initialisation SEEDS. The mass profiles for the two solutions are shown in (d) and (f), respectively. A comparison of the factor time series is shown in (e) where each factor of the 9 factors are colour coded and the 8-factor solution is underlaid in pink. PVOC is the only factor that appears additionally in the 9-factor solution but not in the 8-factor solution.

3.4.3. Multilinear regression analysis for the 9 factor solutions at different SEEDs

The following multilinear regression analysis established which of the SEED solutions created the best fit to co-located measurements, known as external tracers (ET):

$$ET = A + B(SFVOC) + C(PVOC) + D(TRAF1) + E(TRAF2) + F(EVOC) \quad (3.16)$$

where the residuals of the fit, *A*, represent the background concentration of the ET. The contribution to the fit of each factor time series $SFVOC$, $PVOC$, $TRAF1$, $TRAF2$ and $EVOC$ is represented by its corresponding coefficient B, C, D, E and F. The three ET measurements used were black carbon (BC), CO and NO_x and the factors chosen for the regression were the primary organic aerosol (POA) factors as these are expected to be associated with the trend of the ET. The results of this analysis are summarised in Table 3.1.

Table 3.1. Pearson's *r* (Pr) correlations for the pentalinear regressions between 9-factor SEED solutions and the external tracers NO_x, CO and BC. The largest Pr correlation for each regression is highlighted in bold.

SEED No.	*BC Pr*	*CO Pr*	*NO_x Pr*
SEED 0	0.8996	**0.9614**	**0.895**
SEED 1	0.8937	0.9611	0.8922
SEED 2	**0.9008**	0.9613	0.8944
SEED 3	0.8916	0.9579	0.8946
SEED 4	0.893	0.9587	0.8882
SEED 5	0.8937	0.961	0.8902
SEED 6	0.8936	0.9612	0.8928
SEED 7	0.8916	0.9579	0.895
SEED 8	0.8936	0.961	0.8926
SEED 9	0.8921	0.9576	0.8942
SEED 10	0.8941	0.961	0.8921

A solution was chosen based on the highest Pearson's *r* correlations between the multilinear regression fit and the external tracers. From Table 3.1, the SEED 0 yielded the highest correlation with CO and NO_x and the second highest with BC. Solution SEED 0 also had the second lowest Q/Q_{exp} value to SEED 2 but by a small margin (0.000005). The differences between SEED 0 and SEED 2 are therefore marginal and the default solution of SEED 0 was chosen as the final solution.

It should be noted that when the GEN-VOC factor was also incorporated into hexalinear regressions, its regression coefficient for all NO_x was consistently negative for all solutions. Further characterisation of GEN-VOC suggests it is likely linked to diesel emissions (see section 3.4.5.4) which has a strong association with NO_x. GEN-VOC was, therefore, deemed not suitable to use in the regressions. Nevertheless, SEED 0 still gave the highest correlation in the hexalinear regression so is consistent with the choice of SEED 0 based on the pentalinear regressions.

3.4.4. Multilinear regression analysis for the comparison of 7, 8 and 9 factor solutions

The 9-factor SEED 0 solution and the 8-factor solution were compared, along with a 7-factor solution which represented a baseline. The number of variables in the multilinear regression was decreased as follows to include only one SFVOC variable because both the 7- and 8-factor solutions had only one SFVOC factor.

$$ET = A + B(SFVOC) + C(TRAF1) + D(TRAF2) + E(EVOC) \quad (3.17)$$

The time series used for $SFVOC$ in the 9-factor solution was a combined time series of factors SFVOC and PVOC. A singular SFVOC factor time series was used for the 7- and 8-factor solutions. The results from this analysis are presented in Table 3.2 where the correlations for the regressions using 7-, 8- or 9-factor solutions for a given ET have been ranked in magnitude. The Pearson's *r* correlations for the fits to BC and CO are highest for the 9-factor solution and using this solution also yields the lowest total ranking for regressions across all three ETs. Increasing the number of factors to 9, therefore, shows an improved fit to ETs so this was the chosen final solution.

Table 3.2. Pearson's *r* (Pr) correlations for the tetralinear regression of 7-, 8- and 9-factor solutions and the external tracers: NO_x, CO and BC. The magnitudes of the correlations of the fits to a given external tracer are ranked 1st, 2nd and 3rd (in brackets) and the sum of the rankings for each N-factor solution are shown in the bottom row.

No. of factors	BC Pr	CO Pr	NO_x Pr	Total Score
7 factors	0.8998 (2)	0.9497 (3)	**0.8770 (1)**	6
8 factors	0.8976 (3)	0.9543 (2)	0.8732 (2)	7
9 factors	**0.9005 (1)**	**0.9568 (1)**	0.8606 (3)	**5**

3.4.5. Factor identification and composition

3.4.5.1. Traffic factors: TRAF1 and TRAF2

The mass spectra for the two traffic factors have distinct peaks relating to traffic emissions at *m/z* 79 (benzene), *m/z* 93 (toluene), *m/z* 107 (ethylbenzene or xylene) and *m/z* 121 (trimethylbenzene), which are commonly referred to as 'BTEX' species (Figure 3.1a) (Wang et al., 2020b). The large mass of BTEX species means that hydrocarbons dominate the composition of the two traffic factors (59-64% contribution to the total mass) and both have the lowest percentage mass of oxygen containing species (30-31%) (Figure 3.1b). The spatial flux patterns in Figure 3.4 show factor emission fluxes using complete time series with all instances of deposition removed. The maps help to further justify the origin of TRAF1 and TRAF2 as they show strong emissions originating from an area with two bus stops. Buses were frequently seen waiting for passengers here and causing traffic to bottleneck.

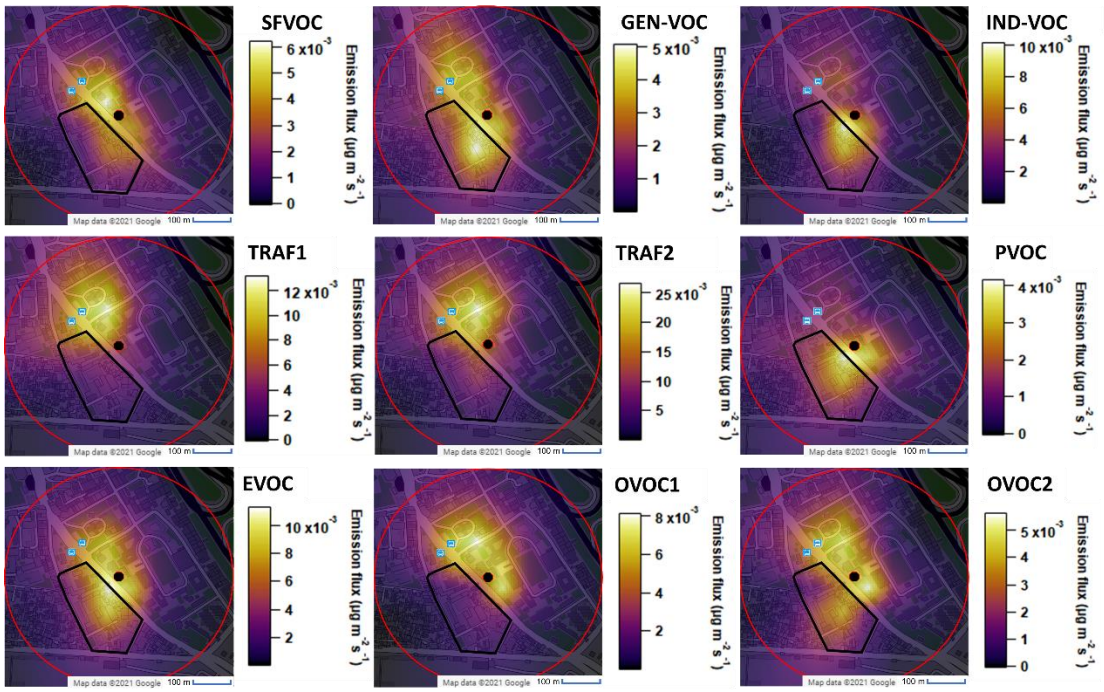

Figure 3.4. Spatial emission flux patterns for each PMF factor. Flux time series covering the whole measurement period are used with instances of deposition removed. The fluxes are allocated based on the maximum of the flux footprint. The red circle marks a 300 m radius around the measurement site (black centre marker). The black area outlines an automotive parts business sector. The locations of two bus stops are labelled with blue bus symbols.

There are notable compositional differences between the TRAF1 and TRAF2 factors, which implies the two factors are related to different fuel or vehicle types. TRAF1 has a number of peaks that are absent in TRAF2, including styrene (*m/z* 105) which is emitted in higher amounts from diesel vehicles than from gasoline vehicles (Elbir et al., 2007). Another key diagnostic peak for diesel tailpipe emissions is naphthalene (*m/z* 129), which is clearly present in TRAF1 but not in TRAF2 (Figure 3.1a). Other less pronounced peaks of napthalenic monoaromatics (*m/z* 119, 133, 147, 161, 175 and 189) and napthalenes (*m/z* 129, 143, 157 and 171) are also higher in TRAF1 than TRAF2. Similar to diesel vehicle emissions, naphthalene-related compounds have previously been shown to be one of the most distinguishing compositional differences in PTR-MS measurements of diesel and gasoline fuel (Erickson et al., 2014). The diesel fuel also had higher cycloalkane

composition (*m/z* 69, 83, 97, 111 and 139) which is again reflected in the TRAF1 factor. The same study also measured higher alkylbenzene species (*m/z* 79, 93, 107, 121, 135, 149, etc.) in gasoline fuel and exhaust emissions which is also consistent with the composition of our TRAF2 factor.

The two traffic factors also separate based on their diurnal cycles: the majority of TRAF1 emissions occur during the evenings and early parts of the morning (Figure 3.5b), whilst TRAF2 emissions peak during midday and gradually decrease throughout the evening. TRAF1 is therefore linked to diesel vehicles, particular heavy goods vehicles (HGV) whose access to the city is restricted during the day. Therefore, TRAF1 represents mostly diesel vehicles, whilst TRAF2 represents the daytime vehicle fleet, i.e. a mixture of gasoline and compressed natural gas (CNG) vehicles. These source assignments are consistent with PMF analysis on co-located HR-TOF-AMS measurements (Cash et al., 2021) and a previous PTR-MS study in Delhi, which similarly identified two different traffic factors (Wang et al., 2020b).

The concentration ratio between TRAF1 and TRAF2 changes across the measurement campaign. There is an initial high peak in TRAF1 concentrations during the Diwali holiday period (04/11/18 - 10/11/18) which is contrasted by low concentrations of TRAF2 (Figure 3.7). This likely reflects the ongoing shipment of goods into the city due to HGVs and the decrease in petrol/CNG usage due to the closure of businesses and places of work caused by the Diwali holiday. The TRAF1:TRAF2 concentration ratio then begins to decrease after Diwali as daily commuters begin to return to work, therefore, causing an increase in petrol and CNG vehicles.

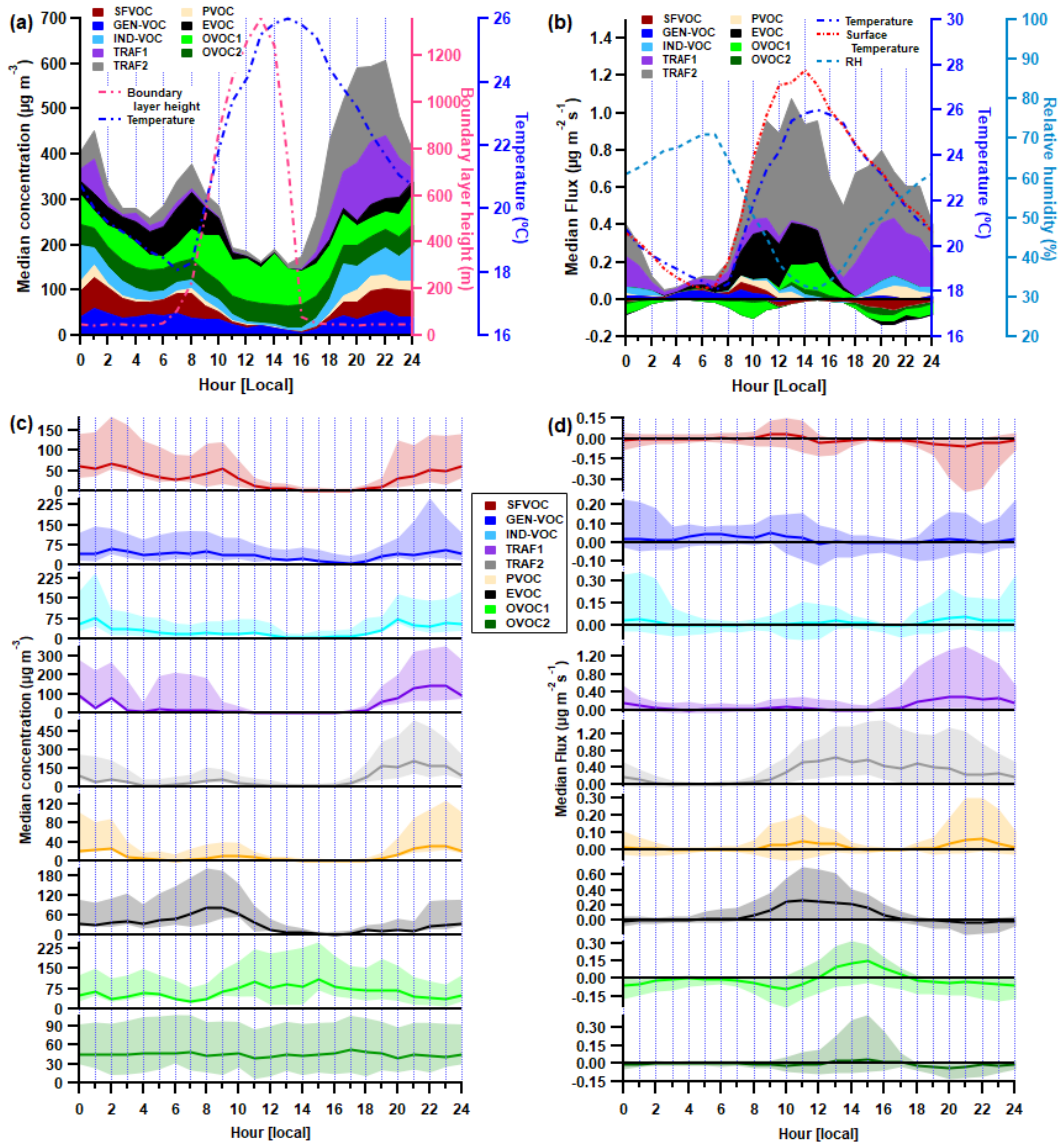

Figure 3.5. PMF factor diurnal cycles showing (a) stacked median concentrations and (b) stacked median fluxes. The dashed lines in (a) and (b) show the temperature, surface temperature, relative humidity, along with the boundary layer height as calculated by the ERA5 land model. The diurnal cycles for concentrations (c) and fluxes (d) are shaded to show the 25th and 75th percentiles.

3.4.5.2. Evaporative VOCs factor

The EVOC factor has a mixture of peaks that overlap with a couple of other factors. Peaks shared with TRAF1 include *m/z* 39 (isoprene fragment ion, $[C_3H_3]^+$), isoprene *m/z* 69 (isoprene), *m/z* 79 (benzene), *m/z* 105 (styrene), *m/z*

121 (trimethylbenzene) and *m/z* 137 (monoterpenes) (Figure 3.1a). It also has similar peaks to the burning sources such as acetonitrile (*m/z* 42), hydoxyacetone (*m/z* 75), vinyl acetate (*m/z* 87) and phenol (*m/z* 95). However, it has the largest contribution from naphthalene (*m/z* 129), tetralin (*m/z* 132), methyl tetralin (*m/z* 146) and dimethyl naphthalene (*m/z* 156) out of the 9 factors which alludes to it being an evaporative source as these are species associated with asphalt emissions (Gasthauer et al., 2008; Khare et al., 2020; Zheng et al., 2018).

Evaporative VOC surface emissions have been observed in a previous VOC concentration source apportionment study in Delhi (Srivastava et al., 2005b). Measurements at two sites near to IGDTUW, the Income Tax Office (ITO) road crossing (~3 km south) and Karol Baugh (~4 km west), showed similarly high contributions from a surface evaporative VOC source (18% and 20%, respectively). Other studies in India have shown the existence of large quantities of evaporative emissions, however, their measurements link directly to emissions from vehicle headspaces or hot soaking and the refuelling of vehicles (Sharma et al., 2015; Srivastava et al., 2005a; Srivastava and Majumdar, 2010).

The evaporative nature of the EVOC source is more apparent from its flux behaviour which increases with temperature during the mornings (Figure 3.5b). It then peaks at around midday and starts to decrease rapidly as the rate of evaporation no longer exceeds the rate of deposition. Additionally, the high abundances of isoprene and monoterpene in the EVOC profile suggests it also includes biogenic emissions, which are also strongly temperature dependent. A further investigation was undertaken to explore the contribution of biogenic emissions on EVOC and is discussed in section 3.5.3.

The EVOC mass profile has large contributions from 1,3-butadiene (*m/z* 55) and styrene (*m/z* 105) peaks (Figure 3.1a) which could arise from the binder used in asphalt. The block polymer styrene-butadiene-styrene (SBS) is

commonly used as a thermoplastic in Indian cities for roads and pavements (Muhmmad Aadil et al., 2019). A number of studies have measured 1,3-butadiene and styrene emissions from SBS-containing asphalt (Li et al., 2020; Liu et al., 2005; Wang et al., 2020a; Xiu et al., 2020). One study also suggested the following species are oxidation products of VOCs emitted from SBS asphalt: 3-buten-2-ol (*m/z* 73), (E)-1,3-butadien-1-ol (*m/z* 71) and methyl vinyl ketone (also *m/z* 71) (Li et al., 2021). Our EVOC mass profile also shows large peaks of these species (Figure 3.1).

Another commonly used binder in Indian cities is the block polymer styrene-isoprene-styrene (SIS) (Muhmmad Aadil et al., 2019). To the authors knowledge, no studies have measured the VOC emissions from SIS containing asphalt but it is reasonable to assume that the main building blocks of this polymer would also be emitted i.e. styrene and isoprene. This could therefore be another source contributing to the high isoprene composition of EVOC, particularly as the isoprene fragment ion $[C_3H_2]^+$ (*m/z* 39) is the highest C_xH_y family peak in EVOC and the isoprene molecular ion peak (*m/z* 69) is greater in EVOC than any other factor (Figure 3.1). Additionally, it is worth noting that, as well as asphalt products, SIS is also used in other applications that can cause evaporative VOC emissions such as vehicle tyres (Naddeo et al., 2021).

The EVOC nitrogen species profile contains the highest contribution from acetonitrile out of all factors (Figure 3.6). Acetonitrile has been reported previously in emissions from asphalt although at relatively low concentrations (Li et al., 2020). This suggests that EVOC also reflects other evaporative sources. A number of possibilities exist. For example, it could be associated with a particular burning phase of biomass burning or be linked to solvent-use in the automotive sector situated nearby. Other nitrogen species within the EVOC profile include the tentatively assigned dimethylformamide (*m/z* 74), pyridine (*m/z* 80), ethylpyridine or methylbenzenamine (*m/z* 94), 4-pyridinol (*m/z* 96), benzonitrile (*m/z* 104) and benzamide (*m/z* 122), furoylacetonitrile (*m/z* 136) and phenylnitroethene (*m/z* 150). There are also large nitrophenol

peaks at *m/z* 140 and *m/z* 154 which are also seen in the burning factors, suggesting it is influenced by the evaporative emissions from solid fuel or biomass burning sources.

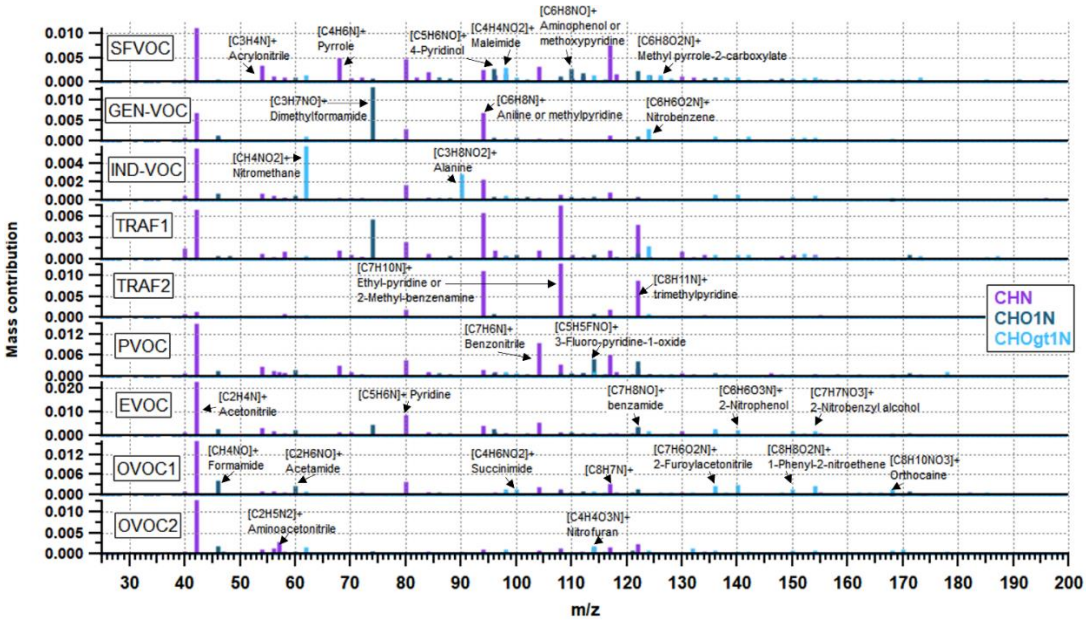

Figure 3.6. Factor mass spectral profiles for nitrogen containing species. The peak labels are tentatively assigned according to the GLOVOCs database (Yáñez-Serrano et al., 2021).

3.4.5.3. Burning-related factors: SFVOC and PVOC

The two factors, SFVOC and PVOC, share similar peaks at *m/z* 42 (acetonitrile), *m/z* 75 (hydroxyacetone), *m/z* 83 (methylfuran), *m/z* 85 (furanone), *m/z* 87 ($[C_4H_6O_2]^+$, an ion with multiple possible parent species including 2,3-dihydro-1,4-dioxin and methyl acrylate) and *m/z* 97 (furfural), which are commonly associated with burning-related sources (Andreae, 2019; Koss et al., 2018). The distinguishing peaks in SFVOC are *m/z* 69 (furan), *m/z* 95 (phenol), *m/z* 111 ($[C_6H_7O_2]^+$, hydroxyphenol, acetylfuran or methylfurfural) and *m/z* 125 (tetramethylfuran). It also has much larger abundances of

dimethylfuran ($[C_6H_9O]^+$) and furfural ($[C_5H_4O_2]^+$). These peaks in SFVOC were also observed in high concentrations during a chamber study in which domestic plastics and municipal waste were burned (Stewart et al., 2021a).

The SFVOC factor exhibits a morning and evening peak in its concentration diurnal cycle (Figure 3.5c). A similar pattern was observed in the concentrations of a solid-fuel organic aerosol (SFOA) burning factor resolved in co-located high-resolution time-of-flight aerosol mass spectrometry (HR-TOF-AMS) measurements (Cash et al., 2021). Additionally, there is a strong correlation between the time series of the AMS-measured SFOA factor and the SFVOC factor (Pearson's r = 0.709). The SFOA factor was attributed to residents burning street waste in the mornings and evenings to clear the streets or for warmth. Figure 3.5d shows that there is an emission of SFVOC in the morning at a similar time (9 a.m.) to the peak in concentrations (Figure 3.5c). However, the fluxes of SFVOC are small but its sources likely exist throughout the city, which suggests most of its sources are located outside the flux footprint.

A previous study in Delhi using PTR-TOF-MS measurements resolved two solid-fuel PMF factors, one of which contained a number of nitrogen species (Wang et al., 2020b). These included $[C_3H_4N]^+$, $[C_4H_6N]^+$, and $[C_7H_6N]^+$ which can be tentatively assigned as acrylonitrile, pyrrole and benzonitrile. The SFVOC factor here contains similar nitrile species but also large peaks for pyridine ($[C_5H_6N]^+$, *m/z* 80) and aniline or methylpyridine ($[C_5H_6N]^+$, *m/z* 94). The nitrophenol peaks observed by Wang et al. (2020b) are also present in SFVOC at *m/z* 140 ($[C_6H_6NO_3]^+$) and *m/z* 154 ($[C_7H_7NO_3]^+$) although they are in much larger abundance in OVOC1. Wang et al. (2020b) suggested these species provide evidence of night-time NO_3 radical chemistry.

The SFVOC factor also contains more $C_xH_yNO_z$ species than reported by Wang et al. (2020b), including peaks such as 4-pyridinol ($[C_5H_6NO]^+$, *m/z* 96), maleimide ($[C_4H_4NO_2]^+$, *m/z* 98, aminophenol or methoxypyridine),

($[C_6H_8NO]^+$, *m/z* 110), benzamide ($[C_7H_8NO]^+$, *m/z* 122), and other smaller peaks (Figure 3.6). This highlights the importance of pyridine-based structures in the composition of SFVOC. Pyridines (including pyridinol) are seen in large amounts from peat burning (Kosyakov et al., 2020). In Delhi, another nitrogen-rich fuel called “dung-cakes” is often used, which are essentially dried cow faeces. GC-MS measurements of VOCs taken while burning dung-cakes have also shown high concentrations of pyridines (Stewart, 2021). The comprehensive range of pyridinic compounds within SFVOC could therefore suggest that dung-cakes are a significant contributor to burning-related VOC concentrations.

The PVOC factor has a large peak in concentration during the evening of Diwali (08/11/18) followed by several smaller evening peaks (Figure 3.7). This trend is similar to the uncalibrated concentration time series for Zn and Pb measured by HR-TOF-AMS. The timings of the increase in Zn or Pb concentrations suggest they arise from pyrotechnical activities such as fireworks or firecrackers and therefore that PVOC is associated with the same activities. The emission of PVOC is infrequent, as shown by its low median flux (Figure 3.5b), but its peak emissions occur during the late evening when fireworks are often set off during Diwali. We therefore define the PVOC factor as burning due to pyrotechnical activity.

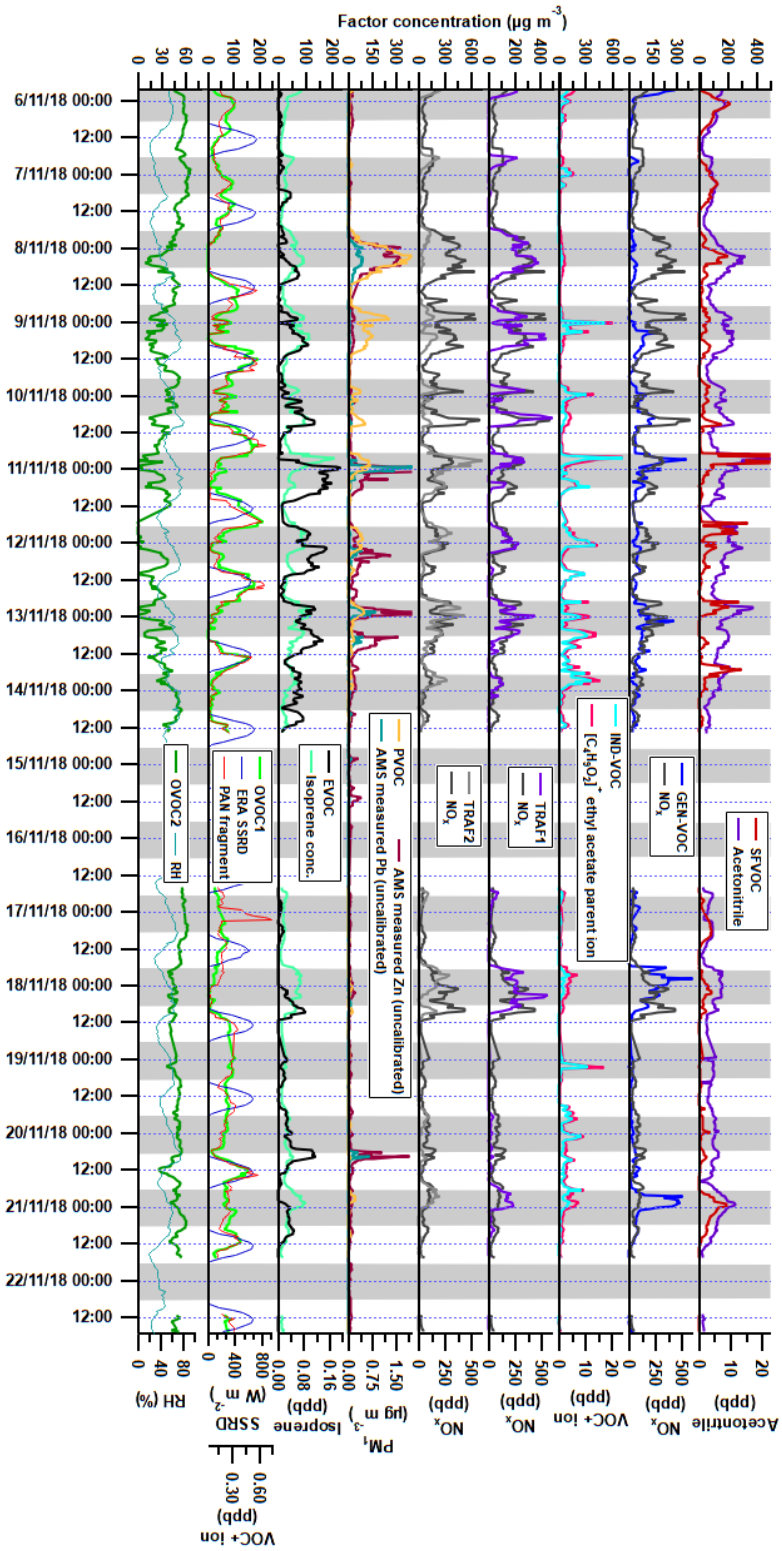

Figure 3.7. Factor concentration time series alongside associated auxiliary measurements. The concentrations of acetonitrile, ethyl acetate parent ion ($[C_4H_9O]^+$), isoprene and peroxyacetic nitric anhydride (PAN) fragment ion ($[C_4H_4O_3]^+$) were measured by the PTR-MS. The PM_1 uncalibrated Zn and Pb concentrations were measured by co-located HR-TOF-AMS. The NO_x concentrations were measured by a dual-channel high-resolution chemiluminescence instrument. The surface solar radiation downwards (SSRD) was obtained from the ERA5 land model (details available at: https://apps.ecmwf.int/codes/grib/param-db?id=169#grib2).

As discussed above, the composition of PVOC is largely similar to SFVOC. It has the markers for biomass burning and, although their intensity is smaller, species connected to plastic burning, such as *m/z* 83 (methylfuran), *m/z* 85 (furanone), furfural (*m/z* 97) and styrene (*m/z* 105). The latter will derive from the plastic packaging often used to protect the fireworks and firecrackers from damp and accidental ignition. It also has some C_xH_y species such as *m/z* 105 (styrene), *m/z* 107 (toluene) and *m/z* 121 (trimethylbenzene) which suggests PVOC is less aged than SFVOC.

3.4.5.4. Factors relating to industrial solvent use (IND-VOC) and electricity generators (GEN-VOC)

The IND-VOC factor contains three dominant mass spectral peaks: *m/z* 43, 61 and 89 (Figure 3.1a). This pattern of peaks has previously been observed in PTR-MS measurements of ethyl acetate, both in a controlled lab study at similar ionisation energies and humidity conditions (Baasandorj et al., 2015), and in ambient atmospheric measurements (Fortner et al., 2009). It is therefore likely that this factor is mainly ethyl acetate and could be linked to its industrial use as a cleaning solvent.

The IND-VOC factor shows large emissions in its spatial flux originating almost exclusively from an automotive parts business sector to the south-west of the measurement site (Figure 3.4). Its concentration time series also shows spikes during the night which may be automotive businesses leaving parts to be cleaned overnight (Figure 3.7). This suggests a link to solvent-use for cleaning automotive parts.

GEN-VOC has a large peak at *m/z* 59, followed by smaller peaks at *m/z* 43, 61, 79 and 93. The peak at 59 *m/z* is most commonly associated with acetone but it may also be due to propanal or methyl vinyl ether, amongst others. The time series for GEN-VOC has a similar pattern to NO_x concentrations but it is not as consistent as the traffic factors (Figure 3.7). This may signify the factor is due to stationary generators, which are commonplace in Delhi, as its mass

profile shows similarities to that measured for stationary diesel generators in Lebanon, particularly the benzene and toluene ratio (Salameh et al., 2014). Although *m/z* 59 has been identified within traffic-related VOCs in previous source apportionment studies (Chen et al., 2014; Crippa et al., 2013; Stojić et al., 2015; Vlasenko et al., 2009), the high abundance observed here has not generally been reported except for a study in Northwest China (Zhou et al., 2019).

The spatial flux pattern for GEN-VOC shows hotspots above the automotive sector, as well as above the northeast sector of IGDTUW which could house diesel generators for the student accommodation. There is also a large peak in the GEN-VOC concentration time series in the late hours of the 20th of November which is not shared amongst other factors or auxiliary measurements (Figure 3.7). This may be evidence of the nearby automotive sector testing diesel engines overnight or maybe a power cut.

The nitrogen composition of GEN-VOC is similar to that of TRAF1 which, as previously discussed, is a factor linked to diesel emissions. Large peaks are seen in both factors for species tentatively assigned as dimethylformamide ($[C_3H_7NO]^+$), aniline or methylpyridine ($[C_6H_8N]^+$), and nitrobenzene ($[C_6H_6NO_2]^+$) (Figure 3.6). The similarity in their nitrogen species composition further supports GEN-VOC being related to stationary diesel combustion.

3.4.5.5. Oxidised VOC factors

The two oxidised factors, OVOC1 and OVOC2, are characterised by their concentration diurnal cycles being less affected by the boundary layer height than those of the primary emitted factors (Figure 3.5a). The OVOC1 concentration time series, in particular, is strongly correlated with that of the peroxyacetic nitric anhydride (PAN) fragment ($[C_2H_5O_3]^+$, Pearson's r = 0.918), and also follows the general trend of the surface solar radiation downwards (SSRD) (Figure 3.7). This suggests that OVOC1 is strongly related to photochemistry. Other high temporal correlations between OVOC1 and PTR-

MS measured ions include maleic anhydride (r = 0.720), succinic anhydride (r = 0.821) and maleic acid (r = 0.671). A link between an oxidised VOC PMF factor and these species has been seen previously in PTR-MS measurements taken in Delhi (Wang et al., 2020b). These species are also associated with biomass burning (Koss et al., 2018) which suggests OVOC1 is most likely formed from the photochemical oxidation of burning-related VOCs.

The nitrophenol peaks observed in SFVOC are also seen in higher abundance in OVOC1 at *m/z* 140 ($[C_6H_6NO_3]^+$) and *m/z* 154 ($[C_7H_7NO_3]^+$), along with an additional peak at *m/z* 168 ($[C_8H_{10}NO_3]^+$). This similarity between SFVOC and OVOC1 supports OVOC1 being mostly oxidised VOCs from solid fuel or biomass burning sources. Additionally, the observation of nitrophenol peaks in a previous study has been linked to night-time NO_3 radical chemistry (Wang et al., 2020b). This suggests that some OVOC1 mass could result from night-time NO_3 radical oxidation, but this contribution is unlikely to be significant because the diurnal cycle for OVOC1 is fairly flat during the night (Figure 3.5c)

In contrast, OVOC2 has peaks at *m/z* 93, 107 and 121 in a similar temporal pattern to the traffic factors. Its time series shows little correlation with PTR-MS measured species or greenhouse gases. However, it has the strongest correlation of all factors (Pearson's r = 0.579) with a low volatility oxygenated organic aerosol (LVOOA) PMF factor measured during the same time period using a HR-TOF-AMS (Cash et al., 2021). This earlier study showed that LVOOA mass is linked to the creation of SOA through the oxidation of traffic emissions. The origin of OVOC2 is, therefore, most likely driven by the oxidation of traffic emissions rather than specific meteorology.

3.4.6. POCP and OH reactivity estimates of PMF factors

The relative contributions of each PMF factor to OH reactivity and photochemical ozone creation potentials (POCP) are shown in Figure 3.8, alongside the contributions of each factor to the total mass. The relative contributions are expressed with respect to both concentrations and fluxes. It

should be noted that these POCP estimates are based on modelled values for maximum incremental reactivities (MIR). This requires the assumption that the atmospheric conditions under which these metrics were modelled are similar to those at the measurement site. As already mentioned, the MIR scale was chosen over other POCP scales as these were modelled under high NO_x conditions which is highly applicable in Delhi.

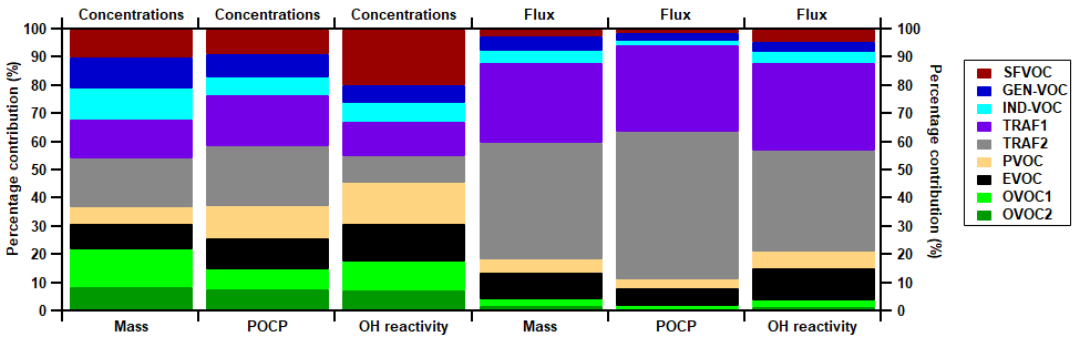

Figure 3.8. The relative contributions of the 9 PMF factors to total mass, OH reactivity and POCP when expressed via absolute concentrations (bars 1-3) and via absolute fluxes (bars 4-6). It should be noted that the average flux for SFVOC and OVOC1 are negative (deposition) as shown in Figure 3.2, hence the use of absolute fluxes and concentrations.

Figure 3.8 shows that the traffic-related VOCs (= TRAF1 + TRAF2) have high contributions to the OH reactivity (22%) and POCP (39%) when expressed by VOC concentrations. They also dominate contributions to OH reactivity (67%) when expressed as the flux of VOCs. The concentration-weighted OH reactivity and POCP mass profiles of each factor are displayed in Figure 3.9 to show the most significant species within each factor. The BTEX species are the largest peaks in the OH reactivity mass profiles for TRAF1 and TRAF2, which are followed by the aniline ion, $[C_6H_7N]^+$ (*m/z* 94) and the acetic acid fragment ion, $[C_2H_3O]^+$ (*m/z* 43) (Figure 3.9). However, TRAF1 has additional high contributions from isoprene (*m/z* 69) and styrene (*m/z* 105).

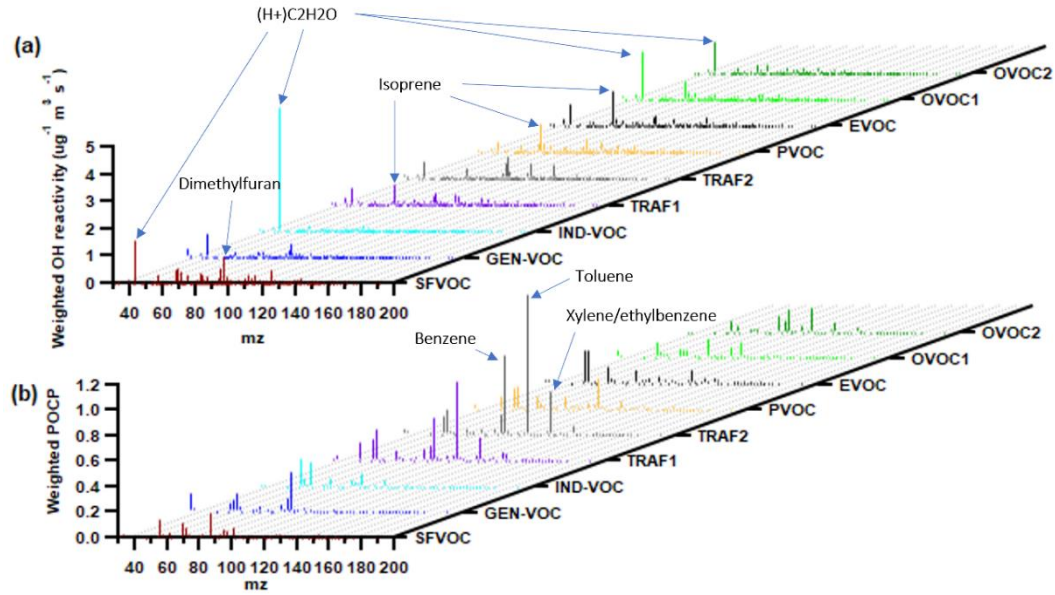

Figure 3.9. Concentration-weighted (a) OH reactivity and (b) POCP mass profiles for each PMF factor.

The concentration-weighted OH reactivity contributions for the SFVOC (20%) and PVOC (14%) burning-related factors (total = 34%) suggest they have the largest effect on the oxidative capacity of the atmosphere above Delhi (Figure 3.8). The most notable species responsible for SFVOC concentration-weighted OH reactivity are the tentatively assigned acetic acid fragment ion, $C_2H_3O^+$ (*m/z* 43), furan (*m/z* 69.034), phenol (*m/z* 95), dimethyl furan (*m/z* 97) and the ion, $[C_8H_{12}O]^+$ (*m/z* 125), which could be a number of species but here it is assigned as trimethylfuran. Similarly, the concentration-weighted OH reactivity of PVOC is dominated by isoprene (*m/z* 69.071), dimethyl furan (*m/z* 97), styrene (*m/z* 105) and trimethylfuran. (*m/z* 125). This highlights the importance of furan species on the oxidising capacity of the atmosphere in Delhi. This observation is supported by other studies that have also shown furan species to be high contributors to measured OH reactivity within biomass burning VOCs (Coggon et al., 2019; Hartikainen et al., 2018).

The localised fluxes of both PVOC and SFVOC are small but, as discussed above, most of their sources are thought to be outside the flux footprint. As a result, their combined OH reactivity flux (10%) and flux-weighted POCP (4%) is small. However, their contributions to concentration-weighted POCP are higher, with SFVOC contributing 9% and PVOC 11.5%. The major ions responsible in SFVOC are 1,3-butadiene (*m/z* 55), furan (*m/z* 69) and 2,3-Butanedione (*m/z* 87), while in PVOC they are 1,3-butadiene (*m/z* 55), butene (*m/z* 57) and ethylbenzene/xylene (*m/z* 107).

The concentration- and flux-weighted OH reactivity and POCP of EVOC were third and fourth highest out of all factors, respectively (Figure 3.8). The ions $[C_4H_7]^+$ and $[C_4H_9]^+$ were responsible for the bulk of the POCP and they represent 1,3-butadiene and butene, respectively. Similarly, a previous study measuring asphalt emissions highlighted these two species, amongst others, as having significant POCP (Li et al., 2020). On the other hand, the OH reactivity of EVOC is mainly due to the acetic acid fragment ion, $[C_2H_3O]^+$, and its isoprene content, with some smaller contributions from phenol, aniline, styrene and tetramethylfuran.

3.5. Discussion

3.5.1. PMF factor deposition fluxes

The average fluxes in Figure 3.2b show net deposition for factors SFVOC and OVOC1, and is, to date, the first reporting of net deposition in source factor apportionment of urban fluxes. This finding is only made possible due to our approach where PMF is applied to the weighted up and down draft concentration measurements and factor fluxes are calculated using the TEA approach. It is not common to observe deposition, particularly in an urban environment as studies have shown deposition occurs mostly above vegetated areas (Nguyen et al., 2015; Park et al., 2013). As Delhi is quite a “green” city,

there are a number of vegetated areas within the flux footprint which could explain the observations of deposition.

Deposition of OVOC1 was a regular occurrence on most days as shown by the 10 a.m. trough in its diurnal cycle (Figure 3.5d). Its consistency can be explained by the balance between the constant deposition of OVOCs against the emissions of OVOCs due to photochemical production occurring below the inlet. This is seen in the diurnal cycle of OVOC1 when net deposition during the early morning becomes net emission as the increasing solar radiation during the late morning drives photochemical production of OVOCs to exceed that depositing (Figure 3.5d).

The median flux of SFVOC is less strong, but the lower 25th percentile indicates a clear period of deposition during the late evening (~9 p.m) (Figure 3.5d). As discussed, the fluxes of SFVOC are small and are likely offset by the deposition of burning plumes originating from outside the flux footprint, making the diurnal pattern uncertain and difficult to interpret.

The deposition spatial flux maps in Figure 3.10 show the deposition flux for the whole time series of OVOC1 and SFVOC, with all instances of emissions removed. The hotspots, or areas of maximum deposition, for both SFVOC and OVOC1 are situated immediately around the tower and overlap with multiple surface types, including road and roof surfaces. For this reason, the nearest neighbour interpolation is not used as it could lead to false interpretations of possible surface types. The deposition of VOCs to a road or roof surface is considered unlikely due to a high surface resistance (Karl et al., 2018; Zhang et al., 2002). A more reasonable explanation is that deposition occurs because there is a group of trees directly beneath the tower. Therefore, caution is required when interpretating these maps, however, these observations perhaps show that vegetation in urban areas could act as a sink of VOCs in Delhi but it is clear from Figure 3.5d that the magnitude of the deposition is small.

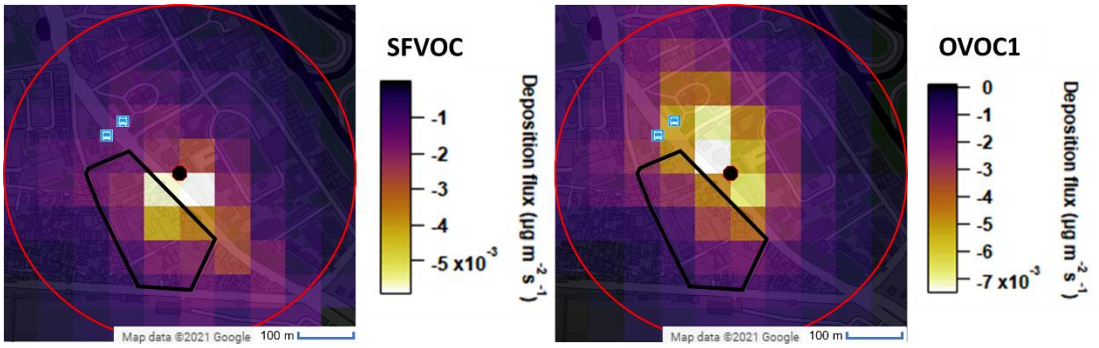

Figure 3.10. Spatial deposition flux patterns for PMF factors, SFVOC and OVOC1, which show net deposition. Maps are shown without the nearest neighbour interpolation. Flux time series covering the whole measurement period are used but instances of emission are removed. The fluxes are allocated based on the maximum of the flux footprint. The faint red circle marks a 300 m radius around the measurement site. The black area outlines an automotive parts business sector.

3.5.2. Isoprene and monoterpenes association with traffic sources

Historically, atmospheric isoprene and monoterpene emissions were viewed as deriving almost exclusively from biogenic sources (Guenther et al., 1995). However, studies have since revealed significant isoprene and monoterpene emissions from anthropogenic sources such as traffic (Borbon et al., 2001; Chang et al., 2014; Hellén et al., 2012), biomass burning (Hellén et al., 2006, 2012), cooking (Klein et al., 2016), domestic heating (Rouvière et al., 2006) and personal-care products (McDonald et al., 2018). It is, therefore, common to measure monoterpenes and isoprene in urban areas that are associated with anthropogenic sources.

In this study, the large *m/z* 81 ($[C_6H_9]^+$ fragment) and *m/z* 137 (monoterpene molecular ion) peaks in TRAF1 suggests the presence of monoterpenes within traffic emissions (Figure 3.1a). Considering all possible monoterpene and sesquiterpene fragments (except those mostly dominated by toluene, xylene/ethylbenzene and trimethylbenzene), it was observed that traffic (= TRAF1+TRAF2) has the highest mass contribution out of all factors (Figure 3.11), accounting for 43% (TRAF1 = 32.5% and TRAF2 = 10.3%) of the

monoterpene concentrations and 90% (TRAF1 = 30.8% and TRAF2 = 59.2%) of the local monoterpene flux. There is also a systematic contribution to TRAF1 and TRAF2 from a comprehensive list of monoterpene related peaks. This reduces the likelihood that other traffic-related compounds also fragment to monoterpene fragment peaks, however, it cannot be ruled out (Figure 3.11).

The mass of each factor at the main molecular ion peak for monoterpenes, *m/z* 137, can be used to estimate the monoterpene contributions of each factor. This gives an estimate which is unlikely to be influenced by non-monoterpene compounds. The TRAF1 factor has the largest contribution to *m/z* 137 ion concentrations (60%) and fluxes (78%). TRAF2 however has only a small contribution to *m/z* 137 concentrations and fluxes (<0.01%).

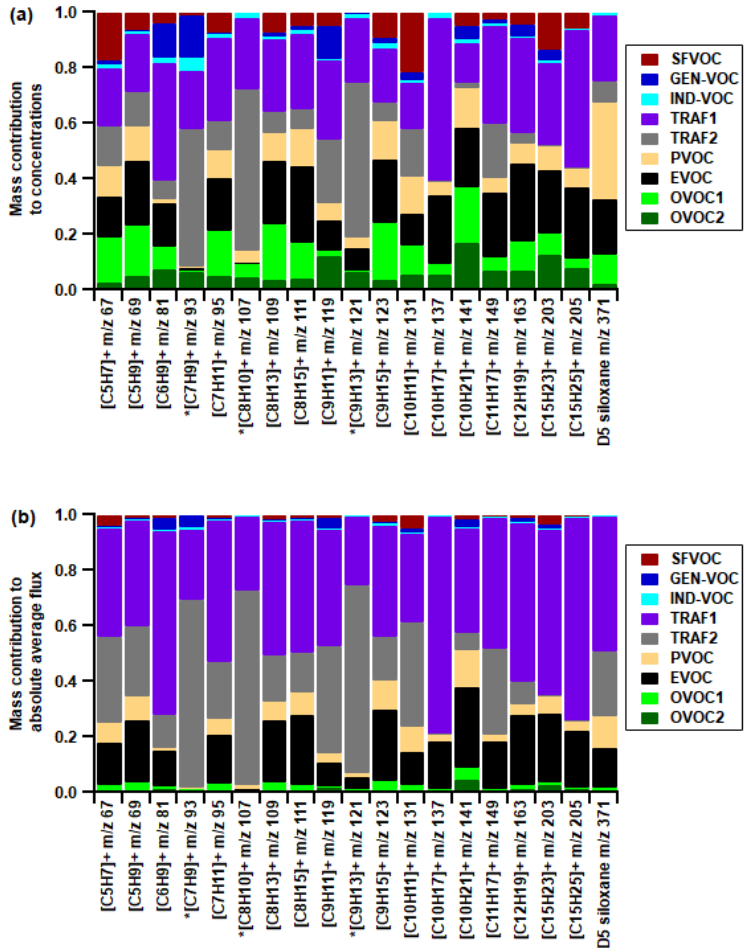

Figure 3.11. Contributions of PMF factor (a) concentrations and (b) absolute average fluxes to D5 siloxane, along with monoterpene and sesquiterpene related PTR-MS measured ions. *The three ions $[C7H9]^+$, $[C8H10]^+$ and $[C9H12]^+$ are also peaks associated with toluene, xylene/ethylbenzene and trimethylbenzene.

The reasons behind TRAF1 containing a substantial amount of the total monoterpene mass are unclear. As discussed, TRAF1 is associated with HGVs which may suggest diesel engine emissions are responsible. There have been Indian-based studies which have experimented with using monoterpenes as diesel fuel additives to improve engine performance (Kumar et al., 2016; Sarkar and Bhattacharyya, 2012). However, it is unknown whether this additive has been incorporated into diesel fuel used in Delhi.

Another explanation could be the use of personal care products by people as they prepare for work and travel using the road systems. This source could then still be wrapped into the TRAF1 factor, due to the similar temporal patterns. Siloxanes are VOCs commonly associated with personal-care products. Measurements of siloxane emissions in the US showed them peaking at rush hour periods and therefore sharing the same time profile as traffic emissions (Coggon et al., 2018). The flux of D5 siloxane in our study has the second highest contribution from TRAF1 which suggests there is a contribution to TRAF1 from personal care products (Figure 3.11).

The highest contributing factor to the D5 siloxane flux is PVOC which is also reasonable if one considers the large gatherings of people igniting and watching the Diwali fireworks. However, the contribution of monoterpenes associated with PVOC is low (Figure 3.11). This means a source with a high siloxane composition does not necessarily mean it also has a high monoterpene composition. This would suggest that TRAF1 could also be influenced by other monoterpene sources than personal care products. It, therefore, remains unclear to why monoterpenes are associated with traffic sources, but the evidence collected in this study suggests monoterpenes are emitted from vehicles in some form. This could point towards the use of air fresheners in cars being the source of monoterpenes, however, more evidence is required to support this.

The implications of monoterpene emissions from traffic sources was highlighted by Nelson et al. (2021) who modelled ozone production when different sources, classes and individual species of VOCs were varied to similate future air quality mitigation strategies. They found that ozone production was second most sensitive to changes in monoterpenes, after changes in aromatics. The same study assumed 50% of monoterpenes concentrations were due to anthropogenic sources and found that ozone production was also highly dependent on traffic reduction. This highlights the significance for ozone mitigation strategies of the findings reported here that

the majority of monoterpene emissions in Dehli (78-90%) originate from traffic sources.

3.5.3. Influence of biogenic emissions on evaporative VOCs

Two of the main controls on evaporative emissions are temperature and solar radiation. This is observed in EVOC (Figure 3.12) where the increase in surface temperature and solar radiation during the morning (9-12 p.m.) is tracked by EVOC. During the afternoon the light intensity drops along with a slight delay in surface temperature, however, EVOC follows the solar radiation more closely, and as a result, there is a higher correlation between EVOC and solar radiation (Pearson's r = 0.484) than with surface temperature (Pearson's r = 0.202).

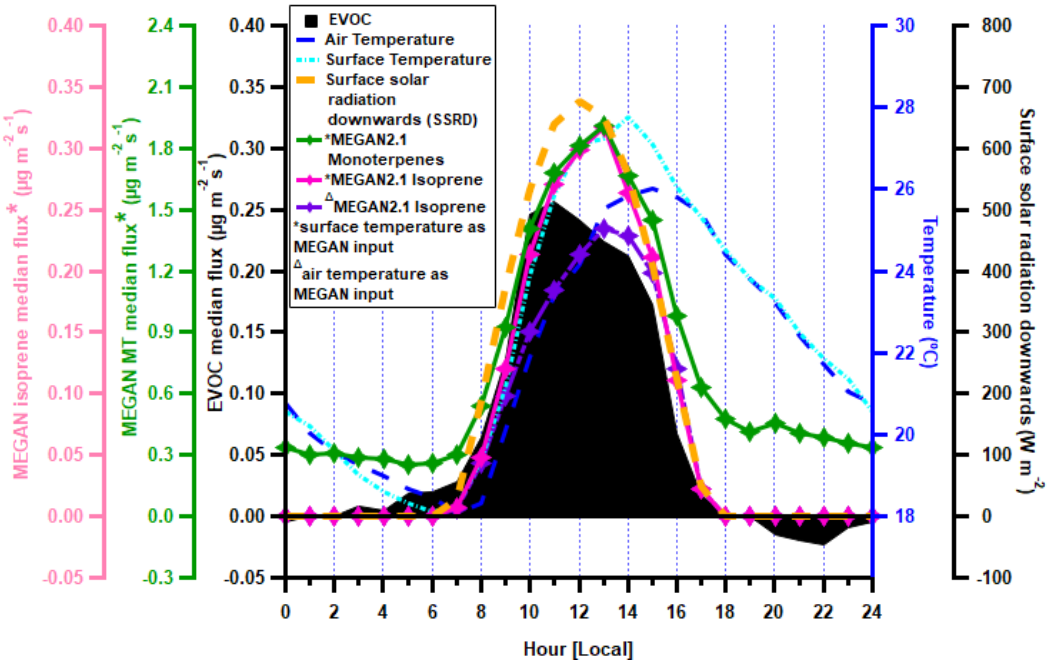

Figure 3.12. EVOC flux diurnal cycle (black) along with MEGAN2.1 estimated isoprene emissions (pink) and monoterpene emissions (green). The surface temperature (cyan) and air temperature (blue) are also shown along with the surface solar radiation downwards (SSRD). *Surface temperature is used as an input for these estimates. The isoprene MEGAN2.1 estimate when using air temperature is also shown (purple) for comparison. As only the trend of biogenic emissions was required the emissions factors for both isoprene and monoterpenes were set to 1.

The associations of EVOC emissions with temperature and light fits with the observed behaviour of emissions from asphalt. Chamber studies by Khare et al. (2020) showed a doubling in total VOC emissions from asphalt samples between 40 and 60^{o}C, and a 300% increase in emissions when exposed to natural and artificial light.

Biogenic emissions are another source of VOCs known to be controlled by temperature and light. These relationships are used in models to predict biogenic VOCs emissions such as MEGAN2.1 (Guenther et al., 2012). The large peaks for isoprene and monoterpenes in the EVOC factor mass profile (Figure 3.1) suggest biogenic VOCs contribute to its composition. However, as discussed previously, the majority of isoprene and monoterpenes in this study appear to be associated with traffic emissions. Therefore, the MEGAN2.1 model was used to predict the biogenic emissions profiles of isoprene and monoterpenes in order to compare with EVOC. Emissions factors were set to 1 in the model as only the temporal pattern in emissions is needed here. The surface and air tempature were used separately in MEGAN2.1 and the two temperature inputs resulted in different diurnal cycles which are presented in Figure 3.12 for isoprene. The temporal profile of predicted isoprene and monoterpene emissions were closer to EVOC when using surface temperature. This suggests that biogenic VOC emissions in Delhi have a stronger relationship with surface temperature than air temperature. As a result, the predictions based on surface temperature were carried forward for comparison with EVOC.

Overall, the diurnal cycles of MEGAN2.1 predicted isoprene and monoterpene emissions closely track that of the EVOC factor flux: the EVOC flux profile has the highest correlations of all factors with MEGAN-predicted emissions of isoprene (Pearson's r = 0.466), monoterpenes (r = 0.433) and sesquiterpenes (r = 0.432). This strongly suggest that EVOC is a mixed source of biogenic and evaporative sources of VOC.

The contribution of biogenic emissions can be calculated from the masses of monoterpene peaks in EVOC. This is assuming the contribution of monoterpenes from other evaportive sources is minimal. From Figure 3.11, the contribution of EVOC to the total of all possible monoterpene and sesquiterpene masses (except those mostly dominated by toluene, xylene/ethylbenzene and trimethylbenzene) is 19% of total concentrations and 4% of localised fluxes. When observing just the mass at *m/z* 137, EVOC contributes 25% to *m/z* 137 concentrations and 18% to *m/z* 137 localised fluxes. In summary, EVOC and, therefore, biogenic emissions are the second highest source of monoterpenes behind traffic (=TRAF1+TRAF2).

3.5.4. Uncertainties and limitations of VOC measurements using PTR-QiTOF-MS and the source apportionment of TEA derived fluxes

3.5.4.1. Uncertainties and limitations associated with PTR-QiTOF-MS measurements

One limitation in PTR-MS VOC measurements is the determination of compound structures as multiple possible isomers are measured at one *m/z*. A best-guess approach was implemented for this study and a comparison of the physical properties of possible compounds (e.g. vapor pressures and boiling points) were used to help determine the structure. Regardless, this limitation creates the potential to over- or underestimate the fluxes, OH reactivity and POCP of some species and sources.

Another limitation is the low PTR-MS measurement sensitivities for small-chained alkane species which is caused by their low proton affinities. Co-located gas chromatography mass spectrometry (GC-MS) measurements of VOCs can be used to establish the fraction of alkanes not quantified by PTR-MS and therefore, not included in PMF factors. These measurements show alkanes strongly contribute to the composition of petrol or liquid-petroleum gas (LPG) source concentrations (Stewart et al., 2021b). The composition of TRAF1 and TRAF2 show some peaks relating to small-chained alkanes but

these are small and have insignificant contributions. This, therefore, suggests traffic emissions are underestimated in this study.

Another study by Nelson et al. (2021) used the same GC-MS measurements to estimate concentration-weighted OH reactivities. They also modelled ozone formation using a range of auxiliary measurements (e.g. NO_x, HONO, SO_2, photolysis rates, etc.) to better quantify ozone formation under the prevailing atmospheric conditions. Sensitivity analysis of ozone formation was performed using variations in VOC classes, sources and individual species of interest. The analysis showed that the aromatic and alkene VOC classes were the largest contributors to OH reactivity. This is similar to observations in this study as the major species responsible for the high OH reactivity in TRAF1, TRAF2 and SFVOC were aromatic. These were in the form of BTEX species for the traffic sources and furan species for SFVOC. Isoprene was also considered a key contributor to OH reactivity in Nelson et al. (2021) and this is seen to have high contributions in factors TRAF1 and PVOC.

The largest contributing VOC class to POCP in Nelson et al., (2021) was aromatics, followed by monoterpenes and then alkenes. The TRAF1 and TRAF2 factors have high contributions from BTEX species, however, monoterpenes are not prominent POCP contributing species in any of the factors. This suggests the POCP for factors that are composed highly of monoterpenes (TRAF1 and EVOC) may be underestimated.

3.5.4.2. Uncertainties and limitations associated with the source apportionment of TEA derived fluxes

There is a lack of studies comparing fluxes derived by eddy covariance (EC) and true-eddy accumulation (TEA) when using modern instruments such as the PTR-QiTOF-MS. It is important this comparison is undertaken to rule out any uncertainty. As previously mentioned in section 3.3.3, the time series for all measured ion fluxes derived by EC were divided by the corresponding ion flux derived by TEA. This resulted in an average gradient of 1 with a relative

standard deviation of 0.89%. This shows the two methods result in virtually numerically identical fluxes and, therefore, the uncertainty introduced by using TEA is minimal.

The most recent study generating factor fluxes is by Karl et al. (2018) who used a non-negative matrix factorisation (NNMF) source apportionment model. Their method relies on the dataset always having net emission fluxes because the negative values of deposition fluxes cannot be processed by NNMF. However, it is clear from our results in Delhi that net deposition factor fluxes are resolved in urban environments, which highlights the importance of using an approach that allows for bi-directional factor fluxes.

A previous study by Kota et al., (2014) used the multilinear-engine 2 (ME-2) to resolve bi-directional factor fluxes from flux measurements. However, they show large flux losses after source apportionment processing which reach as high as ~49% for some species. For the TEA source apportionment method, the flux losses were estimated by summing the EC derived fluxes of all measured ions used in the PMF model (n = 1230) and subtracting the summed flux of all PMF factors. This yields an unresolved flux of 2.27 μg m^{-2} s^{-1} that is only 0.38% of the total flux and equates to the unfitted mass remaining in the residuals after PMF analysis. This suggests that despite the factors being derived using concentrations, the calculated factor fluxes capture the majority of the measured ion fluxes.

Overall, the factor flux results in section 3.4 suggest the TEA source apportionment method can derive bi-directional factor fluxes, for VOCs, that are compositionally accurate. It is also shown that the fluxes calculated are quantitative, with minimal flux losses due to source apportionment and data processing. Future work concentrating on error estimates for each factor flux would be beneficial. This could involve using the constant signal of the PTR-QiTOF-MS internal standard of diiodobenzene within each factor to filter out spurious fluxes and detect for effects of humidity, similar to work carried out in

Millet et al. (2018). There is also a need to account for flux losses due to underestimations in small-chained alkanes and monoterpenes.

3.6. Conclusions

The calculation of quantitative bi-directional fluxes of VOC factors identified by positive matrix factorisation (PMF) has been made possible for the first time through the incorporation of true eddy accumulation calculations. A total of 9 factors were separated, including two traffic factors (TRAF1 and TRAF2), a solid fuel combustion (SFVOC), a pyrotechnical activity factor (PVOC), two industrial factors thought to reflect solvent-use (IND-VOC) and emissions from stationary generators (GEN-VOC), an evaporative emissions factor (EVOC) and two oxidised VOC factors (OVOC1 and OVOC2). Using factor fluxes, spatial flux patterns are presented which show the origin of each factor within a 300 m radius. It was also possible to calculate the OH reactivity flux and flux weighted POCP for each factor.

The measurement site, on the edge of Old Delhi, was shown to be a net source of VOCs, of which, the majority was due to traffic emissions (70% of total flux). Maps showing the spatial flux patterns of the two traffic factors gave large fluxes that concentrated over two bus stops near the measurement site, probably due to the traffic congestion created by waiting buses and passengers boarding. The two traffic factors also differed in their diurnal cycles and chemical makeup, consistent with TRAF1 reflecting HGV diesel traffic (which is banned during the daytime) and TRAF2 reflecting petrol and CNG vehicles. It was also found that 60% of the monoterpene concentrations, and 78% of local fluxes, were attribute to the TRAF1 factor but whether this is via fuel composition/additives, air fresheners or temporal association remains unclear.

The second most significant source in terms of emissions, behind traffic, was found to be EVOCs (10% of the total flux) which showed a strong signature of asphalt emissions. The high peaks of naphthalene and tetralin-based structures being key markers species, along with styrene and 1,3-butadiene which are constituent parts of the adhesives and binders used in asphalt.

The emissions behaviour of EVOC showed a strong relationship with surface temperature and solar radiation. This meant biogenic VOCs also strongly contribute to EVOC as they share similar controls with light and temperature. Assuming all monoterpenes within EVOC originate from biogenic sources, it was estimated that 25% of monoterpene concentrations and 18% of localised fluxes were from biogenic sources.

The burning factor, SFVOC, was linked to sources of municipal waste burning, but local fluxes were small suggesting the concentrations were mainly driven by sources from outside of the footprint. Nitrogen containing species that compose SFVOC were mostly pyridine-based structures, and the common combustion of nitrogen-rich dung-cakes is likely to significantly contribute to SFVOC. PVOC was related to pyrotechnical activity associated with the Diwali festival and is therefore likely infrequent and sporadic over the year. It also shows an inconsistent and small flux depending on the location of the activity.

The IND-VOC factor describes emissions that originate from an automotive business sector near the measurement site which houses businesses selling automotive parts. Its composition was dominated by ethyl acetate which is linked to solvent-use for cleaning automotive parts. Similarly, some of the emissions of GEN-VOC were observed over the automotive sector and it was loosely similar in composition to TRAF1. This, along with night-time peaks in its concentration time series, suggests it was most likely due to stationary diesel generators.

The concentration weighted OH reactivity of the burning-related factors (34% of total OH reactivity) was the highest and was linked to the high furan-based

species content within SFVOC and PVOC. The outcome changes when observing the OH reactivity flux, as the traffic factors dominate the local emissions. Similarly, the flux and concentration weighted POCP were largest for the two traffic factors. This is mostly due to BTEX species and, therefore, means traffic emissions, and BTEX species, were the most significant source of OH radical loss and POCP in Delhi during the post-monsoon.

For the first-time, a deposition flux of VOC PMF factors within an urban environment was observed. This was made possible by the application of PMF to the virtual up and downdraught weighted concentrations and subsequent flux calculation based on the TEA method. Both OVOC1 and SFVOC showed a net deposition flux and their spatial flux patterns suggest OVOC1 and SFVOC may deposit onto vegetation suggesting vegetation could act as a sink of VOCs in Delhi.

Acknowledgements

This work was supported by UK NERC project DelhiFlux under the Newton Bhabha Fund programme Air Pollution and Human Health in a Developing Megacities (APHH-India), NERC reference numbers NE/P016502/1 and NE/P016472/1. James M. Cash is supported by a NERC E3 DTP studentship (NE/L002558/1). These measurements were also supported by the NERC National Capability award SUNRISE (NE/R000131/1). We thank the director of CSIR-National Physical Laboratory for allowing us to carry out this research. This work was also supported by the Earth System Science Organization, Ministry of Earth Sciences, Government of India, under the Indo-UK joint collaboration grant no. MoES/16/19/2017-APHH (DelhiFlux).

References

Andreae, M. O.: Emission of trace gases and aerosols from biomass burning – an updated assessment, Atmos. Chem. Phys., 19(13), 8523–8546, doi:10.5194/acp-19-8523-2019, 2019.

Baasandorj, M., Millet, D. B., Hu, L., Mitroo, D. and Williams, B. J.: Measuring acetic and formic acid by proton-transfer-reaction mass spectrometry: Sensitivity, humidity dependence, and quantifying interferences, Atmos. Meas. Tech., 8(3), 1303–1321, doi:10.5194/amt-8-1303-2015, 2015.

Borbon, A., Fontaine, H., Veillerot, M., Locoge, N., Galloo, J. C. and Guillermo, R.: An investigation into the traffic-related fraction of isoprene at an urban location, Atmos. Environ., 35(22), 3749–3760, doi:10.1016/S1352-2310(01)00170-4, 2001.

Carter, W. P. L.: Development of the SAPRC-07 Chemical Mechanism and Updated Ozone Reactivity Scales, Rep. to Calif. Air Resour. Board, Contract. No. 03-318, 06-408, 07-730, (03), 1–381 [online] Available from: http://www.cert.ucr.edu/~carter, 2010.

Cash, J. M., Langford, B., Di Marco, C., Mullinger, N. J., Allan, J., Reyes-Villegas, E., Joshi, R., Heal, M. R., Acton, W. J. F., Hewitt, C. N., Misztal, P. K., Drysdale, W., Mandal, T. K., Gadi, R., Gurjar, B. R. and Nemitz, E.: Seasonal analysis of submicron aerosol in Old Delhi using high-resolution aerosol mass spectrometry: chemical characterisation, source apportionment and new marker identification, Atmos. Chem. Phys., 21(13), 10133–10158, doi:10.5194/acp-21-10133-2021, 2021.

Chang, C. C., Wang, J. L., Candice Lung, S. C., Chang, C. Y., Lee, P. J., Chew, C., Liao, W. C., Chen, W. N. and Ou-Yang, C. F.: Seasonal characteristics of biogenic and anthropogenic isoprene in tropical-subtropical

urban environments, Atmos. Environ., 99, 298–308, doi:10.1016/j.atmosenv.2014.09.019, 2014.

Chen, W. T., Shao, M., Lu, S. H., Wang, M., Zeng, L. M., Yuan, B. and Liu, Y.: Understanding primary and secondary sources of ambient carbonyl compounds in Beijing using the PMF model, Atmos. Chem. Phys., 14(6), 3047–3062, doi:10.5194/acp-14-3047-2014, 2014.

Chen, Y., Beig, G., Archer-Nicholls, S., Drysdale, W., Acton, W. J. F., Lowe, D., Nelson, B., Lee, J., Ran, L., Wang, Y., Wu, Z., Sahu, S. K., Sokhi, R. S., Singh, V., Gadi, R., Nicholas Hewitt, C., Nemitz, E., Archibald, A., McFiggans, G. and Wild, O.: Avoiding high ozone pollution in Delhi, India, Faraday Discuss., 226, 502–514, doi:10.1039/d0fd00079e, 2021.

Coggon, M. M., McDonald, B. C., Vlasenko, A., Veres, P. R., Bernard, F., Koss, A. R., Yuan, B., Gilman, J. B., Peischl, J., Aikin, K. C., Durant, J., Warneke, C., Li, S. M. and De Gouw, J. A.: Diurnal Variability and Emission Pattern of Decamethylcyclopentasiloxane (D5) from the Application of Personal Care Products in Two North American Cities, Environ. Sci. Technol., 52(10), 5610–5618, doi:10.1021/acs.est.8b00506, 2018.

Coggon, M. M., Lim, C. Y., Koss, A. R., Sekimoto, K., Yuan, B., Gilman, J. B., Hagan, D. H., Selimovic, V., Zarzana, K. J., Brown, S. S., M Roberts, J., Müller, M., Yokelson, R., Wisthaler, A., Krechmer, J. E., Jimenez, J. L., Cappa, C., Kroll, J. H., De Gouw, J. and Warneke, C.: OH chemistry of non-methane organic gases (NMOGs) emitted from laboratory and ambient biomass burning smoke: Evaluating the influence of furans and oxygenated aromatics on ozone and secondary NMOG formation, Atmos. Chem. Phys., 19(23), 14875–14899, doi:10.5194/acp-19-14875-2019, 2019.

Crippa, M., Canonaco, F., Slowik, J. G., El Haddad, I., DeCarlo, P. F., Mohr, C., Heringa, M. F., Chirico, R., Marchand, N., Temime-Roussel, B., Abidi, E., Poulain, L., Wiedensohler, A., Baltensperger, U. and Prévôt, A. S. H.: Primary

and secondary organic aerosol origin by combined gas-particle phase source apportionment, Atmos. Chem. Phys., 13(16), 8411–8426, doi:10.5194/acp-13-8411-2013, 2013.

Desjardins, R. L.: Description and evaluation of a sensible heat flux detector, Boundary-Layer Meteorol., 11(2), 147–154, doi:10.1007/BF02166801, 1977.

Donahue, N. M., Chuang, W., Epstein, S. A., Kroll, J. H., Worsnop, D. R., Robinson, A. L., Adams, P. J. and Pandis, S. N.: Why do organic aerosols exist? Understanding aerosol lifetimes using the two-dimensional volatility basis set, Environ. Chem., 10(3), 151–157, doi:10.1071/EN13022, 2013.

Elbir, T., Cetin, B., Cetin, E., Bayram, A. and Odabasi, M.: Characterization of volatile organic compounds (VOCs) and their sources in the air of Izmir, Turkey, Environ. Monit. Assess., 133(1–3), 149–160, doi:10.1007/s10661-006-9568-z, 2007.

Erickson, M. H., Gueneron, M. and Jobson, B. T.: Measuring long chain alkanes in diesel engine exhaust by thermal desorption PTR-MS, Atmos. Meas. Tech., 7(1), 225–239, doi:10.5194/amt-7-225-2014, 2014.

Fortner, E. C., Zheng, J., Zhang, R., Knighton, W. B., Volkamer, R. M., Sheehy, P., Molina, L. and Andŕe, M.: Measurements of volatile organic compounds using proton transfer reaction-mass spectrometry during the MILAGRO 2006 campaign, Atmos. Chem. Phys., 9(2), 467–481, doi:10.5194/acp-9-467-2009, 2009.

Gani, S., Bhandari, S., Seraj, S., Wang, D. S., Patel, K., Soni, P., Arub, Z., Habib, G., Hildebrandt Ruiz, L. and Apte, J. S.: Submicron aerosol composition in the world's most polluted megacity: The Delhi Aerosol Supersite study, Atmos. Chem. Phys., 19(10), 6843–6859, doi:10.5194/acp-19-6843-2019, 2019.

Gasthauer, E., Mazé, M., Marchand, J. P. and Amouroux, J.: Characterization of asphalt fume composition by GC/MS and effect of temperature, Fuel, 87(7), 1428–1434, doi:10.1016/j.fuel.2007.06.025, 2008.

de Gouw, J. A., Goldan, P. D., Warneke, C., Kuster, W. C., Roberts, J. M., Marchewka, M., Bertman, S. B., Pszenny, A. A. P. and Keene, W. C.: Validation of proton transfer reaction-mass spectrometry (PTR-MS) measurements of gas-phase organic compounds in the atmosphere during the New England Air Quality Study (NEAQS) in 2002, J. Geophys. Res. D Atmos., 108(21), 1–18, doi:10.1029/2003jd003863, 2003.

de Gouw, J. and Warneke, C.: Measurements of volatile organic compounds in the earth's atmosphere using proton-transfer-reaction mass spectrometry, Mass Spectrom. Rev., 26(2), 223–257, doi:10.1002/mas.20119, 2007.

Guenther, A., Hewitt, C. N., Erickson, D., Fall, R., Geron, C., Graedel, T., Harley, P., Klinger, L., Lerdau, M., Mckay, W. A., Pierce, T., Scholes, B., Steinbrecher, R., Tallamraju, R., Taylor, J. and Zimmerman, P.: A global model of natural volatile organic compound emissions, J. Geophys. Res., 100(D5), 8873, doi:10.1029/94JD02950, 1995.

Guenther, A. B., Jiang, X., Heald, C. L., Sakulyanontvittaya, T., Duhl, T., Emmons, L. K. and Wang, X.: The model of emissions of gases and aerosols from nature version 2.1 (MEGAN2.1): An extended and updated framework for modeling biogenic emissions, Geosci. Model Dev., 5(6), 1471–1492, doi:10.5194/gmd-5-1471-2012, 2012.

Hartikainen, A., Yli-Pirilä, P., Tiitta, P., Leskinen, A., Kortelainen, M., Orasche, J., Schnelle-Kreis, J., Lehtinen, K. E. J., Zimmermann, R., Jokiniemi, J. and Sippula, O.: Volatile Organic Compounds from Logwood Combustion: Emissions and Transformation under Dark and Photochemical Aging Conditions in a Smog Chamber, Environ. Sci. Technol., 52(8), 4979–4988, doi:10.1021/acs.est.7b06269, 2018.

Hellén, H., Hakola, H., Pirjola, L., Laurila, T. and Pystynen, K. H.: Ambient air concentrations, source profiles, and source apportionment of 71 different C2-C10 volatile organic compounds in urban and residential areas of Finland, Environ. Sci. Technol., 40(1), 103–108, doi:10.1021/es051659d, 2006.

Hellén, H., Tykkä, T. and Hakola, H.: Importance of monoterpenes and isoprene in urban air in northern Europe, Atmos. Environ., 59, 59–66, doi:10.1016/j.atmosenv.2012.04.049, 2012.

Karl, T., Striednig, M., Graus, M., Hammerle, A. and Wohlfahrt, G.: Urban flux measurements reveal a large pool of oxygenated volatile organic compound emissions, Proc. Natl. Acad. Sci. U. S. A., 115(6), 1186–1191, doi:10.1073/pnas.1714715115, 2018.

Khare, P., Machesky, J., Soto, R., He, M., Presto, A. A. and Gentner, D. R.: Asphalt-related emissions are a major missing nontraditional source of secondary organic aerosol precursors, Sci. Adv., 6(36), doi:10.1126/sciadv.abb9785, 2020.

Klein, F., Platt, S. M., Farren, N. J., Detournay, A., Bruns, E. A., Bozzetti, C., Daellenbach, K. R., Kilic, D., Kumar, N. K., Pieber, S. M., Slowik, J. G., Temime-Roussel, B., Marchand, N., Hamilton, J. F., Baltensperger, U., Prévôt, A. S. H. and El Haddad, I.: Characterization of Gas-Phase Organics Using Proton Transfer Reaction Time-of-Flight Mass Spectrometry: Cooking Emissions, Environ. Sci. Technol., 50(3), 1243–1250, doi:10.1021/acs.est.5b04618, 2016.

Kormann, R. and Meixner, F. X.: An analytical footprint model for non-neutral stratification, Boundary-Layer Meteorol., 99(2), 207–224, doi:10.1023/A:1018991015119, 2001.

Koss, A. R., Sekimoto, K., Gilman, J. B., Selimovic, V., Coggon, M. M., Zarzana, K. J., Yuan, B., Lerner, B. M., Brown, S. S., Jimenez, J. L., Krechmer,

J., Roberts, J. M., Warneke, C., Yokelson, R. J. and De Gouw, J.: Non-methane organic gas emissions from biomass burning: Identification, quantification, and emission factors from PTR-ToF during the FIREX 2016 laboratory experiment, Atmos. Chem. Phys., 18(5), 3299–3319, doi:10.5194/acp-18-3299-2018, 2018.

Kosyakov, D. S., Ul'yanovskii, N. V., Latkin, T. B., Pokryshkin, S. A., Berzhonskis, V. R., Polyakova, O. V. and Lebedev, A. T.: Peat burning – An important source of pyridines in the earth atmosphere, Environ. Pollut., 266, 115109, doi:10.1016/j.envpol.2020.115109, 2020.

Kota, S. H., Park, C., Hale, M. C., Werner, N. D., Schade, G. W. and Ying, Q.: Estimation of VOC emission factors from flux measurements using a receptor model and footprint analysis, Atmos. Environ., 82, 24–35, doi:10.1016/j.atmosenv.2013.09.052, 2014.

Kumar, J. K., Raj, C. S., Gopal, P. and Kumar, P. S.: Blendability and property of turpentine oil with petrol and diesel, Int. J. Chem. Sci., 14(3), 1307–1316, 2016.

Langford, B., Acton, W., Ammann, C., Valach, A. and Nemitz, E.: Eddy-covariance data with low signal-to-noise ratio: Time-lag determination, uncertainties and limit of detection, Atmos. Meas. Tech., 8(10), 4197–4213, doi:10.5194/amt-8-4197-2015, 2015.

Li, N., Jiang, Q., Wang, F., Xie, J., Li, Y., Li, J. and Wu, S.: Emission behavior, environmental impact and priority-controlled pollutants assessment of volatile organic compounds (VOCs) during asphalt pavement construction based on laboratory experiment, J. Hazard. Mater., 398, 122904, doi:10.1016/j.jhazmat.2020.122904, 2020.

Li, N., Jiang, Q., Wang, F., Cui, P., Xie, J., Li, J., Wu, S. and Barbieri, D. M.: Comparative Assessment of Asphalt Volatile Organic Compounds Emission

from field to laboratory, J. Clean. Prod., 278, doi:10.1016/j.jclepro.2020.123479, 2021.

Liu, Y., Shao, M., Zhang, J., Fu, L. and Lu, S.: Distributions and source apportionment of ambient volatile organic compounds in Beijing City, China, J. Environ. Sci. Heal. - Part A Toxic/Hazardous Subst. Environ. Eng., 40(10), 1843–1860, doi:10.1080/10934520500182842, 2005.

McDonald, B. C., de Gouw, J. A., Gilman, J. B., Jathar, S. H., Akherati, A., Cappa, C. D., Jimenez, J. L., Lee-Taylor, J., Hayes, P. L., McKeen, S. A., Cui, Y. Y., Kim, S.-W., Gentner, D. R., Isaacman-VanWertz, G., Goldstein, A. H., Harley, R. A., Frost, G. J., Roberts, J. M., Ryerson, T. B. and Trainer, M.: Volatile chemical products emerging as largest petrochemical source of urban organic emissions, Science, 359(6377), 760–764, doi:10.1126/science.aaq0524, 2018.

Millet, D. B., Alwe, H. D., Chen, X., Deventer, M. J., Griffis, T. J., Holzinger, R., Bertman, S. B., Rickly, P. S., Stevens, P. S., Léonardis, T., Locoge, N., Dusanter, S., Tyndall, G. S., Alvarez, S. L., Erickson, M. H. and Flynn, J. H.: Bidirectional Ecosystem–Atmosphere Fluxes of Volatile Organic Compounds Across the Mass Spectrum: How Many Matter?, ACS Earth Sp. Chem., 2(8), 764–777, doi:10.1021/acsearthspacechem.8b00061, 2018.

Muhmmad Aadil, P., Sonu Ram, E. and Shuab Ahmad, P.: Utilisation of Modified Bitumen in Road Construction, 7th Int. Conf. Adv. Eng. Technol., (March) [online] Available from: www.irjet.net, 2019.

Naddeo, M., Viscusi, G., Gorrasi, G. and Pappalardo, D.: Degradable elastomers: Is there a future in tyre compound formulation?, Molecules, 26(15), 1–16, doi:10.3390/molecules26154454, 2021.

Neftel, A., Spirig, C. and Ammann, C.: Application and test of a simple tool for operational footprint evaluations, Environ. Pollut., 152(3), 644–652, doi:10.1016/j.envpol.2007.06.062, 2008.

Nelson, B. S., Stewart, G. J., Drysdale, W. S., Newland, M. J., Vaughan, A. R., Dunmore, R. E., Edwards, P. M., Lewis, A. C., Hamilton, J. F., Acton, W. J., Hewitt, C. N., Crilley, L. R., Alam, M. S., Åahin, Ü. A., Beddows, D. C. S., Bloss, W. J., Slater, E., Whalley, L. K., Heard, D. E., Cash, J. M., Langford, B., Nemitz, E., Sommariva, R., Cox, S., Shivani, Gadi, R., Gurjar, B. R., Hopkins, J. R., Rickard, A. R. and Lee, J. D.: In situ ozone production is highly sensitive to volatile organic compounds in Delhi, India, Atmos. Chem. Phys., 21(17), 13609–13630, doi:10.5194/acp-21-13609-2021, 2021.

Nemitz, E., Hargreaves, K. J., Neftel, A., Loubet, B., Cellier, P., Dorsey, J. R., Flynn, M., Hensen, A., Weidinger, T., Meszaros, R., Horvath, L., DäCurrency Signmmgen, U., Frühauf, C., Löpmeier, F. J., Gallagher, M. W. and Sutton, M. A.: Intercomparison and assessment of turbulent and physiological exchange parameters of grassland, Biogeosciences, 6(8), 1445–1466, doi:10.5194/bg-6-1445-2009, 2009.

Nguyen, T. B., Crounse, J. D., Teng, A. P., Clair, J. M. S., Paulot, F., Wolfe, G. M. and Wennberg, P. O.: Rapid deposition of oxidized biogenic compounds to a temperate forest, Proc. Natl. Acad. Sci. U. S. A., 112(5), E392–E401, doi:10.1073/pnas.1418702112, 2015.

Paatero, P. and Tapper, U.: Positive matrix factorization: A non-negative factor model with optimal utilization of error estimates of data values, Environmetrics, 5(2), 111–126, doi:10.1002/env.3170050203, 1994.

Park, J. H., Goldstein, A. H., Timkovsky, J., Fares, S., Weber, R., Karlik, J. and Holzinger, R.: Active atmosphere-ecosystem exchange of the vast majority of detected volatile organic compounds, Science, 341(6146), 643–647, doi:10.1126/science.1235053, 2013.

Rouvière, A., Brulfert, G., Baussand, P. and Chollet, J. P.: Monoterpene source emissions from Chamonix in the Alpine Valleys, Atmos. Environ., 40(19), 3613–3620, doi:10.1016/j.atmosenv.2005.09.058, 2006.

Salameh, T., Afif, C., Sauvage, S., Borbon, A. and Locoge, N.: Speciation of non-methane hydrocarbons (NMHCs) from anthropogenic sources in Beirut, Lebanon, Environ. Sci. Pollut. Res., 21(18), 10867–10877, doi:10.1007/s11356-014-2978-5, 2014.

Sarkar, J. and Bhattacharyya, S.: Application of graphene and graphene-based materials in clean energy-related devices Minghui, Arch. Thermodyn., 33(4), 23–40, doi:10.1002/er, 2012.

Sharma, S., Goel, A., Gupta, D., Kumar, A., Mishra, A., Kundu, S., Chatani, S. and Klimont, Z.: Emission inventory of non-methane volatile organic compounds from anthropogenic sources in India, Atmos. Environ., 102(x), 209–219, doi:10.1016/j.atmosenv.2014.11.070, 2015.

Srivastava, A. and Majumdar, D.: Emission inventory of evaporative emissions of VOCs in four metro cities in India, Environ. Monit. Assess., 160(1–4), 315–322, doi:10.1007/s10661-008-0697-4, 2010.

Srivastava, A., Joseph, A. E., More, A. and Patil, S.: Emissions of VOCs at urban petrol retail distribution centres in India (Delhi and Mumbai), Environ. Monit. Assess., 109(1–3), 227–242, doi:10.1007/s10661-005-6292-z, 2005a.

Srivastava, A., Sengupta, B. and Dutta, S. A.: Source apportionment of ambient VOCs in Delhi City, Sci. Total Environ., 343(1–3), 207–220, doi:10.1016/j.scitotenv.2004.10.008, 2005b.

Stewart, G. J.: Sources of non-methane volatile organic compounds in Delhi, India, PhD thesis, York University., 2021.

Stewart, G. J., Acton, W. J. F., Nelson, B. S., Vaughan, A. R., Hopkins, J. R., Arya, R., Mondal, A., Jangirh, R., Ahlawat, S., Yadav, L., Sharma, S. K., Dunmore, R. E., Yunus, S. S. M., Nicholas Hewitt, C., Nemitz, E., Mullinger, N., Gadi, R., Sahu, L. K., Tripathi, N., Rickard, A. R., Lee, J. D., Mandal, T. K. and Hamilton, J. F.: Emissions of non-methane volatile organic compounds from combustion of domestic fuels in Delhi, India, Atmos. Chem. Phys., 21(4), 2383–2406, doi:10.5194/acp-21-2383-2021, 2021a.

Stewart, G. J., Nelson, B. S., Drysdale, W. S., Acton, W. J. F., Vaughan, A. R., Hopkins, J. R., Dunmore, R. E., Hewitt, C. N., Nemitz, E., Mullinger, N., Langford, B., Shivani, Reyes-Villegas, E., Gadi, R., Rickard, A. R., Lee, J. D. and Hamilton, J. F.: Sources of non-methane hydrocarbons in surface air in Delhi, India, Faraday Discuss., 226, 409–431, doi:10.1039/d0fd00087f, 2021b.

Stojić, A., Maletić, D., Stanišić Stojić, S., Mijić, Z. and Šoštarić, A.: Forecasting of VOC emissions from traffic and industry using classification and regression multivariate methods, Sci. Total Environ., 521–522, 19–26, doi:10.1016/j.scitotenv.2015.03.098, 2015.

Taipale, R., Ruuskanen, T. M. and Rinne, J.: Lag time determination in DEC measurements with PTR-MS, Atmos. Meas. Tech., 3(4), 853–862, doi:10.5194/amt-3-853-2010, 2010.

Ulbrich, I. M., Canagaratna, M. R., Zhang, Q., Worsnop, D. R. and Jimenez, J. L.: Interpretation of organic components from Positive Matrix Factorization of aerosol mass spectrometric data, Atmos. Chem. Phys., 9(9), 2891–2918, doi:10.5194/acp-9-2891-2009, 2009.

Venecek, M. A., Carter, W. P. L. and Kleeman, M. J.: Updating the SAPRC Maximum Incremental Reactivity (MIR) scale for the United States from 1988 to 2010, J. Air Waste Manag. Assoc., 68(12), 1301–1316, doi:10.1080/10962247.2018.1498410, 2018.

Vlasenko, A., Slowik, J. G., Bottenheim, J. W., Brickell, P. C., Chang, R. Y. W., Macdonald, A. M., Shantz, N. C., Sjostedt, S. J., Wiebe, H. A., Leaitch, W. R. and Abbatt, J. P. D.: Measurements of VOCs by proton transfer reaction mass spectrometry at a rural Ontario site: Sources and correlation to aerosol composition, J. Geophys. Res., 114(D21), D21305, doi:10.1029/2009JD012025, 2009.

Wang, F., Li, N., Hoff, I., Wu, S., Li, J., Maria Barbieri, D. and Zhang, L.: Characteristics of VOCs generated during production and construction of an asphalt pavement, Transp. Res. Part D Transp. Environ., 87(August), doi:10.1016/j.trd.2020.102517, 2020a.

Wang, L., Slowik, J. G., Tripathi, N., Bhattu, D., Rai, P., Kumar, V., Vats, P., Satish, R., Baltensperger, U., Ganguly, D., Rastogi, N., Sahu, L. K., Tripathi, S. N. and Prévôt, A. S. H.: Source characterization of volatile organic compounds measured by proton-transfer-reaction time-of-flight mass spectrometers in Delhi, India, Atmos. Chem. Phys., 20(16), 9753–9770, doi:10.5194/acp-20-9753-2020, 2020b.

Weng, H., Lin, J., Martin, R., Millet, D. B., Jaeglé, L., Ridley, D., Keller, C., Li, C., Du, M. and Meng, J.: Global high-resolution emissions of soil NOx, sea salt aerosols, and biogenic volatile organic compounds, Sci. Data, 7(1), 1–15, doi:10.1038/s41597-020-0488-5, 2020.

Xiu, M., Wang, X., Morawska, L., Pass, D., Beecroft, A., Mueller, J. F. and Thai, P.: Emissions of particulate matters, volatile organic compounds and polycyclic aromatic hydrocarbons from warm and hot asphalt mixes, J. Clean. Prod., 275, 123094, doi:10.1016/j.jclepro.2020.123094, 2020.

Yáñez-Serrano, A. M., Filella, I., LLusià, J., Gargallo-Garriga, A., Granda, V., Bourtsoukidis, E., Williams, J., Seco, R., Cappellin, L., Werner, C., de Gouw, J. and Peñuelas, J.: GLOVOCS - Master compound assignment guide for

proton transfer reaction mass spectrometry users, Atmos. Environ., 244, 117929, doi:10.1016/j.atmosenv.2020.117929, 2021.

Young, D. E., Allan, J. D., Williams, P. I., Green, D. C., Flynn, M. J., Harrison, R. M., Yin, J., Gallagher, M. W. and Coe, H.: Investigating the annual behaviour of submicron secondary inorganic and organic aerosols in London, Atmos. Chem. Phys., 15(11), 6351–6366, doi:10.5194/acp-15-6351-2015, 2015.

Zhang, L., Moran, M. D., Makar, P. A., Brook, J. R. and Gong, S.: Modelling gaseous dry deposition in AURAMS: A unified regional air-quality modelling system, Atmos. Environ., 36(3), 537–560, doi:10.1016/S1352-2310(01)00447-2, 2002.

Zheng, H., Kong, S., Xing, X., Mao, Y., Hu, T., DIng, Y., Li, G., Liu, D., Li, S. and Qi, S.: Monitoring of volatile organic compounds (VOCs) from an oil and gas station in northwest China for 1 year, Atmos. Chem. Phys., 18(7), 4567–4595, doi:10.5194/acp-18-4567-2018, 2018.

Zhou, X., Li, Z., Zhang, T., Wang, F., Wang, F., Tao, Y., Zhang, X., Wang, F. and Huang, J.: Volatile organic compounds in a typical petrochemical industrialized valley city of northwest China based on high-resolution PTR-MS measurements: Characterization, sources and chemical effects, Sci. Total Environ., 671, 883–896, doi:10.1016/j.scitotenv.2019.03.283, 2019.

Chapter 4

Response of organic aerosol to Delhi's pollution control measures over the period 2011-2018

This chapter is based on a research paper currently in preparation for submission for publication.

Author contributions: I took the PM_{10} measurements using offline-AMS methods with support from Di Marco, C. I interpreted the results with help from Langford, B., Heal, M. R., Di Marco, C., Nemitz, E. I wrote the manuscript with subsequent contributions from all co-authors.

Tuhin K. Mandal and Bhola Ram Gurjar supplied the PM_{10} filter samples from the filter archive at the National Physics Laboratory, New Delhi. Measurements of OC/EC, WSOC and wavelength dispersive x-ray fluorescence were conducted as part of the following studies:

Sharma, S. K., Mandal, T. K., Saxena, M., Rashmi, Rohtash, Sharma, A. and Gautam, R.: Source apportionment of PM10 by using positive matrix factorization at an urban site of Delhi, India, Urban Clim., 10, 656–670, doi:10.1016/j.uclim.2013.11.002, 2014.

Banoo, R., Sharma, S. K., Gadi, R., Gupta, S. and Mandal, T. K.: Seasonal Variation of Carbonaceous Species of PM10 Over Urban Sites of National Capital Region of India, Aerosol Sci. Eng., 4(2), 111–123, doi:10.1007/s41810-020-00058-2, 2020.

Jain, S., Sharma, S. K., Vijayan, N. and Mandal, T. K.: Seasonal characteristics of aerosols (PM2.5 and PM10) and their source apportionment using PMF: A

four year study over Delhi, India, Environ. Pollut., 262, 114337, doi:10.1016/j.envpol.2020.114337, 2020.

Sharma, S. K., Banoo, R. and Mandal, T. K.: Seasonal characteristics and sources of carbonaceous components and elements of PM10 (2010–2019) in Delhi, India, J. Atmos. Chem., 78(4), 251–270, doi:10.1007/s10874-021-09424-x, 2021.

4.1. Abstract

Some of the world's highest air pollution episodes are recorded in Delhi, India and studies have shown particulate matter (PM) is the leading air pollutant to cause adverse health effects on Delhi's population. It is therefore vital to be able to chart PM sources over long time periods to effectively identify trends and evaluate air quality mitigation strategies, particularly as over the past 10 years, multiple air quality measures have been implemented in Delhi but remain unevaluated. An automated offline aerosol mass spectrometry (AMS) method has been developed which has enabled high-throughput analysis, allowing for the extraction of PM filters collected over multiple years. This novel offline-AMS method uses an organic solvent mix of acetone and water to deliver high extraction recoveries of organic aerosol (OA) (95.4 ± 8.3 %). Positive matrix factorisation (PMF) source apportionment was performed on the OA fraction extracted from PM_{10} filter samples collected in Delhi in 2011, 2015 and 2018. Nine factors were resolved which can be grouped into four source categories of OA: traffic, cooking, coal-combustion and burning-related (solid fuel or open burning). Burning-related OA was the largest contributor to PM_{10} OA during the winter and post-monsoon, when total OA concentrations were at their highest. As a result, burning-related OA likely made a significant contribution to acute PM-related health effects in Delhi. Annual averages show a decline in burning-related OA concentrations from 2015 to 2018 (47%). This could be linked to the 2015 ban on open waste burning, and the controls and

incentives to reduce crop-residue burning; however, compositional analysis of OA factors suggests municipal waste burning tracers were still present in 2018 and there is, therefore, scope to reduce burning-related OA further. The shutdown of the two coal power stations, along with initiatives to decrease the popularity of coal use in industry, businesses, and residential homes, resulted in a significant decrease (87%) in coal-combustion OA. This corresponds to a 17% reduction in total OA concentrations, which shows these measures have been effective in reducing in PM_{10}. Increases in annual traffic OA concentrations have likely been partly alleviated by the introduction of the Bharat stage emissions standards for vehicles as the increases do not reflect the rapid increase in population and registered vehicles. However, restrictions on heavy goods vehicles (HGVs) entering the city during the day is linked to large increases in PM_{10} concentrations during the winter and post-monsoon. This is likely because the large influx of diesel-engine HGVs during the early mornings and evenings is timed with a particularly low planetary boundary layer height that enhances surface concentrations.

4.2. Introduction

Air pollution is one of India's biggest health problems. Over the past decade, there has been an increasing fossil fuels demand due to rapid growth in industry, registered vehicles and population (Gulia et al., 2022). Electricity demands have also increased and the majority is generated through coal-fired thermal power stations (~60%) (Yang and Urpelainen, 2019). This, combined with widespread open burning of municipal waste and crop-residue, results in particularly poor air quality. Global estimates for 2019 suggest 17.8% of premature deaths in India can be attributed to air pollution with 10.4% due to ambient particulate matter (PM) (Pandey et al., 2021). One of the most polluted cities in India is Delhi which is a densely populated megacity with over 31.2 million inhabitants (Sharma et al., 2021). The PM_{10} concentrations in Delhi frequently exceed the World Health Organization (WHO) guideline value of 15

μg m^{-3} with an annual average concentration of 222 μg m^{-3} (Sharma et al., 2018). The characterization of the sources of PM is therefore critical in order to improve air quality mitigation strategies.

Aerosol Mass Spectrometry (AMS) has been used for two decades to quantify PM_1 chemical composition (DeCarlo et al., 2006; Hunt and Petrucci, 2002), however, AMS instruments are costly to deploy and require specialist knowledge to operate in the field. Also, they have become more commonplace in India only over the last few years. As a result, measurement campaigns are generally short, particularly when using the high-resolution time-of-flight AMS (HR-TOF-AMS) and there are very limited data prior to 2017. A number of recent studies have conducted HR-TOF-AMS measurements on resuspended airstreams of PM filter samples (offline-AMS) (Bozzetti et al., 2017; Daellenbach et al., 2016, 2017). This enables the high-resolution chemical analysis of PM without the additional cost of HR-TOF-AMS field deployment. Research institutes and statutory monitoring bodies often store filter archives to be reanalysed which creates the opportunity to characterize PM from the past, and the present, using one technique.

The current offline-AMS methods focus on using water as the extracting solvent which limits the fraction of the organic aerosol (OA) component that can be extracted from PM filter samples, particularly as the majority of studies report that water-insoluble OA (WIOA) contributes between 10 and 84% of total OA (Ge et al., 2017; Jayarathne et al., 2018a; Li et al., 2015; Saarikoski et al., 2008; Sun et al., 2011a; Ye et al., 2017). The amount of WIOA is accentuated by the primary organic aerosol (POA) content which originates from sources such as traffic and cooking for which recovery by water extraction is particularly low (Daellenbach et al., 2016). This is therefore an issue when measuring PM in places with high primary emissions where most of the OA measured may therefore not be extracted. Previous studies have shown that the majority of OA in Delhi originates from primary sources (Cash et al., 2021; Reyes-Villegas et al., 2021); therefore, we develop an offline-AMS method

which addresses the issues surrounding OA extraction using an organic solvent mix to extract PM from filter samples. However, there are a number of potential issues with using organic solvents in offline-AMS have which include (Bozzetti et al., 2017):

1. the potential for the solvent to cause a high AMS organics background and
2. the potential for the solvent to interact or react with the extracted sample organics.

Previous studies using organic solvents to extract PM from filters and they have shown a reduction in the organics background after using activated carbon filled diffusion dryers (Chen et al., 2016; Han et al., 2016; Mihara and Mochida, 2011). The study by Mihara and Mochida (2011) who showed good agreement between the mass spectra measured using deuterated or non-deuterated methanol and ethyl acetate solvents to extract PM from filters, even after leaving the samples for 1 week at room temperature. This suggests organic solvents can offer high stability (i.e. resistance to compositional change due to chemical reaction) and creates the possibility of an offline-AMS method with minimal contamination from the solvent.

Over the last 20 years, a series of mitigation strategies have been implemented in Delhi to curb the high concentrations of air pollutants (Table 4.1). There have been a number of vehicle emissions and fuel standards (Bharat stages), which were implemented in 2000, 2005, 2010 and 2018 (Gulia et al., 2018). These have gradually decreased the tailpipe emissions of vehicles in Delhi (and other metro cities). However, the first strategy to have a real effect on air quality was the shift from diesel-engine public transport vehicles to compressed natural gas (CNG) fuelled vehicles in 2001 (Kathuria, 2005; Krelling and Badami, 2022). Although PM_{10} concentrations were observed to decrease in 2001 and 2002, this was short-lived as the increase in registered vehicles meant concentrations continued to increase (Sindhwani and Goyal, 2014). Further diesel-related mitigation strategies were therefore implemented. In 2014, time

restrictions (7:00 a.m. – 10:00 p.m.) were put in place for heavy goods vehicles (HGV) entering the city in order to reduce congestion and midday peaks in traffic emissions. In 2015, there was a ban on open waste burning as studies started to suggest this produced significant air pollutant concentrations (Gulia et al., 2018). In 2016, there was also a ban on luxury diesel vehicles (engines > 2000 cc), a complete ban on HGVs in certain areas of Delhi, and on diesel vehicles that were 10 years or older (Gulia et al., 2018). Finally, there was also a scheme in 2016 that was designed to restrict the number of cars entering the city. This scheme was based on the registered vehicle number plate beginning with an odd or even number. This “Odd-even scheme” has previously been shown as an “unsuccessful” mitigation measure (Chowdhury et al., 2017) causing only a small decrease in air pollutants.

Table 4.1. Air quality mitigation strategies implemented in Delhi over the last 20 years. The table is adapted from that presented in Gulia et al. (2018).

Mitigation strategy	Year	Sources or areas controlled
Bharat stage I	2000	All vehicles
Bharat stage II	2000	Initially in metro cities (including Delhi)
Public transport vehicles moved from diesel to compressed natural gas (CNG) engines	2001	Buses, taxis, three-wheelers
Bharat stage III	2005	Initially only in national capital region (NCR – Delhi included)
Bharat stage IV	2010	Initially only in NCR
Heavy goods vehicle (HGV) restrictions (7:00 a.m. – 10:00 p.m.)	2014	HGVs
Ban on open waste burning	2015	Residents of Delhi
Shutdown of the Rajghat thermal power station	2015	Located in the east of New Delhi
Ban on >2000 cc diesel-engine vehicles	2016	Luxury diesel vehicles
No entry for HGVs in NH-2,10 and 58 area codes	2016	HGVs
Odd-even car scheme	2016	Cars
Deregistration of diesel vehicles older than 10 years or more	2016	Diesel vehicles
Ban on crop-residue burning	2016	Neighbouring states of Uttar Pradesh, Haryana, Punjab, Rajasthan
Bharat stage VI	2018	NCR
Shutdown of the Badarpur thermal power station	2018	Located in the southeast district of Delhi

Some of these strategies are untested for their efficacy and, to the authors' knowledge, the majority of evaluations have been confined to total PM_{10} mass-based measurements (Kathuria, 2005), global satellite observations (Chowdhury et al., 2017) or model simulations (Gulia et al., 2018, 2022; Sindhwani and Goyal, 2014) which do not provide a robust measurement-based link to concentration changes and changes of emissions from specific sectors. Therefore, more detailed analysis of the sources of PM_{10} would be beneficial to improve mitigation strategy evaluations. Our aim is to use a high-

throughput offline-AMS analysis protocol to analyse PM samples collected over multiple years and use this to track the contribution of different sources by performing source apportionment analysis on the organic fraction. The results can then be used to chart the changes in PM sources during times when mitigation strategies were implemented. Therefore, determining whether strategies have successfully decreased PM concentrations from their intended source.

4.3. Methods

4.3.1. Filter sample collection

Filter samples were collected at a 10 m height at the National Physics Laboratory (CSIR-NPL) situated west of the heart of New Delhi (28°38 N, 77°10′ E). The total number of registered vehicles in Delhi was 6.35 million in 2011, which rose to 8.29 million in 2014, and then to over 11 million in 2020 (Jain et al., 2020). This reflects an increasing population which is currently estimated at 31.2 million (Sharma et al., 2021). The NPL campus is surrounded by agricultural fields in the northwest and southwest (~1.5 km), managed by the Indian Agriculture Research Institute (Figure 4.1). There are busy roads to the north, northwest and west (~100 m), along with green parks and forests to the south (~1.2 km). A large industrial area is situated in the southwest (Mayapuri industrial areas, ~5 km). There are also large residential and commercial areas to the northwest (Kirti Nagar, ~3 km), north (Patel Nagar, ~1 km) and northeast (Karol Bagh, ~1 km).

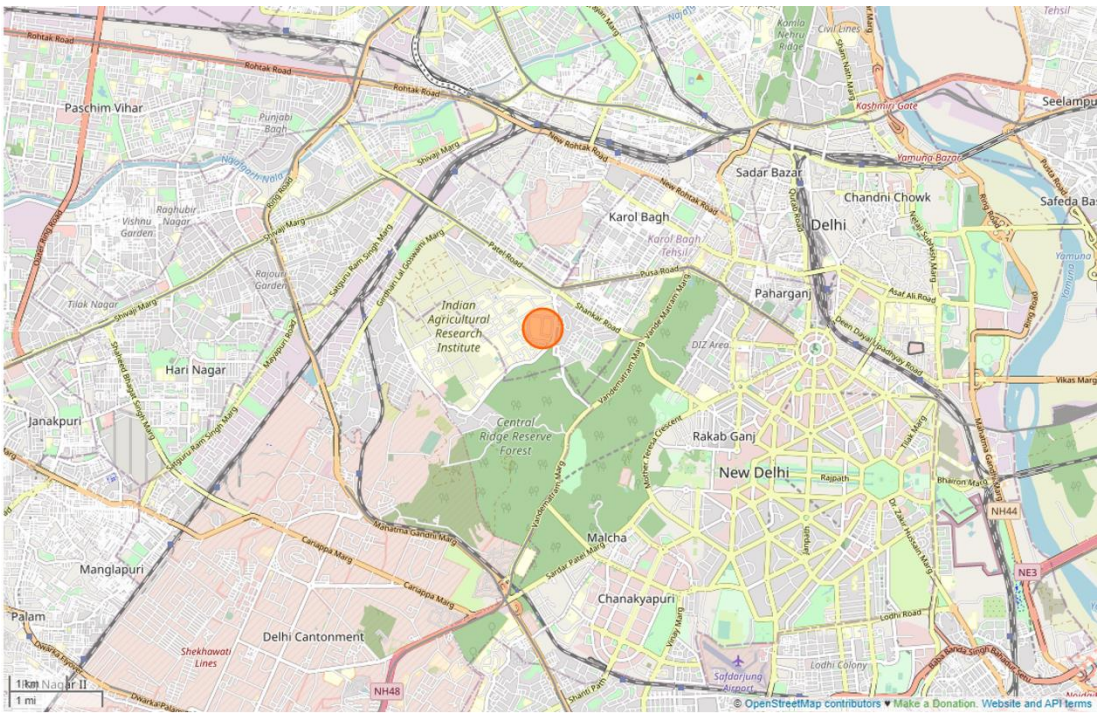

Figure 4.1. Map of New Delhi showing the measurement site location (marked with a circle) and the surrounding area.

For the analyses presented here, the year is split into four seasons: winter (January – February), pre-monsoon/summer (March – May), monsoon (June – September) and post-monsoon (October – December). The seasonal averages of temperature and relative humidity are summarised in Figure 4.2. Temperatures decrease to a minimum of ~3 ^{o}C in the winter, followed by peak temperatures of ~47 ^{o}C in the summer. The monsoon is characterised by large rainfall events which causes a maximum in relative humidity (monsoon average ~ 70%). The post-monsoon and winter seasons exhibit dramatic changes in the diurnal planetary boundary layer height caused by sharp changes in temperature between the day and night. The contraction in the boundary layer during the night causes near-surface pollutant concentrations to increase significantly. As temperatures drop further in the winter, severe fog and haze events occur which causes reduced visibility.

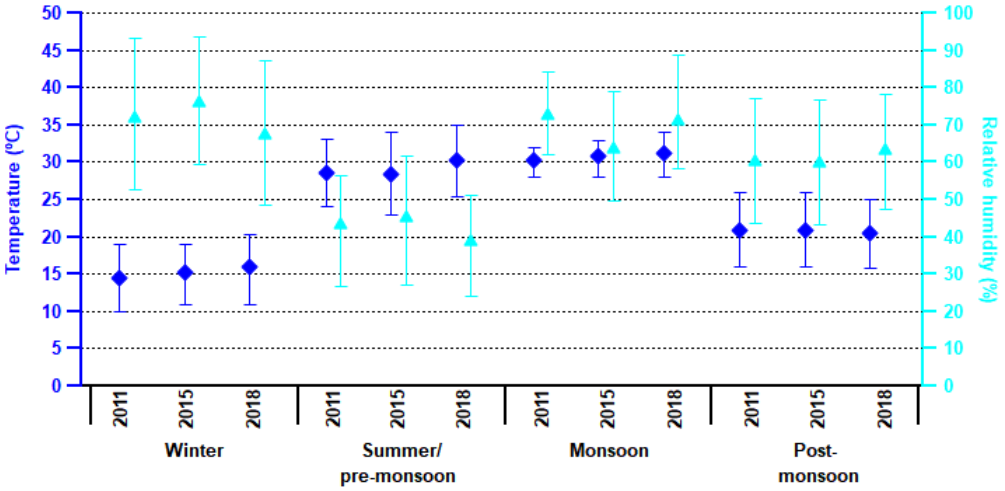

Figure 4.2. Seasonal average temperature (blue diamonds) and relative humidity (cyan triangles) for the years of 2011, 2015 and 2018. The bars show the 25th and 75th interquartile range of the underlying hourly data. Values shown are an average across the entire season.

Filter samples were collected from January until December for the years of 2011 (*n* = 50), 2015 (*n* = 113) and 2018 (*n* = 80). In 2011, the filters were sampled 4-5 times a month on an 8 h basis every Wednesday, during the morning (10:00 to 18:00 hrs) and night (18:00 to 02:00 hrs), using a Respirable Dust Sampler (Model: PEM-RDS 8NL, S/No.:1709; Make: M/s. Polltech Instruments, Mumbai, India). For 2015 and 2018, the filters were sampled over 24 h (10:00 to 10:00) with at least two filters being sampled per week and using a Respirable Dust Sampler (Model: AAS-217 NL; Make: M/s. Ecotech, Delhi, India). The quartz fibre filters (QM-A) were prebaked (550 ^{o}C for 6 h) before sampling at a flow rate of 1.2 m^3 min^{-1} with ± 2% accuracy. The filters were then stored at -20 ^{o}C before being analysed. More information on the sampling method is described in previous studies (Banoo et al., 2020; Jain et al., 2020; Sharma et al., 2014, 2021).

4.3.2. Offline-AMS

A new fully-automated sampling system to perform high-throughput analysis of filter extracts was developed for this study. An overview of the analysis

procedure is shown in Figure 4.3. Filter punches of area 2 cm^2 were first extracted in a solvent (5 mL) and ultrasonicated for 20 minutes at 30 ^oC. A range of solvents were assessed in this study, and the final solvent mix chosen to extract the filter samples was 1:1 acetone (99.8%, for HPLC, Thermo Scientific™) to ultrapure water (18.2 M Ω cm, total organic carbon (TOC) < 5 ppb, 25 ^oC). Further details on how this solvent was chosen is described in Section 4.4.1. The extracts were then filtered (0.45 µm pore size) before being placed in an autosampler. The samples were then injected into a tailor-made nebuliser and aerosolised using compressed argon. All fittings (PEEK or stainless steel), seals (EPDM) and fixtures (stainless steel) were selected specifically for chemical resistance to acetone and other solvents. The generated particles filled a PTFE spray chamber which was fitted with a pressure sensor to ensure consistent aerosol production. The chamber also allowed for the removal of excess liquid into a separate beaker. The aerosol was then dried through a series of dryers which differed according to the solvent. A Perma Pure Nafion™ membrane dryer (model: MD-070, Perma Pure LLC) was used for removal of water from the airstream. For organic solvent removal, diffusion dryers filled with activated carbon were used along with a tailor-made gas-phase denuder filled with activated carbon monolith.

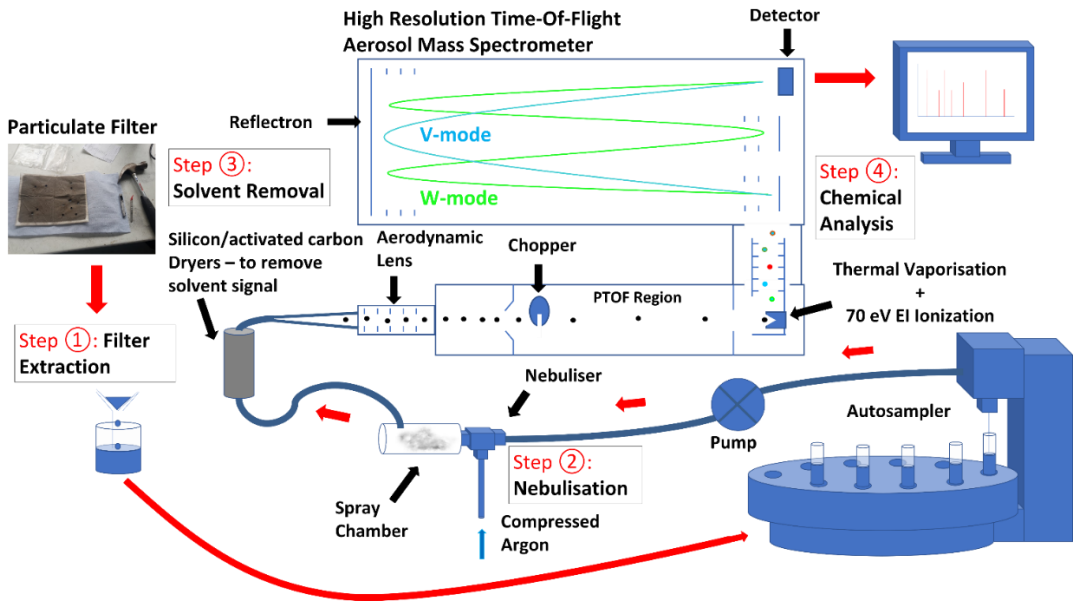

Figure 4.3. Diagram of the automated offline-AMS analysis system constructed for this work. Objects are labelled with black arrows and the flow of sample analysis is shown by red arrows.

The dried aerosol stream then passed through to the inlet of a high-resolution time-of-flight aerosol-mass-spectrometer (HR-TOF-AMS, Aerodyne Research Inc.). The HR-TOF-AMS was operated in V-mode and further operational details and descriptions of the instrument can be found elsewhere (Canagaratna et al., 2007; DeCarlo et al., 2006). In summary, particles pass through a ~PM_1 aerodynamic lens into the particle sizing time-of-flight chamber. Here, a chopper wheel controls the particle beam entering the chamber. Once sized, particles collide with a thermal vaporisation plate (600 ^{o}C) and the resultant non-refractory species are ionised (70 eV). The ions are propelled by a pulsar into the time-of-flight *m/z* analyser before being detected. The measured signal is the difference between the signal measured when the chopper is closed (background spectrum) and open in order to remove background effects. Each filter extract was measured for a total of 5 min at one difference spectrum (= chopper open – chopper closed) per 15 s. This high measurement frequency allowed for anomalies in the aerosol stream to be removed from the 5-min averaged spectra.

In between each sample run, an automated 7-min wash cycle was performed where ultrapure water (18.2 MΩ cm, total organic carbon (TOC) < 5 ppb, 25 ^{o}C) was injected into the sampling system. Samples of the solvent used for extraction were also frequently included in the sample carousel. The solvent spectra and wash cycle spectra were subtracted from the final measurement to reduce memory effects. A typical sample run of AMS measured concentrations of nebuliser generated PM is shown in Figure 4.4. Filter extract concentrations were significantly higher than the concentrations measured during a wash cycle and the pure solvent samples. The solvent organic background concentrations were on average ~1% of the filter sample organics and at a maximum of 2.5%.

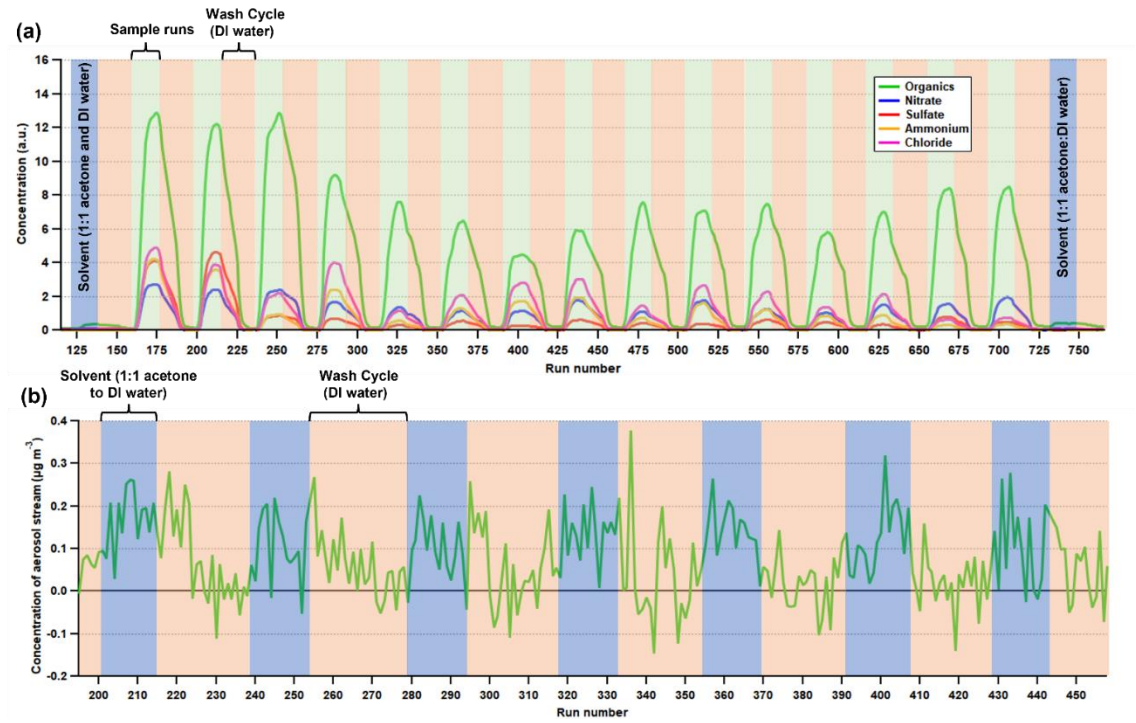

Figure 4.4. Two separate example runs of (a) filter sample (shaded green) and (b) pure extraction solvent (1:1 acetone to deionised ultrapure water, shaded blue). The 7 min wash cycle of deionised (DI) ultrapure water is shaded in orange. Concentrations shown in (b) are of the nebulised aerosol stream measured using the flow rate entering the AMS.

A total of 2078 ions (including isotopes) were fitted (*m/z* 12 – 328) and analysed in SQUIRREL (Sequential Igor data Retrieval) v1.64 and PIKA (Peak Integration by Key Analysis) v1.24 which are coded in IGOR Pro (WaveMetrics, Inc., Portland, OR, USA). Peaks were fitted based on an improvement of the open and closed spectrum residual signals rather than using the difference spectrum residuals as this can cause ambiguity. Peaks were also omitted if their average signal was less than 10 Hz ns^{-1}.

Argon was used as the airbeam correction within SQUIRREL and, given the argon atmosphere, the CO^+ peak (*m/z* 28) was fitted explicitly, rather than assumed to be equal to the signal at of CO_2^+, which is standard practise for ambient AMS analysis where the peak at *m/z* 28 is swamped by N_2. An increase in CO_2^+ was also observed when nebulising pure NH_4NO_3 which has previously been shown to be due to surface ionisation of organics within the instrument (Pieber et al., 2016). This arises from thermal decomposition reactions of NH_4NO_3 particles colliding with charred organic residue left on the particle vaporizer or ion chamber. The corrected CO_2^+ signal, $CO_{2,corr}$, was calculated using the relationship (Pieber et al., 2016):

$$CO_{2,corr} = CO_{2,amb} - \left(\frac{CO_{2,meas}}{NO_{3,meas}}\right)_{NO_4NO_{3,pure}} \times NO_{3,amb} \quad (4.1)$$

The NO_3^+ signal during ambient measurements, $NO_{3,amb}$, is multiplied by the correction ratio ($\left(CO_{2,meas}/NO_{3,meas}\right)_{NO_4NO_{3,pure}}$), which is the ratio of the measured CO_2^+, $CO_{2,meas}$, to the measured NO_3^+, $NO_{3,meas}$, during the nebulisation of pure NH_4NO_3. This is then subtracted from the ambiently measured CO_2^+ signal, $CO_{2,amb}$. During these experiments, the surface ionisation effect was also found to interfere with the CO^+ signal. This has previously been observed in AMS measurements but studies have chosen not to correct for it because not enough measurements were gathered (Pieber et al., 2016). We therefore use the same relationship as Equation 4.1, with all CO_2 terms replaced with CO to find the corrected CO^+ signal. The correction

ratio for CO^+ was found to be higher (6.6%) than for CO_2^+ (3.5%), which shows the need to include this correction when fitting CO^+ independently.

4.3.3. Measurements of OC/EC, WSOC and wavelength dispersive x-ray fluorescence

Organic carbon (OC) and elemental carbon (EC) concentrations were measured, in triplicate, for each filter sample (~0.54 cm^2 punches) using thermal optical carbon analysis (Model: DRI 2001A). The IMPROVE-A protocol was followed which, in brief, ramps the temperature (140, 280, 480, 580, 740 and 840 ^oC) in a helium and oxygen environment (Chow et al., 2004). This allows for the quantification of different fractions of OC (OC1, OC2, OC3 and OC4) and EC (EC1, EC2 and EC3), along with pyrolyzed carbon (OP). Standard solutions of sucrose and of potassium hydrogen phthalate were used for calibration in a 4.8% CO_2 and 95.2% helium atmosphere. Peak area calibrations were performed daily using 5% CH_4 in 95% helium and an error of 3-7% was estimated for OC and EC concentrations.

The water-soluble organic carbon (WSOC) was measured using a total organic carbon (TOC) analyser (Shimadzu TOC-L CPH/CPN, Japan) and a catalytic combustion oxidation method. Punches (~0.4 cm^2) of each PM_{10} filter were extracted in ultrapure Milli-Q water (18.2 M Ω cm) and sonicated in triplicate for 45 min at 50 ^oC. A platinum catalyst at 680 ^oC was used to convert the carbon in filtered (0.2 µm pore) extracts (5-10 mL) into CO_2 which was measured by a nondispersive infrared sensor. Standards of potassium hydrogen phthalate were used for calibration and blank filters were measured every 10 samples in a sample run to correct for background concentrations. A repeatability error of 3-10% was determined based on triplicate sample analysis. The water-insoluble organic carbon (WIOC) was then calculated by subtracting WSOC from the thermal optical carbon analyser OC measurement (WIOC = OC – WSOC).

A Wavelength Dispersive X-ray Fluorescence Spectrometer (WD-XRF, ZSX Primus, Rigaku, Japan) was used to measure the PM_{10} elemental concentrations of Al, B, Ca, Cl, Cr, Cu, Fe, K, Mg, Mn, Mo, Na, Ni, P, Pb, S, Ti, Zn and Zr. Measurements were taken under vacuum at 36 ^{o}C and using a 2.4 kW tube rating. Micro-matter thin-film standards were used for calibration and samples were measured in triplicate with a repeatability error of 5-10%. Detailed information on the calibrations and measurements are described in previous publications for OC/EC, WSOC and WD-XRF measurements (Banoo et al., 2020; Jain et al., 2020; Sharma et al., 2014, 2021).

4.3.4. Meteorological measurements

Temperature and dewpoint temperature measurements were taken at the Indira Ghandi International Airport in New Delhi at 1 h resolution (downloaded at: https://ncdc.noaa.gov/, last access: 03/02/2022). The relative humidity, RH, was calculated using the Magnus approximation:

$$RH = exp^{\left(\frac{bc(Dp-T)}{(c+T)(c+Dp)}\right)}. \quad (4.2)$$

Here, Dp, is the dewpoint temperature and, T, is the air temperature (in ^{o}C), while, b (17.625) and c (243.04 ^{o}C), are constants which were determined to apply to the following set of atmospheric conditions: 0 ^{o}C < T < 60 ^{o}C, 1% < RH < 100% and 0 ^{o}C < Dp < 50 ^{o}C.

The planetary boundary layer (PBL) height and surface solar radiation downwards (SSRD) were taken from the ERA5 land model from the ECMWF (download at: https://cds.climate.copernicus.eu/cdsapp#!/home) at 1 h and 0.25 degree resolution. It should be noted that Nakoudi et al. (2018) found that the ERA5 model overestimated the PBL height in Delhi during convective hours (9 a.m. - 12 p.m.), however, they reported a strong correlation between the SSRD and lidar measurements. For the purpose of this study, only the relative change in PBL height between seasons is considered and the absolute values are not critical to the findings.

4.3.5. Source apportionment

Positive Matrix Factorisation (PMF) is a multivariate analysis tool commonly used to separate a data matrix of pollutant concentration time series into source "factors" (Paatero and Tapper, 1994). In this instance, we use the mass spectral profile of the organic aerosol (number of measured ions m = 816), m, of each filter sample (n = 166) and combine them to form a matrix, $m \times n$, with time series rows of *m/z* species, n. The model can be summarised as:

$$\mathbf{X} = \mathbf{FG} + \mathbf{E} \tag{4.3}$$

where the measured $m \times n$ data matrix, $\mathbf{X}$, is equal to the factor profile $m \times p$ matrix, $\mathbf{F}$, multiplied by the factor time series $p \times n$ matrix, $\mathbf{G}$, plus, the residual $m \times n$ matrix, $\mathbf{E}$. The user determines the number of factors, p, using the value of Q which is calculated as follows:

$$\boldsymbol{Q} = \sum_{\boldsymbol{i=1}}^{\boldsymbol{m}} \sum_{\boldsymbol{j=1}}^{\boldsymbol{n}} \left(\frac{\boldsymbol{e_{ij}}}{\boldsymbol{\sigma_{ij}}}\right)^{\mathbf{2}} \tag{4.4}$$

Here, the residual, e_{ij}, and measurement uncertainty, σ_{ij}, matrices are composed of rows, i, and columns, j. A Q value of 1 would equate to a model solution that perfectly describes the measured data and all measurement uncertainty is found within the residuals. The optimisation of Q is achieved through the increase of p until the change in Q, ΔQ, is small. This shows that an increase in factors no longer improves the solution. The PMF2 algorithm was used in robust-mode using the Multilinear Engine 2 (ME-2) (Paatero, 1999) to explore the a-value space when anchor profiles are used. The PMF Evaluation Tool (PET, v3.00) was used for more general solution exploration as it requires less CPU and less time than ME-2 (Ulbrich et al., 2009). The error matrix was down-weighted based on the conditions set out by Paatero and Hopke (2003). This describes species with a signal-to-noise ratio (SNR) < 2, being down-weighted by a factor of 2 and species with a SNR < 0.2, by a factor of 10.

The error matrix was composed of both the AMS measurement uncertainties, α_{ij}, and the combined background concentrations of the solvent and the wash cycle, β_{ij}. The error has been calculated this way in previous offline-AMS studies (Bozzetti et al., 2017; Daellenbach et al., 2016) and uses the following equation:

$$\sigma_{ij} = \sqrt{\alpha_{ij}^2 + \beta_{ij}^2} \quad (4.5)$$

where, α_{ij}, is calculated according to statistical counting errors and ion-to-ion variability as described in Allan et al. (2003).

4.3.6. Calibration of offline analyses

The input matrices were converted to atmospheric concentrations using the OM/OC ratios measured by offline-AMS, $\left(\frac{OM}{OC}\right)_{offline-AMS}$, and the OC measurements, $OC_{OC/EC}$, made by the thermal optical carbon analyser using the realtionship:

$$OM_{amb} = \left(\frac{OM}{OC}\right)_{offline-AMS} \times OC_{OC/EC} \quad (4.6)$$

in which OM_{amb} is the atmospheric organic matter concentrations calculated in units of μg m^{-3}.

The final 9-factor solution was chosen from over ~100 possible solutions using FPEAK rotations to explore the rotational ambiguity and using initialisation SEEDs. These can be described as pseudorandom starting points from which the PMF model starts its analysis. The stability of each solution was also explored using bootstrapping analysis (50 runs) and the final 9-factor solution was the most stable. ME-2 was also used to anchor each solution to the online-PM_1 profiles previously published in an AMS study conducted in Delhi (Cash et al., 2021). However, there was a significant difference in the profiles of the

PM_{10} filters when run unconstrained compared to the anchored solution, the most significant being the level of oxidation in the primary organic aerosol factors. This caused unusual results that no longer resembled recognisable source factors. We therefore continued to use the unconstrained PMF model solutions and more details on the choice of the solution is shown below.

4.4. Results

4.4.1. Choice of solvent

Previous offline-AMS studies have shown low recoveries of primary organic aerosol (POA) when extracting filters using water. Daellenbach et al. (2016) show an 11% recovery of hydrocarbon-like organic aerosol (HOA) when using water extraction. This is of particular concern when measuring PM in areas where POA concentrations are high and, in the context of our study, to assess the efficacy of emission standards in reducing emissions. Previous measurements show the traffic-related PMF factors, such as HOA and nitrogen-rich HOA (NHOA), to dominate the PM_1 concentrations in Delhi during the majority of the year (Cash et al., 2021). Thus, considering the high concentrations of POA in Delhi, it is beneficial to extract more of the POA mass from filters. The use of organic solvents was therefore explored to recover a greater fraction of OA. However, as highlighted by Bozzetti et al. (2017), the main disadvantage of using an organic solvent as an extractant is the possibility of a high organics background signal. We therefore considered this when choosing the solvent and conducted a series of experiments to explore the solvent effects on the measured PM.

Firstly, to choose the most effective solvent, it is important to understand PM composition. Van Krevelen diagrams can be useful tools to understand the composition of OA as most HR-TOF-AMS literature quotes the H:C and O:C ratios. The bottom right of a Van Krevelen diagram shows the most oxidised composition whilst the top left shows the least (Figure 4.5). It is also possible

to estimate the chemical functionality of OA species using gradients within the diagram. Each gradient represents a step change in oxidation relating to one functional group. For example, the oxidation of alkanes to form alcohols involves the replacement of one hydrogen atom with one oxygen atom and one hydrogen atom and therefore relates to a gradient in H:C ratio of *m* = 0. Similarly, if two hydrogen atoms are replaced by a carbonyl group (R-R′C=O), then this corresponds to a change in -2 hydrogen and +1 oxygen so *m* = -2.

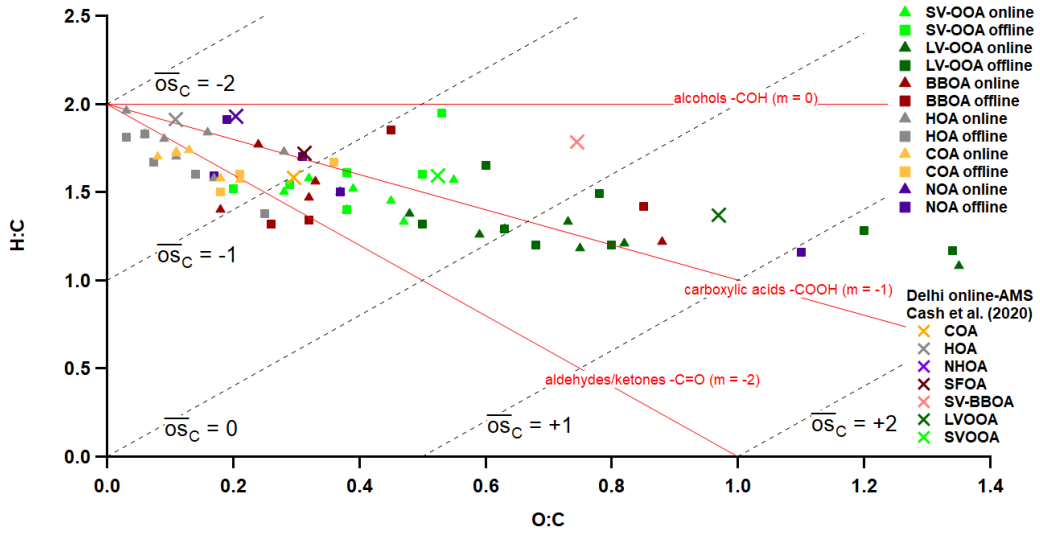

Figure 4.5. Van Krevelen diagram of published H:C and O:C ratios for PMF factors determined from online-AMS (triangles) and offline-AMS (squares) measurements as summarised in Table 4.2. The red lines are characteristic compound gradients which are calculated based on the oxidation of species resulting in the net gain or net loss of oxygen and hydrogen atoms. The effective carbon oxidation state ($\overline{OS}_C$) is denoted by the dashed black lines. The elemental ratios from the online-AMS measurements taken in Delhi by Cash et al. (2021) are represented by crosses and are coloured according to the legend.

Published O:C and H:C ratios (Table 4.2) are presented in the Van Krevelen diagram in Figure 4.5. The POA factors, such as HOA, cooking organic aerosol (COA) and some biomass burning organic aerosol (BBOA) factors, mostly fall on the *m* = -2 gradient. This suggests the functionality of these factors are mostly aldehydes and ketones. The majority of the factors that have high

recoveries when using water extraction are oxygenated factors such as semi-volatility oxygenated OA (SVOOA) and low-volatility oxygenated OA (LVOOA) (Daellenbach et al., 2016). From Figure 4.5, these fall on the carboxylic acid gradient (*m* = -1). This is understandable since -COOH groups have a greater polarity than -COH groups and water extracts polar compounds more efficiently. To dissolve the remaining ketone and aldehyde fraction, a number of possible solvents could be used, including methanol, acetone, ethyl acetate and dichloromethane. Methanol is currently the most used solvent after water in offline-AMS studies (Chen et al., 2016; Han et al., 2016; Mihara and Mochida, 2011), however the polarity of methanol is similar to that of water. This means similar compounds (i.e. polar species) are extracted in water and methanol. Therefore, when using methanol the problem remains that species with R-CH groups (such as alkanes and PAHs), which are dominant in POA, are not effectively extracted. This is supported by Mihara and Mochida (2011) who found the oxygenated composition of extracted PM to be related to the polarity of the solvent.

Table 4.2. Literature H:C and O:C ratios used in the Van Krevelen plot in Figure 4.5.

Literature (online/offline-AMS)	H:C SVOOA	O:C SVOOA	H:C LVOOA	O:C LVOOA	H:C BBOA	O:C BBOA	H:C COA	O:C COA	H:C HOA	O:C HOA	H:C NOA	O:C NOA
Ge et al. (2017) (offline)	1.61	0.38	1.49	0.78	1.85	0.45	1.67	0.36	1.38	0.25		0.19
Ye et al. (2017) (offline)	1.95	0.53	1.28	1.2							1.91	
Timonen et al. (2013) (offline)	1.52	0.2	1.2	0.68	1.34	0.32			1.81	0.03		
Sun et al. (2011a) (offline)	1.6	0.5	1.65	0.6								
Mohr et al. (2012) (offline)	1.58	0.32	1.18	0.75	1.77	0.24	1.57	0.21	1.96	0.03		
Schurman et al. (2015) (online)	1.5	0.28	1.21	0.82	1.22	0.88						
He et al. (2010) (online)					1.4	0.18	1.7	0.08				
Huang et al. (2010) (online)	1.33	0.47	1.38	0.48			1.73	0.11	1.58	0.17		
He et al. (2011) (online)	1.45	0.45	1.26	0.59	1.47	0.32			1.7	0.11		
Crippa et al. (2013) (online)	1.52	0.39	1.33	0.73			1.74	0.13	1.84	0.16		
Ge et al. (2012) (online)					1.56	0.33	1.72	0.11	1.8	0.09		0.37
Sun et al. (2011b) (online)	1.4	0.38	1.29	0.63			1.58	0.18	1.83	0.06	1.5	
Zhu et al. (2016) (online)	1.57	0.55	1.08	1.35					1.73	0.28		
*Cash et al. (2021) (online)	1.59	0.52	1.37	0.97	1.72 (SFOA) 1.79 (SVBBOA)	0.31 (SFOA) 0.74 (SVBBOA)	1.58	0.3	1.91	0.11	1.93 (NHOA)	0.2 (NHOA)

***Factors with slightly different source categories than those listed for other studies but are otherwise comparable.**

We chose a mix of 50% acetone (99.8%, for HPLC, Thermo Scientific™) and 50% ultrapure water (18.2 M Ω cm, total organic carbon (TOC) < 5 ppb, 25 ^{o}C) as the extraction solvent. As discussed, the majority of the water insoluble POA source factors were found to have aldehyde or ketone functionalities and are less oxidised. Acetone is a ketone and has a similar polarity to the majority of the oxidised species in POA. Many alkanes and PAH species are also readily miscible in acetone (Lü et al., 2008; Mlyano and Hayduk, 1986; Sun et al., 1998) and it dissolves the majority of the water insoluble species. Acetone is also miscible with water which means separate extractions are not required. Using acetone as a co-solvent to water is also supported by PAH solubility studies showing the higher co-solvent power of acetone when compared with other common solvents (Kwon and Kwon, 2012; Morris et al., 1988; Sun et al., 1998).

Another consideration is the background signal caused by the solvent which has previously been the main reason behind organic solvents not being used (Bozzetti et al., 2017). However, there are methods to reduce the solvent background. Many studies use diffusion dryers filled with activated carbon and molecular sieves (Chen et al., 2016; Han et al., 2016; Mihara and Mochida, 2011). This technique has been shown to almost remove the background signal when using methanol and ethyl acetate (Mihara and Mochida, 2011). As this technique relies on diffusion, the higher volatility of acetone means it can be efficiently removed from the aerosol stream using diffusion driers. The offline-AMS method described here uses diffusion scrubbers filled with activated carbon granules and monoliths. This technique shows consistently low background concentrations (average signal is ~1 % of filter sample organics) when 1:1 acetone to water is used (Figure 4.4a) which is highly repeatable (Figure 4.4b). Additional experiments were also conducted to assess acetone contamination on known organic samples, as described in Section 4.4.2.2.

4.4.2. Offline-AMS recovery results

4.4.2.1. Online-AMS determined recoveries

The OA recovery of the offline-AMS technique can be determined through a number of methods that are outlined in Daellenbach et al. (2016). One method involves normalising the offline-AMS measured organics signal to the offline-AMS measured sulphate signal. This is then compared to the sulphate normalised organics measured using a co-located online-AMS. The recovery is calculated using the equation:

$$R_{j,SO_4^{2-}} = \frac{Off_j}{Off_{SO_4^{2-}}} \Big/ \frac{On_j}{On_{SO_4^{2-}}} \quad (4.7)$$

Here, R_{j,SO_4^-}, is the recovery of the species, j, and the offline and online signal of j is, Off_j, and, On_j, respectively. These are normalised by the offline and online signals of sulphate: $Off_{SO_4^{2-}}$ and $On_{SO_4^{2-}}$, respectively. This assumes the recovery of sulphate is 100% when using offline-AMS techniques i.e. $Off_{SO_4^{2-}} \approx On_{SO_4^{2-}}$.

This method was used to calculate the OA recovery using online PM_1 measurements taken in Delhi during the pre-monsoon of 2018 (Cash et al., 2021). The same HR-TOF-AMS used to conduct the online measurements was also used for the offline-AMS measurements of $PM_{2.5}$ filters collected during the same time period. The OA recovery results in Figure 4.6a show recoveries higher than 1 which suggests a number of possibilities:

a) refractory sulphate species exist on the $PM_{2.5}$ filter samples that the AMS cannot measure;
b) a larger mass of organics exist on the larger sized $PM_{2.5}$ filter samples that are missed in the online-AMS measurements due to the PM_1 inlet, relative to SO_4^{2-};

c) contamination from the offline-AMS method is causing an increase in the organics;

d) the nebulisation process is causing sulphate to bond to other species to form refractory sulphate that the AMS cannot measure.

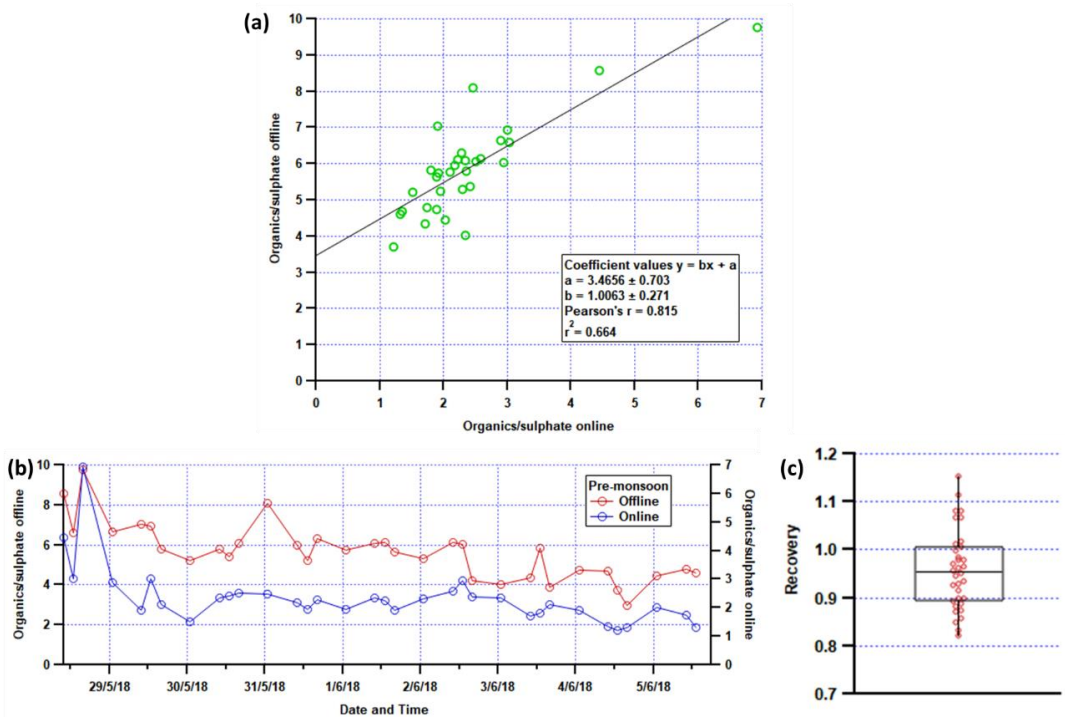

Figure 4.6. Sulphate normalised organics results where the scatterplot of offline vs online is shown in (a) and the sulphate normalised organic concentrations for online- and offline-AMS are also shown in (b). The OM/OC determined recovery is shown in (c).

The effect of possibility (a) could be likely as it has recently been shown from MARGA measurements taken in Delhi that $PM_{2.5}$ sulphate is larger in mass than the sulphate measured in PM_1 (Acharja et al., 2020). Possibility (b) is unlikely as the additional organics arising from a slightly larger size fraction is not likely to cause a 3-fold factor increase in organics. Possibility (c) has validity as the solvent could cause contamination but, for reasons to be discussed in Section 4.4.2.2, this is likely to be minimal and unlikely to cause

a 3-fold factor increase in organics. Another likely possibility is (d), the formation of refractory species of sulphate during nebulisation. In the context on AMS measurements, refractory means the resistance to rapid vaporisation at 600 ^{o}C under vacuum. This has previously been observed in offline-AMS measurements in the presence of large concentrations of metal species such as Na^{+}, Ca^{2+} and Mg^{2+} (Bozzetti et al., 2017). Reactions similar to:

$$2NaCl + (NH_4)_2SO_4 \rightleftharpoons Na_2SO_4 + 2NH_4Cl$$

are proposed, resulting in the formation of sulphate salts, e.g. Na_2SO_4, which are refractory species and are not detected by the AMS. The concentrations of metal species in Delhi are significantly high, particularly Na^{+}, Ca^{2+} and Mg^{2+} (Sharma et al., 2021). This suggests sulphate salts are the likely explanation to the high recovery values.

From Figure 4.6c, the observed trend in measured organics between offline-AMS and online-AMS is still retained, despite the issues surrounding sulphate normalisation. This suggests a recovery method using the organic fraction is more likely to give a better result. A different method is therefore used that relies on the OM/OC measurement from both the online-AMS and offline-AMS techniques. Firstly, the OC measurement, $OC_{online-AMS}$, is obtained from the online-AMS data by using the following equation:

$$OC_{online-AMS} = OM_{online-AMS} / \left(\frac{OM}{OC}\right)_{online-AMS} \quad (4.8)$$

where, $OM_{online-AMS}$ and $\left(\frac{OM}{OC}\right)_{online-AMS}$ are the online measured organics and OM/OC ratio, respectively, measured by the HR-TOF-AMS. The resultant OC measurements can then be fed into Equation 4.6 which gives an offline-AMS organics concentration. The recovery can then be calculated by the equation: $R_{OM} = OM_{amb}/OM_{online-AMS}$ and the results are presented in Figure 4.6d which shows a recovery of 95.4 ± 8.3 %. This suggests that the majority of the organics are extracted and quantified when using 1:1 acetone to water as an

extracting solvent. It is also an improvement over previous recoveries published for water-soluble organic aerosol studies which quote recoveries ranging from 16 to 90 % (Ge et al., 2017; Jayarathne et al., 2018a; Li et al., 2015; Saarikoski et al., 2008; Sun et al., 2011a; Ye et al., 2017).

Despite a high OA recovery prediction, there are likely to be compounds that are not fully extracted in the acetone-water solvent. This means that compound-specific solubilities still apply and future work is required to estimate PMF factor extraction recoveries, like those estimated for water-extraction in Daellenbach et al. (2016). For this study, we are concerned with the relative change in source factors over time. However, it should be noted that the results presented are of the OA fraction that is soluble in 1:1 acetone to water.

4.4.2.2. Recovery of a known organic sample, assessment of solvent contamination and the assessment of particle loss in the AMS inlet

Artificial samples were used to further assess the recovery of organics and whether the organic solvent contaminates the filter extracts. The samples were a mixture of species of known mass and were either dissolved in ultrapure water or in 1:1 acetone to water, as described in Table 4.3.

Table 4.3. Artificial samples of known mass

Sample	Contents	Solvent
Artificial sample S1	NH_4NO_3 (0.0526 g), $(NH_4)_2SO_4$ (0.0525 g), NH_4Cl (0.0538 g) and phthalic acid (0.0606 g)	Ultrapure deionised water
Artificial sample S2	NH_4NO_3 (0.0526 g), $(NH_4)_2SO_4$ (0.0525 g), NH_4Cl (0.0538 g) and phthalic acid (0.0606 g)	Ultrapure deionised water and acetone (1:1)

Two separate dryer setups were used for the different artificial samples: one using only the Perma Pure dryer, and the other using the Perma Pure dryer along with activated carbon granule-filled, and carbon monolith-filled, diffusion dryers.

The recovery of phthalic acid, R_{Pa}, added to each sample was calculated using the equations:

$$(Pa)_{Offline-mass} = \frac{Off_{Org}}{Off_{SO_4^{2-}}} \times (SO_4{}^{2-})_{weighed-mass} \quad (4.9)$$

and

$$R_{Pa} = {(Pa)_{Offline-mass}}\Big/{(Pa)_{weighed-mass}} \quad (4.10)$$

Here, Off_{Org}, is the offline-AMS measured total organics and the $\frac{Off_{Org}}{Off_{SO_4^{2-}}}$ gradient is multiplied by the known mass of sulphate added to the sample, $(SO_4{}^{2-})_{mass}$. The offline-AMS determined mass of phthalic acid, $(Pa)_{Offline-mass}$, is then divided by the known mass of phthalic acid, $(Pa)_{weighed-mass}$.

The details of each run are described in Table 4.4, and the scatterplots used to obtain the $\frac{Off_{Org}}{Off_{SO_4^{2-}}}$ gradients are shown in Figure 4.7a. It is worth noting that the measured AMS signal for artificial sample S2 was on average ~28 times larger for organics (and for sulphate) when at the same dilution as S1. In other words, a sample of the same mass dissolved in the solvent mix (1:1 acetone to water) increased the signal by a factor of ~28 when compared to water dissolution. Sample S2 was therefore diluted in order for its signal to be of a similar magnitude to S1. A likely explanation is the increased miscibility of phthalic acid and an even greater increase in nebulisation efficiency. This

highlights a significant increase in sensitivity when using 1:1 acetone:water compared with water extraction.

Table 4.4. Details and results of artificial sample runs

Run no.	Sample run details	Organic/ sulphate gradient	Sulphate mass (g)	Phthalic acid mass (g)	Calculated organic mass (g)	Phthalic acid recovery (%)
1	Artificial Sample S1 (water) – Perma Pure + activated carbon dryers used	1.2086	0.0382	0.0606	0.0462	76.2
2	Artificial Sample S2 (1:1 acetone to ultrapure DI water) – Perma Pure + activated carbon dryers used	1.3613	0.0382	0.0606	0.0514	85.8
3	Artificial Sample S1 (water) – only Perma Pure dryer used	1.2667	0.0382	0.0606	0.0484	79.8

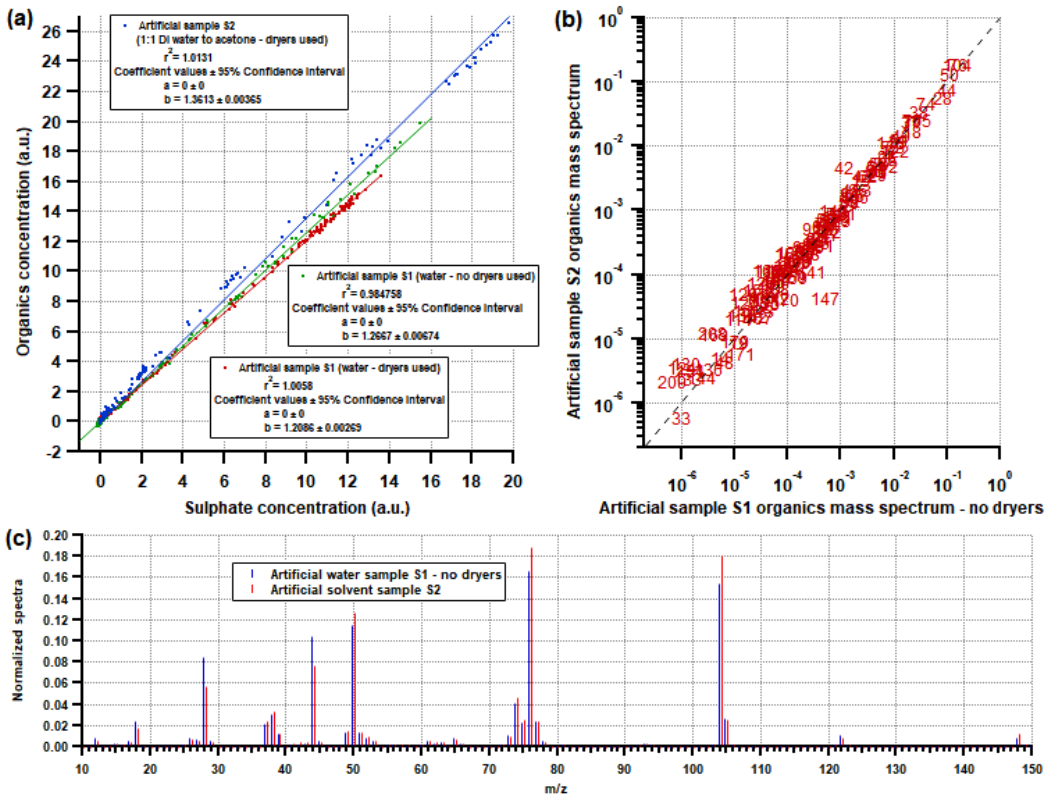

Figure 4.7. Artificial sample results showing (a) scatterplots of the artificial sample runs, along with mass spectral comparisons between sample S2 and sample S1 (no dryers used) in (b) and (c).

Table 4.4 shows the recovery of phthalic acid was higher for sample S2, meaning, the 1:1 acetone-water solvent gave the highest recovery. This is expected as the solubility of phthalic acid in acetone is greater than in water (Long et al., 2005; Long and Yang, 2008). Using the difference in calculated organic mass between runs 1 and 3 (Table 4.4), it is estimated that 5% of extracted phthalic acid is lost when using activated carbon dryer setup.

From the mass spectral comparisons shown in Figures 4.7b and 4.7c, the ratios of peaks closely match when using water and the acetone-water mix. The main peaks relating to phthalic acid (*m/z* 50, 74, 76 and 104) are slightly higher in sample S2 while the peaks associated with CO^+ and CO_2^+ (*m/z* 28 and 44) are higher in sample S1. This suggests there is a small difference in

the fragmentation of phthalic acid when extracted with 1:1 acetone to water compared with water-only extraction. However, if acetone were to contaminate the sample S2 mass spectrum, it would likely show an increase in peaks at *m/z* 27, 28, 29, 39, 43, 44 and 55, over the S1 spectrum. Instead, these peaks have very similar intensities between the two solvents. It is therefore determined that when using 1:1 acetone to water solvent, the contamination of the organics is minimal.

Having established a high degree of recovery using the water/acetone extraction, the measurements were referenced to offline OC measurements to obtain quantitative results as described in Section 4.3.6 above.

4.4.3. Source apportionment results

4.4.3.1. Choice of PMF solution

This section describes the steps to choosing a PMF solution. The correlation of factors with external measurements is often taken as a measure for selecting the physically most likely solution. Here, due to the limited availability of external data, the solution is chosen purely on PMF sensitivity analysis. The solutions were examined for rotational ambiguity using FPEAK. For all solutions, the change with FPEAK (-2 to 2) brought variation in factor mass, however, a clear global minimum is observed in the Q/Q_{exp} solution space when FPEAK = 0. Therefore, all solutions shown are set at FPEAK = 0. Solutions using between 1 to 12 factors were explored; those with more than 10 resulted in factor splitting. Factor splitting can be described as one factor separating into two non-unique factors with similar profiles and time series. It also results in a small drop in Q/Q_{exp} and residuals.

The solution's stability was explored for all possible solutions, by starting the PMF algorithm at different pseudorandom points in time, known as initialisation SEED. The factor masses changed with SEED at 7 and 8 factors, however, they remained stable at 1 to 6 and 9 to 10 factors. The 8, 9 and 10 factor

solution profiles are shown at SEED = 0 in Figure 4.8, along with bar charts showing their factor masses at different SEEDs. The two solutions to be considered are the 9 and 10 factor solutions as these are the most stable with initialisation SEED. The 10-factor solution contains three factors which resemble those previously seen for solid-fuel organic aerosol (SFOA). The factors SFOA1 and SFOA3 show signs of splitting as they have similar profiles and time series. Without more external data, or prior knowledge, the 10-factor solution is discarded as the two SFOA factors are too similar to distinguish as unique.

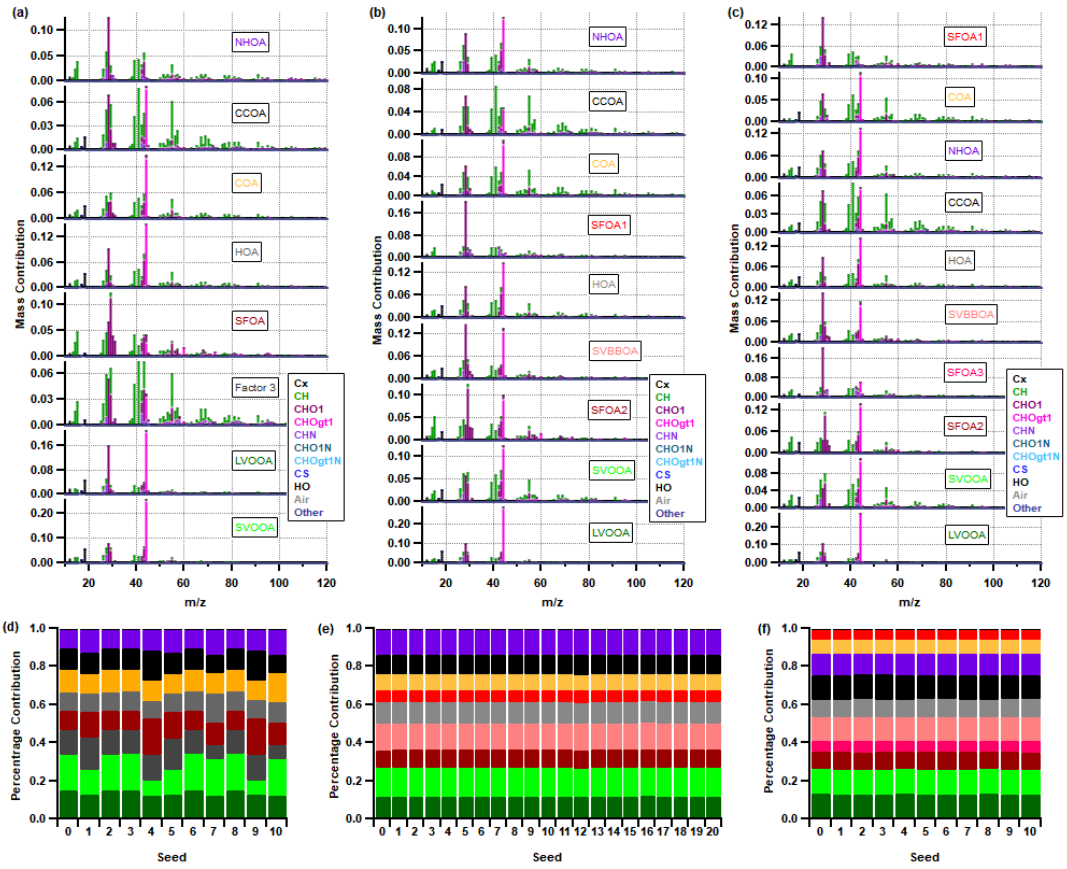

Figure 4.8. The (a) 8, (b) 9 and (c) 10 factor solution profiles along with the factor mass contributions with changing initialisation SEED. The (d) 8 and (f) 10 factor solutions were explored from 1 to 10 SEEDs, while the (e) 9 factor solution was explored using 1 to 20 SEEDs.

There is also a decrease in Q/Q_{exp} with 9 factors (Figure 4.9b) and this corresponds to, mostly, a positive change in the residuals from the 8-factor solution time series (Figure 4.9c). The difference in residuals between the 8 and 10 factor solutions show large negative changes in the residuals. This supports the discarding of the 10-factor solution, and the 9-factor solution is therefore chosen as this best represents the measured data.

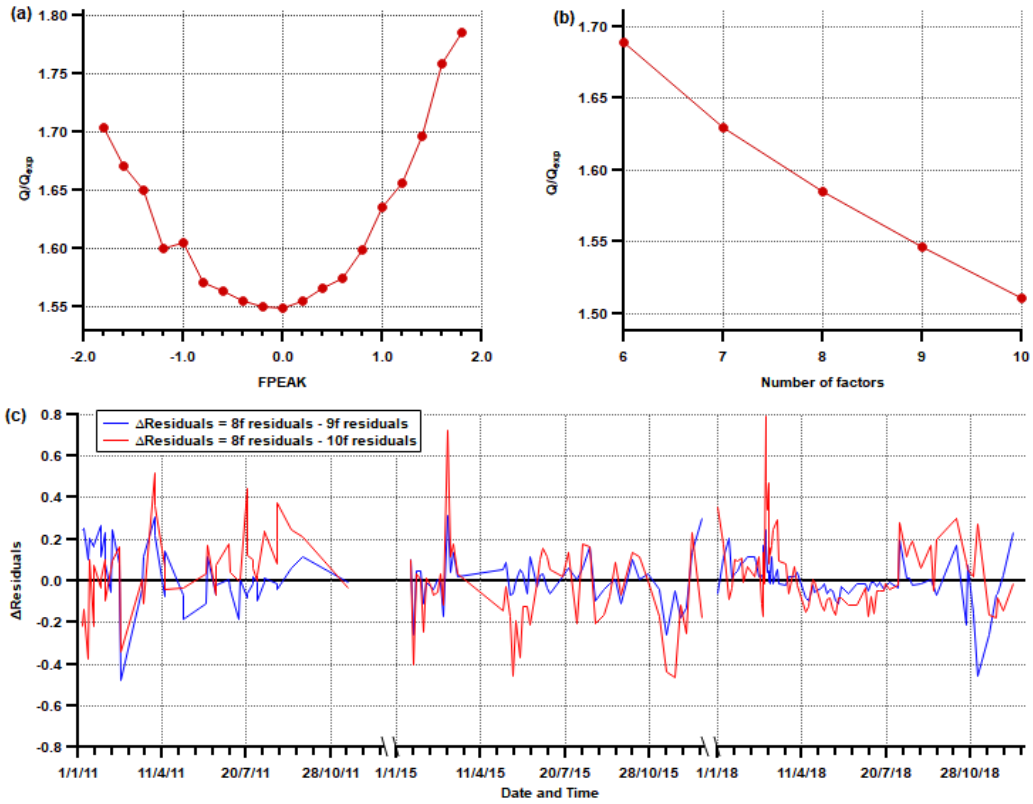

Figure 4.9. Sensitivity analysis of (a) the 9-factor solution with changing FPEAK and (b) the change in *Q*/*Q*exp with the number of factors. The differences between the 8-factor residual time series and either the 9-factor or the 10-factor residual time series are shown in (c) in blue and red, respectively.

It should be noted that solutions based only on the data for one of the three separate years of 2011, 2015 and 2018 were also compared with the chosen 9-factor solution based on the combined dataset. As the 9-factor solution

contains a longer dataset, it was more stable to variations in FPEAKs (-2 to 2) and Initialisation SEED (20 seeds). The solutions for the separate years also contained a lower number of factors (6-7). A similar situation was found in our online measurements (Cash et al., 2021) where we conducted a comparative analysis of PMF solutions produced from the whole dataset, along with solutions from different seasons. The solution that resulted from PMF analysis of the whole dataset was found to have the closest relationship with external tracers. Additionally, the PMF analysis of separate years means factors can vary between years. This makes PMF factors less comparable, so the full-length dataset was therefore used.

4.4.3.2. PMF factor identification

The chosen 9-factor solution includes two traffic-related factors, one named hydrocarbon-like organic aerosol (HOA) and the other named nitrogen-rich HOA (NHOA). There are three burning-related factors, two of which are linked to different sources of solid-fuel burning (SFOA1 and SFOA2), while another is linked to semi-volatility biomass burning OA (SVBBOA). There is also a factor relating to coal-combustion OA (CCOA), another to cooking OA (COA), and two secondary OA factors separated based on volatility: semi-volatility oxygenated OA (SVOOA) and low-volatility OOA (LVOOA). All factor profiles and concentration time series are presented in Figure 4.10, along with the time series of tracers to help identify each factor. The attribution to sources and naming is based on the comparison of mass spectra with those identified in previous studies, including the presence of individual characteristics such as a higher m/z 55 to m/z 57 ratio for COA than for HOA (Mohr et al., 2012) and the presence of *m/z* 60 and *m/z* 73 (levoglucosan) in factors containing biomass burning emissions (see below). Encouragingly, the PMF analysis did not identify a factor that reflected the solvent itself providing further evidence that the scrubbers were efficient in removing the acetone.

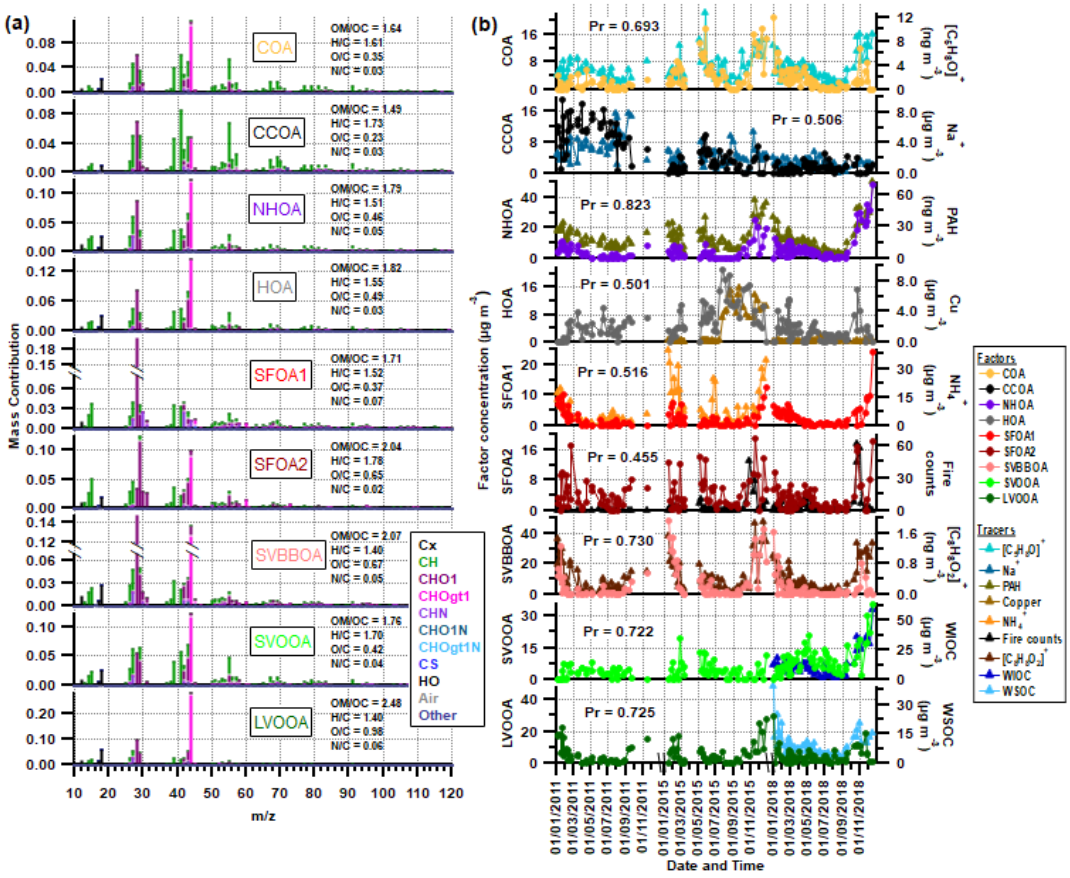

Figure 4.10. (a) Factor profiles and (b) factor concentration time series for the chosen 9-factor solution. The profiles for factors SFOA1 and SVBBOA have split y-axes to display more detail of their composition. Elemental analysis ratios for OM:OC, H:C, O:C and N:C are shown for each factor in (a). The tracer time series (right y-axis) for each factor underlie each graph in (b) and the Pearson's *r* (Pr) correlations between factor and tracer are also shown. Note: for some tracer species, the measurements are not complete for all three years. The AMS measured ions $[C_5H_8O]^+$ and $[C_8H_8O_2]^+$ respectively represent a tracer used to identify cooking OA and a fragment of dibenzodioxin called benzodioxan.

The traffic factor, HOA, has the strongest correlation of all factors with Cu (Figure 4.10) which is a well-known tracer for traffic-related (non-exhaust emission) PM_{10} due to the wear of metallic brake pads on vehicles (Denier van der Gon et al., 2007; Harrison et al., 2021). The second traffic factor, NHOA, has a similar mass profile and elemental composition to HOA, except NHOA has higher nitrogen-containing family peaks (CHN and CHO1N) and a higher

N:C ratio (Figure 4.10). The NHOA factor has previously been measured in Delhi using online-AMS measurements and a similar distinction was made where one traffic factor is richer in nitrogen (Cash et al., 2021). Also, a second study also observed a separation of traffic-related volatile organic compounds (VOCs) into two PMF factors (Wang et al., 2020). These studies have made the link between the second (NHOA) traffic factor and heavy goods vehicle (HGV) restrictions occurring during the day. These restrictions cause a large influx of mostly diesel-engine HGVs into the city during the evenings and early hours of the morning.

Diesel engines are shown to emit large concentrations of PM PAHs (Singh et al., 2010). NHOA shows a strong correlation with PAHs (Pearson's r = 0.823) and this supports diesel emissions contributing to NHOA. Through offline-AMS measurements, a total of 15 PAHs were measured on the filters which are mostly unsubstituted PAH species, all of which have been measured in previous AMS studies (Herring et al., 2015). These species are shown in Figure 4.11, along with PAH profiles for each factor. The breakdown of total PAH mass into factors is also shown, along with the percentage composition of PAHs within each factor. Figure 4.11 shows NHOA has the highest composition of PAHs (0.733%) and contributes the largest PAH mass to total PAH concentrations (21.5%). There is some indication that the NHOA factor has increased over the years.

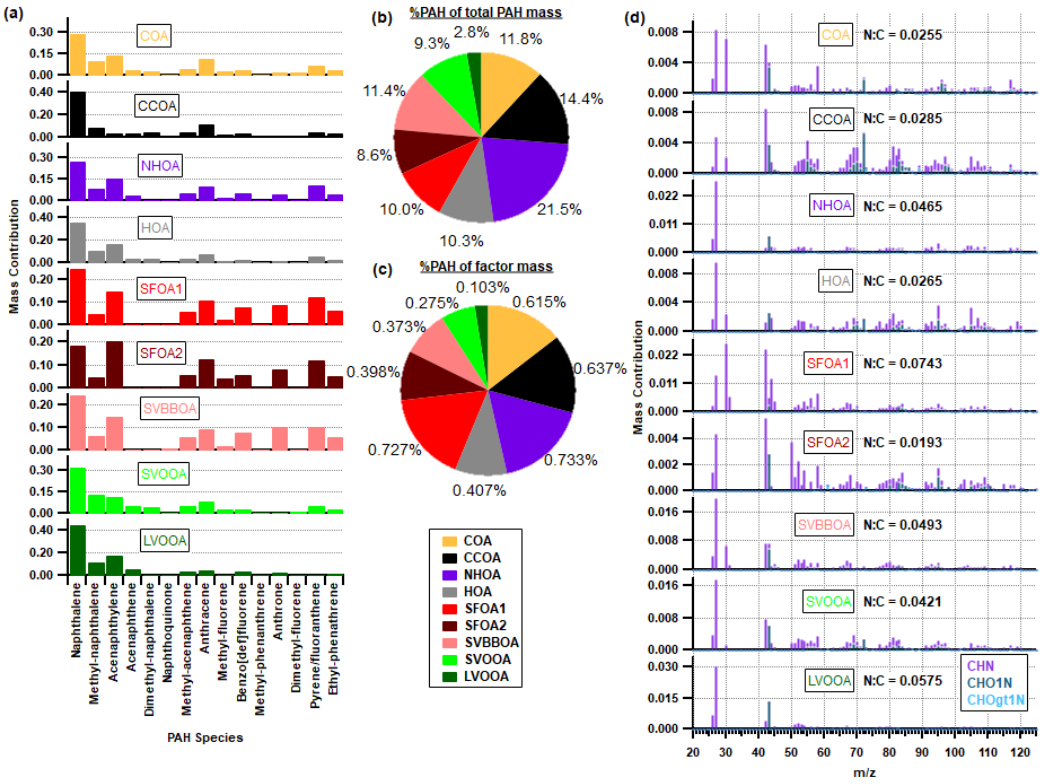

Figure 4.11. Factor profiles for (a) polyaromatic hydrocarbons (PAH) and (d) nitrogen species. The pie charts show (b) the percentage contribution of factors to the total PAH mass and (c) the percentage contribution of PAHs to total factor mass.

The factor mass profile of nitrogen species is also shown in Figure 4.11d. The high N:C ratio of NHOA is mostly due to the *m/z* 27 peak. This relates to the ion, $[CHN]^+$, which is a fragment of multiple possible nitrogen-containing species. Previously, NHOA has been shown to be composed of nitrile species (Cash et al., 2021) but this is not evident in the spectrum in Figure 4.11d. This suggests some of the nitrogen containing species have not been extracted or have volatilized from the filter sample, therefore highlighting a limitation of the offline-AMS technique.

The COA factor has a particularly high *m/z* 55:57 ratio and has a strong correlation with the AMS-measured cooking tracer ion, $[C_5H_8O]^+$ (Figure 4.10). These two characteristics have previously been shown as indicators of cooking

OA (Sun et al., 2016). In a previous study, PM_1 measurements in Delhi suggest COA is highly oxygenated when compared with this type of OA in other cities and, therefore by extension as derived from other cuisines (Cash et al., 2021). This is supported by the measurements shown in this offline study as the COA profile has large *m/z* 28 and 44 peaks. These peaks also make the COA profile look particularly similar to the PM_1 COA profile. It also has a similar set of H:C, O:C and OM:OC ratios. These similarities therefore imply the majority of the PM_{10} COA mass is within the PM_1 fraction.

The time series in Figure 4.10b clearly shows that the concentrations of CCOA slowly decline across the three years. CCOA can be difficult to separate from other fossil fuel emission products such as HOA. However, the CCOA profile in this study does show a ratio of C_xH_y peaks similar to that measured in previous AMS studies (Lin et al., 2019; Xu et al., 2016). There are also other tracers of coal-combustion such as Na^+ to which CCOA shows the strongest correlation out of all factors. Na^+ is often added to coal products in order reduce PM emissions and is mostly bonded to the organic fraction of coal (Reizer and Juda-Rezler, 2016). Out of the available auxiliary measurements, it is also expected that CCOA has a high correlation with Cu and Cr as these are also bonded to the organic fraction. The correlation matrix of PMF factors with external tracers (Figure 4.12) shows a moderate correlation of CCOA with Cr and a low correlation with Cu. However, in an urban setting Cu may be dominated by other sources, such as traffic. Other species bonded to the mineral part of coal include As, Cd, Pb and Zn (Reizer and Juda-Rezler, 2016). These have moderate correlations with Cr which strengthens the suggestion that the moderate correlation between CCOA and Cr is another indicator that CCOA represents coal-combustion.

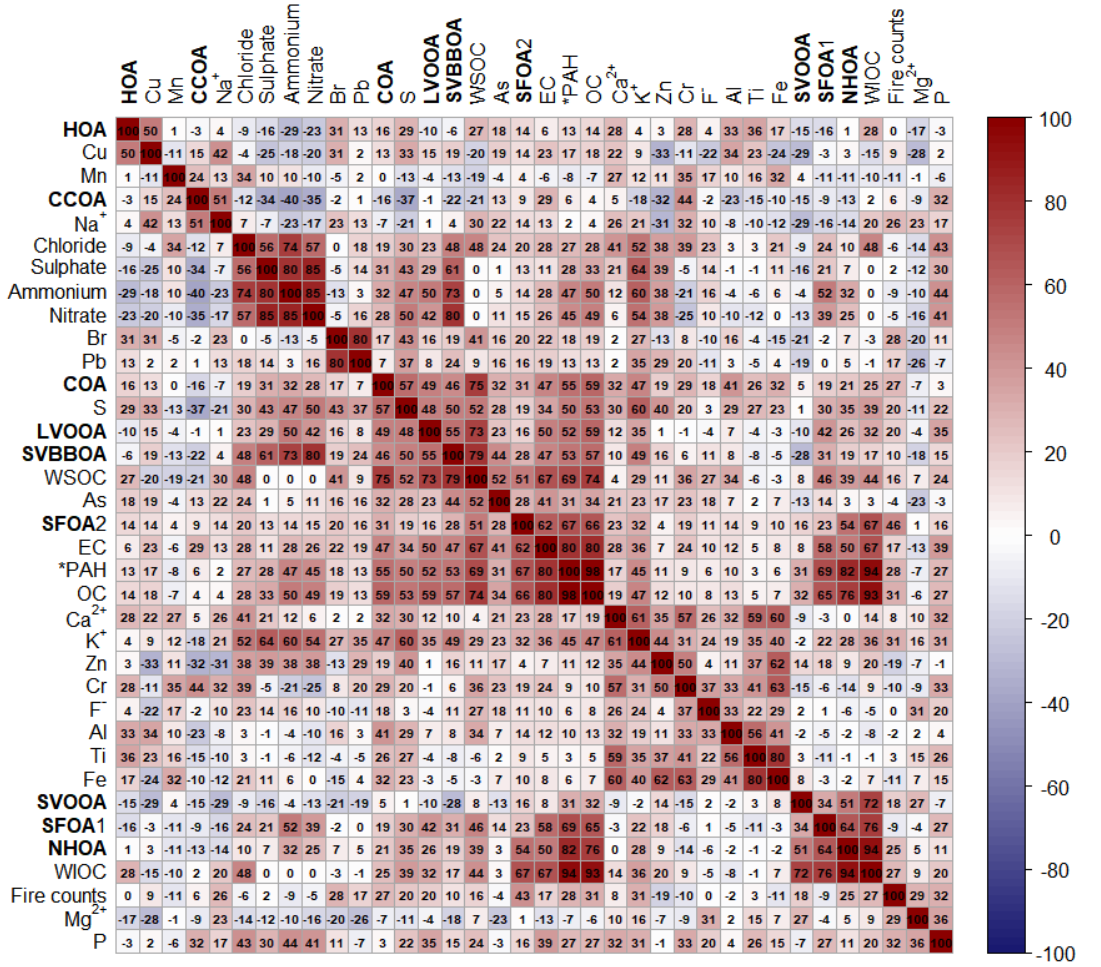

Figure 4.12. Correlation matrix between factors and external tracers. Hierarchical cluster analysis is used to order the Pearson's *r* correlations. The Pearson's *r* correlations are multiplied by 100, hence the scale is from -100 to 100. *The PAH time series is internally measured by the AMS and is the sum of the species described in Figure 4.11.

The three burning-related factors of SFOA1, SFOA2 and SVBBOA represent three different fuel-types which is determined from their composition and through external tracers. SFOA1 has the characteristic levoglucosan *m/z* 60 and 73 indicator peaks, showing the signature of wood burning. It also has the second highest correlation, behind SVBBOA, with NH_4^+ (Pearson's r = 0.516), along with the highest nitrogen content out of all factors (N:C = 0.0743). From Figure 4.11d, the SFOA1 mass profile for nitrogen species shows large peaks at *m/z* 30 ($[C_4HN]^+$), *m/z* 42 ($[C_2H_4N]^+$), *m/z* 44 ($[C_2H_6N]^+$), *m/z* 56 ($[C_3H_6N]^+$)

and *m/z* 58 ($[C_3H_8N]^+$). These peaks have previously been shown to be due to amine compounds in both AMS studies (Bottenus et al., 2018; Docherty et al., 2011) and other MS-based studies (Gohlke and McLafferty, 1962; McLafferty, 1993).

The high nitrogen content of SFOA1 suggests it originates from the burning of nitrogen-rich fuels. There have been numerous studies that compare the PM burning emissions from commonly used solid fuels in Delhi (Jayarathne et al., 2018b; Keene et al., 2006; Pervez et al., 2019). They find that fuels rich in nitrogen, such as dung-cakes, emit large concentrations of ammonium. SFOA1 is therefore likely related to residents burning solid fuels to keep warm during the colder months. This is supported by a general increase of SFOA1 during the post-monsoon and winter seasons, whilst during the summer and monsoon seasons it is close to zero (Figure 4.10b).

The second solid-fuel factor, SFOA2, appears to be a mix of sources. Its large *m/z* 60 and 73 peaks suggest it is heavily influenced by wood or cellulose-based material burning, but, it also has the highest composition of tracer peaks for municipal waste burning such as 1,2- or 1,4-dioxin (*m/z* 84, $[C_4H_4O_2]^+$), furan (*m/z* 68, $[C_4H_4O]^+$), phenol (*m/z* 94, $[C_6H_6O]^+$) and furfural (*m/z* 96, $[C_5H_4O_2]^+$) (Cash et al., 2021; Stewart et al., 2021). It also has the highest correlation of all factors with fire counts (Pearson's r = 0.455). The fire counts are from satellite measurements using the NASA Moderate Resolution Imaging Spectroradiometer (MODIS) sensor (for 2011) and the Visible Infrared Imaging Radiometer Suite (VIIRS) sensor (for 2015 and 2018) (available at: https://earthdata.nasa.gov/earth-observation-data/near-real-time/firms, last access: 18 Jan 2022). The fire counts were limited to a custom polygon encompassing the Haryana region. The vast majority of the fires counted were during April-May and October-November. This identifies the fires as originating from the burning of crop-residue from the wheat and rice harvests.

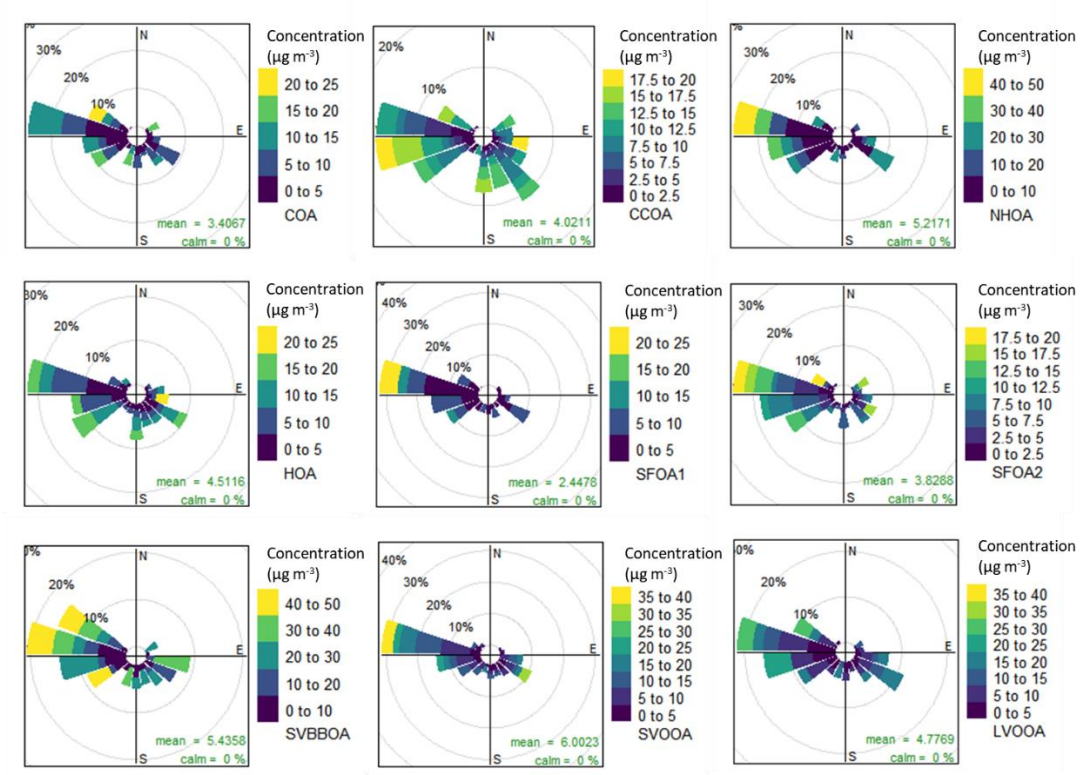

Figure 4.13. Pollution roses for each factor showing wind vectors sized to represent the percentage contribution to the mean concentration. The wind vectors are divided into concentration bins described in the legends.

The third burning-related factor, SVBBOA, has moderately large levoglucosan tracer peaks (*m/z* 60 and 73). It also has a low H:C ratio and a high O:C ratio which indicates it is highly oxidised and therefore more secondary in its composition. This suggests SVBBOA is from a mixture of local sources, city-wide sources, and sources along the Indo-Gangetic plain, as predicted by back-trajectory studies using the same PM_{10} filters (Banoo et al., 2020).

The highest contributions to SVBBOA concentrations arrive via a westerly wind, which is the same for both SFOA1 and SFOA2 (Figure 4.13). The SVBBOA factor may therefore represent an aged and oxidised mixture of SFOA1 and SFOA2. The evidence for this is supported by a high N:C ratio (0.0493) which coincides with N-rich SFOA1. It also has a high correlation with benzodioxan (Pearson's r = 0.730, Figure 4.12) which is an AMS-measured

fragment species of polychlorinated dibenzodioxins (PCDDs). PCDDs have previously been suggested to originate from municipal waste burning (Cash et al., 2021) and are suggested to be a significant source of chloride PM in Delhi. This is supported by SVBBOA having the highest correlation of all the factors with chloride (Pearson's r = 0.480).

The two oxygenated OA factors, SVOOA and LVOOA, have similar profiles but they characteristically differ in their oxygenation as shown by their O:C ratio (Figure 4.10). The large O:C of LVOOA is mostly driven by the large m/z 44 peak, $[CO_2]^+$, which is often thought of as a fragment of acidic functional groups (Duplissy et al., 2011). This means LVOOA is highly water-soluble and, as expected, has a strong correlation with WSOC measurements (Pearson's r = 0.725). Similarly, the higher H:C, and lower O:C, of SVOOA means it is less water-soluble, therefore, it is strongly correlated with water-insoluble organic carbon measurements (WIOC) (Pearson's r = 722). This supports the findings of high recoveries of water-insoluble OA when using this offline-AMS method.

4.5. Discussion

4.5.1. Seasonal and annual comparisons of PM_{10} across 2011, 2015 and 2018

The seasonal average concentrations of PMF factors across the four seasons in each year are shown in Figure 4.14. The highest concentrations of PM_{10} OA for the winter, pre-monsoon and monsoon seasons occurred in 2015. However, the post-monsoon concentrations were comparably high in 2015 and 2018. The post-monsoon of 2018 was meteorologically different to both 2011 and 2015. The temperatures in 2018 were slightly lower and the relative humidity was slightly higher (Figure 4.2). The average planetary boundary layer height (PBL) was also lower during the mornings of the 2018 post-monsoon, as shown by Figure 4.15. Therefore, the lower PBL may have accentuated the PM_{10} concentrations.

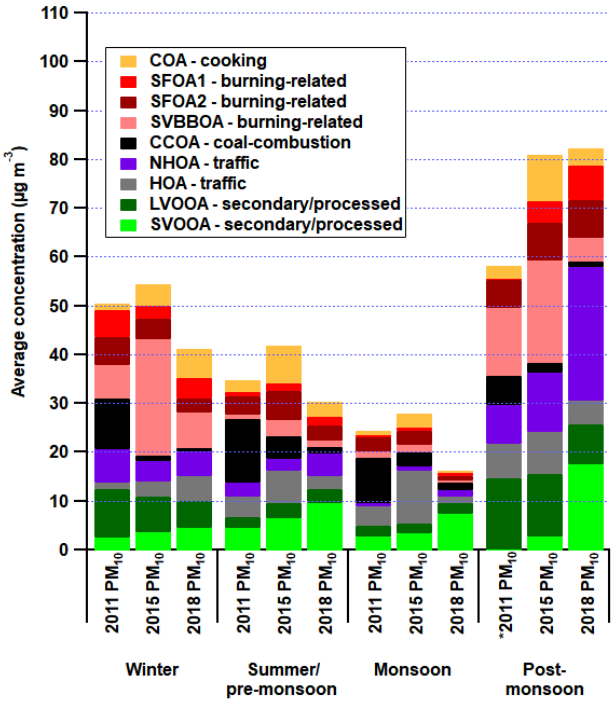

Figure 4.14. Average concentrations of PM_{10} OA factors in each of the four seasons of the years 2011, 2015 and 2018. *The PM_{10} concentrations for factors during the post-monsoon of 2011 are from one filter sample due to the unavailability of filters during this period.

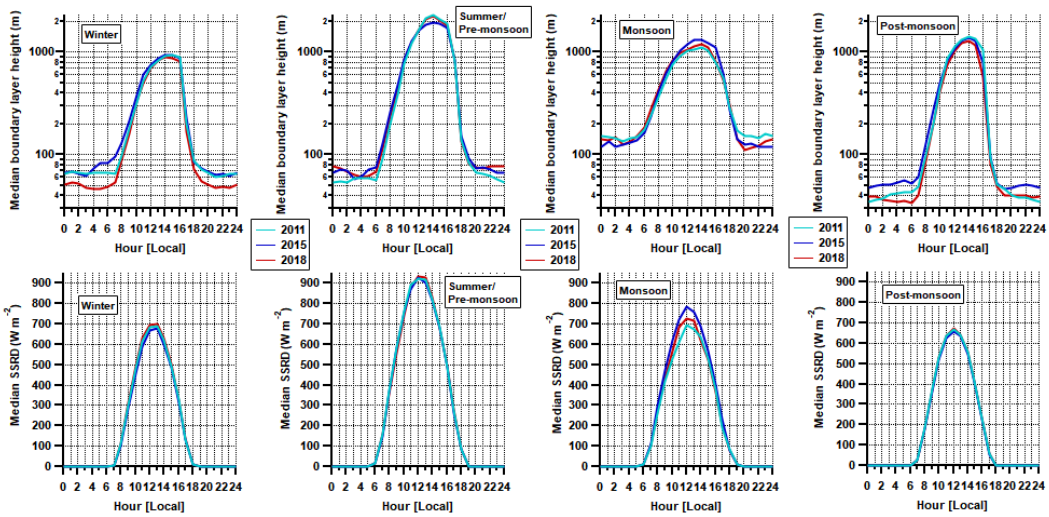

Figure 4.15. Median diurnal cycles of planetary boundary layer height (PBL, first row of graphs) and surface solar radiation downwards (SSRD, second row of graphs) for each of the four seasons. The diurnal cycles for the different years of 2011 (cyan), 2015 (blue) and 2018 (red), are also displayed. The y-axis in graphs displaying PBL are logarithmic in order to show the daily minimum more clearly. Values shown are an average across the entire season.

Figure 4.14 shows that traffic (= NHOA+HOA) is a consistently high contributor to PM_{10} OA in all three years. The consistency of traffic concentrations is mostly due to HOA because NHOA is less consistent across all seasons. NHOA is particularly low in concentration during the monsoon period, suggesting a greater susceptibility to atmospheric washout. However, peak concentrations occur during the post-monsoon which is mostly due to an increase in NHOA.

The rapid increases in population and vehicles from 2011 to 2018 suggest traffic concentrations should also increase significantly each year. However, this is not reflected in the traffic PM_{10} annual averages. This is likely because of the implementation of Bharat stages (Table 4.1) which are emissions standards that aim to improve vehicle technologies mitigating tailpipe emissions. There is also a decrease in traffic concentrations from 2015 to 2018 during the pre-monsoon which is the season least affected by a low boundary layer (Figure 4.15).

COA has a large presence during most seasons which is expected as cooking is a daily activity. However, there is a drop in concentrations during the monsoon period, which is likely due to increased rainfall events causing food vendors and customers to stay inside, as well as washout (Figure 4.14).

CCOA is consistently the largest individual OA factor across the three seasons of winter, summer and monsoon during 2011 (Figure 4.14), showing that coal-combustion was a significant source of OA in 2011. CCOA concentrations then start to decline in 2015 which is expected as the use of coal has decreased in popularity commercially, in homes and, in particular for thermal power stations. During 2018, CCOA concentrations decrease further until almost at zero in October. This coincides with the eventual shutdown of the Badarpur thermal power station (~20 km southeast of the measurement site) in October 2018, following the shutdown of the Rajghat power station in October 2015.

The three burning-related factors of SFOA1, SFOA2 and SVBBOA can be combined to represent the source category of burning-related OA. From Figure 4.14, burning-related OA was the largest contributing source during the winter. It was also the largest OA source during the post-monsoon of 2011 and 2015. This makes burning OA the most significant source when concentrations of PM_{10} are at their highest. This has been observed previously in the PM_1 OA measurements in Delhi where burning-related PM source factors were the highest during the post-monsoon (Cash et al., 2021). Therefore, burning-related emissions are likely to be the largest contributing source to acute PM-related health effects in Delhi.

However, it is important to note that burning-related emissions appear to be on the decline, as the highest mass of burning-related OA is seen in 2015 (Figure 4.14). The emissions then decrease in 2018 which suggests that peak emissions of burning-related PM may have been reached.

Differences in the seasonal averages of individual burning-related OA factors are apparent (Figure 4.14). As discussed, SFOA1 is shown to be linked to wood and dung-cake burning by residents keeping warm during the colder months. This is reflected in the increase in SFOA1 average concentrations in the winter and post-monsoon seasons. For SFOA2, peak concentrations are observed in the post-monsoon season. This was most likely due to its links to crop-residue burning which, from fire count observations, occurs most frequently during October, consistent with the burning of the Kharif season rice residue (Montes et al., 2022).

The seasonal trends in SVOOA and LVOOA suggest different sources influence their formation. The concentrations of LVOOA were generally larger than SVOOA during the winter and post-monsoon (Figure 4.14) but LVOOA was then smaller than SVOOA during the pre-monsoon and monsoon. When examining the trends of other source factors, the burning-related OA sources (SFOA1, SFOA2 and SVBBOA) show a similar pattern to LVOOA, i.e. they were also lower in concentration during the pre-monsoon and monsoon

periods. Therefore, LVOOA most likely has a significant contribution from the oxidation of burning-related emissions. Conversely, SVOOA increased in concentration during the pre-monsoon and monsoon periods. Figure 4.15 shows that the maximum diurnal solar radiation is greatest in the pre-monsoon and monsoon seasons, as expected given these seasons span the summer solstice. This suggests SVOOA is formed through the photooxidation of VOCs and PM.

The LVOOA factor shows a gradual decrease in concentration each year (Figure 4.14) which suggests that, in general, the impact of burning-related PM in Delhi has been diminishing. The opposite trend is apparent for SVOOA, which shows a gradual increase in concentration each year. The increase is not likely to be due to meteorology because solar radiation (i.e. the meteorological control of SVOOA) shows minimal change between each year (Figure 4.15). This suggests that sources of PM affect its formation as well. NHOA also shows a gradual increase each year (Figure 4.14). During 2018, there is a particularly large peak in concentrations during the post-monsoon, which is also reflected in the concentrations of SVOOA. This is supported by a relatively strong correlation between NHOA and SVOOA (Pearson's r = 0.510, Figure 4.12). SVOOA may therefore be influenced by diesel emissions and the annual averages in Figure 4.14 suggest SVOOA could continue to increase in future years without more diesel-focused emission mitigation strategies.

4.5.2. The recovery of primary organic factors using the developed offline-AMS method

Overall, the results in Figure 4.14 show the dominant contributors to OA are primary (POA) factors. As previously discussed, OA recoveries for individual PMF factors are not currently determined for the offline-AMS method used in this study and, therefore the results represent OA that is soluble in 1:1 acetone-water solvent. However, the POA factors that are particularly insoluble in water (e.g. HOA and COA) are dominant in the total OA mass measured. Therefore,

this shows that POA factors can be extracted to give high recoveries when using offline-AMS.

Our previous online-AMS PM_1 measurements in Delhi from 2018 (Cash et al., 2021) confirm a number of important aspects of the offline-AMS method developed in this work. Firstly, the offline-AMS method has retained compositional details such as the high PAH content in factors COA, HOA, NHOA and SFOA. The method also retains important tracer ions even those that are particularly low in concentration such as the benzodioxan ion which relates to PCDDs. Secondly, despite the lower temporal resolution of the filters analysed by offline-AMS, there is a separation of traffic-related PM into two factors, one of which contains a greater N:C ratio (NHOA). Thirdly, the offline-AMS method has delivered similar factor seasonal averages, particularly for the pre-monsoon and monsoon seasons. All the above indicate that the offline-AMS method has successfully captured the majority of the OA in Delhi's atmosphere. Future work aimed at determining PMF factor recoveries when using 1:1 acetone-water solvent would also be beneficial.

The offline analysis presented here identified two factors that were not isolated in the online dataset: the first is CCOA which is consistent with the decline of this component over the years to very small concentrations by 2018. The other is a difference in the split of SFOA into two factors in the offline analysis, distinguishing between biofuels (e.g. dung cakes) and other burning. This may reflect the fact that the solution of the offline analysis is defined also by changes from year to year, whilst the solution of the online data is driven also by diurnal variability.

However, there are some limitations to the developed offline-AMS method which have been highlighted during the discussion. One of these is the lack of nitrogen species in the NHOA mass profile. The quantification and detection of nitrogen species using HR-TOF-AMS is often considered uncertain, although some studies have shown it is possible (Bottenus et al., 2018; Docherty et al., 2011). This is because nitrogen-containing species are often

situated on the tail-end of large neighbouring peaks in the mass spectrum. Therefore, there is already uncertainty involved with measuring N-containing species. However, it is also likely the offline-AMS method does not recover some N-containing species.

There is also a lack of oxygen-containing PAHs in the offline-AMS profiles, which were previously shown to be key peaks in the mass spectra of some PMF factors (Cash et al., 2021). This suggests that some complex and highly insoluble species are not recovered by the offline-AMS method.

4.5.3. The presence of open waste burning

In 2015 and 2016, there were complete bans on open waste and crop-residue burning (Table 4.1), but to what extent these bans have been enforced effectively is uncertain when reviewing literature (Gulia et al., 2018). The general decrease in burning-related OA from 2015 to 2018 could suggest that the bans are having an effect. However, the composition of both SFOA2 and SVBBOA show a substantial amount of their mass originates from municipal waste burning. This suggests that open burning still occurs and it is clear that further mitigation strategies are needed to reduce municipal waste burning PM more effectively, as well as burning as part of industrial processes such as the processing of electronic waste.

4.5.4. The decline in coal combustion

In order to meet the electricity demands of one of the largest populations in the world, India has a large number of coal-fired thermal power stations and a significant percentage of its electricity is generated from these stations (~60%) (Yang and Urpelainen, 2019). Two coal-fired power stations are situated within the national capital territory (NCT) of Delhi: the Rajghat thermal power station (~8 km east) and the Badarpur thermal power station (~20 km southeast).

As discussed in the previous section, the CCOA factor shows a decline in concentrations across the three years (Figure 4.10b). This coincides with the

gradual decrease in popularity of coal being used as a fuel due to public knowledge of air quality issues and government-based decisions to shut down power stations. This can be seen more clearly in the annual wind directional data in Figure 4.16. There is a larger spread of peaks in concentration during 2011 when compared to 2015 and 2018, suggesting a greater number of sources of CCOA were active during 2011. The high peaks in concentrations during 2011 originate from the direction of the two thermal power stations (east and southeast). There are also high concentrations in south westerly winds. This implicates the large industrial areas (~5 km, Mayapuri industrial areas: phase 1 and 2) in this direction which likely relied on coal-combustion for power or industrial-use. High concentrations also originate from the west and northwest which is mostly residential areas and small businesses (~3 km, Kirti Nagar). In these areas coal is used as a fuel for cooking and heating which shows contributions of domestic coal combustion. Domestic coal combustion from cooking using tandoor stoves has previously been shown to be a moderate contributor to $PM_{2.5}$ (Gulia et al., 2018). Modelling of $PM_{2.5}$ emissions sources shows that a ban on coal-fired tandoors in hotels and restaurants could reduce $PM_{2.5}$ concentrations by up to 9% (Gulia et al., 2018).

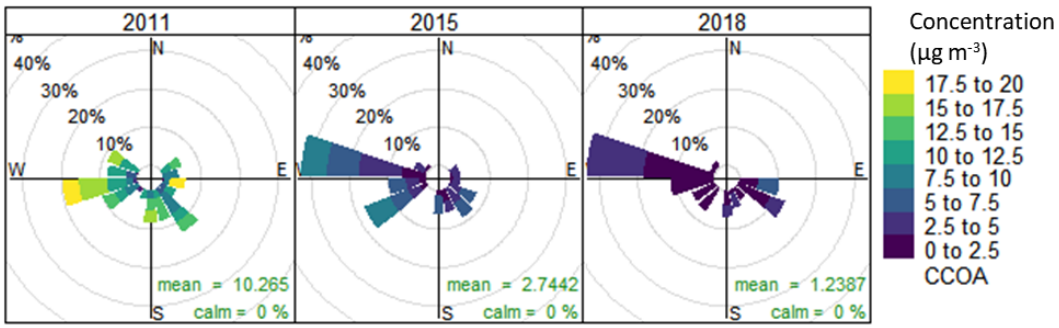

Figure 4.16. Pollution roses for coal-combustion organic aerosol (CCOA) during 2011, 2015 and 2018. The wind vectors are sized to represent the percentage contribution to the mean concentration. The wind vectors are divided into concentration bins described in the legends.

Moving from 2011 to 2015, the contributions of CCOA from the east began to lessen in 2015 and this could mark the gradual decline in use of the Rajghat thermal power station which was eventually shut down in October 2015. The contributions from the west are still the largest but this also decreases in intensity which suggests the domestic use of coal has declined. This coincides with the predicted increase in popularity of electricity, liquid petroleum gas or natural gas being used for heating and cooking in residential homes and small businesses (Negi and Kumar, 2019). There are still large peaks in concentration from the southwest. This suggests that the industrial use of coal is still a high contributor to CCOA in 2015. Although only small contributions are seen from the southeast, however, it is likely that the Badarpur thermal power station still contributes a significant amount to areas of Delhi.

A similar trend is seen when comparing 2015 to 2018, as there is a decrease in the contribution of CCOA from all wind sectors. There are still contributions of CCOA originating from the southeast, however, the shutdown of the Badarpur thermal power station in October 2018 likely means CCOA emissions from this wind sector will be minimal in future years. The west is the largest contributing wind sector for 2018 which suggests coal-combustion still occurs in households and small businesses.

From the wind sector analysis, it is therefore likely that the two power stations had a large influence over CCOA concentrations, particularly during 2011. This combined with the general decrease in use of coal in industry, small businesses, and residential homes, has caused a significant decrease in CCOA. Using the annual averages from 2018 to 2011, there is an 87% decrease in CCOA which results in a predicted 17% decrease in total PM_{10} OA. The decision to shut down the two thermal power stations is therefore shown to be a successful air quality mitigation strategy that effectively reduced the concentrations of PM_{10} from coal-combustion. It is likely that concentrations of CCOA are, however, higher in residential and industrial areas as coal-combustion is still an ongoing practice in homes and businesses.

Further reductions could therefore be seen through the widespread use of electrical appliances for cooking and other non-emitting methods of generating electricity for industry.

The government have recently implemented periodic bans on coal and wood burning for cooking food in restaurants and eateries (Goyal et al., 2019; Jonidi Jafari et al., 2021). It would therefore be beneficial for future studies to investigate the change in PM_{10} due to these measures.

4.5.5. The increase in diesel-related PM concentrations and the efficacy of HGV restrictions

Diesel emissions have previously been compared to CNG and petrol emissions, and are shown to be the largest contributor to PM concentrations in Delhi (Goel and Guttikunda, 2015; Singh et al., 2020). The majority of the traffic PM tailpipe emissions originate from diesel-engine HGVs, despite them being lower in numbers when compared to cars, two-wheelers and three-wheelers (Singh et al., 2018). There is also a moderate contribution from diesel-generator sets which are used by homes and businesses when there are electricity power cuts (Gulia et al., 2018) which tend to be more commonly used during pre-monsoon and monsoon when electricity supplies come under pressure by air conditioning and heavy rain events.

As discussed, the composition of NHOA suggests it is related to diesel-engine emissions. NHOA concentrations are larger than HOA during the post-monsoon and winter, whereas, during the other seasons NHOA is generally of similar or lower concentration. This could be explained by HGV restrictions (7:00 a.m. to 10:00 p.m.) occurring when there is a low PBL height during the winter and post-monsoon (Figure 4.15), thereby amplifying the concentrations. This phenomenon was observed in 2018 when PM_1 concentrations in Delhi were strongly influenced by the low PBL height (Cash et al., 2021). The same study showed strong peaks in the diurnal concentrations of NHOA during the late evening and early morning (Cash et al., 2021). The PBL height was also

lower during the 2018 post-monsoon when compared to 2011 and 2015 (Figure 4.15). This likely further accentuated the concentrations and, as a result, NHOA concentrations are particularly high during this period (Figure 4.14).

Thus, despite the restrictions already in place, there appears to be scope to reduce Delhi's PM concentrations by further targeting diesel emissions. They currently allow for HGVs, the highest emitting vehicle type, to enter the city at a time with unfavourable meteorology. Therefore, if the priority of the HGV restrictions is to reduce PM concentrations (but possibly not exposure), it is likely beneficial to change the restrictions to allow HGVs to enter during the middle of the day, when the PBL is high. However, this does not consider traffic congestion. It would therefore be beneficial for future studies to focus on the change in PM concentrations when HGVs enter the city during the middle of the day, while incorporating the effects of PBL height and traffic flow and people movement.

4.6. Conclusions

This study aimed to use an offline-AMS method to analyse filter samples collected over the years of 2011, 2015 and 2018 at the National Physics Laboratory in Delhi to assess temporal changes in source contributions to Delhi's organic aerosol (OA) in particular and thus particulate matter (PM) in general. For this purpose, a high-throughput offline-AMS method was developed that could measure PM filter archives spanning multiple years, and to extract a high proportion of the primary organic aerosol (POA) fraction. This was achieved through using a solvent mix of 1:1 acetone to water for extraction. Results show that the organic background concentrations were minimal (~1% of the measured signal), and the method gave high recoveries of total OA (95.4 ± 8.3 %) extracted from filters.

The offline-AMS method was used to analyse filter samples collected in 2011, 2015 and 2018 at the National Physics Laboratory in Delhi. Source apportionment analysis was performed on the organic fraction using Positive Matrix Factorisation (PMF). A total of nine factors were resolved which can be grouped into four primary source categories of OA: cooking, traffic, coal-combustion and other burning-related (solid fuel or open waste burning), as well as secondary OA contributions from regional burning and other sources. These results were compared with online-AMS measurements taken during the post-monsoon of 2018 at another location in Delhi. The majority of the compositional traits of PMF factors were resolved in the offline-AMS measurements, for example municipal waste burning tracers and polyaromatic hydrocarbon (PAH) content. The seasonal averages of factors derived from the filter archive also show similar trends despite different measurement sites being used. Therefore, the offline-AMS results accurately show the evolution of PMF sources across multiple years in Delhi. However, future work is required to estimate factor-specific OA recoveries to fully quantify PMF source factors. However, the overall OA recovery is high in this study, therefore, it is unlikely that the absence of factor recoveries will introduce major uncertainty in the measurement.

Annual PM_{10} OA concentrations were the highest during the winter, pre-monsoon and monsoon of 2015. However, peak concentrations were measured during the post-monsoon of 2018 which was consistent with a particularly low planetary boundary layer (PBL) that season. The seasonal analysis of total OA shows, from highest to lowest, the average concentrations are in the order of post-monsoon, winter, pre-monsoon and monsoon.

Burning sources were the largest contributor to OA during the winter and post-monsoon. This is when PM_{10} concentrations are at their highest, therefore, burning-related OA is likely a significant contributor to acute PM-related health effects in Delhi. In 2018, there was also a 47% decrease in burning related OA concentrations which may indicate the peak concentrations were reached in

2015. This could, in part, be due to the 2015 ban on open waste burning and the 2016 ban on crop-residue burning, suggesting, that this mitigation strategy has had some beneficial effect on PM_{10} concentrations. However, compositional analysis of burning-related factors implies a substantial contribution from municipal waste burning which provides evidence that open waste burning is still occurring. This therefore suggests that additional mitigation strategies have the potential to reduce burning related PM concentrations further, such as improved municipal waste collection and more control over small industrial processes.

There is a gradual decline in annual OA measurements from coal-combustion sources which is linked to the shutdown of the Rajghat thermal power station in 2015 and the Badarpur thermal power station in 2018. This mitigation strategy, combined with initiatives to decrease the popularity of coal use in businesses, industry, and residential homes, proved to be effective in reducing OA from coal-combustion sources as there was an 87% decrease. This resulted in a predicted 17% decrease in total PM_{10} OA.

The rapid increase in Delhi's population and registered vehicles coincides with only moderate increases in traffic-related OA concentrations. This is most likely due to tailpipe emission standards causing manufacturers to cut back on vehicle emissions. Therefore, this suggests the introduction of ever more stringent Bharat stage emissions standards has helped to largely counter-balance the increase in vehicle numbers to help control PM_{10} concentrations.

There was a strong increase in OA originating from diesel emissions during the winter and post-monsoon periods over the time-frame covered by the data (2011-2018). This may be a side-effect of an air pollution mitigation strategy which restricts heavy goods vehicles (HGV) entering the city during the daytime (7:00 a.m. – 10:00 p.m.). The restrictions cause a large influx of high PM emitting HGVs into the city at a time when the PBL is particularly low, which causes PM_{10} concentrations to be accentuated. It is suggested that changing the HGV restriction times to allow access in the middle of the day might be

beneficial to reduce PM_{10} concentrations. However, further studies are required to evaluate the resultant effect on congestion and human exposure.

Acknowledgements

This work was supported by UK NERC project DelhiFlux under the Newton Bhabha Fund programme Air Pollution and Human Health in a Developing Megacities (APHH-India), NERC reference numbers NE/P016502/1 and NE/P016472/1. This work was also supported by the Earth System Science Organization, Ministry of Earth Sciences, Government of India, under the Indo-UK joint collaboration grant no. MoES/16/19/2017-APHH (DelhiFlux). A NERC E3 DTP studentship supported James M. Cash (NE/L002558/1). The NERC National Capability award SUNRISE (NE/R000131/1) also supported these measurements. We thank the director of CSIR-National Physical Laboratory for allowing us to carry out this research.

References

Acharja, P., Ali, K., Trivedi, D. K., Safai, P. D., Ghude, S., Prabhakaran, T. and Rajeevan, M.: Characterization of atmospheric trace gases and water soluble inorganic chemical ions of PM1 and PM2.5 at Indira Gandhi International Airport, New Delhi during 2017–18 winter, Sci. Total Environ., 729, 138800, doi:10.1016/j.scitotenv.2020.138800, 2020.

Allan, J. D., Jimenez, J. L., Williams, P. I., Alfarra, M. R., Bower, K. N., Jayne, J. T., Coe, H. and Worsnop, D. R.: Quantitative sampling using an Aerodyne aerosol mass spectrometer 1. Techniques of data interpretation and error analysis, J. Geophys. Res. Atmos., 108(D3), doi:10.1029/2002JD002358, 2003.

Banoo, R., Sharma, S. K., Gadi, R., Gupta, S. and Mandal, T. K.: Seasonal Variation of Carbonaceous Species of PM10 Over Urban Sites of National Capital Region of India, Aerosol Sci. Eng., 4(2), 111–123, doi:10.1007/s41810-020-00058-2, 2020.

Bottenus, C. L. H., Massoli, P., Sueper, D., Canagaratna, M. R., VanderSchelden, G., Jobson, B. T. and VanReken, T. M.: Identification of amines in wintertime ambient particulate material using high resolution aerosol mass spectrometry, Atmos. Environ., 180, 173–183, doi:10.1016/j.atmosenv.2018.01.044, 2018.

Bozzetti, C., Sosedova, Y., Xiao, M., Daellenbach, K. R., Ulevicius, V., Dudoitis, V., Mordas, G., Byčenkienė, S., Plauškaitė, K., Vlachou, A., Golly, B., Chazeau, B., Besombes, J.-L., Baltensperger, U., Jaffrezo, J.-L., Slowik, J. G., El Haddad, I. and Prévôt, A. S. H.: Argon offline-AMS source apportionment of organic aerosol over yearly cycles for an urban, rural, and marine site in northern Europe, Atmos. Chem. Phys., 17(1), 117–141, doi:10.5194/acp-17-117-2017, 2017.

Canagaratna, M. R., Jayne, J. T., Jimenez, J. L., Allan, J. D., Alfarra, M. R., Zhang, Q., Onasch, T. B., Drewnick, F., Coe, H., Middlebrook, A., Delia, A., Williams, L. R., Trimborn, A. M., Northway, M. J., DeCarlo, P. F., Kolb, C. E., Davidovits, P. and Worsnop, D. R.: Chemical and microphysical characterization of ambient aerosols with the aerodyne aerosol mass spectrometer, Mass Spectrom. Rev., 26(2), 185–222, doi:10.1002/mas.20115, 2007.

Cash, J. M., Langford, B., Di Marco, C., Mullinger, N. J., Allan, J., Reyes-Villegas, E., Joshi, R., Heal, M. R., Acton, W. J. F., Hewitt, C. N., Misztal, P. K., Drysdale, W., Mandal, T. K., Gadi, R., Gurjar, B. R. and Nemitz, E.: Seasonal analysis of submicron aerosol in Old Delhi using high-resolution aerosol mass spectrometry: chemical characterisation, source apportionment

and new marker identification, Atmos. Chem. Phys., 21(13), 10133–10158, doi:10.5194/acp-21-10133-2021, 2021.

Chen, Q., Ikemori, F., Higo, H., Asakawa, D. and Mochida, M.: Chemical Structural Characteristics of HULIS and Other Fractionated Organic Matter in Urban Aerosols: Results from Mass Spectral and FT-IR Analysis, Environ. Sci. Technol., 4(50), 1721–1730, doi:10.1021/acs.est.5b05277, 2016.

Chow, J. C., Watson, J. G., Chen, L. W. A., Arnott, W. P., Moosmüller, H. and Fung, K.: Equivalence of elemental carbon by thermal/optical reflectance and transmittance with different temperature protocols, Environ. Sci. Technol., 38(16), 4414–4422, doi:10.1021/es034936u, 2004.

Chowdhury, S., Dey, S., Tripathi, S. N., Beig, G., Mishra, A. K. and Sharma, S.: “Traffic intervention” policy fails to mitigate air pollution in megacity Delhi, Environ. Sci. Policy, 74, 8–13, doi:10.1016/j.envsci.2017.04.018, 2017.

Crippa, M., El Haddad, I., Slowik, J. G., Decarlo, P. F., Mohr, C., Heringa, M. F., Chirico, R., Marchand, N., Sciare, J., Baltensperger, U. and Prévôt, A. S. H.: Identification of marine and continental aerosol sources in Paris using high resolution aerosol mass spectrometry, J. Geophys. Res. Atmos., 118(4), 1950–1963, doi:10.1002/jgrd.50151, 2013.

Daellenbach, K. R., Bozzetti, C., Křepelová, A., Canonaco, F., Wolf, R., Zotter, P., Fermo, P., Crippa, M., Slowik, J. G., Sosedova, Y., Zhang, Y., Huang, R., Poulain, L., Szidat, S., Baltensperger, U., El Haddad, I., H Prévôt, A. S., To, C. and H Prévôt andreprevot, A. S.: Characterization and source apportionment of organic aerosol using offline aerosol mass spectrometry, Atmos. Meas. Tech, 9(1), 8599–8644, doi:10.5194/amt-9-23-2016, 2016.

Daellenbach, K. R., Stefenelli, G., Bozzetti, C., Vlachou, A., Fermo, P., Gonzalez, R., Piazzalunga, A., Colombi, C., Canonaco, F., Hueglin, C., Kasper-Giebl, A., Jaffrezo, J.-L., Bianchi, F., Slowik, J. G., Baltensperger, U.,

El Haddad, I. and Prévôt, A. S. H.: Long-term chemical analysis and organic aerosol source apportionment at 9 sites in Central Europe: Source identification and uncertainty assessment, Atmos. Chem. Phys. Discuss., 17(21), 13265–13282, doi:10.5194/acp-2017-124, 2017.

DeCarlo, P. F., Kimmel, J. R., Trimborn, A., Northway, M. J., Jayne, J. T., Aiken, A. C., Gonin, M., Fuhrer, K., Horvath, T., Docherty, K. S., Worsnop, D. R. and Jimenez, J. L.: Field-Deployable, High-Resolution, Time-of-Flight Aerosol Mass Spectrometer, Anal. Chem., 78(24), 8281–8289, doi:10.1021/ac061249n, 2006.

Denier van der Gon, H. A. C., Hulskotte, J. H. J., Visschedijk, A. J. H. and Schaap, M.: A revised estimate of copper emissions from road transport in UNECE-Europe and its impact on predicted copper concentrations, Atmos. Environ., 41(38), 8697–8710, doi:10.1016/j.atmosenv.2007.07.033, 2007.

Docherty, K. S., Aiken, A. C., Huffman, J. A., Ulbrich, I. M., Decarlo, P. F., Sueper, D., Worsnop, D. R., Snyder, D. C., Peltier, R. E., Weber, R. J., Grover, B. D., Eatough, D. J., Williams, B. J., Goldstein, A. H., Ziemann, P. J. and Jimenez, J. L.: The 2005 Study of Organic Aerosols at Riverside (SOAR-1): Instrumental intercomparisons and fine particle composition, Atmos. Chem. Phys., 11(23), 12387–12420, doi:10.5194/acp-11-12387-2011, 2011.

Duplissy, J., De Carlo, P. F., Dommen, J., Alfarra, M. R., Metzger, A., Barmpadimos, I., Prevot, A. S. H., Weingartner, E., Tritscher, T., Gysel, M., Aiken, A. C., Jimenez, J. L., Canagaratna, M. R., Worsnop, D. R., Collins, D. R., Tomlinson, J. and Baltensperger, U.: Relating hygroscopicity and composition of organic aerosol particulate matter, Atmos. Chem. Phys., 11(3), 1155–1165, doi:10.5194/acp-11-1155-2011, 2011.

Ge, X., Setyan, A., Sun, Y. and Zhang, Q.: Primary and secondary organic aerosols in Fresno, California during wintertime: Results from high resolution

aerosol mass spectrometry, J. Geophys. Res. Atmos., 117(D19301), doi:10.1029/2012JD018026, 2012.

Ge, X., Li, L., Chen, Y., Chen, H., Wu, D., Wang, J., Xie, X., Ge, S., Ye, Z., Xu, J. and Chen, M.: Aerosol characteristics and sources in Yangzhou, China resolved by offline aerosol mass spectrometry and other techniques, Environ. Pollut., 225, 74–85, doi:10.1016/j.envpol.2017.03.044, 2017.

Goel, R. and Guttikunda, S. K.: Evolution of on-road vehicle exhaust emissions in Delhi, Atmos. Environ., 105, 78–90, doi:10.1016/j.atmosenv.2015.01.045, 2015.

Gohlke, R. S. and McLafferty, F. W.: Mass Spectrometric Analysis: Aliphatic Amines, Anal. Chem., 34(10), 1281–1287, doi:10.1021/ac60190a025, 1962.

Goyal, P., Gulia, S., Goyal, S. K. and Kumar, R.: Assessment of the effectiveness of policy interventions for Air Quality Control Regions in Delhi city, Environ. Sci. Pollut. Res., 26(30), 30967–30979, doi:10.1007/s11356-019-06236-1, 2019.

Gulia, S., Mittal, A. and Khare, M.: Quantitative evaluation of source interventions for urban air quality improvement - A case study of Delhi city, Atmos. Pollut. Res., 9(3), 577–583, doi:10.1016/j.apr.2017.12.003, 2018.

Gulia, S., Shukla, N., Padhi, L., Bosu, P., Goyal, S. K. and Kumar, R.: Evolution of air pollution management policies and related research in India, Environ. Challenges, 6, 100431, doi:10.1016/j.envc.2021.100431, 2022.

Han, Y., Kawamura, K., Chen, Q. and Mochida, M.: Formation of high-molecular-weight compounds via the heterogeneous reactions of gaseous C8-C10n-aldehydes in the presence of atmospheric aerosol components, Atmos. Environ., 126, 290–297, doi:10.1016/j.atmosenv.2015.11.050, 2016.

Harrison, R. M., Allan, J., Carruthers, D., Heal, M. R., Lewis, A. C., Marner, B., Murrells, T. and Williams, A.: Non-exhaust vehicle emissions of particulate matter and VOC from road traffic: A review, Atmos. Environ., 262, 118592, doi:https://doi.org/10.1016/j.atmosenv.2021.118592, 2021.

He, L. Y., Lin, Y., Huang, X. F., Guo, S., Xue, L., Su, Q., Hu, M., Luan, S. J. and Zhang, Y. H.: Characterization of high-resolution aerosol mass spectra of primary organic aerosol emissions from Chinese cooking and biomass burning, Atmos. Chem. Phys., 10(23), 11535–11543, doi:10.5194/acp-10-11535-2010, 2010.

He, L. Y., Huang, X. F., Xue, L., Hu, M., Lin, Y., Zheng, J., Zhang, R. and Zhang, Y. H.: Submicron aerosol analysis and organic source apportionment in an urban atmosphere in Pearl River Delta of China using high-resolution aerosol mass spectrometry, J. Geophys. Res. Atmos., 116(12), 1–15, doi:10.1029/2010JD014566, 2011.

Herring, C. L., Faiola, C. L., Massoli, P., Sueper, D., Erickson, M. H., McDonald, J. D., Simpson, C. D., Yost, M. G., Jobson, B. T. and Van Reken, T. M.: New Methodology for Quantifying Polycyclic Aromatic Hydrocarbons (PAHs) Using High-Resolution Aerosol Mass Spectrometry, Aerosol Sci. Technol., 49(11), 1131–1148, doi:10.1080/02786826.2015.1101050, 2015.

Huang, X. F., He, L. Y., Hu, M., Canagaratna, M. R., Sun, Y., Zhang, Q., Zhu, T., Xue, L., Zeng, L. W., Liu, X. G., Zhang, Y. H., Jayne, J. T., Ng, N. L. and Worsnop, D. R.: Highly time-resolved chemical characterization of atmospheric submicron particles during 2008 Beijing Olympic games using an aerodyne high-resolution aerosol mass spectrometer, Atmos. Chem. Phys., 10(18), 8933–8945, doi:10.5194/acp-10-8933-2010, 2010.

Hunt, A. L. and Petrucci, G. A.: Analysis of ultrafine and organic particles by aerosol mass spectrometry, TrAC - Trends Anal. Chem., 21(2), 74–81, doi:10.1016/S0165-9936(01)00138-8, 2002.

Jain, S., Sharma, S. K., Vijayan, N. and Mandal, T. K.: Seasonal characteristics of aerosols (PM2.5 and PM10) and their source apportionment using PMF: A four year study over Delhi, India, Environ. Pollut., 262, 114337, doi:10.1016/j.envpol.2020.114337, 2020.

Jayarathne, T., Stockwell, C. E., Gilbert, A. A., Daugherty, K., Cochrane, M. A., Ryan, K. C., Putra, E. I., Saharjo, B. H., Nurhayati, A. D., Albar, I., Yokelson, R. J. and Stone, E. A.: Chemical characterization of fine particulate matter emitted by peat fires in Central Kalimantan, Indonesia, during the 2015 El Niño, Atmos. Chem. Phys., 18(4), 2585–2600, doi:10.5194/acp-18-2585-2018, 2018a.

Jayarathne, T., Stockwell, C. E., Bhave, P. V, Praveen, P. S., Rathnayake, C. M., Islam, M. R., Panday, A. K., Adhikari, S., Maharjan, R., Goetz, J. D., DeCarlo, P. F., Saikawa, E., Yokelson, R. J. and Stone, E. A.: Nepal Ambient Monitoring and Source Testing Experiment (NAMaSTE): emissions of particulate matter from wood- and dung-fueled cooking fires, garbage and crop residue burning, brick kilns, and other sources, Atmos. Chem. Phys., 18(3), 2259–2286, doi:10.5194/acp-18-2259-2018, 2018b.

Jonidi Jafari, A., Charkhloo, E. and Pasalari, H.: Urban air pollution control policies and strategies: a systematic review, J. Environ. Heal. Sci. Eng., 19(2), 1911–1940, doi:10.1007/s40201-021-00744-4, 2021.

Kathuria, V.: Vehicular Pollution Control in Delhi: Impact of Compressed Natural Gas, Econ. Polit. Wkly., 40(18), 1907–1916 [online] Available from: https://www.jstor.org/stable/4416578, 2005.

Keene, W. C., Lobert, J. M., Crutzen, P. J., Maben, J. R., Scharffe, D. H., Landmann, T., Hély, C. and Brain, C.: Emissions of major gaseous and particulate species during experimental burns of southern African biomass, J. Geophys. Res. Atmos., 111(4), doi:10.1029/2005JD006319, 2006.

Krelling, C. and Badami, M. G.: Cost-effectiveness analysis of compressed natural gas implementation in the public bus transit fleet in Delhi, India, Transp. Policy, 115(August 2020), 49–61, doi:10.1016/j.tranpol.2021.10.019, 2022.

Kwon, H. C. and Kwon, J. H.: Measuring aqueous solubility in the presence of small cosolvent volume fractions by passive dosing, Environ. Sci. Technol., 46(22), 12550–12556, doi:10.1021/es3035363, 2012.

Li, Y.-C., Shu, M., Ho, S. S. H., Wang, C., Cao, J.-J., Wang, G.-H., Wang, X.-X., Wang, K. and Zhao, X.-Q.: Characteristics of PM2.5 emitted from different cooking activities in China, Atmos. Res., 166, 83–91, doi:10.1016/j.atmosres.2015.06.010, 2015.

Lin, C., Ceburnis, D., Huang, R. J., Xu, W., Spohn, T., Martin, D., Buckley, P., Wenger, J., Hellebust, S., Rinaldi, M., Cristina Facchini, M., O'Dowd, C. and Ovadnevaite, J.: Wintertime aerosol dominated by solid-fuel-burning emissions across Ireland: Insight into the spatial and chemical variation in submicron aerosol, Atmos. Chem. Phys., 19(22), 14091–14106, doi:10.5194/acp-19-14091-2019, 2019.

Long, B. and Yang, Z.: Measurements of the solubilties of m-phthalic acid in acetone, ethanol and acetic ether, Fluid Phase Equilib., 266(1–2), 38–41, doi:10.1016/j.fluid.2008.01.014, 2008.

Long, B. W., Wang, L. S. and Wu, J. S.: Solubilities of 1,3-benzenedicarboxylic acid in water + acetic acid solutions, J. Chem. Eng. Data, 50(1), 136–137, doi:10.1021/je049784c, 2005.

Lü, Y., Shi, J. J. and Sun, L.: Investigation of the selection of extraction solvent for extracting the n-alkane from diesel by means of solubility parameters theory, J. Fuel Chem. Technol., 36(3), 297–301, doi:10.1016/S1872-5813(08)60022-5, 2008.

McLafferty, F. W.: Interpretation of Mass Spectra, pp. 25–34, University Science Books., 1993.

Mihara, T. and Mochida, M.: Characterization of solvent-extractable organics in urban aerosols based on mass spectrum analysis and hygroscopic growth measurement, Environ. Sci. Technol., 45(21), 9168–9174, doi:10.1021/es201271w, 2011.

Mlyano, Y. and Hayduk, W.: Solubility of Butane in Several Polar and Nonpolar Solvents and in an Acetone-Butanol Solvent Solution, J. Chem. Eng. Data, 31(1), 77–80, doi:10.1021/je00043a022, 1986.

Mohr, C., DeCarlo, P. F., Heringa, M. F., Chirico, R., Slowik, J. G., Richter, R., Reche, C., Alastuey, A., Querol, X., Seco, R., Peñuelas, J., Jiménez, J. L., Crippa, M., Zimmermann, R., Baltensperger, U. and Prévôt, A. S. H.: Identification and quantification of organic aerosol from cooking and other sources in Barcelona using aerosol mass spectrometer data, Atmos. Chem. Phys., 12(4), 1649–1665, doi:10.5194/acp-12-1649-2012, 2012.

Montes, C., Sapkota, T. and Singh, B.: Seasonal patterns in rice and wheat residue burning and surface PM2.5 concentration in northern India, Atmos. Environ. X, 13, 100154, doi:10.1016/j.aeaoa.2022.100154, 2022.

Morris, K. R., Abramowitz, R., Pinal, R., Davis, P. and Yalkowsky, S. H.: Solubility of aromatic pollutants in mixed solvents, Chemosphere, 17(2), 285–298, doi:https://doi.org/10.1016/0045-6535(88)90221-4, 1988.

Nakoudi, K., Giannakaki, E., Dandou, A., Tombrou, M. and Komppula, M.: Planetary Boundary Layer variability over New Delhi, India, during EUCAARI project, Atmos. Meas. Tech. Discuss., 1–33, doi:10.5194/amt-2018-342, 2018.

Negi, A. and Kumar, A.: Long-term Electricity Demand Scenarios for India: Implications of Energy Efficiency, 2018 Int. Conf. Power Energy, Environ.

Intell. Control. PEEIC 2018, (August), 462–467, doi:10.1109/PEEIC.2018.8665452, 2019.

Paatero, P.: The Multilinear Engine—A Table-Driven, Least Squares Program for Solving Multilinear Problems, Including the n-Way Parallel Factor Analysis Model, J. Comput. Graph. Stat., 8(4), 854–888, doi:10.1080/10618600.1999.10474853, 1999.

Paatero, P. and Hopke, P. K.: Discarding or downweighting high-noise variables in factor analytic models, Anal. Chim. Acta, 490(1–2), 277–289, doi:10.1016/S0003-2670(02)01643-4, 2003.

Paatero, P. and Tapper, U.: Positive matrix factorization: A non-negative factor model with optimal utilization of error estimates of data values, Environmetrics, 5(2), 111–126, doi:10.1002/env.3170050203, 1994.

Pandey, A., Brauer, M., Cropper, M. L., Balakrishnan, K., Mathur, P., Dey, S., Turkgulu, B., Kumar, G. A., Khare, M., Beig, G., Gupta, T., Krishnankutty, R. P., Causey, K., Cohen, A. J., Bhargava, S., Aggarwal, A. N., Agrawal, A., Awasthi, S., Bennitt, F., Bhagwat, S., Bhanumati, P., Burkart, K., Chakma, J. K., Chiles, T. C., Chowdhury, S., Christopher, D. J., Dey, S., Fisher, S., Fraumeni, B., Fuller, R., Ghoshal, A. G., Golechha, M. J., Gupta, P. C., Gupta, R., Gupta, R., Gupta, S., Guttikunda, S., Hanrahan, D., Harikrishnan, S., Jeemon, P., Joshi, T. K., Kant, R., Kant, S., Kaur, T., Koul, P. A., Kumar, P., Kumar, R., Larson, S. L., Lodha, R., Madhipatla, K. K., Mahesh, P. A., Malhotra, R., Managi, S., Martin, K., Mathai, M., Mathew, J. L., Mehrotra, R., Mohan, B. V. M., Mohan, V., Mukhopadhyay, S., Mutreja, P., Naik, N., Nair, S., Pandian, J. D., Pant, P., Perianayagam, A., Prabhakaran, D., Prabhakaran, P., Rath, G. K., Ravi, S., Roy, A., Sabde, Y. D., Salvi, S., Sambandam, S., Sharma, B., Sharma, M., Sharma, S., Sharma, R. S., Shrivastava, A., Singh, S., Singh, V., Smith, R., Stanaway, J. D., Taghian, G., Tandon, N., Thakur, J. S., Thomas, N. J., Toteja, G. S., Varghese, C. M., Venkataraman, C., Venugopal, K. N., Walker, K. D., Watson, A. Y., Wozniak, S., Xavier, D.,

Yadama, G. N., Yadav, G., Shukla, D. K., Bekedam, H. J., et al.: Health and economic impact of air pollution in the states of India: the Global Burden of Disease Study 2019, Lancet Planet. Heal., 5(1), e25–e38, doi:https://doi.org/10.1016/S2542-5196(20)30298-9, 2021.

Pervez, S., Verma, M., Tiwari, S., Chakrabarty, R. K., Watson, J. G., Chow, J. C., Panicker, A. S., Deb, M. K., Siddiqui, M. N. and Pervez, Y. F.: Household solid fuel burning emission characterization and activity levels in India, Sci. Total Environ., 654, 493–504, doi:10.1016/j.scitotenv.2018.11.019, 2019.

Pieber, S. M., El Haddad, I., Slowik, J. G., Canagaratna, M. R., Jayne, J. T., Platt, S. M., Bozzetti, C., Daellenbach, K. R., Fröhlich, R., Vlachou, A., Klein, F., Dommen, J., Miljevic, B., Jiménez, J. L., Worsnop, D. R., Baltensperger, U. and Prévôt, A. S. H.: Inorganic Salt Interference on CO2+ in Aerodyne AMS and ACSM Organic Aerosol Composition Studies, Environ. Sci. Technol., 50(19), 10494–10503, doi:10.1021/acs.est.6b01035, 2016.

Reizer, M. and Juda-Rezler, K.: Explaining the high PM10 concentrations observed in Polish urban areas, Air Qual. Atmos. Heal., 9(5), 517–531, doi:10.1007/s11869-015-0358-z, 2016.

Reyes-Villegas, E., Panda, U., Darbyshire, E., Cash, J. M., Joshi, R., Langford, B., Di Marco, C. F., Mullinger, N. J., Alam, M. S., Crilley, L. R., Rooney, D. J., Acton, W. J. F., Drysdale, W., Nemitz, E., Flynn, M., Voliotis, A., McFiggans, G., Coe, H., Lee, J., Hewitt, C. N., Heal, M. R., Gunthe, S. S., Mandal, T. K., Gurjar, B. R., Shivani, Gadi, R., Singh, S., Soni, V. and Allan, J. D.: PM1 composition and source apportionment at two sites in Delhi, India, across multiple seasons, Atmos. Chem. Phys., 21(15), 11655–11667, doi:10.5194/acp-21-11655-2021, 2021.

Saarikoski, S., Timonen, H., Saarnio, K., Aurela, M., Järvi, L., Keronen, P., Kerminen, V.-M. and Hillamo, R.: Sources of organic carbon in fine particulate

matter in northern European urban air, Atmos. Chem. Phys., 8, 6281–6295, 2008.

Schurman, M. I., Lee, T., Sun, Y., Schichtel, B. A., Kreidenweis, S. M. and Collett, J. L.: Investigating types and sources of organic aerosol in Rocky Mountain National Park using aerosol mass spectrometry, Atmos. Chem. Phys., 15(2), 737–752, doi:10.5194/acp-15-737-2015, 2015.

Sharma, S. K., Mandal, T. K., Saxena, M., Rashmi, Rohtash, Sharma, A. and Gautam, R.: Source apportionment of PM10 by using positive matrix factorization at an urban site of Delhi, India, Urban Clim., 10, 656–670, doi:10.1016/j.uclim.2013.11.002, 2014.

Sharma, S. K., Mandal, T. K., Sharma, A., Saraswati and Jain, S.: Seasonal and annual trends of carbonaceous species of PM10 over a megacity Delhi, India during 2010--2017, J. Atmos. Chem., 75(3), 305–318, doi:10.1007/s10874-018-9379-y, 2018.

Sharma, S. K., Banoo, R. and Mandal, T. K.: Seasonal characteristics and sources of carbonaceous components and elements of PM10 (2010–2019) in Delhi, India, J. Atmos. Chem., 78(4), 251–270, doi:10.1007/s10874-021-09424-x, 2021.

Sindhwani, R. and Goyal, P.: Assessment of traffic-generated gaseous and particulate matter emissions and trends over Delhi (2000-2010), Atmos. Pollut. Res., 5(3), 438–446, doi:10.5094/APR.2014.051, 2014.

Singh, D. P., Gadi, R. and Mandal, T. K.: Emissions of polycyclic aromatic hydrocarbons in the atmosphere: An indian perspective, Hum. Ecol. Risk Assess., 16(5), 1145–1168, doi:10.1080/10807039.2010.512258, 2010.

Singh, V., Sahu, S. K., Kesarkar, A. P. and Biswal, A.: Estimation of high resolution emissions from road transport sector in a megacity Delhi, Urban Clim., 26, 109–120, doi:10.1016/j.uclim.2018.08.011, 2018.

Singh, V., Biswal, A., Kesarkar, A. P., Mor, S. and Ravindra, K.: High resolution vehicular PM10 emissions over megacity Delhi: Relative contributions of exhaust and non-exhaust sources, Sci. Total Environ., 699, 134273, doi:10.1016/j.scitotenv.2019.134273, 2020.

Stewart, G. J., Acton, W. J. F., Nelson, B. S., Vaughan, A. R., Hopkins, J. R., Arya, R., Mondal, A., Jangirh, R., Ahlawat, S., Yadav, L., Sharma, S. K., Dunmore, R. E., Yunus, S. S. M., Nicholas Hewitt, C., Nemitz, E., Mullinger, N., Gadi, R., Sahu, L. K., Tripathi, N., Rickard, A. R., Lee, J. D., Mandal, T. K. and Hamilton, J. F.: Emissions of non-methane volatile organic compounds from combustion of domestic fuels in Delhi, India, Atmos. Chem. Phys., 21(4), 2383–2406, doi:10.5194/acp-21-2383-2021, 2021.

Sun, F., Littlejohn, D. and David Gibson, M.: Ultrasonication extraction and solid phase extraction clean-up for determination of US EPA 16 priority pollutant polycyclic aromatic hydrocarbons in soils by reversed-phase liquid chromatography with ultraviolet absorption detection, Anal. Chim. Acta, 364(1–3), 1–11, doi:10.1016/S0003-2670(98)00186-X, 1998.

Sun, Y., Zhang, Q., Zheng, M., Ding, X., Edgerton, E. S. and Wang, X.: Characterization and Source Apportionment of Water-Soluble Organic Matter in Atmospheric Fine Particles (PM2.5) with High-Resolution Aerosol Mass Spectrometry and GC–MS, Environ. Sci. Technol., 45(11), 4854–4861, doi:10.1021/es200162h, 2011a.

Sun, Y., Du, W., Fu, P., Wang, Q., Li, J., Ge, X., Zhang, Q., Zhu, C., Ren, L., Xu, W., Zhao, J., Han, T., Worsnop, D. R. and Wang, Z.: Primary and secondary aerosols in Beijing in winter: Sources, variations and processes,

Atmos. Chem. Phys., 16(13), 8309–8329, doi:10.5194/acp-16-8309-2016, 2016.

Sun, Y. L., Zhang, Q., Schwab, J. J., Demerjian, K. L., Chen, W. N., Bae, M. S., Hung, H. M., Hogrefe, O., Frank, B., Rattigan, O. V. and Lin, Y. C.: Characterization of the sources and processes of organic and inorganic aerosols in New York city with a high-resolution time-of-flight aerosol mass apectrometer, Atmos. Chem. Phys., 11(4), 1581–1602, doi:10.5194/acp-11-1581-2011, 2011b.

Ulbrich, I. M., Canagaratna, M. R., Zhang, Q., Worsnop, D. R. and Jimenez, J. L.: Interpretation of organic components from Positive Matrix Factorization of aerosol mass spectrometric data, Atmos. Chem. Phys., 9(9), 2891–2918, doi:10.5194/acp-9-2891-2009, 2009.

Wang, L., Slowik, J. G., Tripathi, N., Bhattu, D., Rai, P., Kumar, V., Vats, P., Satish, R., Baltensperger, U., Ganguly, D., Rastogi, N., Sahu, L. K., Tripathi, S. N. and Prévôt, A. S. H.: Source characterization of volatile organic compounds measured by proton-transfer-reaction time-of-flight mass spectrometers in Delhi, India, Atmos. Chem. Phys., 20(16), 9753–9770, doi:10.5194/acp-20-9753-2020, 2020.

Xu, J., Shi, J., Zhang, Q., Ge, X., Canonaco, F., Prévôt, A. S. H., Vonwiller, M., Szidat, S., Ge, J., Ma, J., An, Y., Kang, S. and Qin, D.: Wintertime organic and inorganic aerosols in Lanzhou, China: Sources, processes, and comparison with the results during summer, Atmos. Chem. Phys., 16(23), 14937–14957, doi:10.5194/acp-16-14937-2016, 2016.

Yang, J. and Urpelainen, J.: The future of India’s coal-fired power generation capacity, J. Clean. Prod., 226, 904–912, doi:10.1016/j.jclepro.2019.04.074, 2019.

Ye, Z., Liu, J., Gu, A., Feng, F., Liu, Y., Bi, C., Xu, J., Li, L., Chen, H., Chen, Y., Dai, L., Zhou, Q. and Ge, X.: Chemical characterization of fine particulate matter in Changzhou, China, and source apportionment with offline aerosol mass spectrometry, Atmos. Chem. Phys., 17(4), 2573–2592, doi:10.5194/acp-17-2573-2017, 2017.

Zhu, Q., He, L. Y., Huang, X. F., Cao, L. M., Gong, Z. H., Wang, C., Zhuang, X. and Hu, M.: Atmospheric aerosol compositions and sources at two national background sites in northern and southern China, Atmos. Chem. Phys., 16(15), 10283–10297, doi:10.5194/acp-16-10283-2016, 2016.

Chapter 5

Conclusions and recommendations for future work

This chapter gives a brief overview of the main conclusions and findings for the work carried out in this thesis and formulates some recommendations for further studies. The reader is directed to the conclusions section of each chapter for a more comprehensive interpretation. The focus here is on the synthesis and comparison of the outcomes generated from each chapter in order to assess potential overlaps and develop a more comprehensive picture of the atmospheric composition and sources of VOCs and PM_1 in Delhi. The knowledge from the comparison for the year of overlap (2018) is then carried through to the offline-AMS dataset to help describe the changes in PM_{10} over multiple years in Delhi. Suggestions are also made to direct future studies so as to better understand the atmospheric implications of these findings. Because some of the main aims of this thesis involved the development of novel methods to measure PM and VOCs, there is also a discussion on the advantages and disadvantages of the developed methods, along with suggestions for improvements and further development.

5.1. Synthesising conclusions

5.1.1. New methods of measuring PM and VOCs

This thesis presents novel methods for measuring atmospheric PM and VOCs. For the first time, bi-directional fluxes of VOC PMF factors were presented which show the presence of PMF factor deposition fluxes, despite an observed overall net emission. Previously, source apportionment of fluxes using PMF was limited by the requirement of non-negative input matrices and deposition

fluxes were therefore ignored. This would also have impacted the interpretation of the positive fluxes as these may in reality have been the net result of negative and positive component fluxes associated with different factors. The method described in Chapter 3 negates this issue by first performing PMF analysis on the 30-minute average concentrations associated with the upward and the downward movements of the air separately. Once a solution is found, a numerical simulation of the true-eddy accumulation (TEA) approach is used to calculate the fluxes of each factor. This paves the way for future studies to generate both factor emission and deposition fluxes, therefore providing greater understanding of possible sources and sinks of VOCs and a more robust interpretation of the results. Additionally, the emissions factors generated using the TEA flux source apportionment method can be used in future emission-based modelling studies, leading to more accurate predictions.

This thesis also presents a comparison of eddy covariance (EC) and TEA derived meteorological fluxes. The results showed the half-hourly averages of the two approaches gave close to numerically identical fluxes for all measured ions. It was also shown that the loss of flux due to the TEA source apportionment method was minimal (0.38%) and equated to the unfitted mass remaining in the residuals after PMF analysis. In comparison to previous studies, this is a significant improvement in reducing flux losses. Most of the uncertainty therefore lies within the choice of PMF solution, or the inherent limitations associated with PTR-MS measurements. A key example of this uncertainty is the low sensitivities of the PTR-MS to alkanes. This likely led to underestimation of total VOC emission in the VOC PMF traffic factor.

Another aim of this thesis was to develop an offline-AMS method to analyse filter samples collected over multiple years in Delhi. One of the main issues for the method to handle was the large concentrations of POA in Delhi, which is highly water insoluble. This meant a novel high-throughput method had to be developed that could extract a high percentage of POA, based on a 1:1

acetone-water solvent mix. The method achieved high extraction recoveries of OA with minimal background concentrations due to acetone solvent.

When comparing the offline-AMS data with online-AMS measurements taken during a similar time period in Delhi, the majority of the compositional traits within PMF factors were retained, even for low concentration species such as polyaromatic hydrocarbons. Therefore, this method has clear advantages for the high-throughput analysis of PM filters collected in POA-rich atmospheres such as Delhi. However, the method requires further development for fully quantitative measurements of PM PMF factors. Water-extraction studies use previously determined PMF factor-specific recoveries. The disadvantage of the acetone-water extraction method is that factor-specific recoveries do not exist, so future work is required to determine these recoveries. However, since overall recovery is high, this likely does not introduce a major uncertainty in the measurement.

5.1.2. Comparisons and similarities of real-time measurements of PM and VOCs in Old Delhi

Co-located measurements of PM_1 and VOCs were conducted during 2018 at the Indira Gandhi Delhi Technical University for Women (IGDTUW) in Old Delhi. The PM_1 measurements covered three seasons of pre-monsoon, monsoon and post-monsoon, while the VOC measurements covered just the post-monsoon period. The concentrations of PM_1 were found to be highest during the post-monsoon. PM_1 sulphate was the highest inorganic species during the pre-monsoon and monsoon but this changed to nitrate during the post-monsoon. The inorganic PM_1 chloride showed a significant increase (522%) in concentration in the post-monsoon compared with its pre-monsoon concentrations.

An overview of the concentrations of PM_1 OA PMF factors is presented in **Figure 5.1**, along with the concentrations and fluxes of VOC PMF factors.

These two datasets are the most comparable as the measurements were taken at the same location and during the post-monsoon period of 2018.

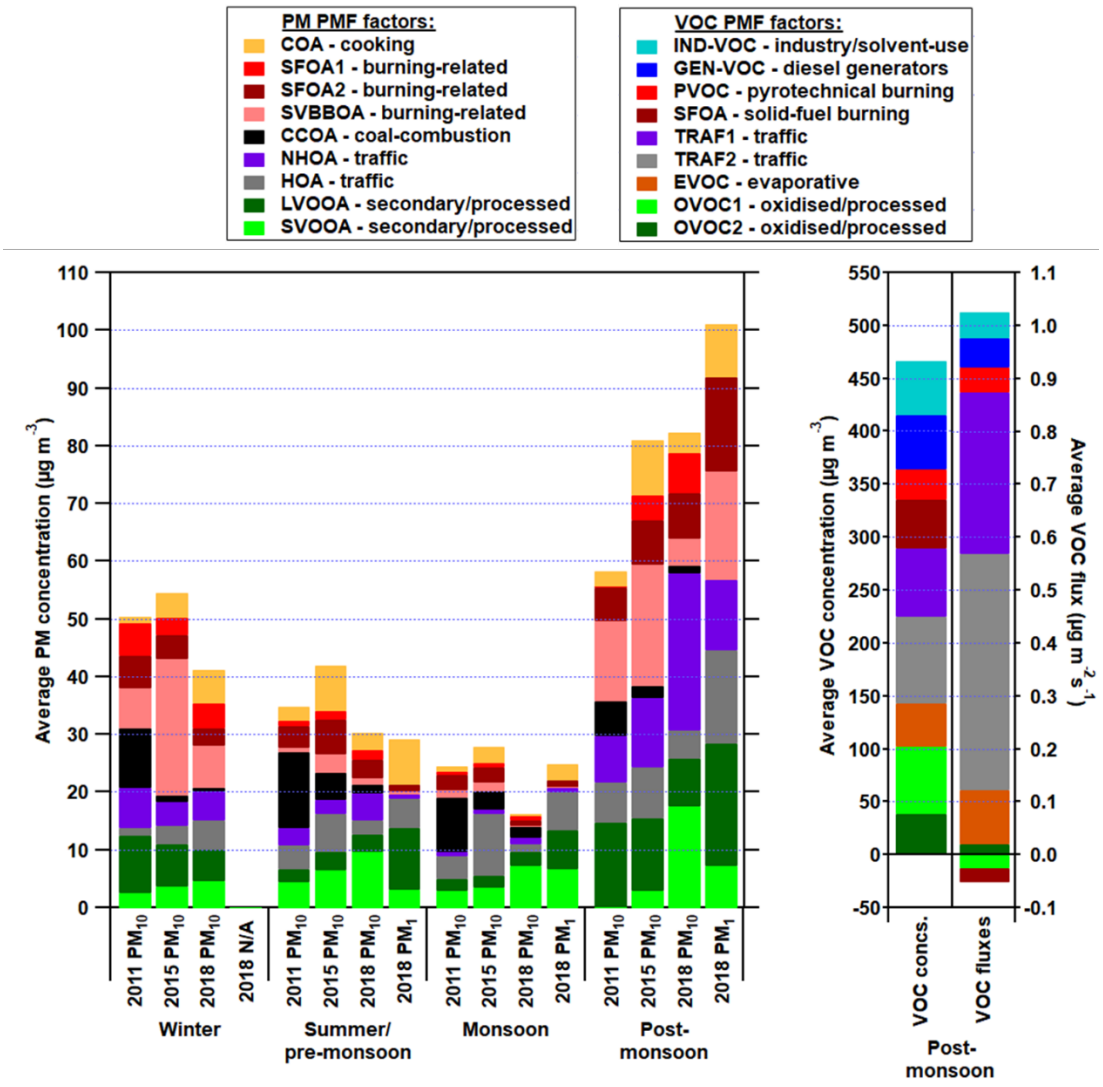

Figure 5.1. Summary chart showing the PMF factor results of the organic compounds in aerosol and gas phase from the three main data chapters in this thesis: the PM_1 online-AMS OA PMF factor concentrations measured during the pre-monsoon, monsoon and post-monsoon of 2018, the VOC PMF factor concentrations and fluxes measured during the post-monsoon of 2018, and the PM_{10} offline-AMS OA PMF factor concentrations measured during all seasons of 2011, 2015 and 2018.

The PM_1 OA traffic factors displayed the highest concentrations of POA during the pre-monsoon and monsoon periods, while during the post-monsoon they were second to the burning-related factors. Therefore, traffic is a significant source of PM_1 OA. Traffic VOC factors were even more dominant in concentrations and were by far the highest source of VOC emissions. The implications of this are exemplified by estimates of the OH reactivity and photochemical ozone creation potential (POCP) of the factors which suggest that traffic VOCs are the greatest source of OH radical loss and have the greatest potential to form ozone.

An emphasis was placed on the high-resolution aspect of the online-HR-TOF-AMS and PTR-QiTOF-MS measurements taken in Old Delhi. This provided in-depth compositional detail and high temporal resolution of PMF factors. As a result, the PMF analyses separated the two datasets into two factors relating to different vehicle fuel-types. The HOA PM_1 factor and the TRAF2 VOC factor both showed compositions that suggested most of their mass was due to emissions from petrol or compressed natural gas (CNG) engines, whilst the composition of NHOA PM_1 and TRAF1 VOC factors suggested the mass of these two factors were due to diesel emissions. The diesel-related factors also appeared to separate based on the temporal activity of heavy good vehicles (HGVs). In Delhi, there are restrictions on HGVs entering the city during the daytime (7:00 a.m. – 10:00 p.m.), which allowed a large influx of highly emitting diesel HGVs to enter during the night and early mornings. The diurnal profile of TRAF1 emission fluxes was showed a clear drop during the day and a peak in the late evening, whereas TRAF2 peaked during the middle of the day. The entry of HGVs is also when the planetary boundary layer (PBL) is at its lowest, which accentuates concentrations. This further supports the findings that the HGV restrictions may be causing an increase in pollutant concentrations, rather than a reduction. However, the impact could be different in terms of human exposure, as more people are outside during the day. The net impact depends on the location of the residential areas with respect to the night-time

diesel traffic as well as the exchange of indoor and outdoor air in relation to building design and ventilation.

The two real-time datasets also showed similarities in burning sources. The PM_1 SFOA factor and the SFVOC factor gave compositions that point towards consistent sources of solid-fuel burning. The most obvious is the burning of cellulose-containing materials, such as wood. There is also evidence of a substantial mass of OA and VOCs being produced from municipal waste burning, the products of which are particularly toxic, and some are carcinogenic (e.g. polychlorinated dibenzodioxins). The SFOA and SFVOC factors also displayed similar diurnal concentration profiles, as their time series were highly correlated. The profiles displayed peaks in concentration during the mornings and evenings which was linked to residents clearing the streets by burning piles of municipal waste. Municipal waste burning was therefore shown to be a significant source of burning-related OA and VOCs. It was also shown to be linked to the high concentrations of PM_1 chloride as the combustion of common plastics, such as polyvinyl chloride (PVC), are known to emit chloride PM. Overall, the concentration results show burning-related sources are a significant source of PM_1 primary and secondary OA as well as VOCs.

There were also differences in the burning-related sources of OA and VOCs. The VOC measurements were made over a shorter time-period and, as a result, the PMF model was able to separate a VOC burning factor, PVOC, which relates to the pyrotechnics associated with the Diwali festival. This source was most likely wrapped into the SFOA factor of the OA measurements as pyrotechnics are known to emit OA as well. However, SVBBOA was only separated in the OA measurements and is linked to the regional transport of OA originating from crop-residue burning. This is expected as VOCs emitted from crop-residue burning would have likely been scavenged as the atmospheric lifetimes of VOCs are shorter than OA, although SVBBOA is likely formed through the atmospheric processing of both primary OA and VOCs (i.e.

through photochemistry in the aerosol and gas phase). SVBBOA also increases significantly during the post-monsoon period which is timed with the rice paddy harvest in October. Another PM_1 species that shows significant increases during the post-monsoon is chloride. From the evidence collected, it was therefore suggested that crop-residue burning is another possible source of the high PM_1 chloride concentrations.

5.1.3. The changes in PM over the last decade and the efficacy of past air quality mitigation strategies

The knowledge gained from the real-time measurements of PM and VOCs was then applied to the offline-AMS dataset in order to identify and contextualise the compositional origins of the PM_{10} OA PMF factors. PM_{10} filter samples were collected during the years of 2011, 2015 and 2018 at the National Physics Laboratory in New Delhi. In comparison to IGDTUW, NPL is in an area which is less densely packed by buildings, people and roads. Instead, it is closer to large industrial areas, green parks and forests. It is also next to agricultural fields which are managed by the Indian Agriculture Research Institute. This would explain why the concentrations of PM_{10} OA at NPL were generally lower than the PM_1 OA measured at IGDTUW despite the difference in size cut-off going the other way. It is well established that secondary organic (and inorganic) PM resides in the accumulation mode which predominantly resides in the PM_1 fraction, whilst primary OA from combustion sources is even smaller. Thus for paired samples, PM_{10} concentrations would not expect to greatly exceed PM_1 concentrations for OA.

The concentration results of PM_{10} OA PMF factors are also summarised in **Figure 5.1** alongside the real-time measurements. The highest PM_{10} OA concentrations were seen during the winter, pre-monsoon, and monsoon of 2015. Throughout all years measured, the post-monsoon gave the highest concentrations, with peak PM_{10} OA concentrations seen in the 2018 post-monsoon period, consistent with a particularly low planetary boundary layer (PBL).

In general, the largest contribution to PM_{10} OA during the winter and post-monsoon was from burning factors (except for the 2018 post-monsoon). There was also a significant decrease (47%) in burning factors going from 2015 to 2018. This could be due to the 2015 and 2016 bans on open waste and stubble burning, which suggests the bans may have caused some reductions in PM_{10} OA. However, the high concentrations of SFOA1 and SFOA2 in 2018 suggest that localised burning still occurs, such as the burning of municipal waste and dung-cakes. Additional mitigation strategies are therefore required to reduce burning sources further. The real-time measurements suggest that large concentrations of OA and VOCs are due to residents burning municipal waste to clean the streets. Therefore, an improvement in municipal waste collection may have the potential to reduce burning-related PM and VOC concentrations.

One air quality mitigation strategy that has proven to be effective is the shutdown of Delhi's two coal-fired thermal power stations. This was evident from the annual decreases in the 'coal-combustion' CCOA factor, which is a PMF factor that had strong links to the two thermal power stations. In 2018, CCOA was reduced by 87% which equates to a 17% decrease in total PM_{10} OA since 2011. The CCOA factor was not resolved in the real-time AMS or VOC measurements in 2018, suggesting the components of CCOA were likely bound within other source factors, such as those associated with SFOA. This therefore supports the findings that coal-combustion is no longer a dominant source of pollutants in Delhi.

Large increases in Delhi's population over the last decade has led to increases in registered vehicles. The effects of this are not seen in the PM_{10} OA concentrations which only showed a moderate increase in annual traffic factors (NHOA and HOA). This suggests that the Bharat stage emissions standards have counter-balanced the otherwise expected increase in tailpipe emissions. However, the previously mentioned HGV restrictions are suggested to accentuate concentrations of PM and VOCs. The real-time measurements showed that NHOA was strongly linked to diesel HGVs and that HOA

represented the daytime vehicle fleet which is mostly fuelled by petrol and CNG. From **Figure 5.1**, the contribution of NHOA was consistently higher than HOA during the winter and post-monsoon. This shows that new measures should be targeted towards emissions from diesel engines and, specifically, from HGVs. Considering the possible accentuation of diesel emissions by the low PBL at night, it may therefore be beneficial to change the timing of HGV restrictions. One example could be to allow HGVs to enter during the day when the PBL is high and atmospheric dispersion is at its greatest. However, further studies are required to estimate the efficacy of this change on pollutant concentrations and exposure.

5.2. Recommendation for future work

5.2.1. Improvements and further method development

This thesis demonstrates the ability to calculate bi-directional VOC PMF factor fluxes, although it does not develop an approach to calculate an associated uncertainty for each factor flux. As discussed, one of the main sources of error involved in using the TEA approach is the inherent uncertainty in PTR-MS measurements. One of the largest uncertainties in PTR-MS measurements is often due to the change in sensitivity of the instrument caused by changes in relative humidity. This occurs mostly due to the creation of water clusters, $H_3O^+(H_2O)$ and the two contaminant ions, NO^+ and O_2^+. These ions cause charge-transfer, or clustering, of analyte VOCs which makes mass spectral interpretation harder due to changes in the fragmentation pattern. A method described by Millet et al. (2018) involves using the internal standard of diiodobenzene ($C_6H_4I_2$), which is now used in most modern PTR-MS instruments and is fed into the instrument at a constant rate. The large mass defect and high internal concentration (relative to its mass) of diiodobenzene means interference from other fragmenting species is unlikely. The diiodobenzene standard therefore provides a constant signal with which to assess whether effects due to humidity generate spurious fluxes. Millet et al.

(2018) calculate the exchange velocity of diiodobenzene and use this as a flux detection limit. The same could be applied to the EC-derived diiodobenzene fluxes within this thesis and a flux detection limit could be determined according to which factor fluxes could be filtered. However, if the mass of diiodobenzene were to be left in the input PMF matrix, this could act as a constant for the determination of individual factor-specific flux errors. Future work could therefore apply this technique of error determination to VOC PMF factor fluxes.

The POCP estimates for VOC PMF factors is shown to be uncertain when compared to previous studies. This is particularly the case for factors with high monoterpene compositions, such as the traffic factors, which are shown to contribute 60% to monoterpene concentrations and 78% to localised fluxes of monoterpenes. Therefore, it would be beneficial if the method for estimating POCP under local conditions could be improved. The current method relies on using maximum incremental reactivity (MIR) weighting parameters; however, there is potential uncertainty in these estimates due to the conditions under which the MIR scale was modelled. An improvement would be to conduct ozone production modelling under the atmospheric conditions found in Delhi, as in the study by Nelson et al. (2021). They used measured concentrations of VOCs, NO, NO_2, HONO, CO, SO_2, O_3 and photolysis rates at IGDTUW to constrain the Master Chemical Mechanism (MCM). This resulted in a set of local ozone production rates for VOC species. These estimates could be used as weighting parameters to estimate more accurate flux- and concentration-weighted POCPs for PMF factors and, unlike general model products, do not rely on the emissions inventory being correct, and on simplified and/or lumped chemistry schemes.

Further development could also be applied to the offline-AMS method because, currently, PMF factor-specific recovery factors do not exist for the 1:1 acetone-water solvent extraction. Determining these recoveries would allow for complete quantification of OA that is compositionally comparable to

online-AMS measurements. Multiple methods could be used to determine factor-specific recoveries. One way is to use the sulphate normalisation method described in Chapter 4. This describes using online-AMS measurements taken in the same location, and during the same time period, as the collection of PM_1 or $PM_{2.5}$ filter samples. However, the work in Chapter 4 described recoveries much higher than 1 when the method was used on filters collected in Delhi. It was found that high concentrations of metal species on the filter could have caused refractory sulphate salts to form after nebulisation. Therefore, the sulphate normalisation method can only be conducted on filter samples that have low metal concentrations. It is also worth noting that a recent study by Acharja et al. (2020) has shown that $PM_{2.5}$ sulphate concentrations were higher than PM_1 sulphate concentrations in Delhi. Therefore, sampling filters using a PM_1 inlet will likely be required for more accurate recoveries. AMS sampling with the standard (PM_1) lens and the more recently developed $PM_{2.5}$ lens (Peck et al., 2016; Xu et al., 2017) would also provide useful insights into the size distribution of both sulphate and OA.

Another method could use OC analysers, such as an OC/EC Sunset Analyser, to give an online or offline total organic carbon (TOC) measurement. The premise of this determination would be to use a similar equation to that described for water-extraction in Daellenbach et al. (2016) and which requires co-located online-AMS measurements:

$$R_{i,k} = R_{i,bulk} \times \frac{off_{i,k}}{on_{i,k}} \quad (5.1)$$

Here, $R_{i,k}$ is the time-dependent factor-specific recovery for factor, k, and the time index is i; while $off_{i,k}$ and $on_{i,k}$ are the time-dependent factor percentage contributions to the overall solution determined through offline-AMS and online-AMS, respectively. The bulk recovery of total OA, $R_{i,bulk}$, could be determined using OC analysis. The median of $R_{i,k}$ for each factor can then be determined and used to scale each factor to ambient concentrations.

5.2.2. Future studies

The second largest VOC-emitting PMF factor measured at IGDTUW was the surface evaporative emissions factor, EVOC. This factor was shown to have a composition indicative of both asphalt evaporative emissions and biogenic emissions. It was also found that EVOC emissions are likely controlled by light and surface temperature, which is consistent with its source origins. The measurements were taken during the post-monsoon which is one of the colder and darker periods of the year. However, the increase in temperature and light during the pre-monsoon may cause EVOC emissions to become more significant. The implications of this are that EVOC may be a significant contributor of OH reactivity and POCP as it is composed of highly reactive compounds such as isoprene and monoterpenes. It would therefore be beneficial to return to IGDTUW and take PTR-MS micrometeorological flux measurements during the warmer and lighter periods of the year, such as the pre-monsoon season.

Elemental analysis of the PM measurements showed high nitrogen content within some PMF factors. Nitrile species were proposed to be responsible for the high nitrogen content within NHOA, whilst N-rich solid fuel burning was suggested to be the cause of the high nitrogen composition of the PM_{10} OA factor, SFOA1. The HR-TOF-AMS is limited in its ability to measure individual N-containing organic compounds due to overlapping peaks within the mass spectrum. It would therefore be beneficial to take measurements using a long-TOF-AMS which would allow for higher resolution chemical analysis (~8000 $m/\Delta m$). This would help to give more detail on the compositional differences between NHOA and HOA. It would also help to better resolve the N-content within factors such as SVBBOA and SFOA1.

The AMS, along with the PTR-QiTOF-MS, is also limited in its volatility range as this thesis does not present measurements of volatile compounds that exist between PM and VOCs. There are low- and semi-volatile organic compounds (LVOCs and SVOCs), which are mostly in the gas phase, and extremely low

volatility organic compounds (ELVOCs), which are mostly in the particle-phase. Being able to measure these species would further the understand of PM formation and the atmospheric processing of VOCs in Delhi. This can be achieved through real-time measurements of LVOCs/SVOCs using a PTR3-TOF or using a Vocus PTR-TOF (Riva et al., 2019). The ELVOCs can be measured using chemical ionization TOF-MS (CI-TOF-MS) instruments such as an iodide chemical ionization time-of-flight mass spectrometer (TOF-CIMS) or a chemical ionization atmospheric pressure interface time-of-flight mass spectrometers (CI-APiTOF) with nitrate and amine reagent ion chemistries.

The work in this thesis has been conducted alongside several other studies that involve measurements taken at IGDTUW during the post-monsoon of 2018. Some of these studies are still being processed and prepared, which means further analyses can be conducted in future work. One such study uses the TEA flux source apportionment method on the unit mass resolution PM_1 measurements. The findings of this study will further our understanding of the surface exchange dynamics of PM_1 in Delhi. Comparisons can also be made with the VOC PMF factor fluxes calculated within this thesis to further our knowledge of the overlapping behaviours of VOCs and PM sources in Delhi. Other studies include the measured fluxes of NO_x, BC and CO taken during the same time period as the real-time measurements of PM_1 and VOCs (the post-monsoon of 2018). Further analysis of these measurements, alongside the VOC PMF factor flux measurements, could be used to compare with emissions inventories for Delhi, much like the study by Squires et al. (2020) conducted for measurements in Beijing. This could mean more accurate emissions inventories are calculated, therefore, leading to improved model predictions of atmospheric pollutants.

This work includes two contrasting measurement sites and, although they cover a wide range of pollutant sources, there could be other sources missed which were not within the proximity of the measurement site. Pollutant concentrations and fluxes are also likely to change when comparing one area

of the city to another. Therefore, it would be beneficial to replicate these studies at different measurement sites and increase the number of years measured. This would mean the results would be more representative of the whole city and a greater weight could be placed on reviewing air quality mitigation strategies.

A final remark is aimed towards the proposed changes to HGV restrictions and the implementation of an improved waste management system in Delhi. These changes are untested and further studies are required to assess whether they would lead to reductions in atmospheric PM and VOCs. The movement of HGV restrictions to the middle of the day to increase dispersion of diesel emitted PM and VOCs, will likely cause increases in congestion. Therefore, future modelling studies combining modelling of traffic flow, atmospheric transport and chemistry, as well as exposure could investigate the proposed changes and estimate its effects on congestion and human exposure. Similarly, modelling studies can also assess the potential reductions in PM and VOCs due to a decrease in municipal waste burning. This will help to determine whether an improved waste management system in Delhi would lead to reduced air pollutant concentrations.

References

Acharja, P., Ali, K., Trivedi, D. K., Safai, P. D., Ghude, S., Prabhakaran, T. and Rajeevan, M.: Characterization of atmospheric trace gases and water soluble inorganic chemical ions of PM1 and PM2.5 at Indira Gandhi International Airport, New Delhi during 2017–18 winter, Sci. Total Environ., 729, 138800, doi:10.1016/j.scitotenv.2020.138800, 2020.

Daellenbach, K. R., Bozzetti, C., Křepelová, A., Canonaco, F., Wolf, R., Zotter, P., Fermo, P., Crippa, M., Slowik, J. G., Sosedova, Y., Zhang, Y., Huang, R., Poulain, L., Szidat, S., Baltensperger, U., El Haddad, I., H Prévôt, A. S., To, C.

and H Prévôt andreprevot, A. S.: Characterization and source apportionment of organic aerosol using offline aerosol mass spectrometry, Atmos. Meas. Tech, 9(1), 8599–8644, doi:10.5194/amt-9-23-2016, 2016.

Millet, D. B., Alwe, H. D., Chen, X., Deventer, M. J., Griffis, T. J., Holzinger, R., Bertman, S. B., Rickly, P. S., Stevens, P. S., Léonardis, T., Locoge, N., Dusanter, S., Tyndall, G. S., Alvarez, S. L., Erickson, M. H. and Flynn, J. H.: Bidirectional Ecosystem–Atmosphere Fluxes of Volatile Organic Compounds Across the Mass Spectrum: How Many Matter?, ACS Earth Sp. Chem., 2(8), 764–777, doi:10.1021/acsearthspacechem.8b00061, 2018.

Nelson, B. S., Stewart, G. J., Drysdale, W. S., Newland, M. J., Vaughan, A. R., Dunmore, R. E., Edwards, P. M., Lewis, A. C., Hamilton, J. F., Acton, W. J., Hewitt, C. N., Crilley, L. R., Alam, M. S., Åahin, Ü. A., Beddows, D. C. S., Bloss, W. J., Slater, E., Whalley, L. K., Heard, D. E., Cash, J. M., Langford, B., Nemitz, E., Sommariva, R., Cox, S., Shivani, Gadi, R., Gurjar, B. R., Hopkins, J. R., Rickard, A. R. and Lee, J. D.: In situ ozone production is highly sensitive to volatile organic compounds in Delhi, India, Atmos. Chem. Phys., 21(17), 13609–13630, doi:10.5194/acp-21-13609-2021, 2021.

Peck, J., Gonzalez, L. A., Williams, L. R., Xu, W., Croteau, P. L., Timko, M. T., Jayne, J. T., Worsnop, D. R., Miake-Lye, R. C. and Smith, K. A.: Development of an aerosol mass spectrometer lens system for PM2.5, Aerosol Sci. Technol., 50(8), 781–789, doi:10.1080/02786826.2016.1190444, 2016.

Riva, M., Rantala, P., Krechmer, E. J., Peräkylä, O., Zhang, Y., Heikkinen, L., Garmash, O., Yan, C., Kulmala, M., Worsnop, D. and Ehn, M.: Evaluating the performance of five different chemical ionization techniques for detecting gaseous oxygenated organic species, Atmos. Meas. Tech., 12(4), 2403–2421, doi:10.5194/amt-12-2403-2019, 2019.

Squires, F., Nemitz, E., Langford, B., Wild, O., Drysdale, W., Acton, W. J. F., Fu, P., Grimmond, C. S. B., Hamilton, J., Hewitt, C. N., Hollaway, M., Kotthaus,

S., Lee, J., Metzger, S., Pingintha-Durden, N., Shaw, M., Vaughan, A., Wang, X., Wu, R., Zhang, Q. and Zhang, Y.: Measurements of traffic dominated pollutant emissions in a Chinese megacity, Atmos. Chem. Phys., 1–33, doi:10.5194/acp-2019-1105, 2020.

Xu, W., Croteau, P., Williams, L., Canagaratna, M., Onasch, T., Cross, E., Zhang, X., Robinson, W., Worsnop, D. and Jayne, J.: Laboratory characterization of an aerosol chemical speciation monitor with PM2.5 measurement capability, Aerosol Sci. Technol., 51(1), 69–83, doi:10.1080/02786826.2016.1241859, 2017.

Appendix 1: Supplementary information for Chapter 2

This contains the supplementary information for Chapter 2: Seasonal analysis of submicron aerosol in Old Delhi using high resolution aerosol mass spectrometry: Chemical characterisation, source apportionment and new marker identification.

Supplement of Atmos. Chem. Phys., 21, 10133–10158, 2021, https://doi.org/10.5194/acp-21-10133-2021-supplement

Table S2.1. List of abbreviations

Abbreviations	
IGDTUW	**Indira Gandhi Delhi Technical University for Women**
HR-ToF-AMS	**High-resolution time-of-flight aerosol mass spectrometer**
PTR-QiTOF-MS	**High-resolution proton transfer reaction mass spectrometer**
PM_1	**Sub-micron particulate matter**
SOA	**Secondary organic aerosol**
VOC	**Volatile organic compound**
OrgNO	**Organic nitrogen oxide species**
BC	**Black carbon**
LWC	**Liquid water content**
PCDDs	**Polychlorinated dibenzodioxins**
PCDFs	**Polychlorinated dibenzofurans**
$\overline{OS_C}$	**Carbon oxidation state**
PMF	**Positive Matrix Factorisation**
COA	**Cooking organic aerosol**
NHOA	**Nitrogen-containing hydrocarbon-like organic aerosol**
SFOA	**Solid fuel organic aerosol**
HOA	**Hydrocarbon-like organic aerosol**
SVBBOA	**Semi-volatility biomass burning organic aerosol**
LVOOA	**Low-volatility oxygenated organic aerosol**
SVOOA	**Semi-volatility oxygenated organic aerosol**
PAH	**Polyaromatic hydrocarbons**
UnSubPAH	**Unsubstituted PAH**
MPAH	**Methyl-substituted PAH**
OPAH	**Oxidised PAH**
NOPAH	**Nitrogen-oxygen substituted PAH**
APAH	**Amino PAH**
VK	**Van Krevelen**

Table S2.2. Relative ionisation efficiencies (RIE), ionisation efficiencies (IE) and collection efficiencies (CE)

Season	IE	RIE NH_4^+	RIE SO_4^{2-}	RIE Cl^-	CE
Pre-monsoon	2.92E-07	4	1.45	2.07	0.5
Monsoon	2.92E-07	4	1.45	2.07	0.5
Post-monsoon preflux period (11/10/18 - 03/11/18)	2.89E-07	4	1.45	2.07	0.5
Post-monsoon Diwali period (05/11/18 - 14/11/18)	3.14E-07	4	1.45	1.05	0.8
Post-monsoon post-Diwali (14/11/18 - 23/11/18)	3.14E-07	4	1.45	1.05	0.5

S2.1. Method for determining the best Organic PMF solution

This section describes the method for obtaining the organic-only PMF solution and the flow chart in Figure S2.1 illustrates the separate steps to the analysis. The details of each step are described in detail below. Four main complications arose when analysing this dataset using PMF:

1. The solutions changed with different initialisation SEEDS.

And decisions had to be made about:

2. whether to conduct PMF analysis on the separate periods (Pre-Monsoon, Monsoon, Post-Monsoon) individually, or whether to combine all the periods into one single PMF analysis,
3. whether to use the full recorded mass spectrum for the analysis or to cut off the spectrum at <120 *m/z,*
4. On the number of factors PMF could distinguish.

PMF analysis was therefore conducted on the separate measurement periods (pre-monsoon, monsoon and post-monsoon) and on all the measurement periods combined. For each period, and the all-combined case, PMF was

conducted on separate organic matrices which excluded or included peaks >120 *m/z*. These analyses are respectively referred to as <120 *m/z* and >120 *m/z* in Figure S2.1. The rotational ambiguity of each solution was explored (-3 to 3, steps of 0.2) and consistently showed little variation with different FPEAKs. This led to all solutions being set to FPEAK = 0.

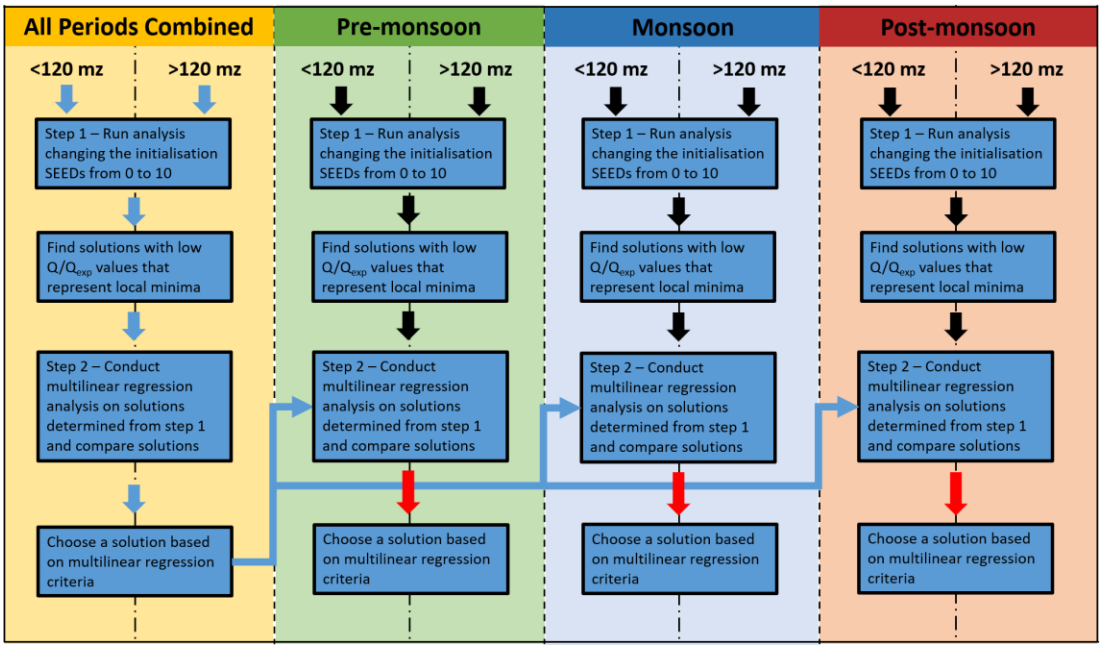

Figure S2.1. Flow chart to show the steps to finding a PMF solution. First the analysis was conducted on the all periods combined case and these solutions were then compared with the step 2 analysis of each period separately, as illustrated with the blue arrows. The solution which matched the multilinear regression criteria more closely was then chosen, as illustrated by the red arrows.

S2.1.1. Step 1 – choose Q/Q_{exp} local minima out of 0 to 10 initialisation SEEDS

Initialisation SEEDS were explored from 0 to 10 for each analysis and almost all the solutions showed variation when the initialisation SEED was altered. Due to the large number of solutions this created, solutions were chosen from each set of 0 to 10 SEEDS based on their Q/Q_{exp}. Chosen solutions showed

Q/Q_{exp} values that were clear local minima in the solution space. Exceptions were made for S0 solutions as these represent a baseline solution for comparison. Some additional solutions were also chosen based on their chemical resemblance to source factors. Other solutions were removed due to obvious factor splitting, following a procedure described in detail in the supplementary information of Allan et al. (2010). They were then taken to the next step where they were compared using multilinear regression analysis.

Variation in the number of factors was also explored for each analysis. A set of between 5-7 factors was found to best describe the measurements without obvious time-series splitting. However, solutions with less obvious splitting were not fully explored until after multilinear regression analysis as this removes bias due to the user's choice in the number of factors, one of the largest forms of error in use of the PMF algorithm (Ulbrich et al., 2009). The time series splitting was further explored post-regression analysis.

S2.1.2. Step 2 – Conduct multilinear regression analysis on solutions chosen from step 1

In order to reduce the subjectivity of choosing a solution, they were compared using multilinear regression analyses where the factors were combined to fit an external tracer, ET (Allan et al., 2010; Young et al., 2015; Reyes-Villegas et al., 2016):

$$ET = A + B(SFOA) + C(COA) + D(HOA) \quad \text{(S2.1)}$$

The three external tracers used here were the concentrations of NO_x, CO and BC measured at the same site (only BC was available for the Monsoon period). The coefficients are valuable ways of verifying the solution fit where A is an indication of the background concentration of the tracer. The other three coefficients, B, C and D, are gradients to the fit which show the contribution of each factor.

The strategy to choosing a solution from multilinear regression analysis involves a search for a compromise of characteristics which is summarised as follows.

Multilinear Regression Criteria:

1. A solution with a low chi-square value shows a higher correlation of its multilinear fit with the *ET*
2. The solution should contain factors which contribute more strongly to certain *ET*s. This includes:
    a. Strong contributions of HOA to NO_x above all other factors
    b. SFOA contribution close to or above zero for BC
    c. COA contribution close to or above zero for BC
3. An estimated background concentration which is near background levels for the *ET*
4. A low Q/Q_{exp}

The COA coefficient, C, has previously been expected to be near zero as cooking activities are not commonly associated with the production of NO_x or CO (Reyes-Villegas et al., 2016). It may however be possible that burning of organic material contributes to COA in Delhi. Cooking food over open fires is a major practice in the city which is likely to produce BC and means COA and BC are likely to correlate. It is also suggested that Q/Q_{exp} should only be compared between solutions from the same period as the length of dataset will likely strongly influence this value. Additionally, an increase in number of factors will lower Q/Q_{exp} due to an increase in degrees of freedom. These two influences were therefore considered when choosing a solution.

The graphs in Figure S2.2 to Figure S2.5 show the different solutions chosen in step 1 along the x axis. They have specific labels which are summarised in Table S2.3. An example of this is “6f_ac_<120mz_S0_C1”, where the ‘6f’ indicates it is a 6-factor solution, ‘S0’ indicates this is the solution found at SEED 0 and solutions with ‘<120mz’ in their name include ions up to 120 *m/z*.

Those with ‘ac’ in their name have been resolved from the all-combined analysis case (all periods analysed in one PMF analysis). If the solution does not include prefixes ‘ac’ or ‘<120mz’, they include ions up to 328 *m/z* and have not been resolved from the all-combined case. Solutions with ‘C1’ indicates a specific combination of factors used for the $SFOA$ variable in Eq. (S2.1). The $SFOA$ variable could be an SFOA factor time series alone (C1) or a combined time series of an SFOA and an SVBBOA factor (C2), if both were resolved in the solution. The SVBBOA factors had secondary characteristics and the SFOA factors were primary. As a result of this, they caused significantly different fit results when combined or separated. In order to remove any bias resulting from this, these combinations were explored at this stage rather than later.

Table S2.3. A description of labels used to define a solution

Label (Xf_ac_<120*m/z*_SX_CX)	**Description**
Xf, where X=1,2,3,n	The number of factors
ac	If present, this indicates it is resolved from the all-combined analysis case (all periods analysed in one PMF analysis). Otherwise, the solution is limited to a specific measurement period
<120mz	If present, this indicates the solution is limited to include ions up to *m/z* 120. Otherwise, ions up to *m/z* 385 are included
SX, where X=1,2,3,n	The SEED number
CX, where X=1,2,3,n	Indicates a specific combination of factors used for the $\boldsymbol{SFOA}$ variable in Eq. (S2.1) C1 an SFOA factor time series alone is used for the $\boldsymbol{SFOA}$ variable C2 a combined time series of an SFOA and an SVBBOA factor C3 a combined time series of two SFOA factors (for solutions that produce two SFOA factors)

The post-monsoon period analysis (Figure S2.5) also produce solutions with two SFOA factors. The two SFOA factors were therefore combined to give $SFOA$ (= SFOA1 + SFOA2) and these solutions are labelled ‘C3’.

The high signals seen at masses >120 *m/z* carry important information such as polyaromatic hydrocarbon (PAH) composition. Similar PMF analyses have been conducted where the solution fit was improved through the addition of masses up to 385 *m/z* (Aiken et al., 2009; Docherty et al., 2011; Sun et al., 2016; Zhang et al., 2018). In order to validate this, every possible solution obtained using a >120 *m/z* solution was compared to a <120 *m/z* solution.

The strategy to finding the final solution first involved finding the most robust solutions for the all-combined case to then compare with the period-specific analyses (Figure S2.1). Figure S2.2(a) shows the CO trilinear analyses for the all-combined case where COA consistently contributes negatively to the fit for all solutions. COA may therefore have little importance when considering a solution for the CO fit. The SFOA contribution has a large range between solutions and its significance is uncertain without prior knowledge. The chi-square value is therefore a better indication of the most accurate solution to fit CO. The two solutions with the lowest chi-square values are 7f_ac_S1_C1 and 7f_ac_S1_C2. For the NO_x analysis in Figure S2.2(b), There is a similar set of contributions for each factor and a consistently strong contribution of the traffic factor, HOA. The chi-square is again an important parameter for choosing the best solution. The same two solutions give the lowest values: 7f_ac_S1_C1 and 7f_ac_S1_C2.

In Figure S2.2(c), the contribution of factors to BC varies, with some solutions showing above or near zero COA contribution. Using the multilinear regression criteria described above, a number of solutions can therefore be chosen including: 7f_ac_<120mz_S0_C1, 7f_ac_<120mz_S0_C2, 7f_ac_<120mz_S1_C1, 7f_ac_<120mz_S1_C2, 7f_ac_S0_C1, 7f_ac_S1_C1, 7f_ac_S1_C2, 6f_ac_<120mz_S0_C1 and 6f_ac_<120mz_S0_C2. Considering that both 7f_ac_S1_C1 and 7f_ac_S1_C2 were the most robust in the NO_x and CO analyses as well, these solutions are likely the most robust solutions. However, each C1 solution has a lower chi-square value which suggests that the burning-related factors fit *ET*s

stronger when separated. 7f_ac_S1_C1 is therefore the chosen solution for the all-combined case.

In order to account for differences in composition between the three periods, seven of the solutions were taken from the all-combined case to compare with the separate period analyses. Five of the C1 solutions in the list above were used, along with the two solutions: 6f_ac_S0 and 6f_ac_S3, in order to add comparisons of 6f solutions with masses >120 *m*/*z*. The same method was then used to determine the most robust solution for the separate period analyses. The Monsoon period analysis includes only BC as an external tracer because measurements of other tracers were not available. The solution with the strongest fit to external tracers for the pre-monsoon (Figure S2.3) and monsoon periods (Figure S2.4) is the all-combined case solution, 7f_ac_S1_C1. In Figure S2.5, there are however two solutions for the post-monsoon (7f_ac_S1_C1 and 6f_<120mz_S0_C3) which are very similar in their trilinear analysis parameters and both are near equal in their fit to external tracers. As both are valid solutions, the chosen solution is 7f_ac_S1_C1 as it represents the primary factors well in the two other periods and it also maintains consistency in representing organic source factors for Old Delhi.

It should be noted that the calculation of a common PMF solution for the combined dataset was possible because no major interventions to the instrument were required during the measurements that could have caused a change in the relative sensitivities to the various ions, such as change of filaments, venting of the instrument, or major retuning of the mass spectrometer.

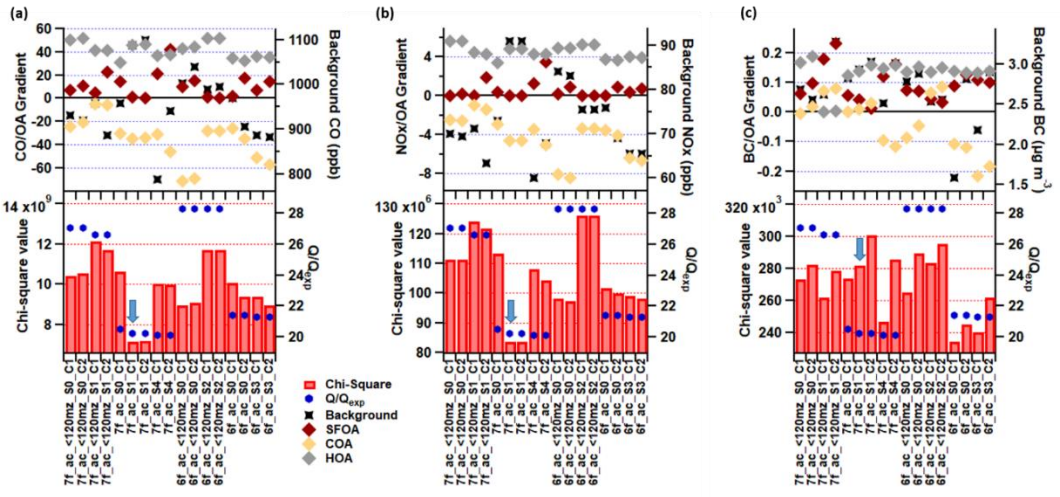

Figure S2.2. Trilinear regression analysis results for the PMF solutions taken from the all-periods-combined case. Results are shown for the fit using (a) CO, (b) NO_x and (c) BC as external tracers. Gradient contributions for factors SFOA, COA and HOA are shown alongside the background concentration of the tracer (black) which is estimated using the intercept of the linear regression. The chi-square value (red markers), the Q/Q_{exp} (blue markers) and the chosen final solution (labelled with a blue arrow) are also shown below.

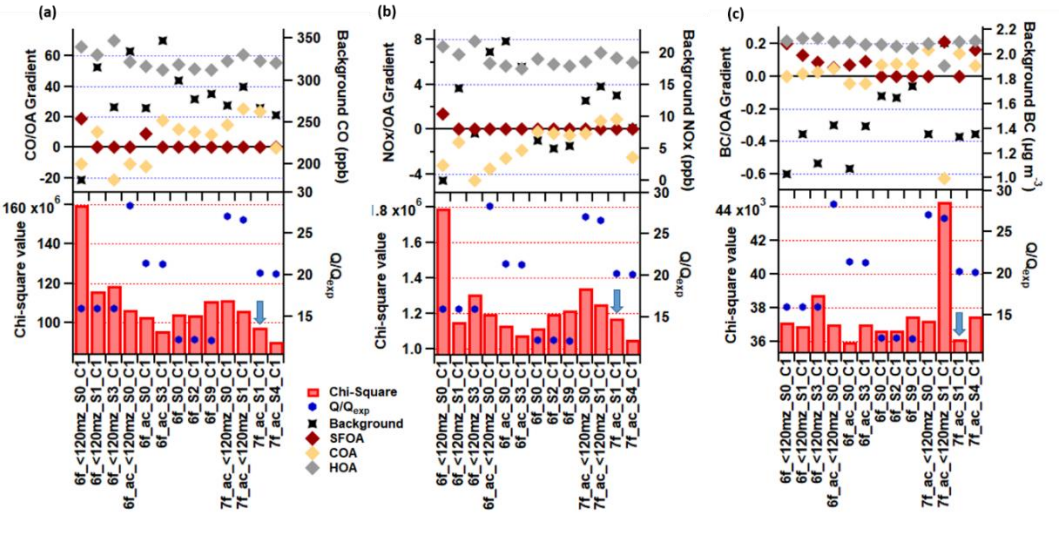

Figure S2.3. Trilinear regression analysis results for the Pre-Monsoon period analysis. Results are shown for the fit using (a) CO, (b) NO_x and (c) BC as external tracers. Gradient contributions for factors SFOA, COA and HOA are shown alongside the background concentration of the tracer (black) which is estimated using the intercept of the linear regression. The chi-square value (red markers), the Q/Q_{exp} (blue markers) and the chosen final solution (labelled with a blue arrow) are also shown below.

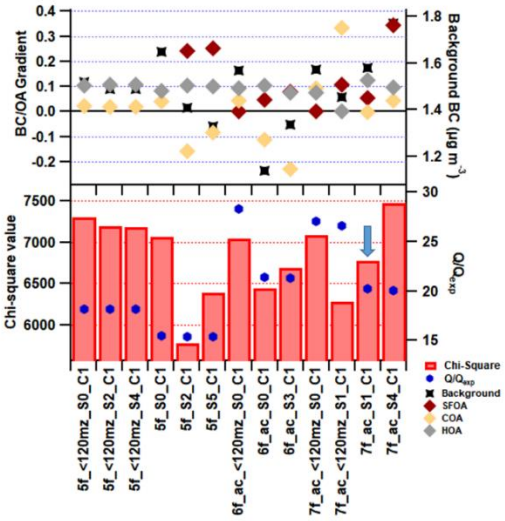

Figure S2.4. Bi- and trilinear regression analysis results for the Monsoon using BC as an external tracer. Gradient contributions for factors SFOA, COA and HOA are shown alongside the background concentration of the tracer (black) which is estimated using the intercept of the linear regression. The chi-square value (red markers), the Q/Q_{exp} (blue markers) and the chosen final solution (labelled with a blue arrow) are also shown below.

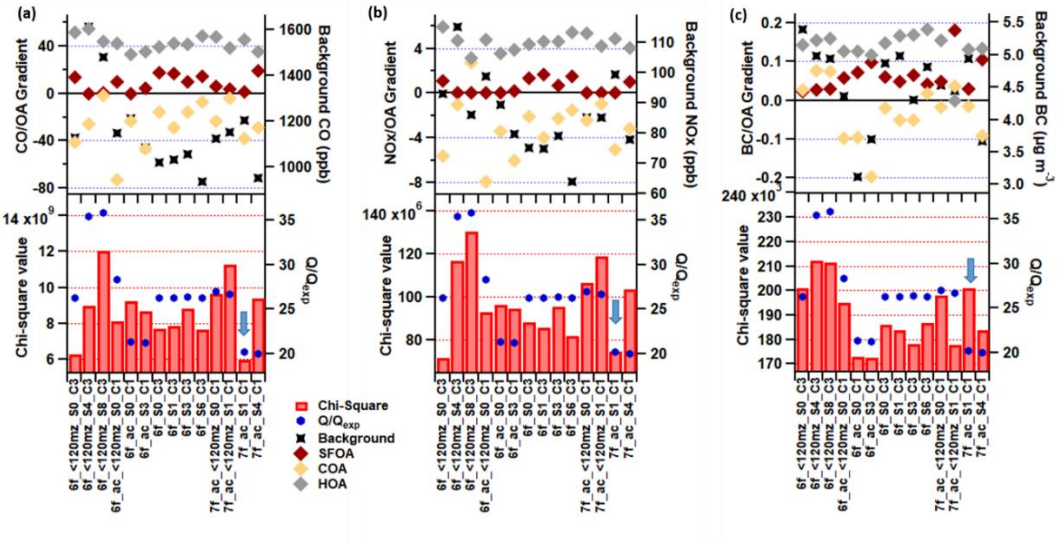

Figure S2.5. Trilinear regression analysis results for the Post-Monsoon period analysis. Results are shown for the fit using (a) CO, (b) NO_x and (c) BC as external tracers. Gradient contributions for factors SFOA, COA and HOA are shown alongside the background concentration of the tracer (black) which is estimated using the intercept of the linear regression. The chi-square value (red markers), the Q/Q_{exp} (blue markers) and the chosen final solution (labelled with a blue arrow) are also shown below.

S2.2. Determining if the traffic factors (NHOA and HOA) and burning factors (SFOA and SVBBOA) are more meaningful if separated or combined

In an attempt to assess if the nitrogen containing peaks (*m/z* 41 $[C_2H_3N]^+$, *m/z* 43 $[C_2H_5N]^+$, *m/z* 55 $[C_3H_5N]^+$, *m/z* 57 $[C_3H_7N]^+$, *m/z* 83 $[C_5H_9N]^+$, *m/*z 97 $[C_6H_{11}N]^+$) are solely responsible for the NHOA factor being resolved, these peaks were systematically down-weighted during separate PMF analyses by a factor of 2, 10 and 100. The results gave a similar solution that still separated into two traffic related factors which differed in their nitrogen content due to the above peak list.

As shown in the previous section, the separation of burning-related factors gave larger correlations with the external tracers. However, the SVBBOA factor was not included to simplify the analysis. This section includes a separate variable for SVBBOA in order to further establish if SFOA and SVBBOA should be separated or combined to form one time series. Similarly, the difference between the traffic factors NHOA and HOA is also investigated to see if the two create a better fit to external tracers when separated or when combined, to assess how robust the identified NHOA factor is. This analysis was applied to the chosen solution (7f_ac_S1_C1) and using Pearson's r correlations shown in Table S2.4, the two traffic factors showed a negligible change in correlation with external tracers when separated or combined. Similarly, the two burning factors showed little improvement in correlations when combined. Therefore, further multilinear regression analysis was carried out.

Penta- and tetralinear analyses were carried out using similar equations to Eq. (S2.1) but the number of factors, and therefore coefficients, were increased. The pentalinear equation is of the form:

$$ET = A + B(SFOA) + C(COA) + D(HOA) + E(NHOA) + F(SVBBOA) \quad \text{(S2.2)}$$

which does not include a combination of factors. The two tetralinear analyses correspond to two different combinations of factors. The Tetra_B1 analysis uses the equation:

$$ET = A + B(SFOA) + C(COA) + D(HOA_{tot}) + E(SVBBOA), \quad \text{(S2.3)}$$

where HOA_{tot} is the sum of NHOA and HOA. The Tetra_B2 analysis uses the equation:

$$ET = A + B(SFOA_{tot}) + C(COA) + D(HOA) + E(NHOA), \quad \text{(S2.4)}$$

where $SFOA_{tot}$ = SFOA + SVBBOA. The trilinear analysis uses Eq. (S2.1) with combinations *COA*, HOA_{tot} and $SFOA_{tot}$. These results are shown in Figure S2.6 and the chi-square values are summarised in Table S2.4 where a decrease in the chi-square is seen for the pentalinear analysis, i.e. when NHOA and HOA are separated, and this suggests that they are separate source factors. It also supports the findings shown in Section S2.1 as the chi-square decreases when SFOA and SVBBOA are separated. Additionally, Figure S2.6 also shows a significant difference in contribution based on the external tracer BC. The contribution of NHOA to BC in the Penta and Tetra_B2 analyses is particularly low but the HOA contribution is high. This further supports that they are from different sources.

Table S2.4. External tracer correlation summary showing the Pearson's r correlations for the traffic-related (NHOA and HOA) and burning-related (SFOA and SVBBOA) factors when their time series are combined (e.g. $SFOA_{tot}$ = SFOA + SVBBOA) or separated. The chi-square values for the multilinear regression analyses are also summarised for the Tri, Tetra_B1, Tetra_B2 and Penta cases (see Section S2.2 for explanation).

Pearson's r correlations	*CO*	*NO_x*	*BC*	*Acetonitrile*
SFOA	0.460	0.376	0.551	0.749
SVBBOA	0.531	0.447	0.618	0.607
$SFOA_{tot}$ = SFOA + SVBBOA	0.547	0.451	0.642	0.758
NHOA	0.850	0.770	0.697	0.735
HOA	0.879	0.853	0.637	0.685
HOA_{tot} = HOA + NHOA	0.911	0.855	0.701	0.725
Chi-squared – Multilinear Regressions	**CO**	**NO_x**	**BC**	
ET(Tri) – SFOA = $SFOA_{tot}$ and HOA = HOA_{tot}	7.18e+9	8.38e+7	2.82e+5	-
ET(Tetra_B1) – SFOA = $SFOA_{tot}$	7.12e+9	8.19e+7	2.38e+5	-
ET(Tetra_B2) – HOA = HOA_{tot}	7.14e+9	8.10e+7	2.42e+5	-
ET(Penta) – all separated	7.11e+9	8.10e+7	2.27e+5	-

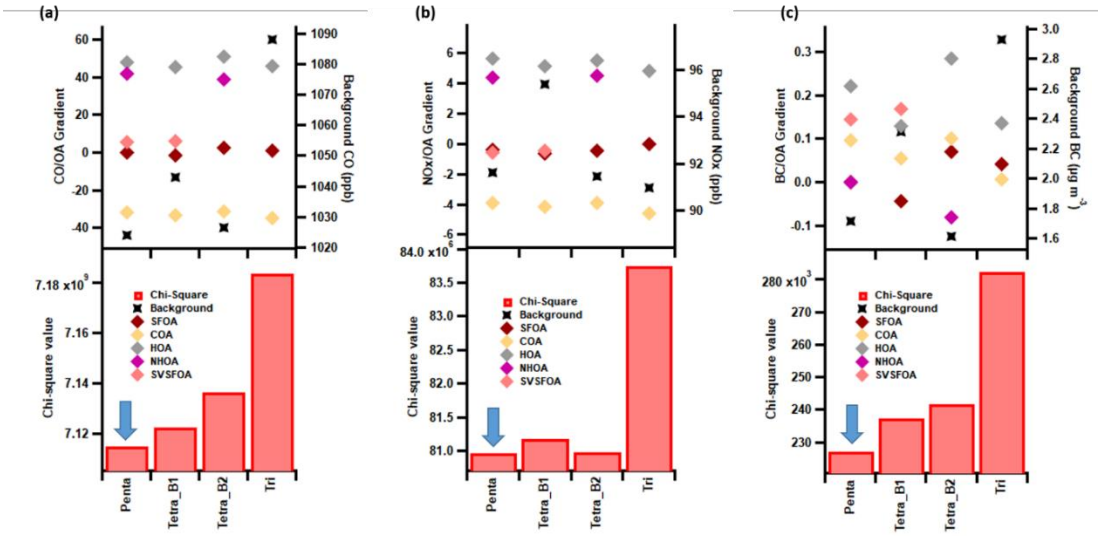

Figure S2.6. Multilinear regression analysis results for 7f_ac_S1 solution showing four difference combinations of factors. Results are shown for the fit using (a) CO, (b) NO_x and (c) BC as external tracers. Gradient contributions for factors are coloured according to the legend and are shown alongside the background concentration of the tracer (black) which is estimated using the intercept of the linear regression. The chi-square value (red markers) and the chosen final solution (labelled with a blue arrow) are also shown below.

S2.3. Method for determining the Inorganic-Organic PMF solution

The method described in Section S2.1 for the organic PMF analysis was also applied to the Inorg-Org PMF solutions. In brief, the previous organics analysis showed that a more robust solution is produced using all the measurement periods combined and including the larger masses (>120 *m/z*). This was therefore carried into the Inorg-Org PMF analysis. The rotational ambiguity was explored and again showed little variation between FPEAKS (-2 to 2, steps of 0.2). The mass contributions are the same to 0.1 % between FPEAKS which lead to setting FPEAK = 0.

Through exploring different initialisation SEEDS, the solutions changed, and multilinear regression analysis was carried out in the same method as described in Section S2.1. The results are summarised in Figure S2.7 and the same three external tracers were used. The organic PMF analysis in Section S2.1 and Section S2.2 also determined that, in most cases, the solution correlated with external tracers more strongly when factors were separated. The regression variables therefore increase with the number of factors and there are up to 6 variables used in the fit. The factors chosen for the fit are primary in nature and those that were not identifiable are labelled as primary organic aerosol (POA).

The solution chosen was 9f_S3 which gave a close to zero COA factor contribution and consistently gave low chi-square values for all three tracers. The solution 10f_S5 is an equally strong solution but there is not enough *a priori* information to discern if there is a credible separation into 10 factors i.e. unknown or non-specific factors were resolved past 9 factors. Additionally, the 9f_S3 is the most comparable to the organic-only PMF solution chosen.

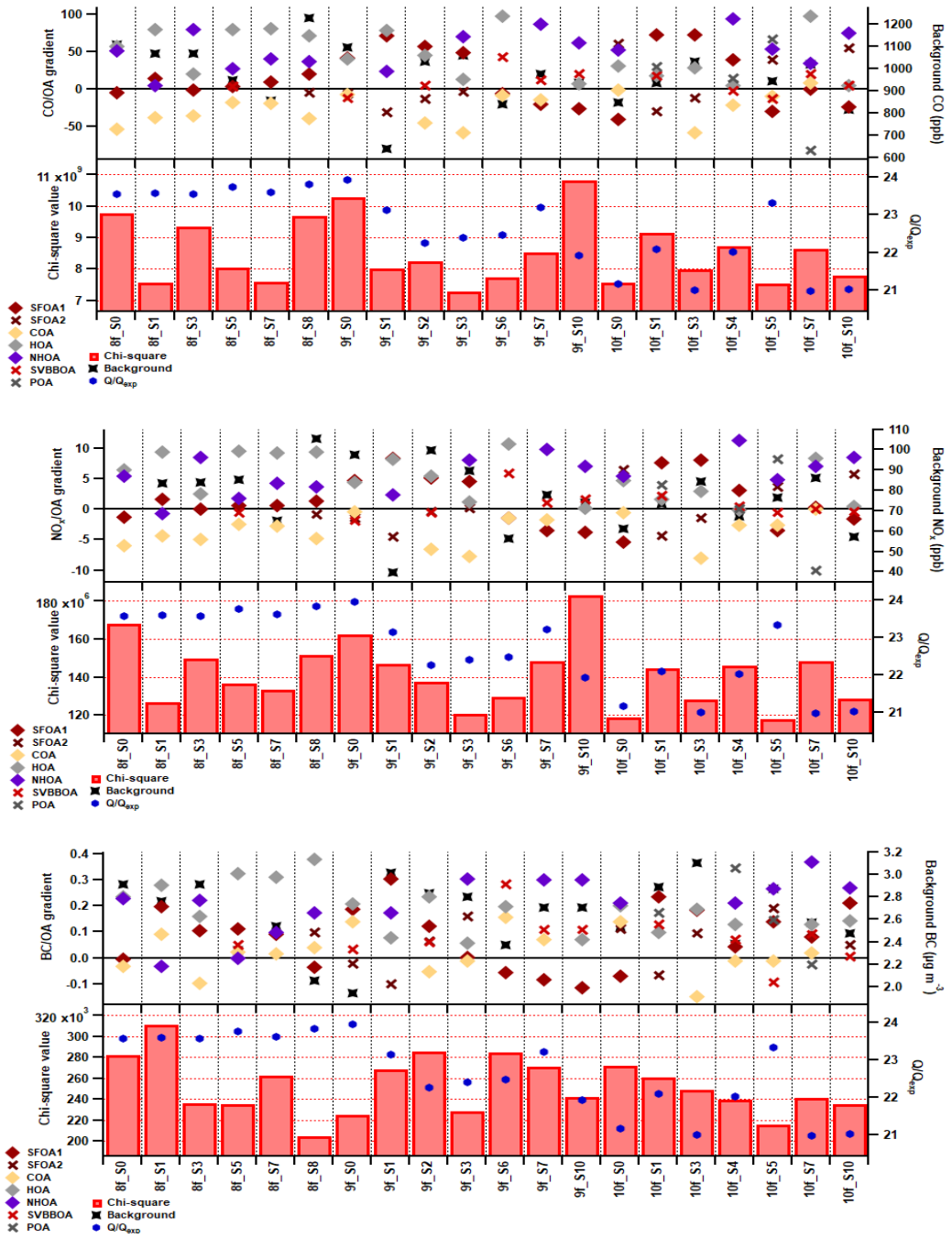

Figure S2.7. Multilinear regression for Inorg-Org PMF solutions. Results are shown for the fit using (a) CO, (b) NO_x and (c) BC as external tracers. The chi-square value for the fit is shown using red bars and the Q/Q_{exp} with blue markers. Gradient contributions for each factor are shown alongside the background concentration of the tracer (black) which is estimated using the intercept of the linear regression.

S2.4. Mean and standard deviations for species concentrations along with species concentration as a function of wind direction

All values for concentration summary graphs, Figures 2.1 and 2.7, are shown in Table S2.5 and includes mean, median and standard deviations for the three measurement periods.

Table S2.5. Mean and standard deviations for species concentrations during each measurement period

	Pre-monsoon (averaging interval = 784.67 hours)			*Monsoon (averaging interval = 369.75 hours)*			*Post-monsoon (averaging interval = 1072.25 hours)*		
Species	**Mean (µg m^{-3})**	**Median (µg m^{-3})**	**Standard deviation (µg m^{-3})**	**Mean (µg m^{-3})**	**Median (µg m^{-3})**	**Standard deviation (µg m^{-3})**	**Mean (µg m^{-3})**	**Median (µg m^{-3})**	**Standard deviation (µg m^{-3})**
Chloride	1.29	0.44	2.57	0.99	0.37	1.66	8.03	4.45	10.17
Ammonium	4.16	3.90	2.35	3.75	3.39	2.04	8.82	6.97	6.31
Nitrate	2.31	1.50	2.39	3.14	2.41	2.66	13.08	11.11	8.65
Sulphate	13.05	12.71	6.39	11.29	9.90	5.56	11.14	10.02	7.44
BC	3.47	2.59	3.13	2.54	1.90	2.23	8.50	5.98	7.04
Organics	29.16	26.12	22.96	24.98	21.43	16.63	104.32	83.20	78.38
COA	7.84	5.61	8.73	2.83	1.79	3.57	9.60	6.91	13.76
NHOA	0.83	0.00	2.46	0.76	0.19	1.33	12.56	4.04	20.39
SFOA	1.16	0.07	3.51	1.36	0.50	3.33	17.00	8.92	26.18
HOA	5.13	3.07	6.90	6.55	4.84	5.62	16.57	8.24	20.83
SVBBOA	0.53	0.00	1.18	0.01	0.00	0.11	19.60	15.27	16.13
LVOOA	10.59	10.68	7.36	6.71	6.32	5.11	21.65	19.91	12.59
SVOOA	3.26	1.57	4.76	6.81	5.41	5.81	7.72	6.26	6.86

The polar graphs for AMS measured aerosol chemical species concentrations are presented in Figure S2.8 and show each 30-minute average measurement on the radius against the wind direction displayed as an angle. Some of the pollution roses shown in the main manuscript do not show very distinct directional behaviours for the various species. The polar plots offer additional information about the highest values which are seen more clearly in Figure S2.8 and show the direction of possible high source contributors.

The diurnal cycle for chloride in the main manuscript shows a high morning peak at ~7-8 a.m. (Figure 2.3). The pollution roses for each diurnal hour in

Figure S2.9 shows this morning peak in more detail and suggests chloride originates from multiple directions. This helps to explain that chloride may be from multiple sources.

The polar graphs for PMF factors in Figure S2.10 are also used to help identify the wind directional preference of the highest outliers. The majority of the primary factors, NHOA, SFOA and COA, show strong outliers towards the south-east which is the same wind direction for which there are large peaks in polyaromatic hydrocarbons.

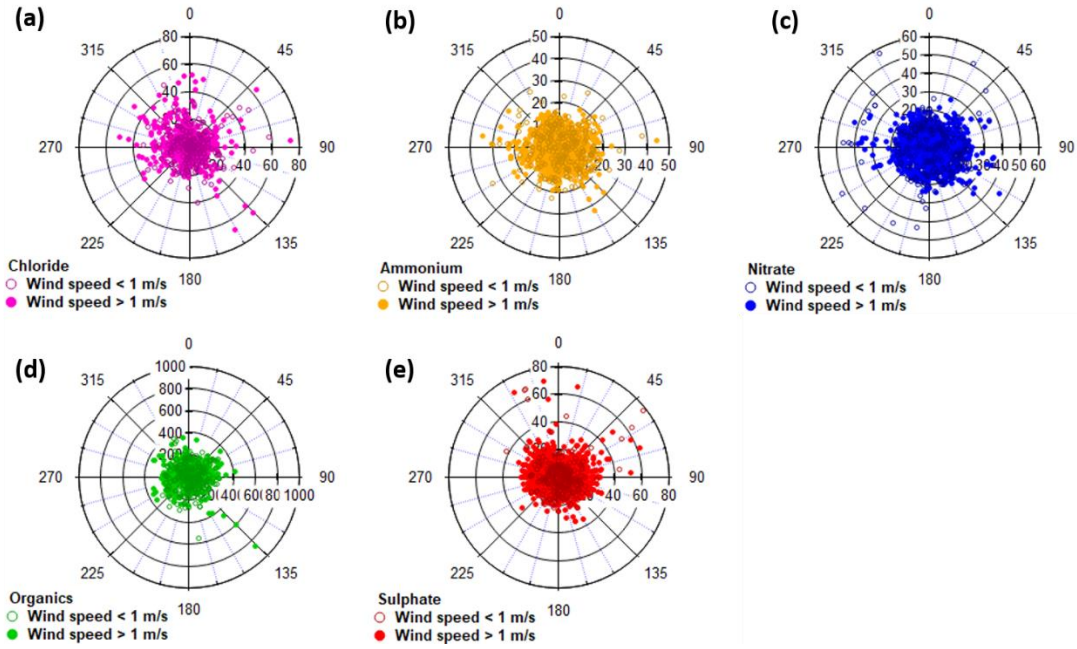

Figure S2.8. Polar graphs showing the concentrations (in μg m^{-3}) by wind direction for chloride, ammonium, nitrate, sulphate and organics for all measurement periods combined. Each point represents a 5-minute measurement. Open symbols show concentrations for winds speeds <1 m s^{-1} and closed symbols for wind speeds >1 m s^{-1}.

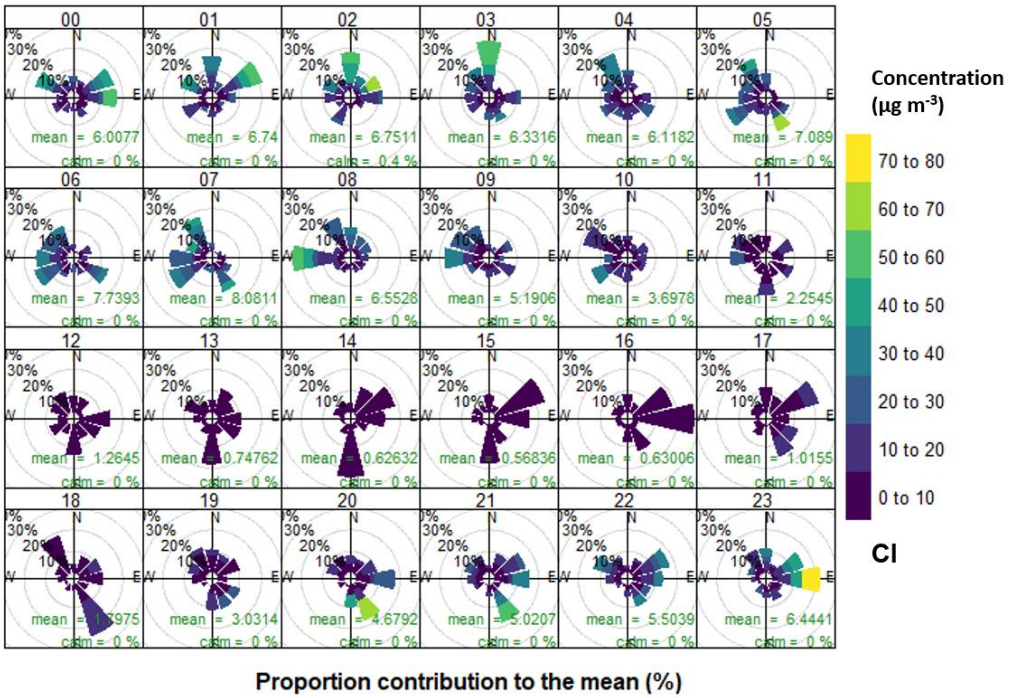

Figure S2.9. Chloride pollution roses for each diurnal hour for all measurement periods combined, where the data is binned into 30º wind vectors and the size of each bin is proportional to its contribution to the mean concentration. The counts are divided into concentration bins based on the colour scale in the legend. Units are µg m^{-3}.

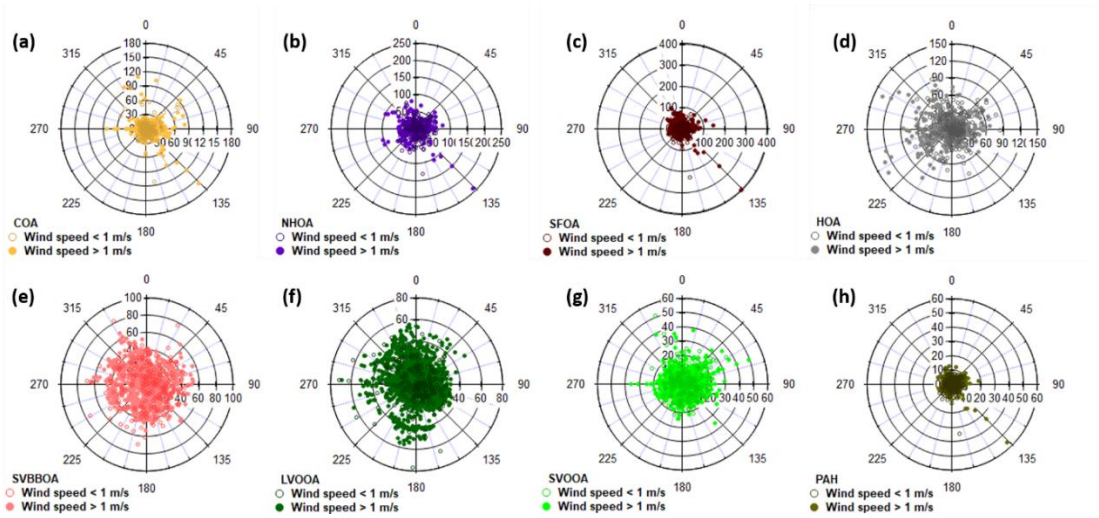

Figure S2.10. Polar graphs showing the concentrations (in µg m^{-3}) by wind direction for the factor solutions: (a) COA, (b) NHOA, (c) SFOA, (d) HOA, (e) SVBBOA, (f) LVOOA and (g) SVOOA. (h) PAH polar graph shows uncalibrated concentrations (a.u.) by wind direction. Each point represents a 30-minute average measurement. Open symbols show concentrations for winds speeds <1 m s^{-1} and closed symbols for wind speeds >1 m s^{-1}.

S2.5. Determination of the contribution of nitrogen compounds within PMF factors

As described in the main manuscript, the PMF factors NHOA and SVBBOA include a series of nitrogen-containing peaks. Figure S2.11 shows particular fragmentation patterns for each factor that can be used to distinguish the nitrogen-containing compounds responsible. The NHOA factor has prominent peaks at *m/z* 41 ($[C_2H_3N]^+$), *m/z* 43 ($[C_2H_5N]^+$), *m/z* 55 ($[C_3H_5N]^+$), *m/z* 57 ($[C_3H_7N]^+$), *m/z* 83 ($[C_5H_9N]^+$), *m/*z 97 ($[C_6H_{11}N]^+$) (Figure 2.5). The origin of these ions could be from nitrile compounds (R-C≡N) as the peaks at *m/z* 41 ($[C_2H_3N]^+$) and *m/*z 97 ($[C_6H_{11}N]^+$) have shown to be characteristically large for nitriles in standard 70 eV impact ionisation (McLafferty, 1962). They also have an even-to-odd carbon-to-nitrogen preference due to the nitrile fragmentation pattern in mass spectra (Simoneit et al., 2003; Abas et al., 2004). This is further supported by the comparison of NHOA with nitrile 70 eV spectra available on the NIST Chemistry WebBook (https://webbook.nist.gov/chemistry) (Figure S2.11). The relatively short carbon-chain nitrile compounds, for example, dodecanenitrile, tetradecanenitrile, hexadecanenitrile and octadecanenitrile, have particularly similar spectra and peak ratios to that of NHOA. To further support the evidence that nitrile compounds exist within the NHOA signature, its time series was compared with known nitrile VOC compounds (Brilli et al., 2014) measured using the PTR-MS. The correlation results are shown in Figure S2.12 where NHOA shows the strongest Pearson's *r* correlations with nitriles and other $C_xH_yN_z$ species.

The factor SVBBOA however has prominent peaks at peaks at *m/z* 43 ($[CHNO]^+$), *m/z* 44 ($[CH_2NO]^+$) and *m/z* 45 ($[CH_3NO]^+$), and lower intensity peaks at *m/z* 42 ($[CNO]^+$), *m/z* 46 ($[CH_4NO]^+$) and *m/z* 59 ($[C_2H_5NO]^+$) (Figure S2.11). This ratio of peaks is characteristic of primary amides where a large contribution from *m/z* 44 is a result of an α-cleavage fragmentation leaving a $[O=C=NH_2]^+$ ion (Pavia et al., 2014; Nicolescu, 2017; Fokoue et al., 2018). The absence of a high intensity *m/z* 59 peak could point to the majority being low molecular weight amides, because once above three carbon atoms, the amide

will undergo a McLafferty rearrangement and produce a $[H_2N\text{-}(C{=}O)\text{-}OH]^+$ ion. It is, however, uncertain how much of an influence the large $[CO_2]^+$ signal has on the fit of the $[CH_2NO]^+$ peak. The residuals of the peak fitting for the open and closed mass spectrum improved once $[CH_2NO]^+$ was fitted but this cannot rule out the large overlapping signals from $[CO_2]^+$.

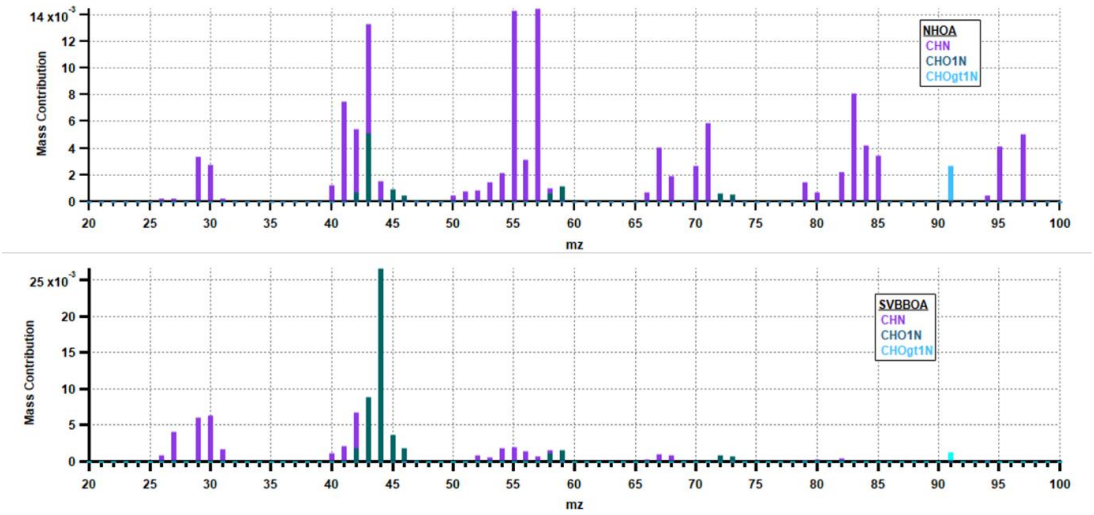

Figure S2.11. Mass spectra for the NHOA and SVBBOA factors showing the different nitrogen-containing chemical moieties.

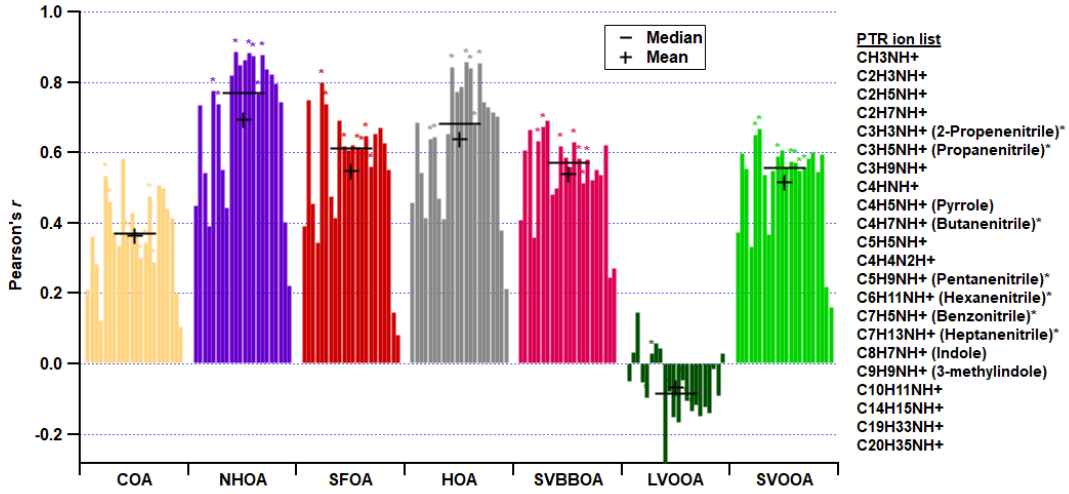

Figure S2.12. Correlation coefficients between Org-only PMF factors with $C_xH_yN_z$ family species measured using the PTR-MS. Chemical names for species are assigned based on literature presented in Brilli et al. (2014) and species marked with * are known nitrile compounds. The PTR ion list corresponds to the correlations going from left to right for each factor.

S2.6. Polyaromatic hydrocarbon (PAH) factor mass spectra

The PAH composition of PMF factors offers a unique look into explaining the origin of AMS factors. The difference between NHOA and HOA is further highlighted by their PAH mass spectra where NHOA contains a much larger fraction of the total PAH mass. A large percentage of OPAH mass in NHOA is due to the species dibenzodioxin (*m/z* 183 and 184), dibenzopyran and acenaphthoquinone (*m/z* 181 and 182). NHOA has other high OPAH species including naphthaldehyde (*m/z* 155 and 156) and anthrone (*m/z* 193 and 194) but these are shared amongst other factors as well. The NHOA factor also contributes the highest relative amounts of amino PAHs (APAH) and nitrogen-oxygen substituted PAHs (NOPAH) which coincides with this factor containing more nitrogen (Figure 2.10). The more prominent NOPAH and APAH peaks are nitro-acephthlene (*m/z* 198), nitro-fluorene (*m/z* 210 and 211), aminopyrene and carbazole (*m/z* 216 and 217), nitro-anthracene and nitro-phenathrene (*m/z* 223), chrysenamine (*m/z* 242 and 243), and dibenzocarbazole and amino benzopyrene (*m/z* 266 and 267). There are also

large methyl-substituted PAHs (MPAH) and UnSubPAH peaks in the NHOA factor including methyl-acenaphthalene (*m/z* 167), methyl-phenanthrene (*m/z* 191) and the ion $[C_{20}H_{12}]^+$ (*m/z* 251 and 252) which represents a number of benzopyrene and benzofluoranthene species that have the same mass (see Figure S2.13 for full list).

The PAH composition of COA is mainly UnSubPAHs and contributes the largest amount of UnSubPAHs out of all factors (Figure 2.10). Its defining peaks correspond to naphthalene (*m/z* 127 and 128), methyl-naphthalene (*m/z* 141 and 142), acenaphthylene (*m/z* 151 and 152), fluorene (*m/z* 165 and 166), anthracene/phenanthrene (*m/z* 177 and 178), benzo[def]fluorene (*m/z* 189 and 190), and pyrene/fluoranthene/acephenanthrylene (*m/z* 201 and 202).

The two burning factors, SFOA and SVBBOA, share similar PAH peaks however SVBBOA are much lower in abundance. A large portion of their PAH mass is OPAH and this is reflected by defining OPAH peaks such as indanone (*m/z* 131 and 132), napthaldehyde (*m/z* 155 and 156), dibenzofuran (*m/z* 167 and 168), dibenzopyran and acenaphthoquinone (*m/z* 181 and 182), dibenzodioxin and hydroxy-dibenzofuran (*m/z* 183 and 184), anthrone (*m/z* 193 and 194), and anthraquinone (*m/z* 207 and 208). Both factors also have prominent UnSubPAHs such as acenaphthylene (*m/z* 151 and 152), fluorene (*m/z* 165) and pyrene/fluoranthene/acephenanthrylene (*m/z* 201 and 202). However, SFOA has a larger naphthalene (*m/z* 127 and 128) content.

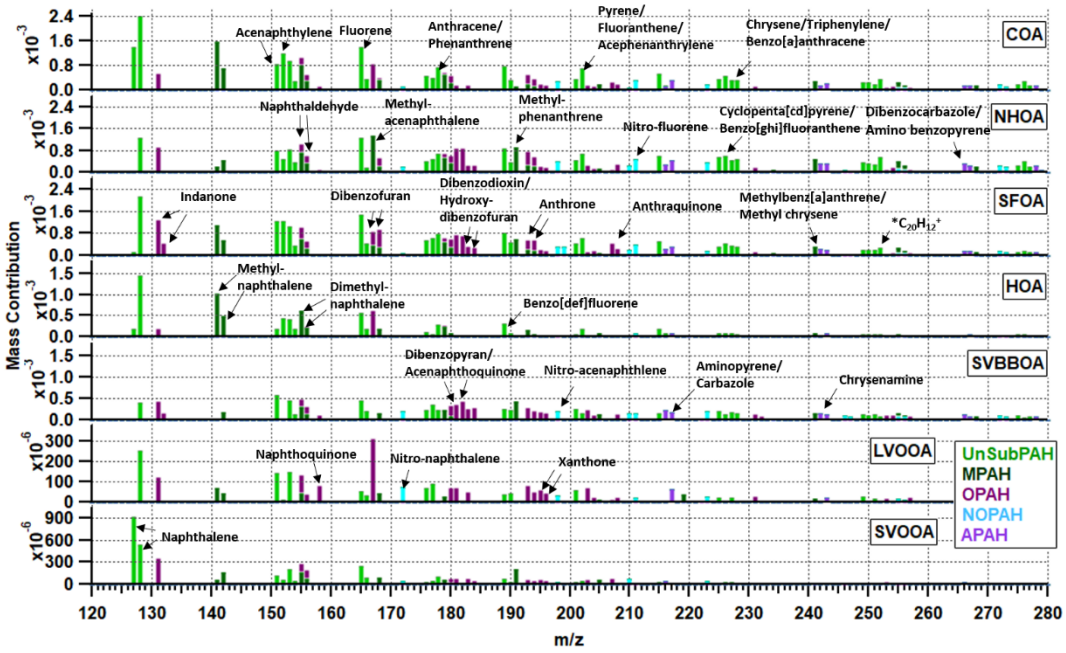

Figure S2.13. PAH factor mass spectra showing The PAH families: UnSubPAH, MPAH, OPAH, NOPAH and APAH. *The peak at m/z 252 relating to the ion $[C_{20}H_{12}]^+$ is a list of PAHs overlapping in mass and includes benzo[b]-, benzo[j]- and benzo[k]flouranthene, along with benzo[a]- and benzo[e]pyrene.

S2.7. AMS and PTR-QiTOF correlation mass spectra

The correlations between AMS measured ions and the seven PMF factors are presented in Figure S2.14. The AMS correlation mass spectra offer an alternate view to factor mass spectra. They show which AMS ions correlate strongly with factor time series while removing the influence of ion concentration. This means high *m/z* peaks exist due to their strong association in time and space with a factor, irrespective of the ion signal. A PTR-QiTOF correlation mass spectrum is also shown for the measurements of VOCs taken at the same site during the post monsoon period (Figure S2.14).

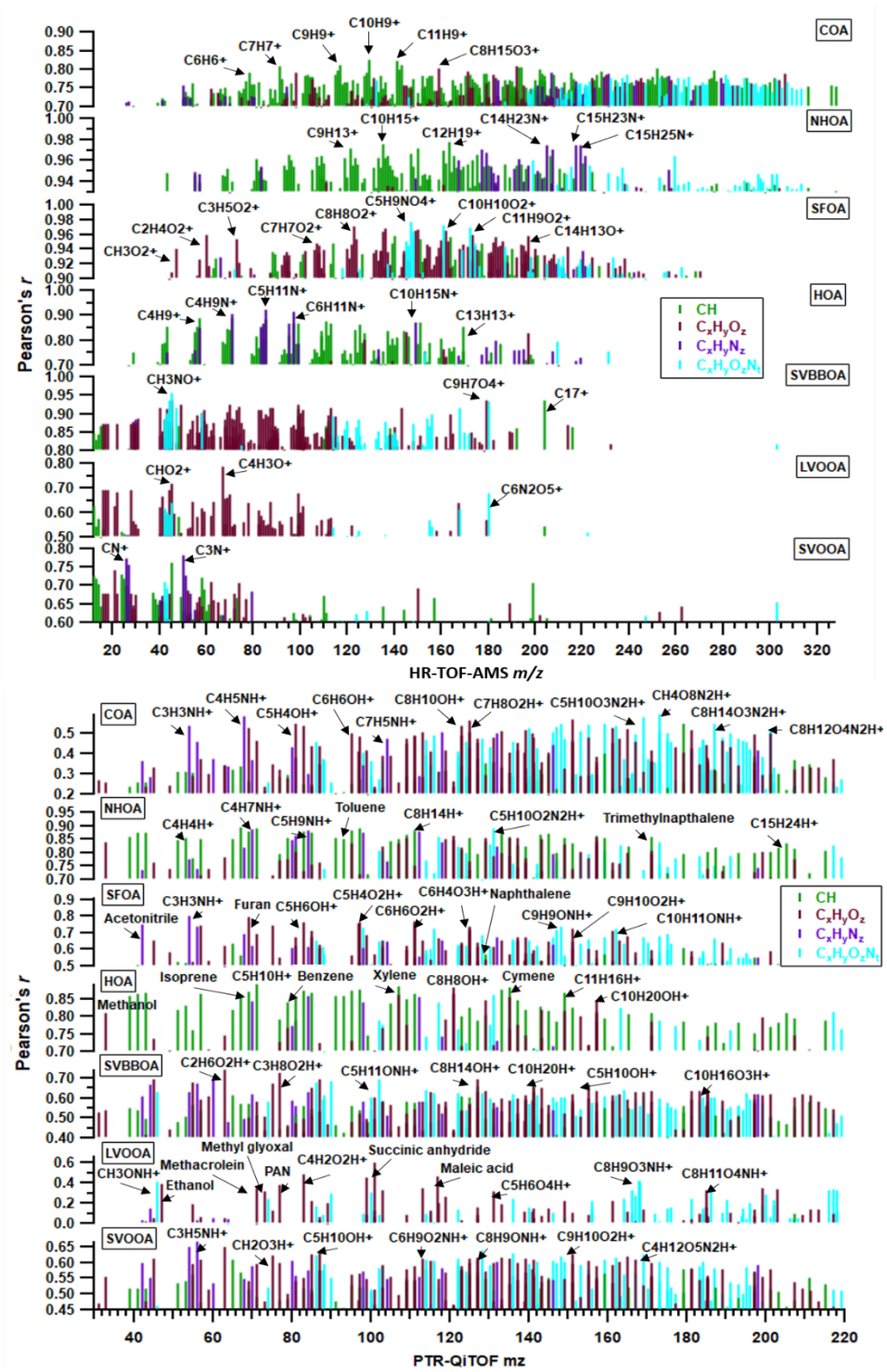

Figure S2.14. AMS and PTR-QiTOF correlation mass spectra where the y-axis shows the Pearson's r correlation coefficient between each m/z and the respective factor. Peaks are coloured based on the chemical composition described in the legend.

S2.8. Elemental ratio comparisons with literature using a Van Krevelen diagram

The Van Krevelen (VK) diagram of H:C ratio versus O:C ratio has previously been used in AMS studies to determine the level of oxidation of measured organic aerosol (Heald et al., 2010; Kroll et al., 2011; Ng et al., 2011; Canagaratna et al., 2015). The gradients in carbon oxidation states ($\overline{OS}_C$) show how aerosol moves from a less oxidised form in the top left ($\overline{OS}_C$ = -2) to a more oxidised form in the bottom right ($\overline{OS}_C$ = +2). It can also be used to estimate the reaction type that is occurring for the oxidation of aerosol. A gradient of zero with an increasing $\overline{OS}_C$, shows the addition of alcohol groups (R-COH) as there is an increase in both one oxygen and one hydrogen atom. The gradient of -1 shows the increase of two oxygen atoms for one hydrogen atom which suggests the addition of a carboxylic acid group or the simultaneous increase in both a carbonyl (R-C=O) and an alcohol group (R-C-OH). The final common reaction gradient is -2 which corresponds to an increase in a carbonyl (R-C=O) group as two hydrogen atoms are lost for an increase in one oxygen atom.

The O:C and H:C literature values for different PMF factors are shown in a VK diagram in Figure S2.15 and are tabulated in Table S2.6. The VK diagram shows a large spread of $\overline{OS}_C$ for the more oxidised PMF factors, such as LVOOA and SVOOA. Conversely, the primary factors, HOA and COA, both have a small window of $\overline{OS}_C$ but BBOA values can be variable. The PMF factors determined in this study in Delhi fall within similar compositional windows to literature with only the COA and SVBBOA factors showing significant differences. As discussed in the manuscript, the difference in Delhi COA is likely due to its high carboxylic acid content which is supported by its position being close to the -1 gradient in Figure S2.15. The SVBBOA factor is close to the zero gradient which may suggest it contains more alcohol functional groups. This is consistent with the time series of this factor having the strongest correlation (Pearson' *r* = 0.651) with aerosol liquid water content (LWC) since alcohol groups tend to create compounds that are water soluble.

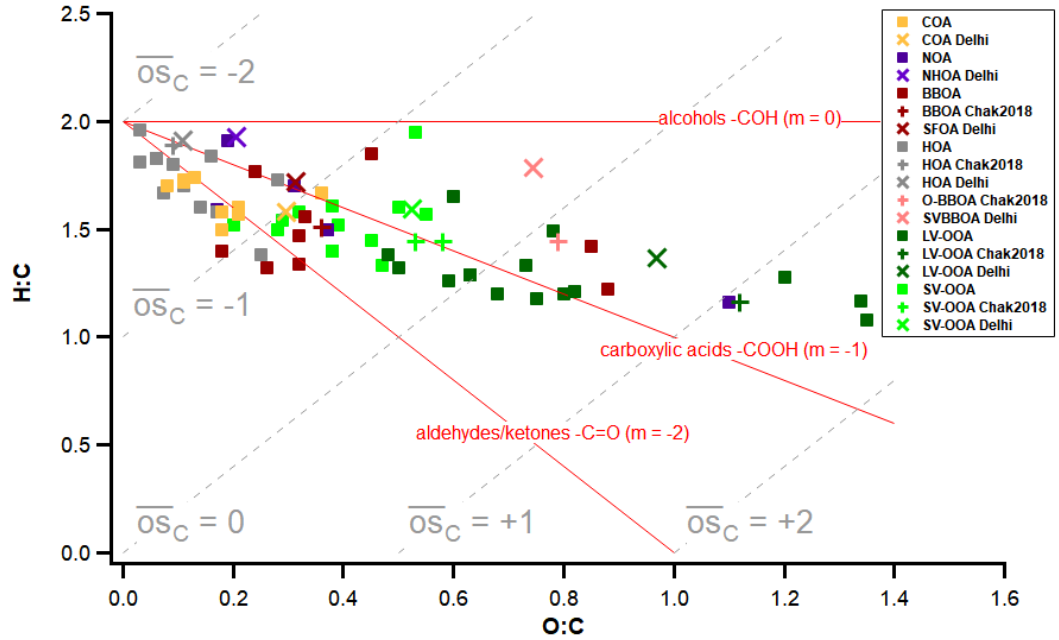

Figure S2.15. Van Krevelen (VK) diagram for the mass spectra of the organic aerosol factors listed in Table S2.6. The data labelled with Chak2018 are from the study by Chakraborty et al. (2018) and those labelled with Delhi are values from this study.

Table S2.6. Literature values of O:C and H:C ratios for mass spectra of AMS organic aerosol factors from selected studies around the world.

Literature	*Country*	*O:C SVOOA*	*H:C SVOOA*	*O:C LVOOA*	*H:C LVOOA*	*O:C BBOA*	*H:C BBOA*	*O:C COA*	*H:C COA*	*O:C HOA*	*H:C HOA*	*O:C NOA*	*H:C NOA*
Ye et al. (2017)	Changzhou, China	0.53	1.95	1.2	1.28							0.19	1.91
Timonen et al. (2013)	Helsinki, Finland	0.2	1.52	0.68	1.2	0.32	1.34			0.03	1.81		
Sun et al. (2011a)	Alabama, USA	0.5	1.6	0.6	1.65								
Sun et al. (2011b)	New York, USA	0.38	1.4	0.63	1.29			0.18	1.5	0.06	1.83	0.37	1.5
Bottenus et al. (2018)	Washington, USA	0.29	1.54	0.5	1.32	0.26	1.32			0.074	1.67	0.17	1.59
Zhang et al. (2018)	Northern Himalayas, China			1.34	1.17	0.85	1.42					1.1	1.16
Mohr et al. (2012)	Barcelona, Spain	0.32	1.58	0.75	1.18	0.24	1.77	0.21	1.57	0.03	1.96		
Schurman et al. (2015)	Colorado, USA	0.28	1.5	0.82	1.21	0.88	1.22						
He et al. (2010)	lab-based simulation study					0.18	1.4	0.08	1.7				
Huang et al. (2010)	Beijing, China	0.47	1.33	0.48	1.38			0.11	1.73	0.17	1.58		
He et al. (2011)	Shenzhen, China	0.45	1.45	0.59	1.26	0.32	1.47			0.11	1.7		
Crippa et al. (2013)	Paris, France	0.39	1.52	0.73	1.33			0.13	1.74	0.16	1.84		
Ge et al. (2012)	California, USA					0.33	1.56	0.11	1.72	0.09	1.8		
Zhu et al. (2016)	Jiangsu, China and Hainan, China	0.55	1.57	1.35	1.08					0.28	1.73		
Chakraborty et al. (2018)	Delhi, India	SVOOA1 = 0.58 SVOOA2 = 0.53	SVOOA1 = 1.44 SVOOA2 = 1.44	1.12	1.16	BBOA = 0.36, O-BBOA = 0.79	BBOA = 1.51, O-BBOA = 1.44			0.09	1.89		
This Study	Delhi, India	0.52	1.59	0.97	1.37	SFOA = 0.31, SVBBOA = 0.74	SFOA = 1.72, SVBBOA = 1.79	0.30	1.58	NHOA = 0.20 HOA = 0.11	NHOA = 1.93 HOA = 1.91		

S2.9. Monitoring Site Map

The monitoring site (28°39'51.8"N 77°13'55.2"E) at the Indira Gandhi Delhi Technical University for Women (IGDTUW) is shown in Figure S2.16 which is located ~500-750 m from the Yamuna river where a large cremation site is situated along the banks of the river.

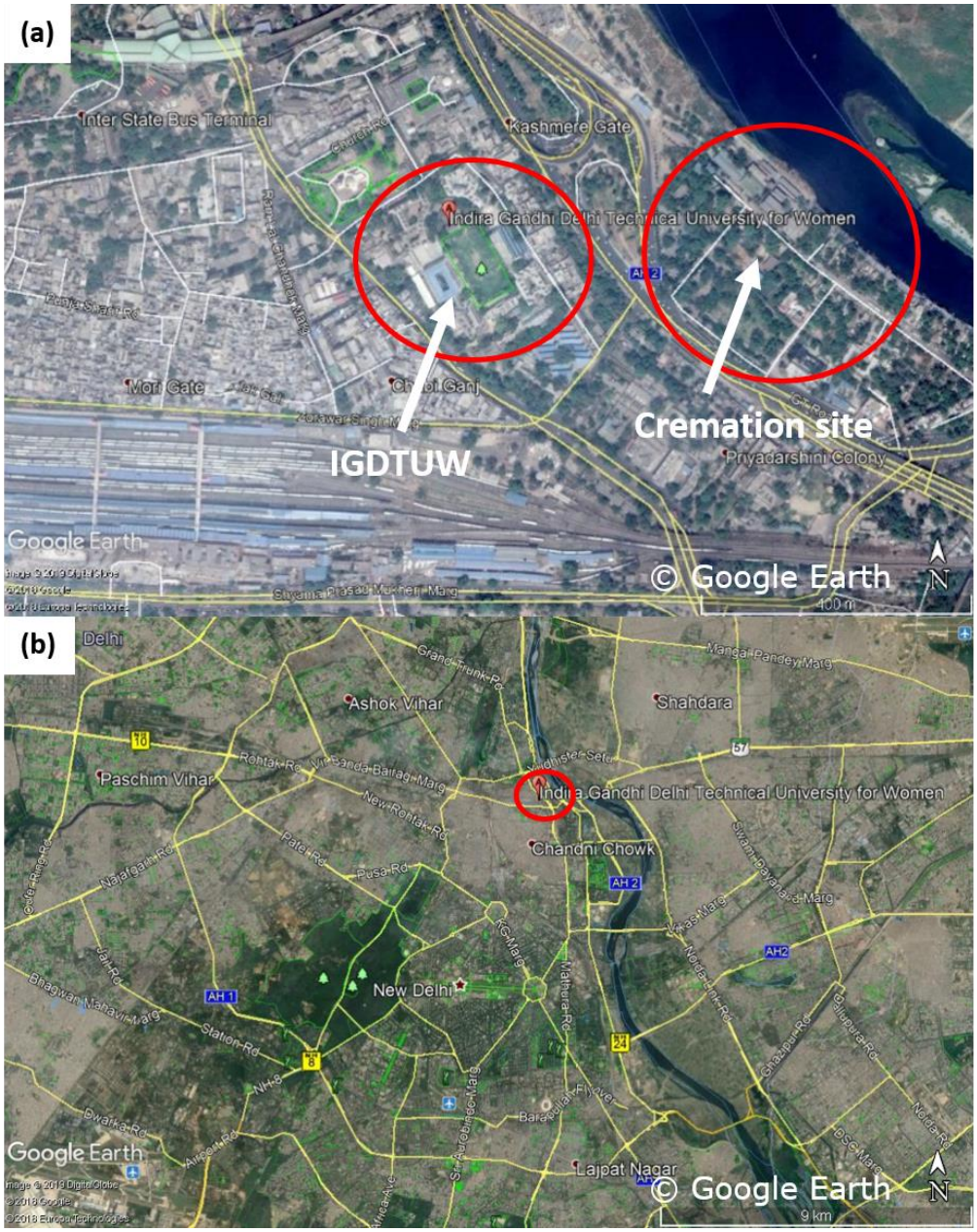

Figure S2.16. Monitoring site map on (a) small and (b) large scale. The red circles show the monitoring site location and a nearby large cremation site in (a).

S2.10. Inorganic-organic PMF solution results

The PMF analysis on the inorganic and organic combined matrix gave a 9-factor solution which was chosen using the described method in Section S2.3. There are common factors between the organic-only and inorganic-organic PMF solutions. These include two traffic factors: a hydrocarbon-like organic aerosol factor (HOA) and an N-rich HOA factor (NHOA), a cooking OA (COA) factor and two secondary factors: semi-volatility oxygenated OA (SVOOA) and low volatility OOA (LVOOA). There are also two burning factors where one is similarly named solid fuel OA (SFOA) and the other is a Cl-rich SFOA factor (Cl-SFOA). There are also two factors containing mainly inorganic mass where one is rich in sulphate (SO_4-OA) and the other is rich in nitrate (NO_3-OA). The factor mass profiles and their diurnal cycles during each measurement period are summarised in Figure S2.17.

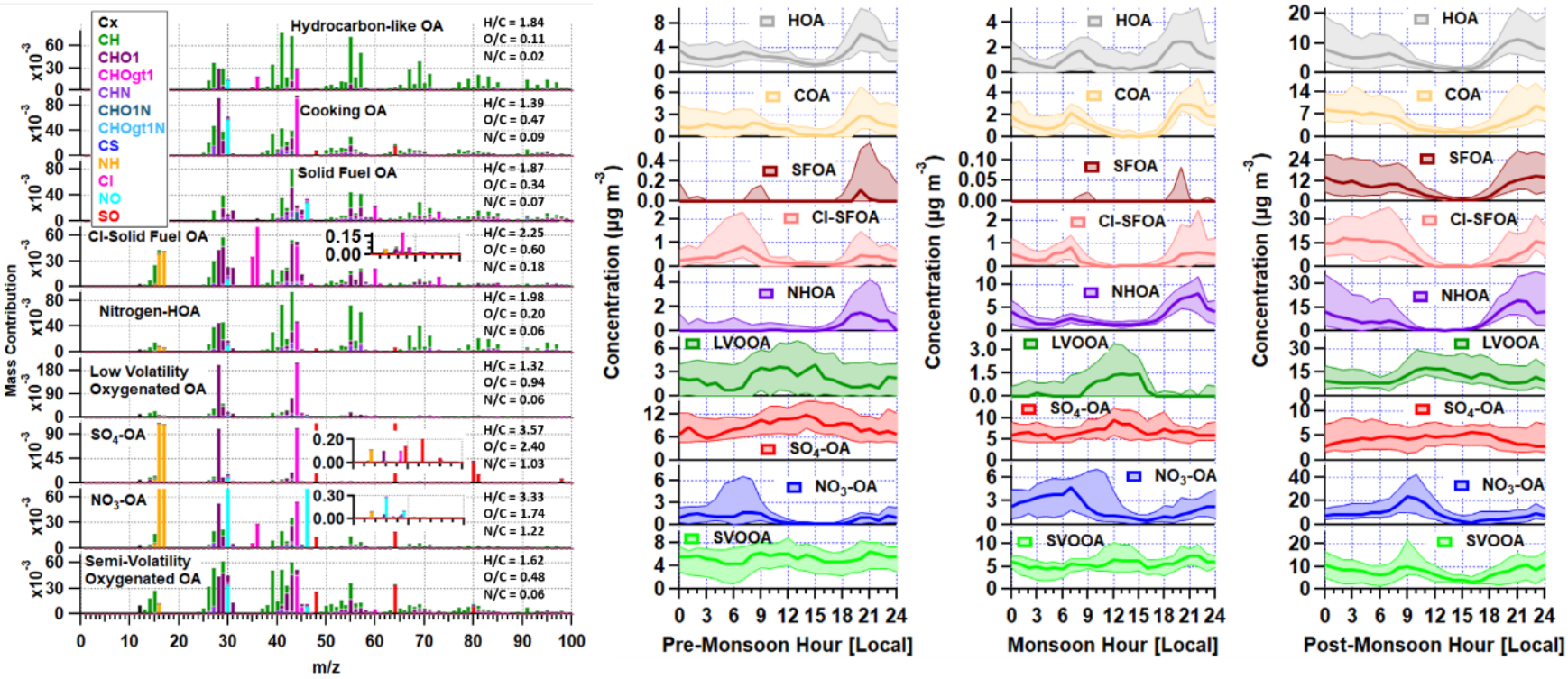

Figure S2.17. Inorganic-organic PMF solution mass profiles along with the diurnal cycles for each measurement period. The mass profiles for Cl-solid fuel OA (Cl-SFOA), SO_4-OA and NO_3-OA are dominated by certain peaks and their scales are adjusted to show the full spectrum. Small images of these factors on a larger scale are included to show the scale of the dominant peaks.

Their similarities to the organic-only solution and inorganic AMS species (nitrate, chloride and sulphate) are shown using time series and Pearson's *r* correlations in Figure S2.18. Here, the primary factors and inorganic factors show strong correlations with the organic-only factors and inorganic AMS species, respectively. However, secondary factors such as SVOOA are weakly correlated. Therefore, this suggests that inorganic aerosol may be contributing to secondary factors and causing a difference in mass. Evidence of this is seen in Figure S2.19 where SVOOA is shown to have a large percentage of sulphate. There is also a difference in burning factors where the organic-only solution has a secondary (SVBBOA) and a primary (SFOA) factor compared to the two primary factors of the inorganic-organic solution. This is mostly due to the majority of the chloride aerosol being associated with burning aerosol in the Cl-SFOA factor. As described in Section 2.5.3 of Chapter 2, the factor SVBBOA is thought to be associated with crop residue burning transported to Delhi from outside the city. For the inorganic-organic solution, the increased burning OA in the post-monsoon during the crop burning cycle is also resolved via factor SFOA. However, most of the oxidised mass has moved into LVOOA which therefore creates two primary factors. SFOA is therefore likely to be associated to wood burning in general rather than being resolved due to a specific source such as crop residue burning. This is also evident in the pre-monsoon and monsoon periods where SFOA is generally higher in mass than the organic-only solution SVBBOA.

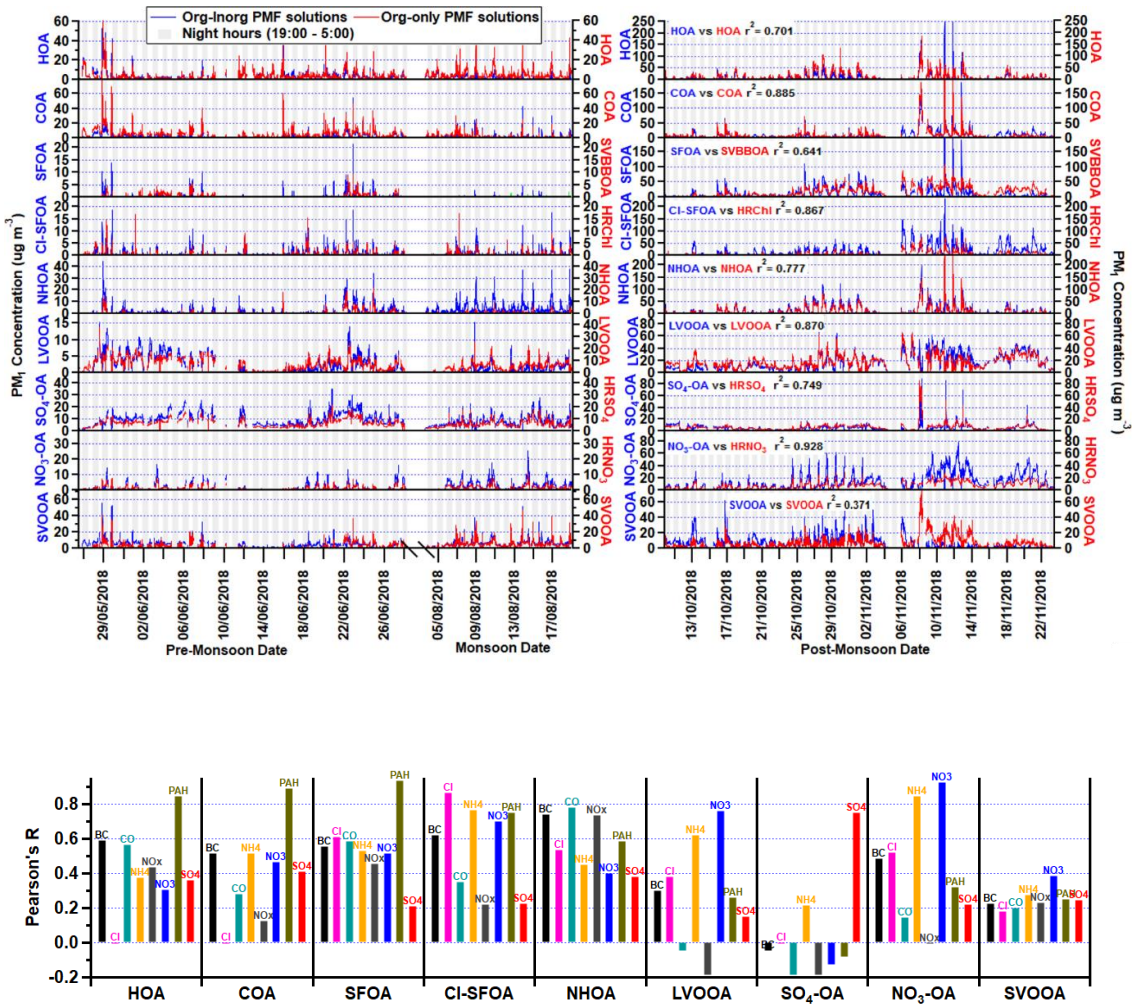

Figure S2.18. Top panel: inorganic-organic PMF solution times series (blue) along with overlaid organic-only factor time series and HR aerosol species (red). The Pearson's *r* correlations for each comparison are shown in the legend. Note: the scale changes between measurement periods and the left and right axes for LVOOA factors are different. Bottom panel: Pearson's *r* correlations between inorganic-organic solution factors and auxiliary measurements.

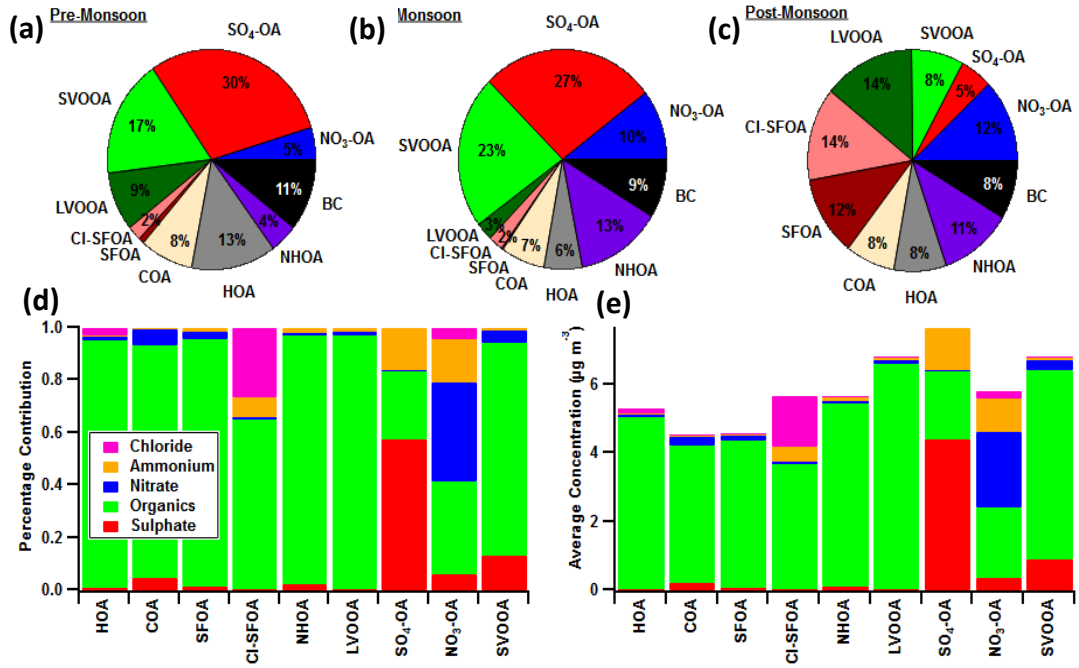

Figure S2.19. Percentage contribution of PMF factors to total PM_1 during each measurement period (a, b and c), along with the percentage contribution of AMS species to each factor (d). The average concentration of AMS species within each factor is also summarised in (e).

S2.11. Organic nitrogen oxide monsoon diurnal cycle

The elemental analysis in Section 2.4.4. shows the N:C diurnal cycle (Figure 2.11) which peaks at night during the monsoon period. The peak is suggested to be due to dark oxidation of volatile organic compounds via nitrate radicals. The N:C diurnal cycle is shown along with the diurnal cycle for organic nitrogen oxide species (OrgNO) in Figure S2.20 which shows a variable rise in OrgNO during the morning hours (00:00-07:00). OrgNO is an estimate with a large margin of error (± 20%) and this is shown using error bars (Kiendler-Scharr et al., 2016). The differences between the N:C and OrgNO diurnal cycles during the morning may therefore be within the uncertainty range. There is also a general rise and fall in the interquartile range between 00:00 and 07:00 which follows the N:C diurnal cycle. This may suggest that this rise is due to OrgNO formation via nitrate radical oxidation.

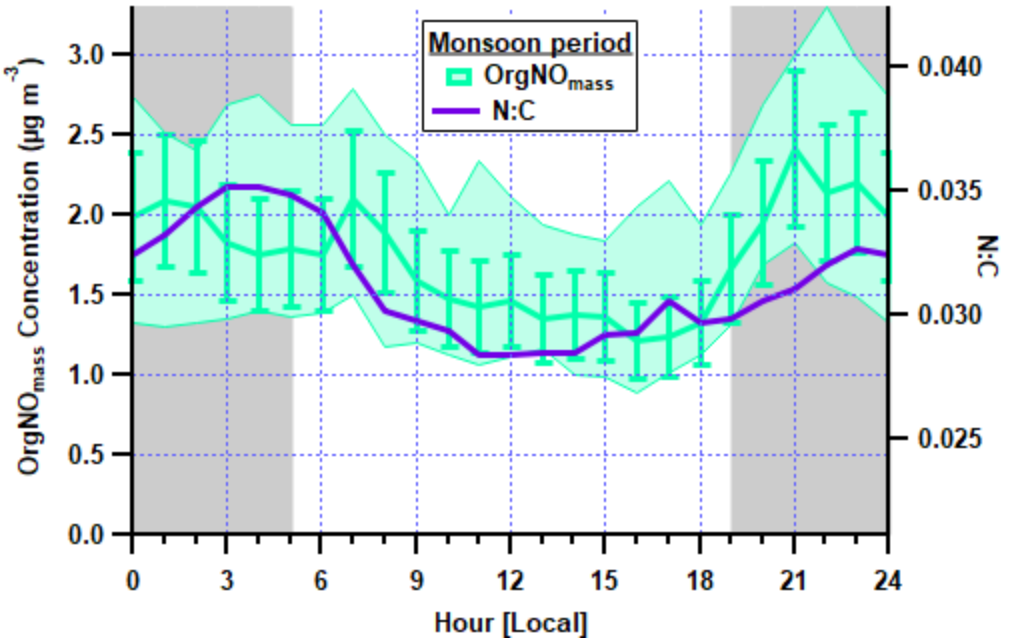

Figure S2.20. Median diurnal cycles for organic nitrogen oxide species (OrgNO$_{mass}$) and N:C ratio. The OrgNO$_{mass}$ interquartile range is shown using shading and its uncertainty (± 20%) is shown using error bars. The grey shading indicates the dark hours of the day.

References

Abas, M. R. Bin, Rahman, N. A., Omar, N. Y. M. J., Maah, M. J., Samah, A. A., Oros, D. R., Otto, A. and Simoneit, B. R. T.: Organic composition of aerosol particulate matter during a haze episode in Kuala Lumpur, Malaysia, Atmos. Environ., 38(25), 4223–4241, doi:10.1016/j.atmosenv.2004.01.048, 2004.

Aiken, A. C., Salcedo, D., Cubison, M. J., Huffman, J. A., DeCarlo, P. F., Ulbrich, I. M., Docherty, K. S., Sueper, D., Kimmel, J. R., Worsnop, D. R., Trimborn, A., Northway, M., Stone, E. A., Schauer, J. J., Volkamer, R. M., Fortner, E., de Foy, B., Wang, J., Laskin, A., Shutthanandan, V., Zheng, J., Zhang, R., Gaffney, J., Marley, N. A., Paredes-Miranda, G., Arnott, W. P., Molina, L. T., Sosa, G. and Jimenez, J. L.: Mexico City aerosol analysis during MILAGRO using high resolution aerosol mass spectrometry at the urban supersite (T0) - Part 1: Fine particle composition and organic source

apportionment, Atmos. Chem. Phys., 9(17), 6633–6653, doi:10.5194/acp-9-6633-2009, 2009.

Allan, J. D., Williams, P. I., Morgan, W. T., Martin, C. L., Flynn, M. J., Lee, J., Nemitz, E., Phillips, G. J., Gallagher, M. W. and Coe, H.: Contributions from transport, solid fuel burning and cooking to primary organic aerosols in two UK cities, Atmos. Chem. Phys., 10(2), 647–668, doi:10.5194/acp-10-647-2010, 2010.

Bottenus, C. L. H., Massoli, P., Sueper, D., Canagaratna, M. R., VanderSchelden, G., Jobson, B. T. and VanReken, T. M.: Identification of amines in wintertime ambient particulate material using high resolution aerosol mass spectrometry, Atmos. Environ., 180, 173–183, doi:10.1016/j.atmosenv.2018.01.044, 2018.

Brilli, F., Gioli, B., Ciccioli, P., Zona, D., Loreto, F., Janssens, I. A. and Ceulemans, R.: Proton Transfer Reaction Time-of-Flight Mass Spectrometric (PTR-TOF-MS) determination of volatile organic compounds (VOCs) emitted from a biomass fire developed under stable nocturnal conditions, Atmos. Environ., 97, 54–67, doi:10.1016/j.atmosenv.2014.08.007, 2014.

Canagaratna, M. R., Jimenez, J. L., Kroll, J. H., Chen, Q., Kessler, S. H., Massoli, P., Hildebrandt Ruiz, L., Fortner, E., Williams, L. R., Wilson, K. R., Surratt, J. D., Donahue, N. M., Jayne, J. T. and Worsnop, D. R.: Elemental ratio measurements of organic compounds using aerosol mass spectrometry: Characterization, improved calibration, and implications, Atmos. Chem. Phys., 15(1), 253–272, doi:10.5194/acp-15-253-2015, 2015.

Chakraborty, A., Mandariya, A. K., Chakraborti, R., Gupta, T. and Tripathi, S. N.: Realtime chemical characterization of post monsoon organic aerosols in a polluted urban city: Sources, composition, and comparison with other seasons, Environ. Pollut., 232, 310–321, doi:10.1016/j.envpol.2017.09.079, 2018.

Crippa, M., El Haddad, I., Slowik, J. G., Decarlo, P. F., Mohr, C., Heringa, M. F., Chirico, R., Marchand, N., Sciare, J., Baltensperger, U. and Prévôt, A. S. H.: Identification of marine and continental aerosol sources in Paris using high resolution aerosol mass spectrometry, J. Geophys. Res. Atmos., 118(4), 1950–1963, doi:10.1002/jgrd.50151, 2013.

Docherty, K. S., Aiken, A. C., Huffman, J. A., Ulbrich, I. M., Decarlo, P. F., Sueper, D., Worsnop, D. R., Snyder, D. C., Peltier, R. E., Weber, R. J., Grover, B. D., Eatough, D. J., Williams, B. J., Goldstein, A. H., Ziemann, P. J. and Jimenez, J. L.: The 2005 Study of Organic Aerosols at Riverside (SOAR-1): Instrumental intercomparisons and fine particle composition, Atmos. Chem. Phys., 11(23), 12387–12420, doi:10.5194/acp-11-12387-2011, 2011.

Fokoue, H. H., Marques, J. V., Correia, M. V., Yamaguchi, L. F., Qu, X., Aires-De-Sousa, J., Scotti, M. T., Lopes, N. P. and Kato, M. J.: Fragmentation pattern of amides by EI and HRESI: Study of protonation sites using DFT-3LYP data, RSC Adv., 8(38), 21407–21413, doi:10.1039/c7ra00408g, 2018.

Ge, X., Setyan, A., Sun, Y. and Zhang, Q.: Primary and secondary organic aerosols in Fresno, California during wintertime: Results from high resolution aerosol mass spectrometry, J. Geophys. Res. Atmos., 117(D19301), doi:10.1029/2012JD018026, 2012.

He, L. Y., Lin, Y., Huang, X. F., Guo, S., Xue, L., Su, Q., Hu, M., Luan, S. J. and Zhang, Y. H.: Characterization of high-resolution aerosol mass spectra of primary organic aerosol emissions from Chinese cooking and biomass burning, Atmos. Chem. Phys., 10(23), 11535–11543, doi:10.5194/acp-10-11535-2010, 2010.

He, L. Y., Huang, X. F., Xue, L., Hu, M., Lin, Y., Zheng, J., Zhang, R. and Zhang, Y. H.: Submicron aerosol analysis and organic source apportionment in an urban atmosphere in Pearl River Delta of China using high-resolution

aerosol mass spectrometry, J. Geophys. Res. Atmos., 116(12), 1–15, doi:10.1029/2010JD014566, 2011.

Heald, C. L., Kroll, J. H., Jimenez, J. L., Docherty, K. S., Decarlo, P. F., Aiken, A. C., Chen, Q., Martin, S. T., Farmer, D. K. and Artaxo, P.: A simplified description of the evolution of organic aerosol composition in the atmosphere, Geophys. Res. Lett., 37(8), doi:10.1029/2010GL042737, 2010.

Huang, X. F., He, L. Y., Hu, M., Canagaratna, M. R., Sun, Y., Zhang, Q., Zhu, T., Xue, L., Zeng, L. W., Liu, X. G., Zhang, Y. H., Jayne, J. T., Ng, N. L. and Worsnop, D. R.: Highly time-resolved chemical characterization of atmospheric submicron particles during 2008 Beijing Olympic games using an aerodyne high-resolution aerosol mass spectrometer, Atmos. Chem. Phys., 10(18), 8933–8945, doi:10.5194/acp-10-8933-2010, 2010.

Kiendler-Scharr, A., Mensah, A. A., Friese, E., Topping, D., Nemitz, E., Prevot, A. S. H., Äijälä, M., Allan, J., Canonaco, F., Canagaratna, M., Carbone, S., Crippa, M., Dall Osto, M., Day, D. A., De Carlo, P., Di Marco, C. F., Elbern, H., Eriksson, A., Freney, E., Hao, L., Herrmann, H., Hildebrandt, L., Hillamo, R., Jimenez, J. L., Laaksonen, A., McFiggans, G., Mohr, C., O'Dowd, C., Otjes, R., Ovadnevaite, J., Pandis, S. N., Poulain, L., Schlag, P., Sellegri, K., Swietlicki, E., Tiitta, P., Vermeulen, A., Wahner, A., Worsnop, D. and Wu, H. C.: Ubiquity of organic nitrates from nighttime chemistry in the European submicron aerosol, Geophys. Res. Lett., 43(14), 7735–7744, doi:10.1002/2016GL069239, 2016.

Kroll, J. H., Donahue, N. M., Jimenez, J. L., Kessler, S. H., Canagaratna, M. R., Wilson, K. R., Altieri, K. E., Mazzoleni, L. R., Wozniak, A. S., Bluhm, H., Mysak, E. R., Smith, J. D., Kolb, C. E. and Worsnop, D. R.: Carbon oxidation state as a metric for describing the chemistry of atmospheric organic aerosol, Nat. Chem., 3(2), 133–139, doi:10.1038/nchem.948, 2011.

McLafferty, F. W.: Mass Spectrometric Analysis: Aliphatic Nitriles, Anal. Chem., 34(1), 26–30, doi:10.1021/ac60181a005, 1962.

Mohr, C., DeCarlo, P. F., Heringa, M. F., Chirico, R., Slowik, J. G., Richter, R., Reche, C., Alastuey, A., Querol, X., Seco, R., Peñuelas, J., Jiménez, J. L., Crippa, M., Zimmermann, R., Baltensperger, U. and Prévôt, A. S. H.: Identification and quantification of organic aerosol from cooking and other sources in Barcelona using aerosol mass spectrometer data, Atmos. Chem. Phys., 12(4), 1649–1665, doi:10.5194/acp-12-1649-2012, 2012.

Ng, N. L., Canagaratna, M. R., Jimenez, J. L., Chhabra, P. S., Seinfeld, J. H. and Worsnop, D. R.: Changes in organic aerosol composition with aging inferred from aerosol mass spectra, Atmos. Chem. Phys., 11(13), 6465–6474, doi:10.5194/acp-11-6465-2011, 2011.

Nicolescu, T. O.: Interpretation of mass spectra, in Mass Spectrometry, pp. 24–78, Intech Open: London, UK., 2017.

Pavia, D. L., Lampman, G. M., Kriz, G. S. and Vyvyan, J. A.: Introduction to Spectroscopy, Cengage Learning., 2014.

Reyes-Villegas, E., Green, D. C., Priestman, M., Canonaco, F., Coe, H., Prévôt, A. S. H. and Allan, J. D.: Organic aerosol source apportionment in London 2013 with ME-2: Exploring the solution space with annual and seasonal analysis, Atmos. Chem. Phys., 16(24), 15545–15559, doi:10.5194/acp-16-15545-2016, 2016.

Schurman, M. I., Lee, T., Sun, Y., Schichtel, B. A., Kreidenweis, S. M. and Collett, J. L.: Investigating types and sources of organic aerosol in Rocky Mountain National Park using aerosol mass spectrometry, Atmos. Chem. Phys., 15(2), 737–752, doi:10.5194/acp-15-737-2015, 2015.

Simoneit, B. R. T., Rushdi, A. I., Abas, M. R. B. and Didyk, B. M.: Alkyl amides and nitriles as novel tracers for biomass burning, Environ. Sci. Technol., 37(1), 16–21, doi:10.1021/es020811y, 2003.

Sun, Y., Zhang, Q., Zheng, M., Ding, X., Edgerton, E. S. and Wang, X.: Characterization and Source Apportionment of Water-Soluble Organic Matter in Atmospheric Fine Particles (PM 2.5) with High-Resolution Aerosol Mass Spectrometry and GC–MS, Environ. Sci. Technol., 45(11), 4854–4861, doi:10.1021/es200162h, 2011a.

Sun, Y., Du, W., Fu, P., Wang, Q., Li, J., Ge, X., Zhang, Q., Zhu, C., Ren, L., Xu, W., Zhao, J., Han, T., Worsnop, D. R. and Wang, Z.: Primary and secondary aerosols in Beijing in winter: Sources, variations and processes, Atmos. Chem. Phys., 16(13), 8309–8329, doi:10.5194/acp-16-8309-2016, 2016.

Sun, Y. L., Zhang, Q., Schwab, J. J., Demerjian, K. L., Chen, W. N., Bae, M. S., Hung, H. M., Hogrefe, O., Frank, B., Rattigan, O. V. and Lin, Y. C.: Characterization of the sources and processes of organic and inorganic aerosols in New York city with a high-resolution time-of-flight aerosol mass apectrometer, Atmos. Chem. Phys., 11(4), 1581–1602, doi:10.5194/acp-11-1581-2011, 2011b.

Timonen, H., Carbone, S., Aurela, M., Saarnio, K., Saarikoski, S., Ng, N. L., Canagaratna, M. R., Kulmala, M., Kerminen, V. M., Worsnop, D. R. and Hillamo, R.: Characteristics, sources and water-solubility of ambient submicron organic aerosol in springtime in Helsinki, Finland, J. Aerosol Sci., 56, 61–77, doi:10.1016/j.jaerosci.2012.06.005, 2013.

Ulbrich, I. M., Canagaratna, M. R., Zhang, Q., Worsnop, D. R. and Jimenez, J. L.: Interpretation of organic components from Positive Matrix Factorization of aerosol mass spectrometric data, Atmos. Chem. Phys., 9(9), 2891–2918, doi:10.5194/acp-9-2891-2009, 2009.

Ye, Z., Liu, J., Gu, A., Feng, F., Liu, Y., Bi, C., Xu, J., Li, L., Chen, H., Chen, Y., Dai, L., Zhou, Q. and Ge, X.: Chemical characterization of fine particulate matter in Changzhou, China, and source apportionment with offline aerosol mass spectrometry, Atmos. Chem. Phys., 17(4), 2573–2592, doi:10.5194/acp-17-2573-2017, 2017.

Young, D. E., Allan, J. D., Williams, P. I., Green, D. C., Harrison, R. M., Yin, J., Flynn, M. J., Gallagher, M. W. and Coe, H.: Investigating a two-component model of solid fuel organic aerosol in London: Processes, PM1 contributions, and seasonality, Atmos. Chem. Phys., 15(5), 2429–2443, doi:10.5194/acp-15-2429-2015, 2015.

Zhang, X., Xu, J., Kang, S., Liu, Y. and Zhang, Q.: Chemical characterization of long-range transport biomass burning emissions to the Himalayas: Insights from high-resolution aerosol mass spectrometry, Atmos. Chem. Phys., 18(7), 4617–4638, doi:10.5194/acp-18-4617-2018, 2018.

Zhu, Q., He, L. Y., Huang, X. F., Cao, L. M., Gong, Z. H., Wang, C., Zhuang, X. and Hu, M.: Atmospheric aerosol compositions and sources at two national background sites in northern and southern China, Atmos. Chem. Phys., 16(15), 10283–10297, doi:10.5194/acp-16-10283-2016, 2016.